Structural and Functional Characterization of Catalase HPII of *Escherichia coli*

by

Vikash Kumar Jha

A thesis

submitted to the Faculty of Graduate Studies

in partial fulfillment of the requirements for the degree of

DOCTOR OF PHILOSOPHY

Department of Microbiology

University of Manitoba

Winnipeg, Manitoba

Canada

ABSTRACT

Catalase HPII of *Escherichia coli* is similar in sequence and structure to other catalases including the conservation of several residues on both the distal and proximal sides of the active center heme. The roles of many residues on the distal side of the heme have been well characterized. By contrast, very few residues on the proximal side of the heme or in the plane of the heme have been investigated. The primary goal of this thesis is to develop a better understanding of the role of the residues and structural features at the core of catalases and in the lateral access channel. The results demonstrate that a break in molecular symmetry does not have any functional significance. Mutations of the residues involved caused little change in catalytic, biochemical or structural properties of the enzyme. The group of conserved arginines including R125, R165 and R422 adjacent to the heme propionates is critical for heme binding and proper folding of the protein such that none of the alanine variants resulted in accumulation of folded protein and only the R125K and R422K variants accumulated active and folded protein. Mutation of conserved phenylalanine at 413, ~13 Å from heme on its proximal side to alanine, lysine, glutamate, glutamine and tyrosine surprisingly resulted in variants that were inefficient in the conversion of heme *b* to heme *d* and differed from the native HPII in their resistance to inhibitors despite retaining near WT activities. F413Y was even more unusual in presenting two bands after SDS-PAGE, indicating that main chain cleavage had occurred. Inactivation of the F413Y protein in the H128N/F413Y double variant prevented cleavage suggesting it was related to catalytic activity. Mass spectrometry suggested protein cleavage had occurred at the N-terminus between residues 110 and 130, and this was confirmed in the crystal structure. Replacing Ile274, which is situated adjacent to the heme edge at the entrance to the lateral channel, with a Cys resulted in the heme being covalently linked to the protein through a Cys-vinyl bond which is hypersensitive to X-ray irradiation being largely degraded within seconds of exposure to the X-ray beam.

ACKNOWLEDGEMENTS

I take this opportunity to extend my sincere and heartfelt gratitude and acknowledge all those people who have helped me through this task of completing my Ph.D thesis. First and foremost, I would like to thank my advisor, Dr. Peter Loewen, for giving me the opportunity to work in his lab, making things seem simple for me during the work and providing financial support throughout the study period. Discussions with him and his expert suggestions have always encouraged and inspired me during the course of my doctoral program. I am grateful to the Thesis and Review Committee members, especially Dr. Pavel Dibrov, Dr. Ivan Oresnik and Dr. Jorg Stetefeld for their valuable suggestions and constructive views during my reviews and discussions. I would also like to thank my external examiner Dr. Zongchao Jia for accepting to review the thesis. I am thankful to Mr. Jacek Switala for his thorough assistance and cooperation; to the past and present Loewen lab members, Rahul Singh, Amarbeer Kaur, Taweewat Deemagarn, Vania Nunes, Ben Wisemen, Jacylyn Villanueva, Munmun Nandi, Tuhin Guha for their support and friendship. My thanks also go to Dr. Brian Mark for his expert opinion and suggestions in my structural work. I am also thankful to Dr. Lynda Donald for her assistance in mass spectrometry work, our collaborator in Spain Prof. Ignacio Fita for his constructive suggestions. The assistance I received from Dr. Linda Camroon, Sharon Berg, Madeleine Harris and Veronica Larmour is gratefully acknowledged. The staff members of Canada Light Source (CLS) Saskatoon are also greatly acknowledged for allowing me to use the synchrotron X-ray source. The graduate fellowship fundings from Faculty of Science and Faculty of Graduate Studies are also acknowledged.

I would like to express my sincere thanks to my wife Tanushree, whose constant love and support played a vital and indispensable role in the completion of this work. Last but certainly not the least my special thanks go to my parents who always stood by me and supported me in their own ways.

Thank you all...

TABLE OF CONTENTS

LIST OF FIGURES

LIST OF TABLES

LIST OF ABBREVIATIONS

Å	Angstrom
A	Absorbance
AA	Amino acid
ADP	Adenosine diphosphate
AMP	Adenosine monophosphate
Amp^R	Ampicillin resistant
ATP	Adenosine triphosphate
bp (s)	Base pair (s)
BpKatG	*Burkholderia pseudomallei* catalase-peroxidase
BLC	Bovine liver catalase
$CaCl_2$	Calcium chloride
CatF	Catalase from *Pseudomonas syringae*
Cat1	Catalase from *Neurospora crassa*
Cat3	Catalase from *Neurospora crassa*
C*c*P	Cytochrome *c* peroxidase
Ci	Curie
CIP	Calf intestinal alkaline phosphatase
CO_2	Carbon dioxide
Cu	Copper
°C	Degree centigrade or celcius
Da	Dalton
dATP	Deoxyadenosine triphosphate
DEAE	Diethylaminoethyl
DMSO	Dimethylsulfoxide
DNA	Deoxribonucleic acid
dNTP	Deoxyribonicleotide triphosphate
e^-	Electron
*Ec*KatG	Catalase-peroxidase from *Escherichia coli*
EDTA	Ethylene diamine tetraactic acid
EFC	*Enterobacter faecalis* catalase
EKTA	*Exiguobacterium oxidotolerance* catalase
EPR	Electron paramagnetic resonance
Fe	Iron

g	Gram
H^+	Proton
HEC	Human erythrocyte catalase
*Hm*KatG	Catalase-peroxidase from *Haloarcula marismortui*
H_2O	Water
HPI	Hydroperoxidase I or catalase-peroxidase from *Escherichia coli*
HPII	Hydroperoxidase II or catalase from *Escherichia coli*
HPC	*Helicobacter pylori* catalase
HPLC	High pressure liquid chromatography
HRP	Horseradish peroxidase
KatE	*Escherichia coli* catalase or HPII
kb	Kilobase
k_{cat}	Turnover number
kDa	KiloDalton
K_M	Michealis-Menten constant
KPi	Potassium phosphate buffer
L	Liter/s
LB	Luria-Bertani
LiCl	Lithium chloride
LPC	Catalase from *Lactobacillus plantarum*
µg	Microgram
µl	Microliter
µM	Micromolar
M	Molar
MALDI	Matrix-assisted laser desorption/ionization
mg	Milligram
$MgSO_4$	Magnesium sulphate
min	Minute
ml	Milliliter
MLC	*Micrococcus lysodeikticus* catalase
mM	Millimolar
Mn	Manganese
*Mt*KatG	Catalase peroxidase from *Mycobacterium tuberculosis*
NaCl	Sodium chloride

NaCN	Sodium cyanide
Na_2CO_3	Sodium carbonate
NAD	Nicotinamide adenine dinucleotide (oxidized)
NADH	Nicotinamide adenine dinucleotide (reduced)
NADPH	Nicotinamide adenine dinucleotide phosphate
Na_2HPO_4	Sodium phosphate monobasic
NaH_2PO_4	Sodium phosphate dibasic
NaN_3	Sodium azide
NaOH	Sodium hydroxide
ng	Nanogram
NH_2OH	Hydroxylamine
nm	Nanometer
nM	Nanomolar
NMR	Nuclear magnetic resonance
OD	Optical density
O_2	Oxygen molecule
PAGE	Polyacrylamide gel electrophoresis
PCR	Polymerase chain reaction
PDB	Protein Data Bank
PEG	Polyethylene glycol
PMC	*Proteus mirabilis* catalase
PMSF	Phenylmethylsulfonyl fluoride
Por	Porphyrin
$Por^{\bullet+}$	Porphyrin π-cation radical
PVC	*Penicillium vitale* catalase
RNA	Ribonucleic acid
RNase	Ribonuclease
RT	Room temperature
S	Sulphur
SCCA	*Saccharomyces cerevisiae* catalase
SDS	Sodium dodecyl sulfate
sec	Second
SOD	Superoxide dismutase
SO_4^{2-}	Sulphate ion

*Sy*KatG	Catalase-peroxidase from *Synechocystis PCC 6803*
TAE	Tris-acetate-EDTA
TBE	Tris-borate-EDTA
TE	Tris-EDTA
TOF	Time of flight
TTC	Catalase from *Thermus thermophilus*
U	Units
UV	Ultraviolet
V	Volts
V_{max}	Maximum velocity
VSC	*Vibrio salmonicida* catalase
v/v	Volume per unit volume
w/v	Weight per unit volume
WT	Wild type
Zn	Zinc

1. GENERAL INTRODUCTION

1.1. Oxygen: a paradox for aerobic life

The earth's atmosphere in the earliest stages of biological evolution, about 3.5 billion years ago, was nearly devoid of oxygen, and therefore, the earliest cells were anaerobic. They oxidised organic compounds to CO_2, transferring electrons to SO_4^{2-} instead of O_2. With the rise of O_2-producing photosynthetic cyanobacteria, the earth's atmosphere progressively became richer in oxygen as they succeeded in linking photosynthetic electron flow from water through photosystems I and II to oxygen production in the oxygen evolving complex (Margit et al. 2009). This provided aerobic organisms an energetic advantage, leading to their predominance over their anaerobic counterparts in an oxygen rich environment. Continued elaboration of photosynthesis and cellular respiration ultimately led to the evolution of more complex multicellular organisms such as plants and animals (Campbell and Reese, 2005). Responding to evolutionary pressure some lineages of microorganisms gave rise to aerobes that obtained energy from the transfer of electrons to O_2 as the terminal electron acceptor. However these changes came at a price, because both the chemical and metabolic reduction of O_2 results in the production of highly toxic and reactive forms of oxygen which are inherently dangerous to an organism's existence.

This 'dark side' of oxygen relates directly to the fact that each oxygen atom has one unpaired electron in its outer valence shell, giving molecular oxygen two unpaired electrons. Thus, atomic oxygen is a free radical and molecular oxygen is a di-radical (Davies, 1995). The one electron reduction of molecular oxygen generates reactive intermediates and the reductive environment of the cellular milieu provides ample opportunities for oxygen to

undergo the unproductive and potentially dangerous univalent reductions shown below (Imlay, 1999).

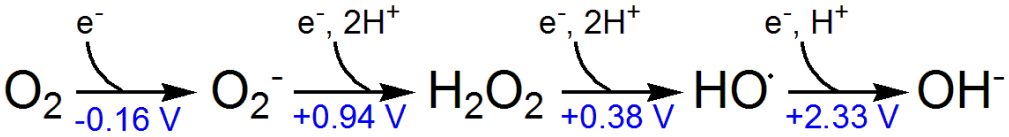

The values in blue are the standard reduction potentials for each of the reductions revealing the energetically favourable nature of all the reactions except the first, and even it involves a low enough energy barrier to be easily driven by many biologically relevant reactions. Thus, we have the oxygen paradox. Its reduction provides a great competitive advantage to organisms adapted to using it as a terminal electron acceptor, but its reduction generates highly reactive products that are damaging to the same organisms.

1.1.1. Oxidative stress

Oxygen is essential for most living organisms, with the exception of a rather small group of anaerobic bacteria and some heterotrophic organisms that are adapted to growth with or without oxygen. Aerobic organisms use molecular oxygen (O_2) for respiration or oxidation of nutrients to obtain energy in the form of ATP. However, the presence of oxygen in the cell leads to the production of reactive by-products of oxygen, such as hydrogen peroxide (H_2O_2), the superoxide anion ($O_2^{\bullet-}$), and the hydroxyl radical ($OH^{\bullet}$) commonly referred to as “reactive oxygen species” (ROS). When the generation of ROS is higher than the rate of their elimination, a state of oxidative stress is created. Recently, Jones redefined oxidative stress as “a disruption of redox signalling and control” bringing antioxidant enzymes into the picture (Jones, 2006). This definition makes the point that it is the accumulation of ROS in excess of the cell's defence capacity that is deleterious. Scientific

research has shown that oxidative stress directly or indirectly is the major cause of several diseases in both plants (apoptosis and necrosis) and humans (arthrosclerosis, diabetes, chronic degenerative diseases, muscular dystrophy, various genetic and nervous disorders like Trisomy 21 syndrome and amylotrophic lateral sclerosis cancer and aging) (Halliwell and Gutteridge, 1999).

1.1.2. Biology, Chemistry, and Fate of Reactive Oxygen Species

Aerobic organisms use molecular oxygen (O_2) to generate energy in the form of ATP by the process of oxidative phosphorylation where O_2 acts as a terminal electron acceptor and is reduced to water. In eukaryotic organisms oxidative phosphorylation takes place in mitochondria and in bacteria it occurs in the plasma membrane. Whereas the concerted tetravalent reduction of oxygen by the mitochondrial cytochrome oxidase to produce water (Reaction 1) is considered to be a relatively safe process;

$$O_2 + 4H^+ + 4e^- \rightarrow 2H_2O \qquad \text{Reaction 1}$$

the univalent reduction of oxygen to ROS by the uncontrolled electron transfer by several membrane-associated respiratory chain enzymes is more harmful (Cabiscol et.al. 2000). Experimental data indicate that, in *Escherichia coli*, the respiratory chain can account for as much as 87% of the total H_2O_2 production (Gonzalez and Demple, 1995), but prokaryotes are also often challenged by harsh environments giving rise to ROS from other sources as well (Figure 1.1).

In eukaryotes, ROS are generated by the enzymes especially in the kidney, where oxygen is used to metabolize many different compounds including amines, prostaglandins, purines, amino acids, etc. (Storey, 1996). ROS are also generated from the oxidation of small molecules (such as flavins, catecholmines, hydroquinones, etc.) by microsomal

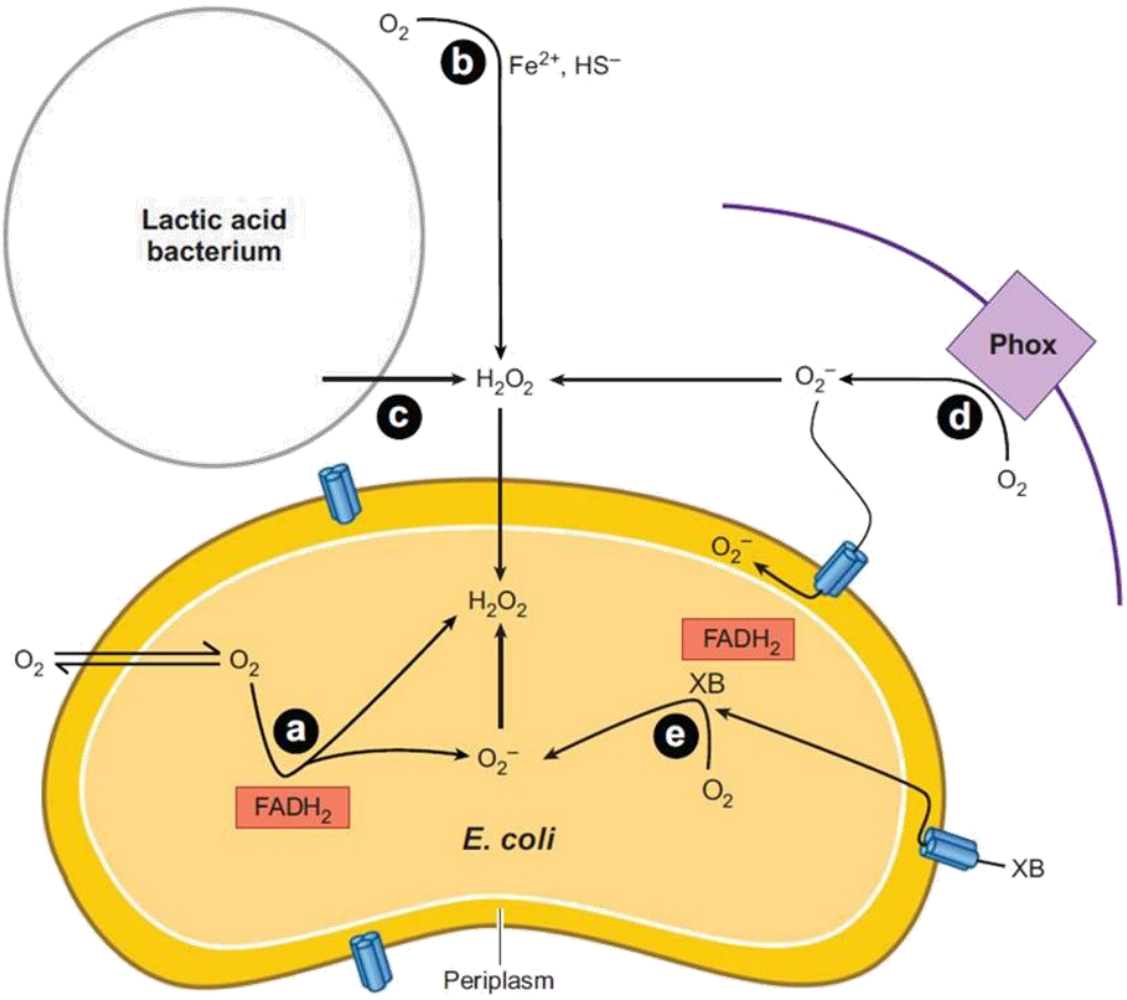

Figure 1.1. Some of the sources of oxidative stress in bacteria. **(a)** Intracellular enzyme autoxidation results in the production of both superoxide anion and hydrogen peroxide. **(b)** Environmental redox reactions produce hydrogen peroxide which being uncharged penetrates membranes. **(c)** H_2O_2 is released by competing microbes. **(d)** Phagosomal NADPH oxidase generates superoxide ion. **(e)** Redox-cycling xenobiotics (XB) including antibiotics also generate superoxide ion. (*Imlay, 2008*).

cytochromes P450 and b5, xanthine dehydrogenases, and monoamine oxidases, (Ding et al., 1997), oxidation of NADPH by NADPH oxidase, the oxidation of xanthine by xanthine oxidases, and by the leakage of electrons from the electron transport chain (Sayre et al., 2001). Much of the ROS damage is caused by hydroxyl radicals ($OH^{\bullet}$) generated from H_2O_2 via the Fenton reaction (reaction 2), involving iron or other divalent metal ions such as copper (Fenton, 1894).

$$Fe^{II} + H_2O_2 \rightarrow Fe^{III} + OH^{-} + OH^{\bullet} \qquad \text{Reaction 2}$$

The resulting Fe^{III} or Cu^{II} can be reduced by $O_2^{\bullet -}$ in the Haber-Weiss reaction (reaction 3) so that it is recycled for use in the Fenton reaction. Thus, the simultaneous presence of H_2O_2, $O_2^{\bullet -}$, and Fe^{II} is a dangerous source of $OH^{\bullet}$ formation (Smirnoff, 2005).

$$O_2^{\bullet -} + H_2O_2 \xrightarrow{Fe^{II}} O_2 + OH^{\bullet} + OH^{-} \qquad \text{Reaction 3}$$

Damage by the highly reactive hydroxyl radical is usually close to the site of its formation, and its influence increases substantially when the cells are defective in maintaining iron homeostasis (Figure 1.2) or in other situations such as X-irradiation generating the hydroxyl radical and UV irradiation generating various other radicals (Sies, 1997).

The biological targets for these highly reactive oxygen species include DNA, RNA, proteins, and lipids. In particular, the reaction of free radicals with polyunsaturated fatty acids in membranes leads to lipid peroxidation and a reduction in membrane fluidity, which can disrupt the properties of membrane bound proteins. Free radical reactions frequently amplify one another generating more radicals (lipid peroxides), which convert more polyunsaturated fatty acids to a variety of products (Lushchack, 2001). Increased production

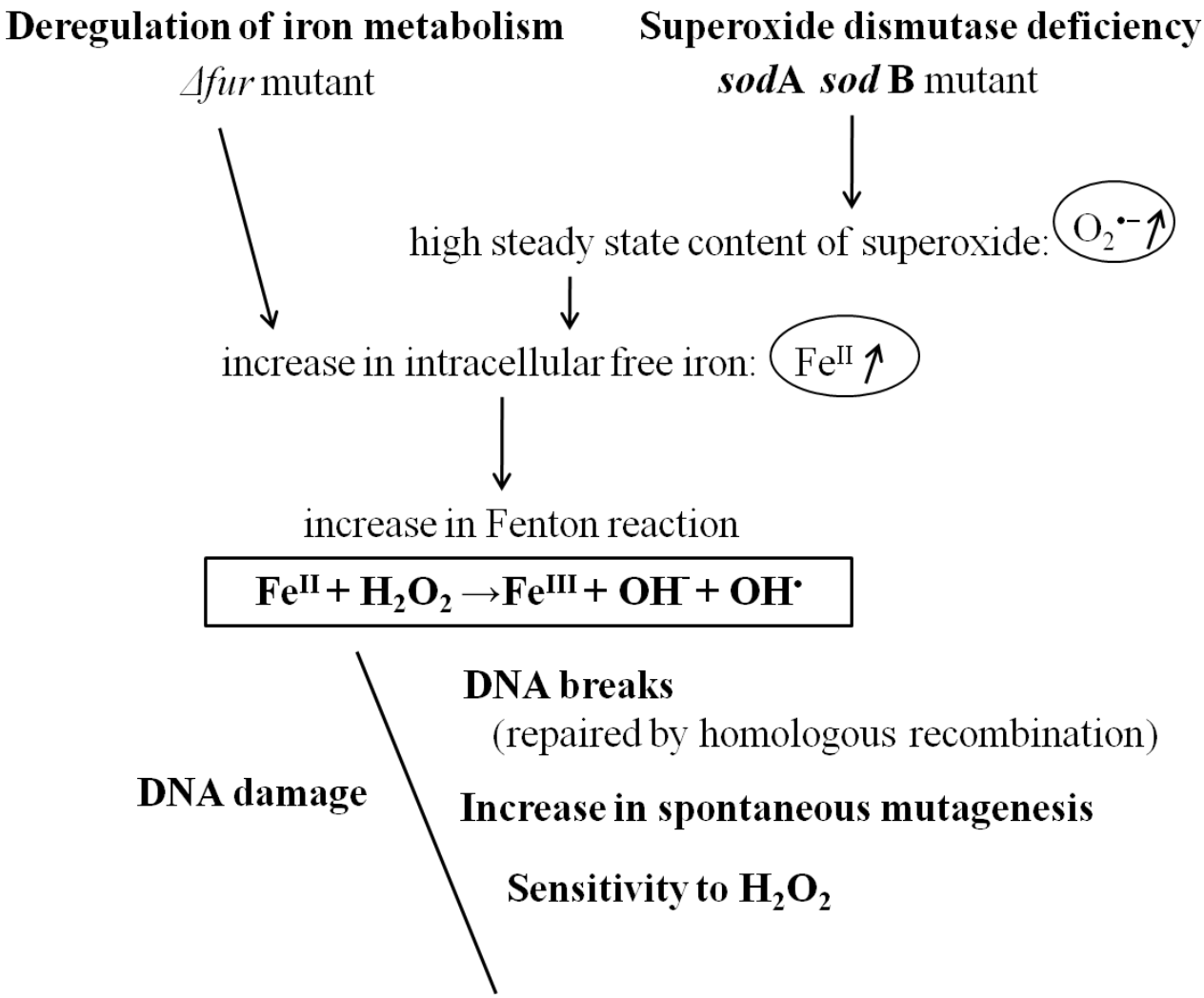

Figure 1.2. Similar effects of iron homeostasis deregulation and superoxide-mediated oxidative stress in *E.coli.* Fur protein usually modulates bacterial iron-responsive gene regulation and is responsible for iron homeostasis. Similar effects and coordination is likely to exist in other bacteria (prepared from Touati, 2000).

of perhydroxyl radicals leads to the formation of lipid hydroperoxides that produce a family of reactive alpha-beta unsaturated aldehydes including 4-HNE (4-hydroxynonenal), 4-ONE (4-oxo-2-nonenal), and acrolein (Sayre et al., 2006). Unlike reactive free radicals, these lipid peroxidation products are rather long lived and can therefore diffuse across membranes, allowing the reactive aldehyde-containing lipids to covalently modify proteins throughout the cell and relatively far away from the initial site of ROS formation. (Grimsrud et al., 2008).

ROS also attack DNA, producing chain breaks. In *E. coli*, as little as 1 µM intracellular H_2O_2 causes crippling levels of DNA damage. It attacks both the nitrogen bases and the sugar moieties producing single and double strand breaks in the backbone, adducts of base and sugar groups, and cross-links to other molecules, lesions that block replication (Sies, 1993 ; Sies and Menck, 1992). The spectrum of adducts in oxidized DNA in vitro and in vivo includes more than 20 known products, including damage to all four bases including thymine-tyrosine cross links (Dizdaroglu, 1992) and the production of 8-hydroxyguanine (8-oxoG) by hydroxyl radical (Candeias and Steenken, 1993). $O_2^{\cdot-}$ promotes DNA damage indirectly by releasing iron from damaged 4Fe-4S dehydratase clusters (Keyer and Imlay, 1996). In addition, ROS also reacts with proteins causing the modification of amino acids including the oxidation of cysteine, methionine, histidine, tyrosine, phenylalanine and tryptophan (Fucci et al., 1983; Stadtman, 1990; Smith et al., 1992; Stadtman, 1993). Excess of superoxide has been shown to release free iron from 4Fe-4S cluster-containing enzymes of the dehydratase-lyase family (such as aconitase, fumarase A and B, and isopropylmalate isomerase) that can then activate the Fenton reaction (Flint et al., 1993 and Jang and Imlay, 2006) thereby aggravating the damage. All these modifications are deleterious to the cell,

since they lead to loss of function of membranes and proteins and block DNA replication or cause mutations.

In fact, the effects of ROS are not all negative. There is increasing evidence for the involvement of ROS in redox signalling pathways which may contribute to normal cell function such as cell proliferation, differentiation, and migration in mammalian cells (Rhee, 2000 and 2006; Sundaresan, 1995). In addition, ROS act as an important component of both animal and plant defence responses against bacterial pathogens (Tenhaken et al., 1995; Nathan and Shiloh, 2000).

1.1.3. ROS defence systems and strategies

As oxygen levels in the atmosphere increased and ROS became more common, organisms had to evolve defense mechanisms to maintain ROS at non-harmful levels and to repair oxidative damage. Over time, an array of strategies for such protection arose that can be divided into three categories: (1) prevention of ROS generation; (2) free radical chain termination and detoxification of radicals by antioxidant enzymes and quenchers; and (3) repair of damaged products, including DNA and proteins. All three categories include both enzymatic and non-enzymatic components.

1.1.3a. Non-enzymatic defences

Some molecules are constitutively produced to maintain an intracellular reducing environment or to scavenge ROS. These include cofactors and small peptides such as NADPH and NADH, glutathione (GSH), and thioredoxins, β-carotene, ascorbic acid (Vitamin C), and α-tocopherol (Vitamin E) that scavenge reactive oxygen and nitrogen species. GSH is present at high concentrations in most bacteria which maintain a strong

reducing environment inside the cell, and its reduced form is maintained by glutathione reductase utilizing NADPH as electron donor (Cabiscol, 2000). GSH can act directly as an ROS scavenger or more importantly as a cofactor of enzymes involved in oxidative stress protection. Thioredoxins (Trxs) are another group of small ubiquitous proteins found in all living organisms. They are efficient thiol-disulphide reductants and together with the glutaredoxins are responsible for maintaining the cellular oxidative environment (Aslund et al., 1997). The available data suggest that thioredoxins are a very important part of the complex regulatory networks that control the bacterial oxidative stress response, and most likely, many additional physiological functions. Trxs also function as singlet oxygen quenchers and hydroxyl radical scavengers (Das and Das, 2000).

Vitamin C has also traditionally been regarded as a potent reducing agent and scavenger of free radicals in biological systems (Buettner and Jurkiewicz, 1996). The antioxidant property of Vitamin C is attributed to its mono-anionic form at physiological pH which allows it to undergo facile one electron oxidations generating the ascorbate free radical (AFR). Ascorbate has the capability to undergo one electron oxidations and this process generates ascorbate free radical (AFR). In reaction 4, $AscH^-$ represents ascorbate, $X^\bullet$ represents oxidizing species and $Asc^{\bullet-}$ represents AFR.

$$AscH^- + X^\bullet \rightarrow Asc^{\bullet-} + XH \qquad \text{Reaction 4}$$

Because AFR is relatively unreactive compared to all other reactive oxygen and nitrogen species including α-tocopherol and glutathione radical, ascorbate oxidation replaces potentially damaging radicals with the less reactive AFR (Duarte and Lunec, 2005). Vitamin E or α-tocopherol is a potent lipid-soluble antioxidant which functions as a peroxyl radical scavenger that maintains the integrity of long chain polyunsaturated fatty acids in the

membranes, which in turn maintains their bioactivity and preserves membrane characteristics and function (fluidity, phase separation, and lipid domains) (Traber and Atkinson 2007).

1.1.3b. Enzymatic defences

Enzymatic detoxification of ROS constitutes a major component of bacterial and eukaryotic oxidative stress defence systems and involves enzymes such as superoxide dismutases, catalases and peroxidases. Basal levels of these enzymes work in concert to remove endogenously produced ROS and keep their levels within physiologically safe limits. The primary superoxide removing enzymes or superoxide-dismutases are found in almost all aerobic organisms and in some anaerobic organisms. They catalyze the conversion of $O_2^{\bullet -}$ to O_2 and H_2O_2 (Reaction 5).

$$2O_2^{\bullet -} + 2H^+ \rightarrow H_2O_2 + O_2 \qquad \text{Reaction 5}$$

Three types of SOD, varying primarily in their metal cofactor, have been identified, the copper-zinc type (CuZnSOD), the manganese type (MnSOD), and the iron type (FeSOD), and all three are produced in *E.coli* (Niederhoffer et al., 1990; Compan and Touati, 1993; Benov and Fridovich, 1994).

Catalases are another group of protective enzymes that scavenge H_2O_2 by dismutating it to oxygen and water (Reaction 6). Thus, H_2O_2 produced by SOD, or any other source, is removed by catalases.

$$2H_2O_2 \rightarrow 2H_2O + O_2 \qquad \text{Reaction 6}$$

The importance of catalases as a major ROS scavenger is evident in the fact that almost all aerobic organisms from prokaryotes to eukaryotes produce one or more catalases. They are either constitutively expressed or induced in response to oxidative stress, either

directly to H_2O_2 levels or to the presence of other active oxygen species. Symbiotic and pathogenic organisms generally contain more catalase gene paralogues. For example, the soil-bacterium *Sinorhizobium meliloti* which makes symbiotic association with Medicago species produces two monofunctional catalases, KatA and KatC and a catalase-peroxidase KatG, but only KatA is induced upon exposure to H_2O_2 (Jamet et al., 2003). The genome of the filamentous fungus *Neurospora crassa* contains genes encoding three different monofunctional catalases, a catalase-peroxidase and several peroxidases (Galagan et al., 2003). Similarly, the phytopathogenic fungi *Aspergillus fumigatus* expresses two monofunctional catalases (one is present in the conidia and other in mycelia) and a catalase-peroxidase (in mycelia) (Paris et al., 2003). Contrary to the earlier suggestions, some obligate anaerobes have been shown to contain typical catalases, including strains of *Desulfovibrio*. *D. gigas* expresses catalase constitutively but it is not fully saturated with the prosthetic heme group (Dos Santos et al., 2000). The strict anaerobe *Methanobrevibacter arboriphilus* also exhibits catalase activity with maximum expression in stationary phase. The activity significantly increases upon addition of hemin in the growth medium, and the purified protein strongly resembles a monofunctional catalase (Shima et al., 2001). Enhanced expression of catalases is also observed in *Clostridium acetobutyricum* upon addition of hemin (Brioukhanov and Netrusov, 2004).

Yet another group of enzymes that utilizes H_2O_2 as substrate are the peroxidases, which are widespread in nature. Similar to catalases, peroxidases catalyze the degradation of H_2O_2 to water, but utilize a variety of intracellular organic molecules as electron donors in place of H_2O_2 (Reaction 7).

$$RH_2 + H_2O_2 \rightarrow R + 2H_2O \qquad \text{Reaction 7}$$

Alkyl hydroperoxidases, including AhpCF, a two-component NADH peroxidase of *E. coli* and other bacteria utilize H_2O_2 at a rate of 4×10^7 $M^{-1}sec^{-1}$ and act as potent scavengers of H_2O_2 (Parsonage et al., 2005). As a result of the combination of catalases and peroxidases, the steady state concentration of H_2O_2 does not exceed 20 nM despite being produced at the rate of 15 µM/s in aerobically growing *E. coli* (Seaver and Imlay, 2001).

In addition to this combination of non-enzymatic and enzymatic strategies, microbes employ several other strategies to control the production of ROS and/or their damage including controlling the levels of unincorporated iron (see page 3 and figure 1.2) and repairing damaged proteins and DNA. The primary control of iron homeostasis in most bacteria is mediated by the Fur protein (Andrews et al., 2003). Studies have shown that *fur* mutants exhibit high rates of mutagenesis and *fur recA* mutants, which are also defective in the repair of oxidatively damaged DNA, are non-viable in aerobic media (Touati et al., 1995). *fur* mutants have also been shown to be more susceptible to DNA damage by exogenous H_2O_2 (Keyer and Imlay, 1996). Thus, Fur protein plays an important role in protecting the cell generally and preventing DNA damage specifically. Most bacteria also produce an iron storage/binding protein called ferritin, which is strongly induced as a part of the OxyR and PerR systems in some H_2O_2 stressed bacteria (Rocha and Smith, 2004). Organisms also produce proteins that repair the oxidatively damaged iron-sulfur clusters of enzymes including YtfE and YggX in *E. coli* (Pomposiello et al., 2003; Justino et al., 2007). Increased expression of *ytfE* upon exposure to nitric oxide led to the conclusion that YtfE is critical for the repair of iron-sulfur clusters damaged by oxidative and nitrosative stress conditions, but the mechanism remains undefined (Justino et al., 2007).

DNA repair enzymes include the DNA glycosylases such as MutM (excises oxidized purines prior to replication), MutY (specifically corrects 8-oxoG:A base pairs), and MutT (hydrolyzes 8-oxodGTP to 8-oxodGMP) of the base excision repair (BER) pathway (Fowler and Schaaper, 1997) along with endonucleases III and IV. Endonuclease IV is the only component of the BER system that is induced in *E. coli* in response to oxidative stress (by the SoxRS regulator) (Chan and Weiss, 1987), but the remaining enzymes are constitutively expressed, presumably to cope with the DNA damage that is produced by endogenous H_2O_2.

1.2. Catalases

Catalases, also known as hydroperoxidases, have been studied for over a century. Catalase activity in the form of oxygen evolution was first noted by Thenard in 1811, but the cause of the activity remained unknown until 1901 when Lowe coined the term "catalase" and applied it to the protein responsible for the oxygen evolution. Twenty two years later Warburg (1923) demonstrated that the active site or center of catalase contains iron, and in 1936, Stern demonstrated that protophorphyrin IX was at the active center of catalases. Catalase functions to degrade hydrogen peroxide into water and oxygen (Reaction 6) and this very simple reaction has become highly important for aerobic organisms both to remove excessive H_2O_2 and to maintain H_2O_2 levels appropriate for its role in signalling pathways (Veal et al., 2007). The catalatic mechanism will be discussed later in appropriate sections.

Three protein families, unrelated on the basis of sequence, structure and active site exhibit significant catalase activities. Two of the protein families are heme enzymes: monofunctional catalases and bifunctional catalase-peroxidases. Monofunctional catalases comprise the most abundant group spread among Eubacteria, Archaebacteria, Protista, Fungi, Plantae, and Animalia, whereas catalase-peroxidases are less widespread, and are not

found in plants and animals. Non-heme manganese-containing catalases found only in bacteria comprise the third family of catalases (Klotz and Loewen, 2003; Zamocky et al., 2008).

Additionally, several heme-containing proteins, including most peroxidases, metmyoglobin, and methemoglobin have been observed to exhibit a low level of catalatic activity (Nicholls et al., 2001). Among these enzymes, multifunctional chloroperoxidase from the ascomycete *Caldariomyces fumago* exhibits the highest catalase activity (Thomas et al., 1970).

1.2.1. Catalase expression and regulation in response to oxidative stress

Genetic responses to oxidative stress occur in all aerobic organisms involving transcriptional modulators that sense oxidative stress and activate regulons of related genes. The mechanism of regulation depends on the specific signal but may occur at the level of transcription, translation, protein activity, or targeted proteolysis. Regulation of oxidative stress enzymes in response to H_2O_2 have been extensively studied in bacteria such as *Escherichia coli* (Loewen, 1985; Demple, 1991; Hengge-Aronis R, 2000; Manchado et al., 2000; Zheng et al., 2001) and *Bacillus subtilis* (Chen et al., 1995; Helmann et al., 2003), and in fungi *Saccharomyces cerevisiae* (Jamieson et al., 1994; Godon et al., 1998; Cyrne et al., 2003; Molina-Navarro et al., 2008)

Regarding the physiology of catalase expression and its control in bacteria, *Escherichia coli* is well studied. The earliest studies on catalase gene expression and regulation in *E.coli* were initiated in early 1980s and have been the subject of several reviews (Loewen, 1985; Mulvey et al., 1990; Loewen et al., 1998). *E. coli* cells express several defense systems against ROS, of which the primary ones are mediated by the

transcription factor OxyR and the sigma factor RpoS (σ^S). *E. coli* OxyR was the first peroxide-sensing transcription factor to be well characterized (Zheng et al., 1998; Storz and Zheng, 2000). The initial reaction of OxyR with H_2O_2 oxidizes Cys-199 (Zheng et al., 1998 and Kiley and Storz, 2004) which then reacts with another conserved cysteine, Cys-208, to form an intramolecular disulphide bond (Choi et al., 2001). Whereas reduced OxyR binds only to its own promoter thereby autoregulating its own expression, a conformational change caused by disulfide bond formation allows it to bind to promoters of the OxyR regulon, activating transcription. OxyR oxidation is a very rapid and sensitive process which occurs within 30 seconds with an intracellular H_2O_2 concentration as low as 0.1 µM (Toledano et al., 2004). The oxidized OxyR is reduced with a half-time of 5 min (Aslund et al., 1999) by glutaredoxin 1 (GrxA) using glutathione as electron source (Zheng et al., 1998). OxyR controls the genes encoding the catalase-peroxidase, KatG or HPI (*katG*), glutathione reductase (*gorA*), glutaredoxin 1 (*grxA*), alkyl hydroperoxide reductase (*ahpCF*) and a protective nonspecific DNA-binding protein Dps (Demple, 1991; Lushchak, 2001). For example, KatG levels are 100-fold higher when OxyR is oxidized (Storz et al., 1990).

Unlike HPI, HPII (KatE) is not induced by H_2O_2 and the levels of HPII in an *oxyR* mutant are similar to those in the wild type strain indicating that *katE* is not a member of *oxyR* regulon (Schellhorn and Hassan, 1988). Levels of HPII are about 10-20 times higher in stationary phase cells than in exponentially growing cultures. KatF (renamed RpoS or σ^S) was shown to control the levels of HPII in stationary phase (Loewen and Triggs, 1984; Mulvey et al., 1990), leading to the conclusion that HPII is controlled as a part of the RpoS regulon (Loewen and Hengge-Aronis, 1994). A comprehensive microarray-based transcriptome analysis has shown that almost 500 genes (about 10% of the *E.coli* genome)

are directly or indirectly regulated by RpoS in response to environmental stress or during entry into stationary phase (Lacour and Landini, 2004; Patten et al., 2004; Weber et al., 2005). RpoS itself is regulated at the level of transcription, translation, protein stability and protease activity. Numerous factors, including small molecules, small regulatory RNAs and regulatory proteins have been identified that play a role in the complex regulation of RpoS and many more may be identified in the future. The low levels of σ^s found in exponentially growing cells (Lange and Hengge-Aronis, 1994) are attributed to the rapid proteolytic degradation of RpoS by the ATP dependent protease ClpXP after recognition by RssB (Muffler et al., 1996; Schweder et al., 1996). RssB binds directly to σ^s and targets it to ClpXP (Zhou et al., 2001; Klauck et al., 2001). Bougdour and Gottesman recently demonstrated the involvement of yet another small protein IraP with a role in the inhibition of σ^s proteolysis through direct interaction with RssB under phosphate starvation and stationary-phase (Bougdour et al., 2006). Subsequently, they showed that the expression of *iraP* mRNA is positively regulated by ppGpp under phosphate starvation (Bougdour and Gottesman, 2007) thereby providing a clear explanation for earlier observations (Gentry et al., 1993; Spira and Yagil, 1998).

It has been shown in *Escherichia coli* and *Salmonella enterica* that growth in stationary phase in rich medium such as Luria-Bertani, leads to a dramatic increase of >30 fold in RpoS abundance (Mulvey et al., 1990; Gentry et al., 1993; Hirsch and Elliott, 2002). This is mediated by Fis, a DNA-binding protein present at high levels in exponential phase, but not in stationary phase, that binds to a site in the major *rpo*S promoter causing repression of transcription (Hirsch and Elliott, 2005). Another level of control is evident in the upregulation of *rpo*S expression by polyamines, including putrescine, spermidine and

spermine, but the mechanism remains unclear (Tkachenko et al., 2001; Jung and Kim, 2003).

1.3. Heme-containing monofunctional catalases

Monofunctional heme-containing catalases are the largest group of H_2O_2 degrading enzymes. The catalatic reaction pathway in this class of catalase involves two distinct stages. In the first stage, the resting enzyme is oxidized by one molecule of H_2O_2 to form an oxyferryl intermediate called Compound I (Cpd I) in which one oxidation equivalent is removed from the iron becoming Fe^{IV} and one from the porphyrin ring generating a porphyrin cation radical (Reaction 8). During this step, the H_2O_2 is cleaved with one oxygen being reduced to water and the second becoming coordinated to the iron. In the second stage, Cpd I is reduced back to the resting state by a second H_2O_2 molecule releasing H_2O and O_2 as products (Reaction 9). In this case, the axial oxygen (bound to iron of Cpd I) atom is reduced to water and both oxygens of the O_2 are derived from the reducing H_2O_2 (Alfonso et al. 2007).

$$\text{Por-Fe}^{III} + H_2O_2 \rightarrow \text{Por}^{\bullet+}\text{Fe}^{IV}\text{=O} + H_2O \qquad \text{Reaction 8}$$

$$\text{Por}^{\bullet+}\text{Fe}^{IV}\text{=O} + H_2O_2 \rightarrow \text{Por-Fe}^{III} + H_2O + O_2 \qquad \text{Reaction 9}$$

Despite having a common two-stage reaction mechanism, monofunctional catalases from different organisms can exhibit profoundly different reactivities (Switala and Loewen, 2002). The reasons for these great variations in activity are not fully understood, but may, at least in part, arise from the delocalization of the porphyrin radical to other locations in the protein generating Cpd I* species ($\text{Por-Fe}^{IV}\text{=O/protein}^{\bullet}$). In some catalases, especially small subunit catalases, Cpd I may undergo one-electron reduction under low H_2O_2 concentration

and in the presence of external one-electron donors to form high-valent inactive intermediate Compound II (Cpd II) (Figure 1.3), which may exist in two different protonation states (Reaction 10) (Nicholls et al., 2001; Rovira et al., 2005). Cpd II may also be generated through one-electron quenching of the protein radical from Cpd I*, but evidence is limited.

$$Por^{\bullet+}Fe^{IV}=O + AH \rightarrow Por\text{-}Fe^{IV}\text{-}OH + A^{\bullet} \qquad \text{Reaction 10}$$

Cpd II differs from Cpd I* in having had the porphyrin or protein radical quenched in a one electron transfer and the resulting oxyferryl species (Fe^{IV}-OH) is reduced only very slowly back to the resting state (Reaction 11). Consistent with this reaction model, subtle differences have been noted among the crystal structures of the oxyferryl derivatives of different catalases. For example, Cpd I of PVC appears to contain predominantly an oxoferryl $Por^{\bullet+}Fe^{IV}=O$ species with a shorter Fe-O bond length than that observed in the presumed Por-Fe^{IV}-OH $AA^{\bullet+}$ Cpd I* of HPC (Alfonso et al. 2007). Also Cpd I of CcP, MLC and BpKatG have longer than expected Fe-O bond lengths (~1.9 Å) consistent with a hydroxoferryl group similar to that characterized in Cpd II of myoglobin. These differences in the nature of intermediates might be responsible for varying kinetic properties among catalases.

$$Por\text{-}Fe^{IV}\text{-}OH + AH \rightarrow Por\text{-}Fe^{III} + H_2O + A^{\bullet} \qquad \text{Reaction 11}$$

In mammalian and yeast catalases peroxidatic reactions (Reaction 12) have been observed at low H_2O_2 concentrations, but the catalatic reaction predominates at higher H_2O_2 concentrations. (Vetrano et al., 2005; Zamocky and Koller, 1999).

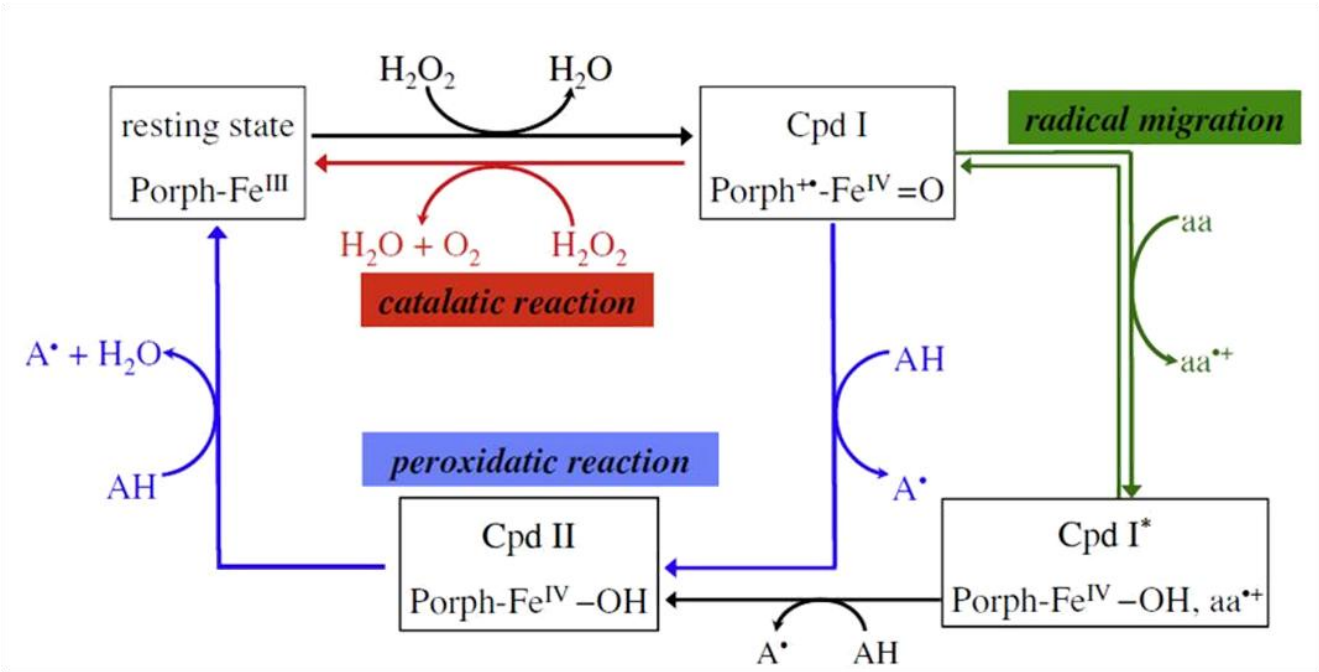

Figure 1.3. Reaction scheme showing the reaction intermediates formed during catalytic cycle of monofunctional catalases, peroxidases and catalase-peroxidases. The branch shown in green is well characterized in peroxidases and catalase-peroxidases, but still unconfirmed in monofunctional catalases.

$$Por^{\bullet+}Fe^{IV}=O + CH_3CH_2OH \rightarrow Por\text{-}Fe^{III} + CH_3CHO + H_2O \qquad \text{Reaction 12}$$

1.3.1. Distribution and Phylogeny of monofunctional catalases

Analysis of prokaryotic and eukaryotic genomes reveals that genes coding for monofunctional heme-containing catalases represent the largest group of H_2O_2-degrading enzymes. Currently, 943 DNA sequences contain this typical motif (Zamocky et al., 2008). PeroxiBase presently contains > 290 completed protein sequences of monofunctional catalases.

First attempts to classify the various enzymes with significant catalytic activity were made in 1989 by Goldberg and Hochman, who divided catalases into 3 subgroups: typical, atypical and catalase-peroxidases. With the ever increasing number of complete nucleotide and protein sequences, distinct homologies were detected, which led to several updated phylogenetic classification of catalases (von Ossowski et al., 1993, Klotz et al., 1997 and Klotz and Loewen, 2003). The most recent analysis by Klotz and Loewen (2003) confirmed the existence of three main clades that were segregated rather early in the evolution of this gene family through at least two gene-duplication events (Loewen, 2003). Clade 1 contains small subunit (55-69 kDa) catalases of bacterial, algal and plant origins with heme *b* as the cofactor. Clade 2 contains large subunit (75-84 kDa) catalases of eubacterial, archaebacterial and fungal origin with heme *d* as cofactor. The large subunit enzymes contain the basic small subunit core with extended N-terminal and C-terminal domains. Clade 3 also contains small subunit catalases of bacterial, archaebacterial, fungal, protista, plant and animal origins with heme *b* as cofactor. A sub-group of this clade can bind NADPH as a second redox-active cofactor, the role of which will be discussed below. Many bacteria possessing

catalase gene paralogues of the first two clades also have a representative in this clade (Zamocky et al., 2008).

1.3.2. Kinetic and biochemical properties

Many catalases from different organisms have been purified and characterized and shown to exhibit a wide range of biochemical and kinetic properties (Nadler et al., 1986; Nicholls et al., 2001). Recent comparison of 16 common catalases from different organisms, including both small and large subunit enzymes, revealed great divergence in properties within the catalase family (Switala and Loewen 2002). All catalases have an absorbance spectrum with a characteristic strong band at ~407 nm, the Soret band, arising from the heme moiety. The ratio of A_{407} to A_{280} or R_z (Reinheitszahl) value varies among catalases depending on the heme type and aromatic amino acid content and provides a measure of enzyme purity. Catalases also typically suffer irreversible inhibition following treatment with 3-amino-1,2,4-triazol. Catalases do not follow Michaelis-Menten kinetics except at very low substrate concentrations, and different enzymes are affected differently at higher substrate concentrations. Small subunit catalases do exhibit Michaelis-Menten-like dependence of velocity on H_2O_2 concentrations below 200 mM, but begin to suffer inactivation above 300-500 mM concentrations (Chelikani et al. 2004). On the other hand, large subunit catalases are relatively insensitive to the damaging effects of H_2O_2 at concentrations up to 3 M for *E. coli* KatE and 5 M for *Aspergillus niger* KatA, and they exceed the predicted Michaelis-Menten V_{max}. The observed k_{cat} values range from 54000 sec^{-1} (*Pseudomonas aeruginosa* KatB) to 833,000 sec^{-1} (*Proteus mirabilis*) and the $[H_2O_2]$ at $V_{max}/2$ ranges from 38-599 mM over the pH range of 4.0 to 9.0. Large subunit catalases exhibit high resistance to both thermal denaturation and proteolysis compared even to small

subunit catalases. For example, *E. coli* KatE retains activity to over 80 °C and inactivation occurs with a T_m of 83 °C compared to 56 °C for BLC. Proteolysis resistance was evident in the retention of activity even after treatement with a 1:1 ratio of proteinase K for 16 hr at 37 °C (Chelikani et al., 2005). These two features, (1) enhanced resistance to thermal denaturation and (2) proteolytic cleavage were initially attributed to the interweaving of the 80 N-terminal residues of one subunit through a loop on an adjacent subunit (Chelikani et al., 2003). However removal of 75 N-terminal residues did not significantly reduce the thermal stability of the enzyme whereas removal of the 150 C-terminal domain lowered the T_m for loss of activity by 25 °C (Chelikani et al., 2005), suggesting that the C-terminal domain in fact plays a more important role than the N-terminal domain in enzyme stability. Catalases generally are sensitive to many ligands that bind in the heme cavity including cyanide, azide, hydroxylamine, aminotriazol and a variety of sulfhydryl reagents, although the sensitivity varies considerably.

1.3.3. Structural and functional properties of monofunctional catalases

The crystal structures of 14 monofunctional catalase have been determined, including BLC (Fita and Rossmann, 1985), PVC (Vainshtein et al., 1986), MLC (Murshudov et al., 1992), PMC (Gouet et al., 1995), HPII (Bravo et al., 1997), SCC-A (Mate et al., 1999), HEC (Putnam et al., 2000), CatF (Carpena et al., 2003), Cat-1 (Diaz et al., 2004), EFC (Hakansson et al., 2004), HPC (Alfonso-Prieto et al., 2007), EKTA (Hara et al., 2007), VSC (Riise et al., 2007), and Cat-3 (Diaz etal., 2009) (Table 1.1.). All known monofunctional catalases are homotetrameric enzymes. Although some important differences in the primary structure are found among them, the 3D structure appears well conserved. Each subunit has four distinct structural regions: the N-terminal/amino-terminal arm, an antiparallel eight-

stranded β-barrel, the connecting domain, sometimes referred as ‘wrapping domain’ and the α-helical domain (Figure 1.4 A). Residues in the amino-terminal arm form a "hook" that feeds through a loop in the wrapping domain of an adjacent subunit to form an interwoven structure (Bravo et al., 1997). A portion of the amino terminus interacts with the third subunit partially covering each other’s heme pocket (Figure 1.4 C). The amino acid residues in the antiparallel beta barrel form a sheet that is part of the heme pocket and the residues are important for catalysis. The wrapping loop consists of many conserved proline residues including P432, P436, P439, and P462 (HPII numbering) and are probably important for the interaction between subunits. Two of the four α-helical domains (α10 and α12) build the site for NADPH binding in small subunit clade 3 catalases. The large subunit catalases possess an extra C-terminal domain of about 150 residues, called the flavodoxin-like domain according to its fold (Bravo et al. 1995). The β-barrel, the wrapping loop, and the α-helical domain are almost identical in PVC, HPII, CAT-1, and CAT-3 and the major differences are observed in the N-terminal end and in the C-terminal domain (Diaz et al., 2009). HPII contains an extended N-terminal region of about 70 residues, both of which seem to contribute to the increased resistance to thermal denaturation and proteolysis. It is tempting to speculate about a mechanistic connection between the increased size of these large catalases and their functional peculiarities, including the conversion of heme *b* to *d*, the absence of bound NADPH and the low or even no tendency towards compound II formation (Loewen, 1997).

A single subunit of a tetrameric small subunit catalase shows a globular structure carrying an extended amino terminal arm, most of which is buried between neighbouring subunits (Figure 1.5). The central core structure of the subunit is formed by an 8-stranded β-

barrel domain of about 250 residues. According to sequence alignments this domain is nearly identical in length in all species, and clearly is the most conserved part of the enzyme. This domain also bears many catalytically and structurally important residues in a characteristic three-dimensional organization. One part of the barrel is oriented towards the surface allowing intersubunit contacts, whereas the internal parts harbour several essential amino acid residues including His74, Ser113, Asn147 and Tyr357 (BLC numbering). All these residues are found to be conserved among catalases. In HPII the equivalent residues are His128, Ser167, Asn201 and Tyr415 (Figure 1.4 B) (Bravo et al., 1995). Whereas His128 has been implicated as an essential residue for catalysis, Asn201 is not absolutely required for catalysis but is still important in facilitating the reaction. The importance of the distal side His128 and Asn201 has recently been assessed using X-ray crystallographic data and *ab initio* molecular dynamics (MD) simulation techniques leading to the conclusion that the conformational changes of histidine during the reaction facilitate proton transfer from the substrate to the heme cofactor. The movement of asparagine towards the main channel provides space to accommodate the oxygen released during catalysis (Vidossich et al., 2010). In all heme containing monofunctional catalases, a tyrosine (Tyr415 in HPII) on the proximal side of the heme occupies the fifth coordination site on the heme iron where it modulates heme iron reactivity and stabilizes higher oxidation states (Visser, 2006). Two channels are clearly distinguishable leading from the surface to the distal side of the heme pocket (Bravo et al., 1999). The main channel, approaching the heme distal side pocket perpendicular to the plane of the heme is approximately 35 Å in length and is considered to be the primary entry route for substrate H_2O_2. In small subunit catalases, the main channel

Table 1.1. List of known 3D structures of monofunctional heme catalases, bifunctional catalase-peroxidases, and non-heme catalases (as of November 2010).

Enzyme source	Type	Cofactor	PDB code	Reference
Monofunctional heme catalases				
Bovine liver	Small subunit clade 3	heme *b*	8CAT, 4BLC	Fita et al., 1986; Ko et al., 1999
Penicillium vitale	Large subunit clade 2	heme *d*	4CAT	Vainshtein et al., 1986
Micrococcus lysodeikticus	Small subunit clade 3	heme *b*	1GWE, 1GWF	Murshudov et al., 1982, 2002
Proteus mirabilis	Small subunit clade 3	heme *b*	1M85	Gouet et al., 1995
Escherichia coli	Large subunit clade 2	heme *d*	1IPH, 1GGE	Bravo et al., 1995, 1999
Saccharomyces cerevisiae	Small subunit clade 3	heme *b*	1A4E	Mate et al., 1999
Human erythrocyte	Small subunit clade 3	heme *b*	1DGB	Putnam et al., 2000
Pseudomonas syringae	Small subunit clade 1	heme *b*	1M7S	Carpena et al., 2003
Neurospora crassa	Large subunit clade 2	heme *d*	1SY7	Diaz et al., 2004
Neurospora crassa	Large subunit clade 2	heme *b*	3EJ6	Diaz et al., 2004
Enterobacter faecalis	Small subunit clade 3	heme *b*	1SI8	Hakansson et al., 2004
Helicobacter pylori	Small subunit clade 3	heme *b*	1QWL	Loewen et al., 2004
Exiguobacterium oxidotolerance	Small subunit clade 1	heme *b*	2J2M	Hara et al., 2007
Vibrio salmonicida	Small subunit clade 3	heme *b*	2ISA	Riise et al., 2007
Biofunctional catalase-peroxidases				
Haloarcula marismortui	Archaebacterial KatG	heme *b*	1ITK	Yamada et al., 2002
Synechococcus PCC 7942	Eubacterial KatG	heme *b*	1UB2	Wada et al., 2002
Burkholderia pseudomallei	Eubacterial KatG	heme *b*	1MWV	Carpena et al., 2003
Mycobacterium tuberculosis	Eubacterial KatG	heme *b*	1SJ2	Bertrand et al., 2004
Escherichia coli	Eubacterial KatG	heme *b*	1U2K	Carpena et al., 2004
Non-heme / Mn Catalases				
Thermus thermophilus	clade 1	di-manganese	2CWL, 2V8U	Antonyuk et al., 2000
Lactobacillus plantarum	clade 3	di-manganese	1JKU	Barynin et al., 2001

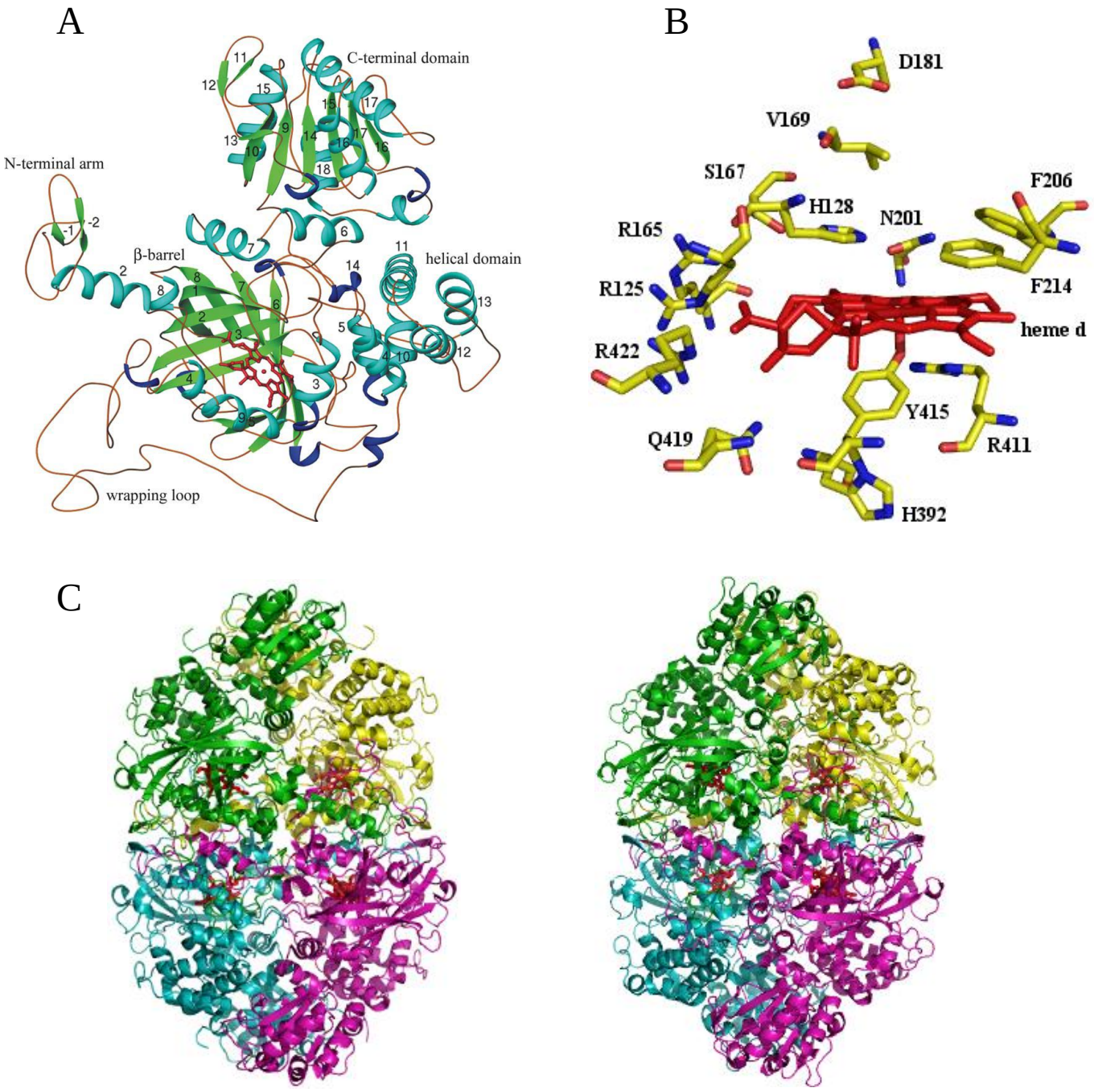

Figure 1.4. Cartoon representation of the structure of large subunit catalases. Panel A: single subunit showing secondary structures. Panel B: residues in the heme pocket and in the main substrate access channel. Panel C: on the left is the *N. crassa* CAT-3 tetramer and on the right is the *E. coli* HPII tetramer. Subunits are color coded. Hemes are represented by red sticks.

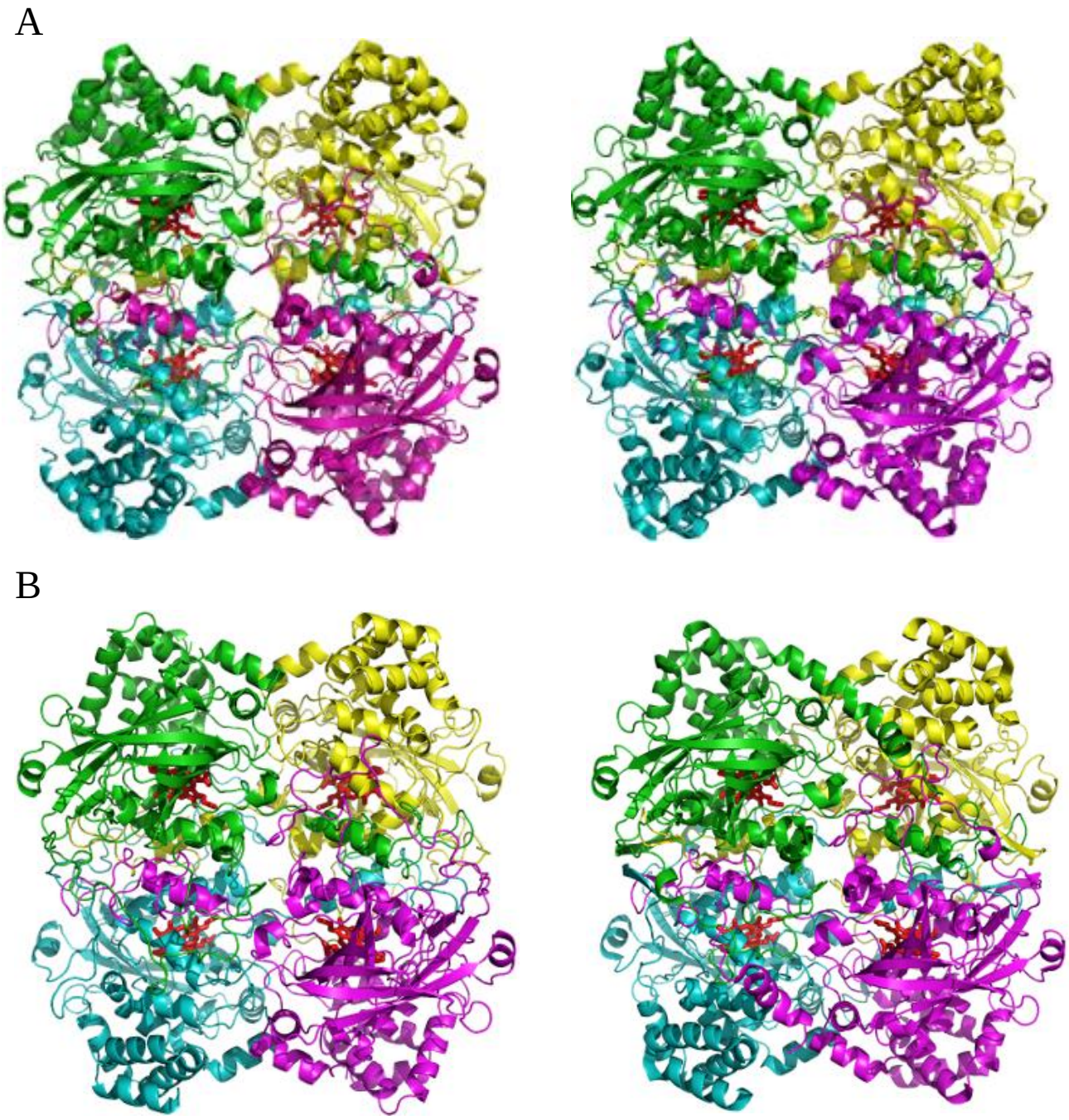

Figure 1.5. Cartoon representation of the small subunit catalase tetramers. Panel (A) on the left is the catalase from *Pseudomonas syringae* and on the right is from *Vibrio salmonicida*, both clade 1 catalase. Panel (B) on the left is the catalase from *Saccharomyces cereviseae* and on the right is the catalase from Human erythrocyte. The four hemes are represented by red sticks.

has a funnel shape that varies somewhat among the different catalases depending on the residues along its surface. Within the heme cavity the key catalytic residues include a His and an Asn (128 and 201 respectively in KatE). The incoming H_2O_2 forms a hydrogen bond with the His, 4 Å above the heme, and one oxygen associates with the heme iron. As the OH bond stretches, the proton is transferred from the oxygen attached to the iron to the non-associated oxygen producing water and Cpd I (Fita and Rossmann, 1985). The role of the conserved distal Asn201 is to stabilize and polarize the peroxide. During the reduction of Cpd I back to resting state (Reaction 9), the second H_2O_2 forms hydrogen bonds with Fe^{IV}=O and His128. This allows the transfer of one hydrogen atom and two electrons from H_2O_2 to the oxyferryl species and a second proton to the imidazole, giving rise to molecular oxygen. Conformational changes in the histidine facilitate electron transfer and product formation (Alfonso-Prieto et al., 2009 and Vidossich et al., 2010).

Subtle differences have been observed in the architecture of the channels among the small subunit catalases. For example, the lower part of the channel from the heme up to Asp109 is narrower by 0.5-1 Å than those of other enzymes because of the small shift in the locations of Phe134 and Phe145 and the presence of Ile146 in place of a Val present in many other catalases. Above Asp109, the HPC channel opens into a cavity whereas BLC, PMC, HEC and CatF channels become progressively larger with a funnel shape, the CATA channel forms a small cavity and the MLC channel remains narrow (Loewen et al., 2004). The conserved aspartate in the channel (Asp109 in HPC or 181 in KatE) enhances the catalatic reaction >10-fold, a property ascribed to its involvement in the generation of an electrical potential field in combination with the positively charged heme iron. The electrical dipoles of water and H_2O_2 are aligned in the potential field placing the substrate in an

optimal orientation for interaction with the active site residues upon entry into the heme cavity (Chelikani et al., 2003).

A second or minor channel approaches the heme active site laterally, beginning on the surface near the NADPH binding pocket. In those catalases that bind NADPH, the channel is blocked, but in all other enzymes, including KatE, the channel can potentially be used to access the heme pocket either for substrate entry or product exhaust. A third channel leading from the heme to the central cavity, the central channel, has been noted in the structures of large subunit catalases (Bravo et al., 1997 and 1999; Diaz et al., 2004). Although the main channel could in theory serve both as an entry and exhaust channel, increased catalytic efficiency might be realized from using one channel for substrate entry and a second for product exhaust. The only experimental evidence that the alternate channels play any role is found in KatE where opening the lateral channel by removing a Glu-Arg bridge enhanced enzyme activity (Sevinc et al., 1999). Similar evidence does not exist for the central channel.

The crystal structures of various catalases have revealed a number of unusual modifications, particularly in the large subunit enzymes, KatE from *E. coli* and Cat-1 from *N. crassa*. The side chain of the fifth ligand tyrosine is covalently cross linked to an imidazole in KatE (His392-Tyr415, Bravo et al., 1997) and a sulfhydryl group in Cat-1 (Cys356-Tyr379, Diaz et al., 2004). Conjecture about the role of these modifications have included involvement in the self-catalyzed conversion of heme *b* to heme *d* (Bravo et al., 1997 and 1999) and prevention of the one electron reduction of Cpd I to Cpd II to make the enzyme more resistant to substrate inactivation (Diaz et al., 2004 and 2009). Two other large

subunit catalases PVC and *N. crassa* Cat-3 do not contain this modification, but a comparision of their properties with either KatE or Cat-1 have not been reported.

1.3.4. Heme type and orientations in heme catalases

The four heme groups are deeply buried within the core structure of the enzyme, at least 20Å apart from the protein surface (Figure 1.4 and 1.5). The heme pocket is defined by residues from the β-barrel (distal side and along the edges of pyrrole rings I, II and III), from the domain connection (proximal side) and from the N-terminal arm of the R-related subunit (lining the edges of pyrrole rings I and IV) (Zamocky and Koller 1999), and is well conserved on both distal and proximal sides. For example, His74, Ser113, Asn147, Arg353 and Tyr357 in BLC can be equated with His128, Ser167, Asn201, Arg411 and Tyr415 in HPII (Figure 1.4 B). All of the small subunit clade 3 catalases have heme *b* as the cofactor, whereas the large subunit catalases HPII, PVC, and CAT-1 have heme *d* (Figure 1.6 A). Conversion of heme *b* to heme *d* involves oxidation of carbons 12 and 13 along with formation of a spirolactone on C13. The modifications cause characteristic changes to the absorbance spectrum in the charge transfer region including the appearance of a strong band at 590 nm (Murshudov et al. 1996). An autocatalytic mechanism involving Cpd I was proposed for the conversion in HPII and PVC, whereas in Cat1 the involvement of singlet oxygen has been proposed (Diaz et al., 2004). In contrast, CAT-3, also a large subunit catalase, contains heme *b* (Diaz et al., 2009). Subtle differences in the orientation of conserved Ser414, Gln419, and Arg422 (HPII numbering) among these four large subunit catalases has also been implicated in regulating the heme modification and presence or absence of the modification to the tyrosine (Diaz et al., 2009).

Two heme orientations with respect to conserved His128 have been observed among catalases. In small subunit clade 3 catalases the heme is oriented with the active site His located above ring III, whereas in the large subunit clade 2 catalases, the heme is flipped 180° resulting in the active site His being located over ring IV (Figure 1.6 B) (Carpena et al., 2003). A similar orientation has been observed in CatF, a clade 1 catalase, which suggests that, the 'normal' and, in view of probable evolutionary development, original orientation of heme in catalases is His IV.

1.3.5. Role of NADPH binding in catalases

A number of clade 3 catalases bind NADPH, either very tightly as in BLC, HEC, and PMC or with lower affinity as in MLC or CATA. Tightest binding is reported for BLC, HEC and PMC with a K_d of 10 nM (Kirkman et al. 1987), whereas the binding is much weaker in CATA with a K_d of 2 µM (Herzog et al. 1997). On the other hand, NADPH does not bind to clade 1 catalases, for example CatF (Carpena et al., 2003), or to the large subunit clade 2 enzymes, PVC, HPII, and Cat-1, where the putative binding site deviates significantly from those in clade 3 enzymes. In the enzymes that bind NADPH the binding site structures are highly conserved. Signature residues for NADPH binding in BLC are His193, Arg202, Val301, and His304. The only clade 3 catalase so far characterised that does not bind NADPH is *Helicobacter pylori* (HPC) where the equivalent four residues are Tyr175, Arg184, Ile283, and Thr286 (Loewen et al., 2004). The inability of the large subunit catalases to bind NADPH has been attributed to their extended C-terminal region and the absence of signature amino acid residues forming the putative NADPH binding pockets (Sevinc et al., 1999). The NADPH binding cavity of catalases is close to the enzyme surface,

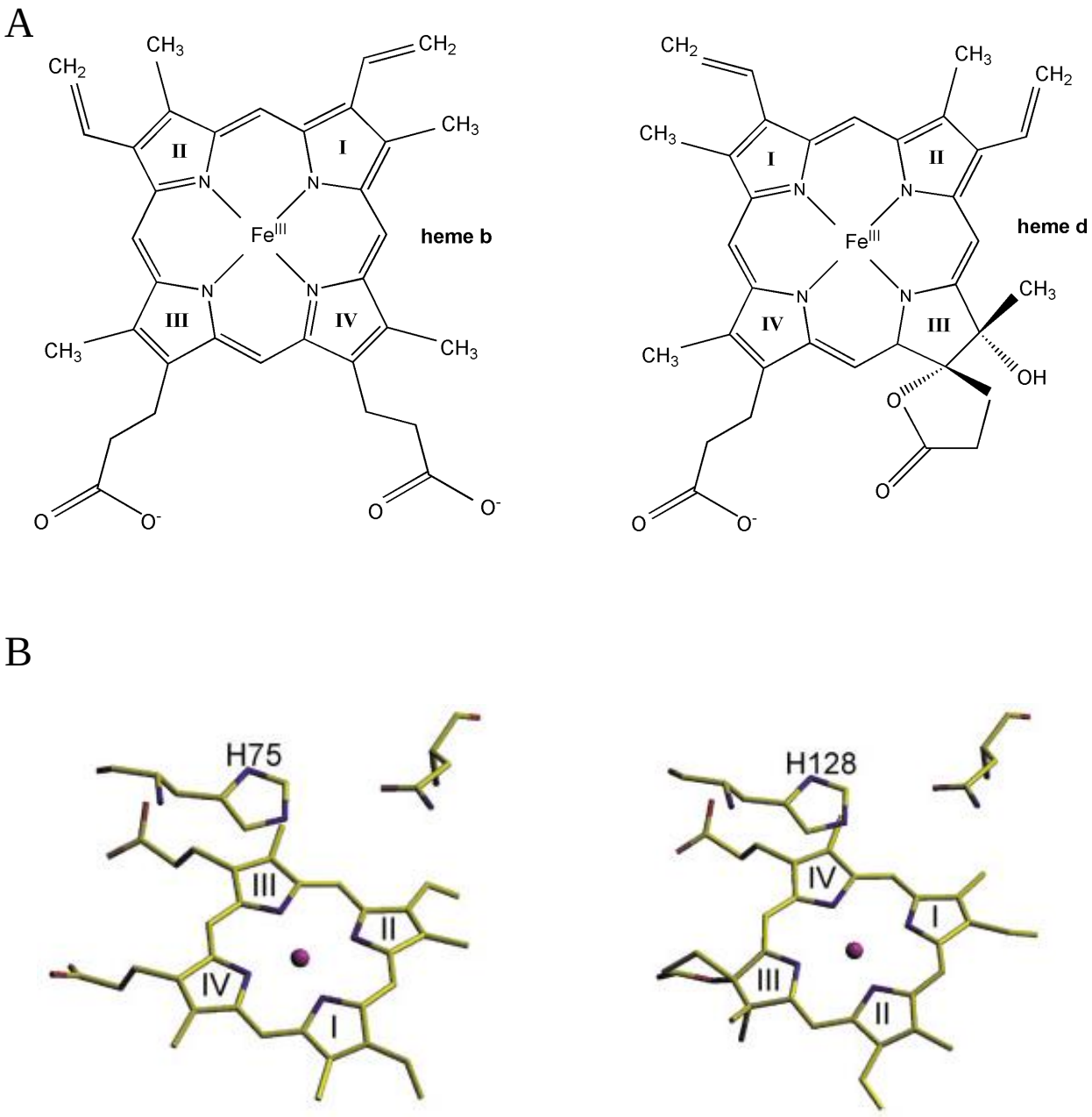

Figure 1.6. Heme types and orientations in catalases. Panel A: on the left is the structure of heme *b*, found in small subunit catalases and on the right is the heme *d*, found only in large subunit catalases. Panel B: shown on the left is the orientation of heme observed mostly in small subunit clade 3 catalases and on the right orientation of heme observed in large subunit catalases and some small subunit clade 1 catalases.

~20 Å from the nearest heme iron (Putnam et al., 2000) and is formed by residues from the β-barrel and the α-helical domain. This part of the molecule is covered by the extra domain in large-subunit catalases (Zamocky and Koller, 1999).

The role of bound NADPH in catalases seems to be to act as an electron source to prevent the accumulation of inactive Cpd II (Kirkman and Gaetani, 1987; Hillar et al., 1992, 1994). Clade 1 and clade 2 enzymes do not seem to form Cpd II and therefore have no need for NADPH. Unfortunately, the final story is not complete because as part of the suggestion that NADPH both decreases the formation of compound II and increases the rate of removal of Cpd I, the dissociation of $NADP^+$ to be replaced by new NADPH was proposed (Kirkman et al., 1999). However, $NADP^+$ does not dissociate from the enzyme, but rather is reduced back to NADPH while bound to BLC suggesting the existence of reductase and transhydrogenase activities. The implied mechanisms for multiple NADPH interactions remain unknown (Gaetani et al., 2005). Recently Sicking and co-workers attempted to investigate the functional role of NADPH in Clade 3 catalases by scrutinizing and comparing the structures of 13 available X-ray structures of heme catalases. They observed striking similarities among the Clade 3 NADPH-binding catalases and concluded that NADPH in Clade 3 catalases prevents the formation of inactive Cpd II through electron tunnelling involving a conserved water (only in Clade 3 catalases) adjacent to the 4-vinyl group of heme and a Thr-Pro linkage, with proline in the van der Walls contact with the dihydro- nicotinamide group of NADPH (Sicking et al., 2008).

In addition to its role in the recycling mechanism, experiments with CATA indicate that binding of NADPH stabilizes the quaternary structure, which is in agreement with

Gouet et al., who proposed that NADPH binding in PMC causes slight structural changes (Gouet et al., 1995).

1.4. Bifunctional catalase-peroxidases

Catalase-peroxidases form a second distinct group of heme catalases. They are also commonly called as KatGs after the encoding gene, *katG* (Loewen et al., 1985; Triggs-Raine et al., 1988). The importance of this enzyme in the research community increased substantially in 1992 when it was confirmed that mutations in the *katG* gene in *Mycobacterium tuberculosis* were responsible for the development of resistance to the antitubercular drug isoniazid (INH) (Zhang et al., 1992). Members of KatGs have been found in bacteria, archaebacteria and a few fungi (Welinder, 1992; Klotz and Loewen, 2003; Zamocky et al., 2007) and exhibit sequence similarity to the class I peroxidases such as ascorbate peroxidase (APX) of plants and cytochrome C peroxidase (CCP) of fungus. As the name indicates KatGs are enzymes which unlike monofunctional catalases possess both catalase and peroxidase activity, catalyzing both reactions 6 and 7.

As expected for a catalase and a peroxidase, the first step in the reaction involves the formation of Cpd I and release of a water molecule (Reaction 8). The enzyme differs from the monofunctional enzymes in presenting two pathways for Cpd I reduction, as a catalase and as a peroxidase. In the presence of higher concentrations of H_2O_2, KatGs act preferentially as catalases, using H_2O_2 as a two-electron donor, but with the added ability to utilize organic substrates as one-electron donors. KatGs rapidly form Cpd I* species with electrons from several different tyrosine and tryptophan residues giving up an electron to quench the porphyrin radical (Reaction 13) (Figure 1.3) (Chouchane et al., 2002; Ivancich et al., 2003; Yu et al., 2003; Jakopitsch et al., 2004).

$$AA\ Por^{\bullet+}Fe^{IV}=O \rightarrow Por\text{-}Fe^{IV}\text{-}OH\ AA^{\bullet+} \qquad \text{Reaction 13}$$

Two specific tryptophans in BpKatG, Trp139 and Trp153, have been identified as sites of stable radical formation (Singh et al., 2007) along with the adduct tyrosine (Suarez et al., 2009). Thus three unique Cpd I* have been identified: Por-Fe^{IV}-OH $Trp153^{+\bullet}$, Por-Fe^{IV}-OH $Trp139^{+\bullet}$ and Por-Fe^{IV}-OH $MY^{\bullet}W$.

1.4.1. Distribution and phylogeny of catalase-peroxidases

The evolutionary and phylogenetic classification of KatGs have been revisited in several different reports since 1991. In the first review, Welinder proposed that the katG gene arose through a gene duplication and fusion event (Welinder, 1991, 1992). Subsequently, phlogenetic surveys by Faguy and Doolittle (2000), Klotz and Loewen (2003) and finally Passardi et al (2007) have included ever increasing numbers of sequences in their comparisons, but in all cases arriving at a rather chaotic tree lacking in substantive subgroups.

1.4.2. Kinetic and biochemical properties of KatGs

Typically KatGs are found as homodimers of 80 kDa subunits with very similar catalase and peroxidase kinetic properties (Singh et al., 2008). In addition to these basic activities for which the enzyme is named, KatGs also catalyze NADH oxidase activity, and INH lyase activity and an isonicotinyl-NAD synthase activity (Singh et al., 2004) (Figure 1.7). The latter activity is responsible for the activation of INH as an anti-tubercular drug in *M. tuberculosis* (Zhang et al., 1992; Lei et al., 2000).

1.4.3. Structural and functional properties of KatGs

Crystal structures of four KatGs are available: HmKatG (Yamada et al., 2002), SyKatG (Wada et al., 2002), BpKatG (Carpena et al., 2003), and MtKatG (Bertrand et al., 2004). In addition the structure of the C-terminal domain of EcKatG or HPI is also available (Carpena et al., 2004) (Table 1.1.). KatGs are homodimers with each subunit composed of two domains with extensive structural similarity (Figure 1.8 A). While the N-terminal domains have greater sequence similarity to plant APXs and fungal CCPs and bind heme *b* as part of the active site, the C-terminal domains have greater sequence deviation, and do not bind heme, making them functionally inactive (Carpena et al., 2004).

Crystal structures from four KatGs have revealed structural features conserved between class I peroxidases and KatGs together with features unique to KatGs (Smulevich et al., 2006). Among the structural features conserved between KatGs and class I peroxidases are the triads His279/Trp330/Asp389 (BpKatG numbering) and His112/Arg108/Trp111, respectively on the proximal and distal side of heme (Figure 1.8 B). His112 is required for both catalase and peroxidase reactions. During Cpd I formation His112 acts as a proton acceptor and Arg108 as a charge stabilizer (Regelsberger et al., 2000; Hillar et al., 2000). Among the features unique to KatGs is the covalently linked adduct joining the side chains of Trp111, Tyr1238 and Met264 in the vicinity of active site (Donald et al., 2003 and Jakopitsch et al., 2003). Disruption of this covalent adduct significantly decreases the catalase activity but does not affect the peroxidase activity (Jakopitsch et al., 2003; Ghiladi et al., 2005) suggesting that a complete cross-link is required for the catalase activity. Other residues shown to specifically modulate catalase activity are Arg108, Asp141 and Arg426. Arg108 and Asp141 have been shown to modulate the catalase reaction by controlling

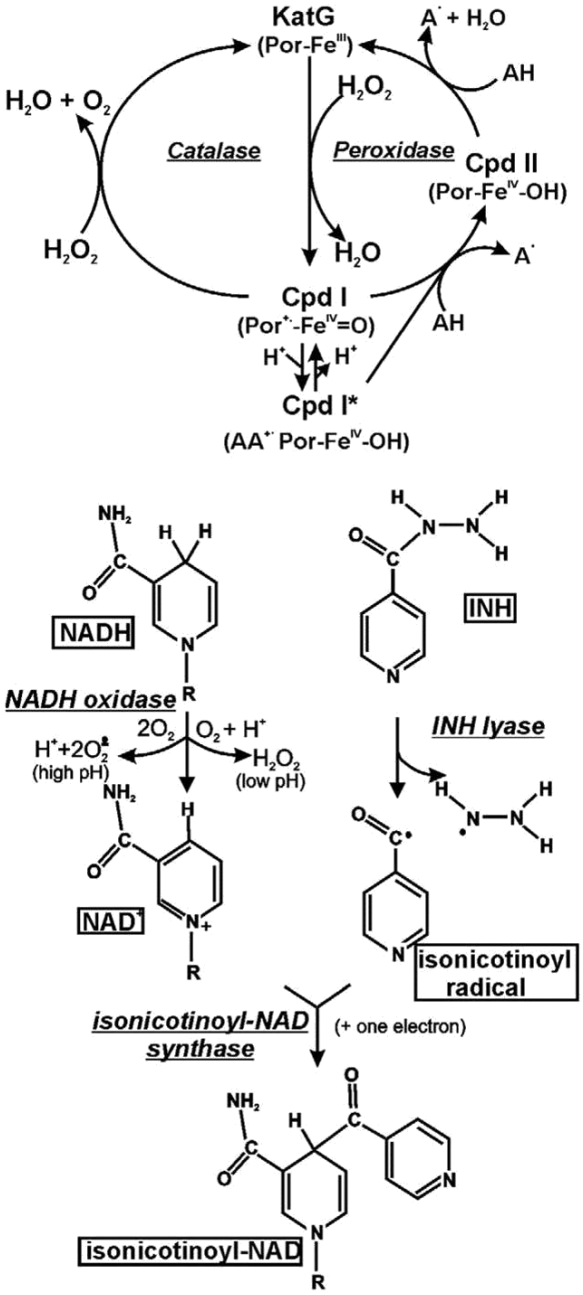

Figure 1.7. Scheme outlining the various reactions catalyzed by KatGs: At the top are shown the catalase and peroxidase reactions. At the bottom are shown the NADH oxidase, INH lyase, and isonicotinoyl-NAD synthase reaction cycle (Figure adopted from Singh et al., 2008 paper).

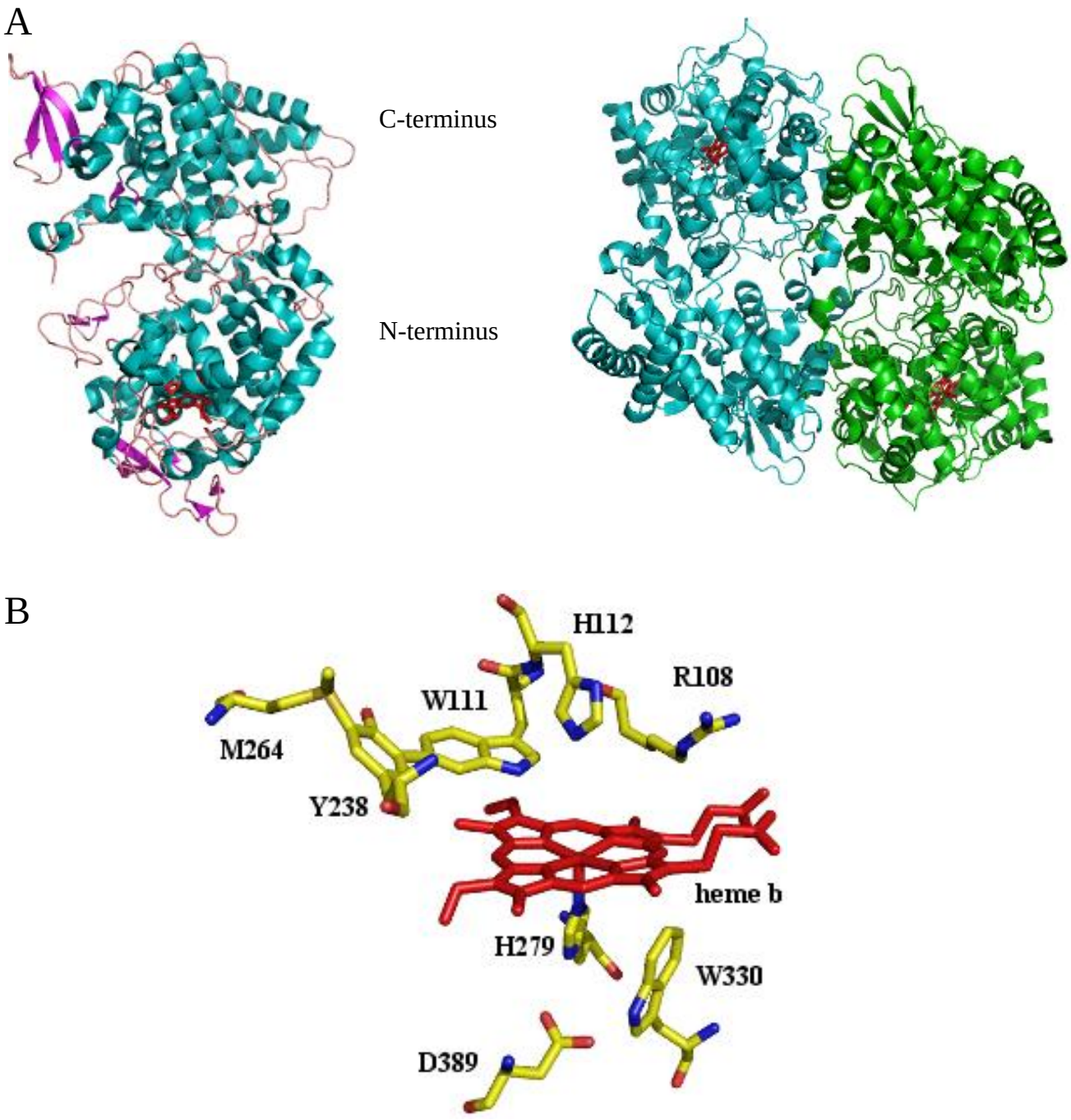

Figure 1.8. Structure of catalase-peroxidase from *Burkholderia pseudomallei*. Panel A: on the left is the monomeric unit and on the right is the dimeric unit in relation to each other. Panel B: catalytically important residues on the distal and proximal side of heme. Figure was prepared from coordinates from 1MWV from PDB.

the entry of the substrate into the heme cavity (Deemagarn et al., 2007). Arg426 is involved in modulating catalase and peroxidase activities, and possibly NADH oxidase activity (Carpena et al., 2005; Carpena et al., 2006).

1.5. Non-heme or Manganese containing catalases (Mn-catalases)

Manganese catalases are a minor family of catalases found only in bacteria. To date only four Mn-catalases have been characterized in detail ((Kono and Fridovich, 1983; Allgood and Perry, 1986; Kagawa et al., 1999; Amo et al., 2002) but a large number have been identified in sequencing projects.

The three-dimensional structures of two distinct representatives of manganese catalase are known: TTC (Antonyuk et al., 2000) and LPC (Barynin et al., 2001). The structures reveal that the enzymes exist as homohexamer of six identical subunits (Figure 1.9 A, B & C). The central four-helix bundle domain of each subunit serves as the scaffolding for the catalytic active site and has conserved residues for bridging two manganese ions (Figure 1.9 A & B and Figure 1.10).

As the name Mn-catalase implies, they contain a manganese rich reaction center that catalyzes the catalatic dismutation of H_2O_2, but by a reaction pathway that is very different from that in heme catalases. The dimanganese cluster can exist in one of the four different forms Mn^{II}-Mn^{II} ($Mn^{II}{}_2$), Mn^{II}-Mn^{III}, Mn^{III}-Mn^{III} ($Mn^{III}{}_2$), or Mn^{III}-Mn^{IV} (Whittaker et al., 1999), of which $Mn^{II}{}_2$ and $Mn^{III}{}_2$ are equally stable and active while the other two are inactive (Figure 1.11). As a result, the order of oxidation and reduction is not fixed and depending on the resting state of the enzyme, the reaction sequence will start as either an oxidation or a reduction (reaction 14 and 15).

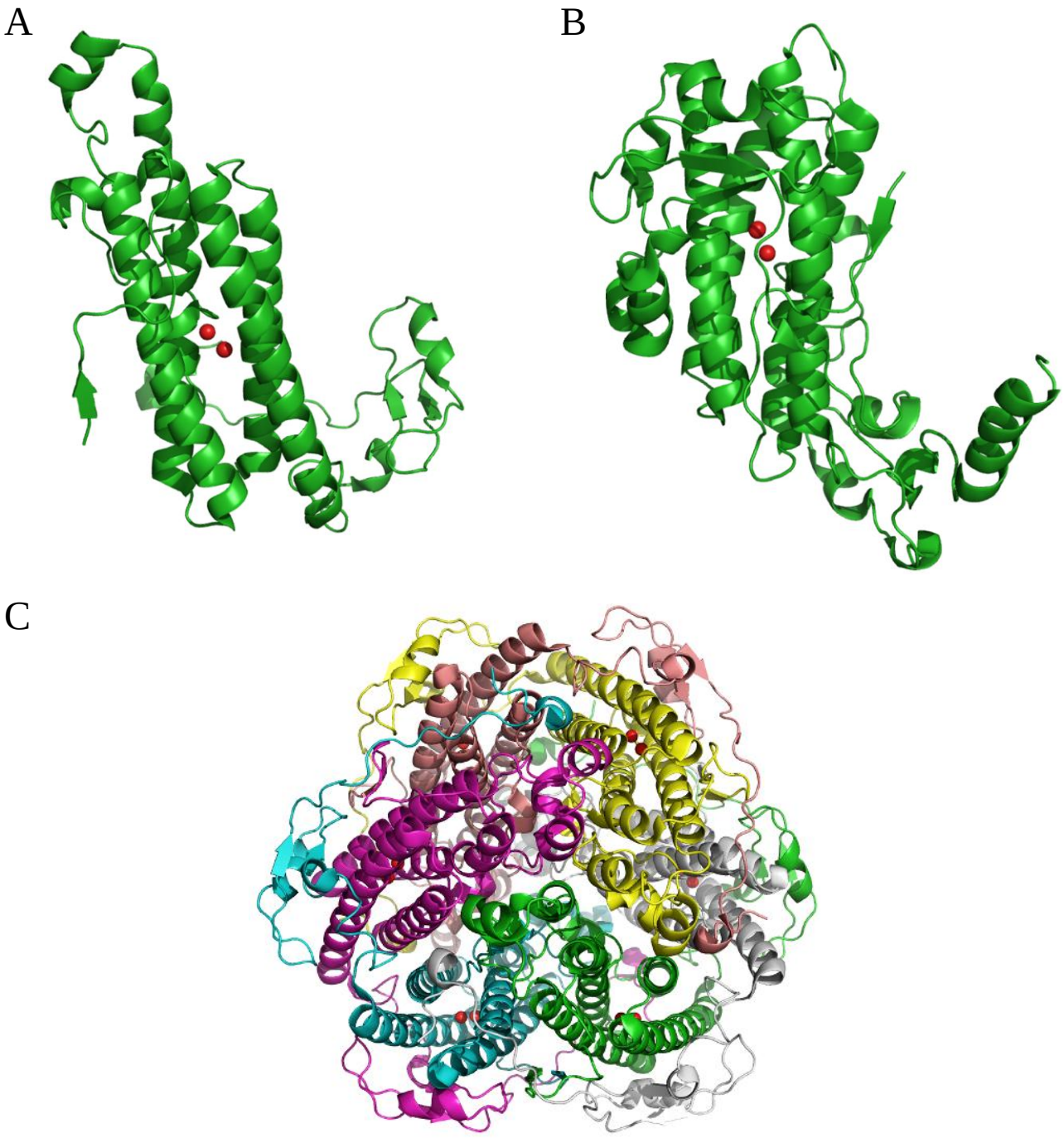

Figure 1.9. Cartoon representation of the structure of manganese catalase with bound Mn ions. Panel A: a single subunit of *Lactobacillus plantarum* (LPC). Panel B: a single subunit of *Thermus thermophilus* (TTC). Panel C: the homohexameric form of LPC. Mn ions are represented with red spheres. Figures were prepared from coordinates coordinates in 2V8U (TTC) and 1JKU (LPC) from PDB.

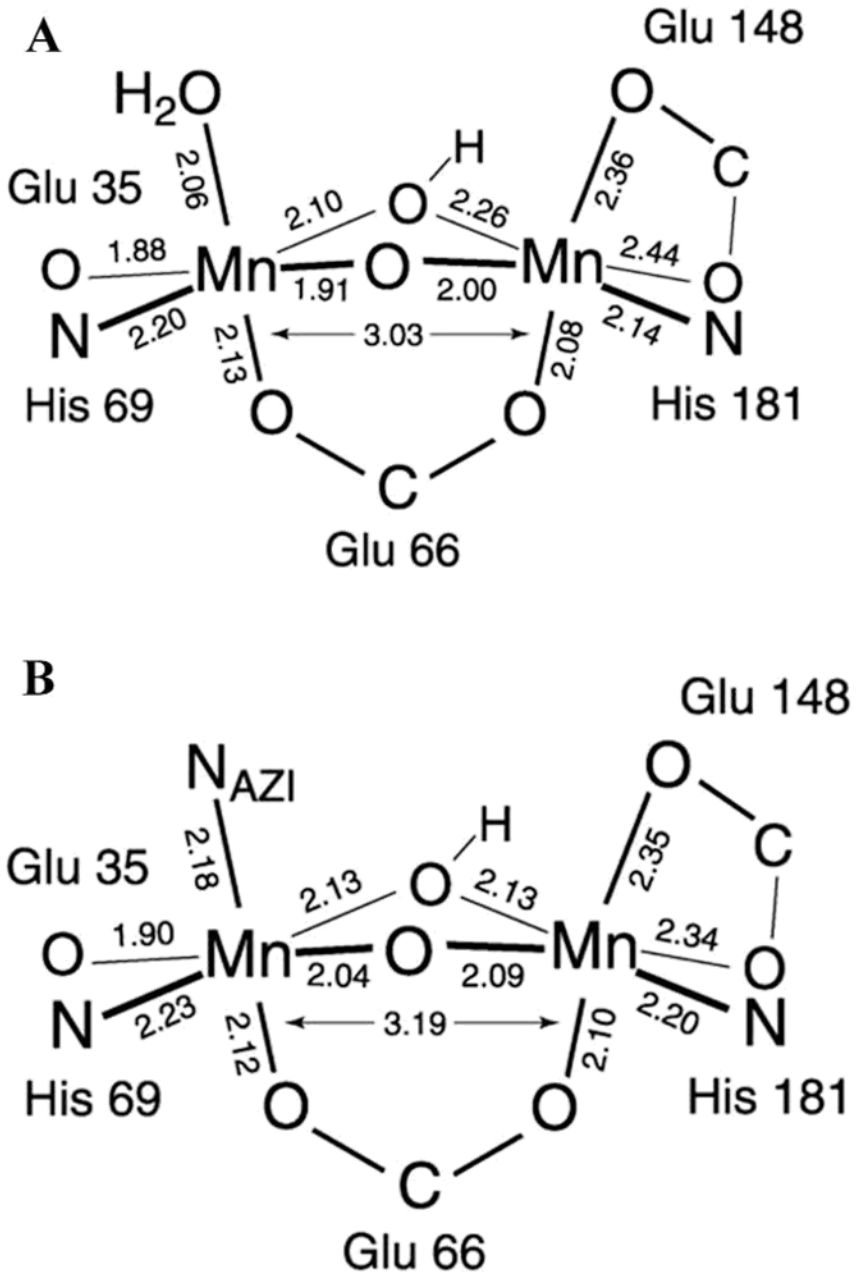

Figure 1.10. View of the dinuclear Mn complex at the active site in *Lactobacillus plantarum* (LPC) catalase. Panel A: conserved catalytically important residues at the Mn active centre. Cl^- binding replaces the central water between two Mn ions. Panel B: active centre showing mode of azide binding and inhibition.

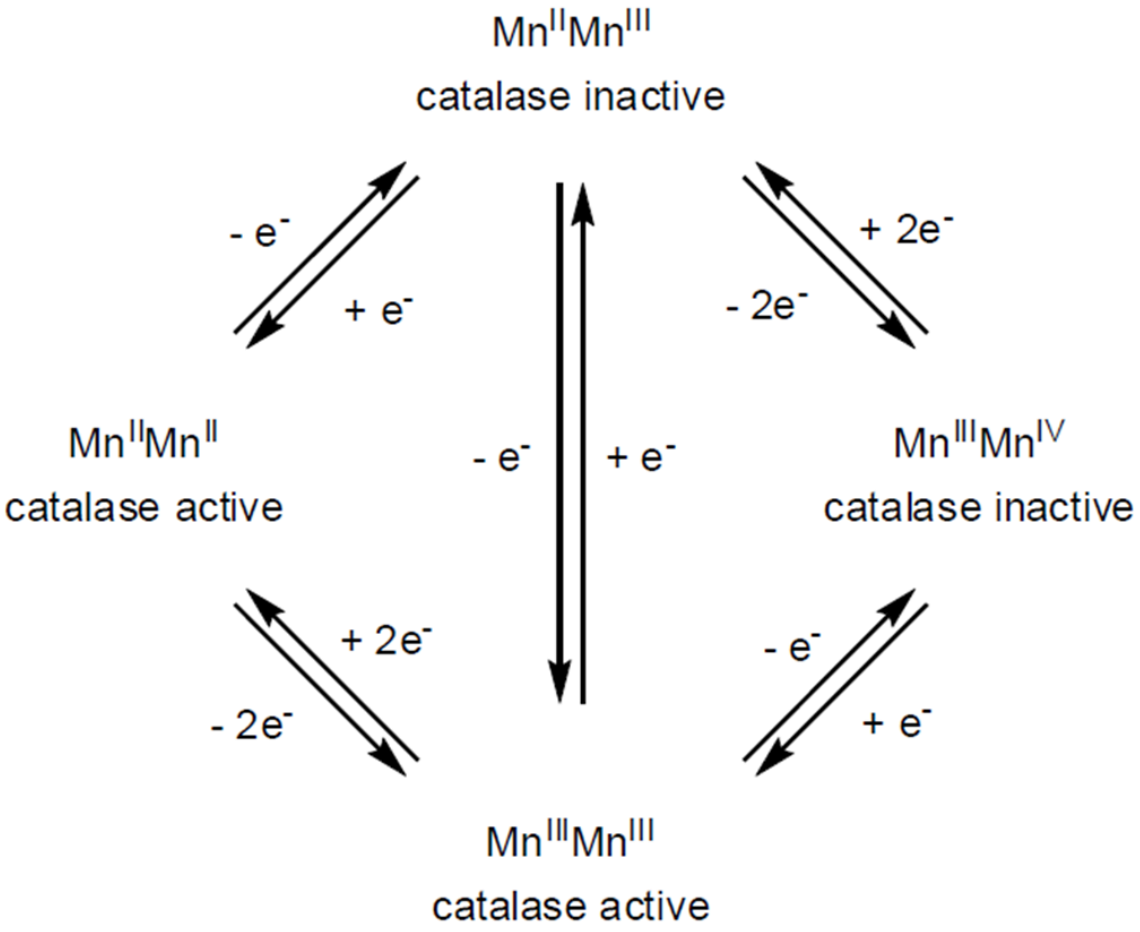

Figure 1.11. Interconversion among the different redox states of the manganese catalase enzymes. Treatment of Mn-catalase with NH_2OH in the presence of H_2O_2 leads to complete conversion of the enzyme to the inactive Mn^{III}-Mn^{IV} state (via Mn^{II}-Mn^{III}). In contrast, treatment with NH_2OH in the absence of H_2O_2 of either the Mn^{III}_2 enzyme or the inactive Mn^{III}-Mn^{IV} form yields the Mn^{II}_2 state, with full restoration of activity.

$H_2O_2 + Mn^{II}\text{-}Mn^{II}\ (2H^+) \rightarrow Mn^{III}\text{-}Mn^{III} + 2\ H_2O$ Reaction 14

$H_2O_2 + Mn^{III}\text{-}Mn^{III} \rightarrow Mn^{II}\text{-}Mn^{II}\ (2\ H^+) + O_2$ Reaction 15

In contrast to heme containing catalases, no reactive intermediates are formed, and both product waters are formed in one step.

1.6. Goal and objective of thesis

KatE of *E. coli* has the largest subunit of all characterized catalases and the extended N- and C-terminal ends produce a complicated system of intersubunit interactions. For example, 75 residues of the N-terminal extension extend through a loop on an adjacent subunit, effectively tying the two subunits together while residues from one N-terminal arm interact with residues from the other three subunits. This complex quaternary structure undoubtedly plays a significant role in the stability and specificity of the enzyme. In addition, it has resulted in some unusual structural features that have not been explored with regards to their function and significance. Most strikingly breaks in molecular symmetry have been observed giving rise to conjecture about unusual types of intersubunit cooperativity. How this relates to the conclusions from kinetic studies that suggested only half of the subunits are active is also unclear. Inter-subunit contacts between His449 residues along the molecular axis in native HPII already require small departures from perfect molecular symmetry (Bravo et al., 1999) and could be the trigger of an asymmetric behavior during catalysis (Melik-Adamyan et al., 2001). A second area of the protein that has not received extensive attention is the lateral channel. Whereas, the residues in the main channel have been investigated extensively both biochemically and structurally, the role of residues forming the second or the lateral channel remains to be investigated.

The primary goal of this thesis is to develop a better understanding of the role of the residues and structural features at the core of catalases and in the lateral access channel. The underlying methods will include site directed mutagenesis of targeted residues followed by enzymatic characterization and X-ray crystal structure determination. The residues targeted for mutagenesis are shown in Figure 1.12.

The specific objectives of this study are:

1. To investigate the role of residues involved in breaking the molecular symmetry with the object of identifying the function, if any, of the symmetry changes and of identifying the role of residues on the proximal side of the heme.
2. To investigate the function of the hydrogen bonded matrix involving H119, S421, and D417 at the core of subunit-subunit interactions.
3. To determine the role of three conserved arginines clustered around the heme carboxyl group.
4. To investigate the role of the lateral channel and specifically the involvement of I274 at the entrance to the channel.
5. To characterize the structures of variants of E530 in the main channel to gain insight into their kinetic properties.

```
1    MSQHNEKNPH QHQSPLHDSS EAKPGMDSLA PEDGSHRPAA EPTPPGAQPT
51   APGSLKAPDT RNEKLNSLED VRKGSENYAL TTNQGVRIAD DQNSLRAGSR
101  GPTLLEDFIL REKITHFDHE RIPERIVHAR GSAAHGYFQP YKSLSDITKA
151  DFLSDPNKIT PVFVRFSTVQ GGAGSADTVR DIRGFATKFY TEEGIFDLVG
201  NNTPIFFIQD AHKFPDFVHA VKPEPHWAIP QGQSAHDTFW DYVSLQPETL
251  HNVMWAMSDR GIPRSYRTME GFGIHTFRLI NAEGKATFVR FHWKPLAGKA
301  SLVWDEAQKL TGRDPDFHRR ELWEAIEAGD FPEYELGFQL IPEEDEFKFD
351  FDLLDPTKLI PEELVPVQRV GKMVLNRNPD NFFAENEQAA FHPGHIVPGL
401  DFTNDPLLQG RLFSYTDTQI SRLGGPNFHE IPINRPTCPY HNFQRDGMHR
451  MGIDTNPANY EPNSINDNWP RETPPGPKRG GFESYQERVE GNKVRERSPS
501  FGEYYSHPRL FWLSQTPFEQ RHIVDGFSFE LSKVVRPYIR ERVVDQLAHI
551  DLTLAQAVAK NLGIELTDDQ LNITPPPDVN GLKKDPSLSL YAIPDGDVKG
601  RVVAILLNDE VRSADLLAIL KALKAKGVHA KLLYSRMGEV TADDGTVLPI
651  AATFAGAPSL TVDAVIVPCG NIADIADNGD ANYYLMEAYK HLKPIALAGD
701  ARKFKATIKI ADQGEEGIVE ADSADGSFMD ELLTLMAAHR VWSRIPKIDK
751  IPA
```

Figure 1.12. Amino acid sequence of *Escherichia coli* catalase HPII (KatE). The residues targeted for mutation/replacement are colored in red.

2. MATERIALS AND METHODS

2.1. *Escherichia coli* strains, plasmids and bacteriophage

E.coli strains, plasmids and bacteriophage used in this study are listed in Table 2.1. The *E.coli katE* gene, encoding HPII catalase, was originally cloned into pKS+ (Stratagene Cloning Systems) to generate the plasmid pAMKatE72 (von Ossowski *et al.*, 1991). Strain CJ236, harboring plasmid clone pAMKatE72 and various pAMKatE72 subclones (Figure 2.1) was used for the generation of uracil-containing, single stranded DNA templates employed for site-directed mutagenesis. Helper phage R408 was used for infection of strain CJ236 to generate single stranded DNA. Strain NM522 was used as host for all plasmids and routine cloning. Strain JM109 was used for production of plasmid DNA for double stranded DNA sequencing. Strain UM255, which is catalase negative, was used for variant KatE expression and subsequent production of variant HPII proteins.

2.2. Biochemical and common reagents

All standard chemicals and biochemical reagents, used in the course of this study were usually of the highest grade available and obtained from either Sigma Chemical Co. (St. Louis, Missouri), or from Fisher Scientific Ltd. (Mississauga, Ontario). Restriction enzymes, polynucleotide kinase, and T4 DNA ligase were obtained from Invitrogen Canada Inc. (Burlington, Ontario). Unmodified T7 DNA polymerase was purchased from New England Biolabs Ltd. (Pickering, Ontario). The sequencing kit was purchased from USB Corporation (Cleveland, Ohio). Media components used for growth of *E. coli* cultures were obtained from DIFCO (U.S.A). Unless otherwise stated, solutions were prepared using reverse osmosis deionized water.

Table 2.1. Genotypes and sources of *Escherichia coli* strains, plasmids and bacteriophage used in this study.

	Genotype		Source
Strains			
CJ 236	*dut*1 *ung*1*thi*-1 *relA1/*pCj105/*cam*^{1}F$^{'}$		Kunkel *et al.*, 1987
NM 522	*sup*E Δ(*lac-pro*AB) *hsd-5* [F' *pro*AB *lac*I^{q} *lac*ZΔ 15]		Mead *et al.*, 1985
UM255	*pro leu rpsl hsd*M *hsd*R *end*I *lacy kat*G2 *kat*E12::*Tn10 rec*A		Mulvey *et al.*, 1988
JM109	*rec*A1 *sup*E44 *end*A1 *hsd*R17 *gyr*A96 *rel*A1 *thi*Δ(*lac-pro*AB)		Yanisch-Perron *et al.*, 1985
Plasmids			
pAM*kat*E72 (pKS^{+}P-C, *kat*E clone)		Amp^{r}	von Ossowski *et al.*, 1991
pKS^{-}E-H (subclone II)		Amp^{r}	von Ossowski *et al.*, 1991
pKS^{+}E-C (subclone III)		Amp^{r}	von Ossowski *et al.*, 1991
Bacteriophage			
R408 (helper phage)			Stratagene Cloning Systems

2.3. Media, growth conditions and storage of cultures

E.coli cultures were routinely grown in LB (Luria-Bertani) medium containing 10 g/L tryptone, 5 g/L yeast extract and 5 g/L NaCl. Solid LB media contained 15 g/L agar. Ampicillin was added to a concentration of 100 μg/ml in both solid and liquid medium to select for plasmid harbouring cells. Chloramphenicol was added to 40 μg/ml in order to maintain the presence of the F' episome for the growth of strain CJ236. *E.coli* strains on the solid medium were always grown at 37 ^{o}C while cells in the liquid media were either grown at 37 ^{o}C or 28 ^{o}C. Liquid cultures were grown with vigorous aeration in shake flasks. Long term storage of stock cultures was in 24% dimethylsulfoxide (DMSO) and 15% glycerol at -60 ^{o}C. Bacteriophage R408 was maintained at 4 ^{o}C in LB supernatant.

2.4. DNA manipulation

2.4.1. Preparation of synthetic oligonucleotides

Oligonucleotides used for mutagenesis were purchased commercially from Invitrogen (Burlington, Ontario) in non-phosphorylated form. The concentration of oligonucleotide DNA was determined spectrophotometrically at 260 nm, where 1 absorbance unit corresponded to ~40 μg/ml single stranded DNA (Sambrook *et al.*, (1989). Oligonucleotides used for site-directed mutagenesis were phosphorylated at the 5' end using T_4 DNA Kinase (Invitrogen) according to the procedure of Ausubel *et al.* (1989). Approximately 100 ng of oligonucleotide DNA in a volume of 25 μl containing 1 mM ATP and 10 U of kinase were incubated in appropriately diluted buffer supplied by the manufacturer at 37 ^{o}C for 30 mins. The reaction was terminated by heat inactivation at 65 ^{o}C for 5 min.

2.4.2. In vitro site-directed mutagenesis strategy

Site-directed mutagenesis of *E.coli katE* was performed according to the methodology described by the Kunkel *et al.*, 1987 with modifications. A simplified restriction map of *E.coli katE* indicating the locations of individual subclone fragments is shown in Figure 2.1. The subclones rather than the whole gene were mutagenized in order to limit the amount of sequencing needed to confirm the desired mutation in the subclone both after mutagenesis and after reinsertion of the subclone into the *katE* gene for protein expression. Target codons for mutagenesis were selected from the DNA sequence of *katE* shown in Figure 2.2. The DNA sequences of the oligonucleotides used for mutagenesis are listed in Table 2.2. Mutagenesis was performed by annealing the phosphorylated oligonucleotides encoding the desired base modification to uracil-containing single-stranded DNA templates obtained from the appropriate pBluescript phagemid subclone, propagated in the CJ236 strain. The complementary DNA strand was then synthesized *in vitro* by unmodified T7 DNA polymerase (New England Biolabs) using the annealed oligonucleotide as the primer. The 3' and 5' ends of the completed complementary strand were ligated by adding T4 DNA ligase (Invitrogen) to the reaction mixture. The double-stranded DNA was then transformed into NM522 strain so that the uracil-containing DNA strand was degraded. Plasmid DNA recovered from the transformants was further transformed into JM109 strain. Plasmid DNA was again recovered from this strain and used to screen for the desired mutation in the plasmid subclone by DNA sequencing. Once the desired mutation was identified, the complete sequence of the subclone was ascertained to ensure that no other base changes had been introduced. The mutated subclone was then used to construct the entire *katE* gene, which was then sequenced over the region containing the mutation for final

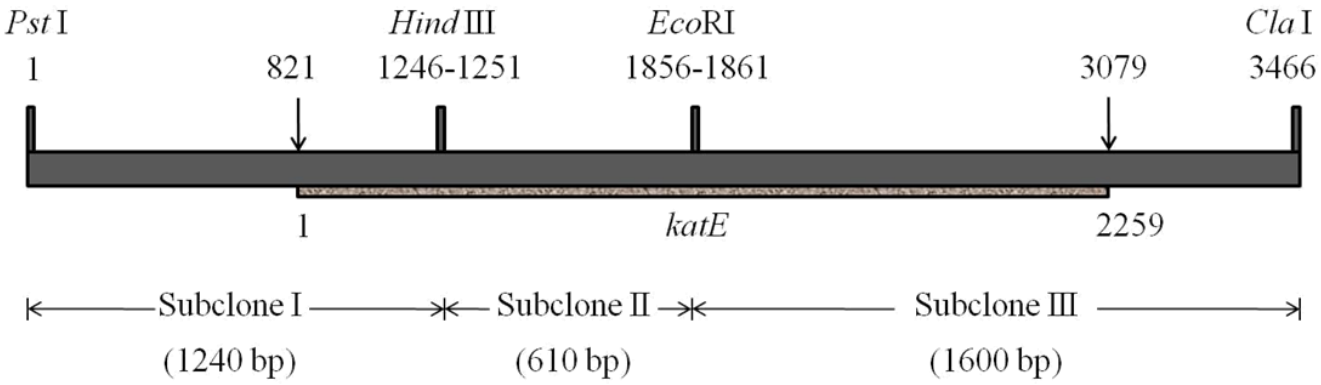

Figure 2.1. Simplified restriction map of the cloned 3466 bp chromosomal insert in pAMKatE72. The 2259 nucleotide long *KatE* open reading frame (▭) is shown as part of the chromosomal insert (▬). Three subclones (I, II, and III) employed in site-directed mutagenesis are also shown. (redrawn from von Ossowski et al., 1991).

Figure 2.2. The DNA sequence and corresponding amino acid sequence of *E. coli kat*E showing the restriction sites (sequences in blue) and the target codons selected for mutagenesis (red dash) in this study. The sequencing primers used are shown with small arrows (in red) (Sequence from von Ossowski et al., 1991). SD (in green) represents Shine-Dalgarno sequence or ribosome binding site.

Escherichia coli katE (HPII or KatE)

```
CTGCAGCCTTTCTTTAAAAGAGTCGAAAGCCAGGCTTTTAATATTTAAATCACCATAATT   60
GACGTCGGAAAGAAATTTTCTCAGCTTTCGGTCCGAAAATTATAAATTTAGTGGTATTAA
 PstI

ACTCTGTATTAAGTTTGTAGAAAACATCTCCCGCCTCATATTGTTAACAAAATTATTATC  120
TGAGACATAATTCAAACATCTTTTGTAGAGGGCGGAGTATAACAATTGTTTTAATAATAG

TCATTTAAATCTAAGTCATTTACAATATAAGTTTAAGAGCGACGCCACAGGATGAACTAT  180
AGTAAATTTAGATTCAGTAAATGTTATATTCAAATTCTCGCTGCGGTGTCCTACTTGATA

CAAAAATAGCTCATCATGATTAGCAAAACTTAACCATTTTAAAATAAATAAACAATTAAA  240
GTTTTTATCGAGTAGTACTAATCGTTTTGAATTGGTAAAATTTTATTTATTTGTTAATTT

GAAAAAAGATCACTTATTTATAGCAATAGATCGTCAAAGGCAGCTTTTTGTTACAGGTGG  300
CTTTTTTCTAGTGAATAAATATCGTTATCTAGCAGTTTCCGTCGAAAAACAATGTCCACC

TTTGAATGAATGTAGCAACGAAATACAGAATTTCAGGTCATGTAACTCCCGGCAAACCGG  360
AAACTTACTTACATCGTTGCTTTATGTCTTAAACTCCAGTACATTGAGGGCCGTTTGGCC

GAGGTATGTAATCCTTACTCAGTCACTTCCCCTTCCTGGCGGATCTGATTTGCCCAACGT  420
CTCCATACATTAGGAATGAGTCAGTGAAGGGGAAGGACCGCCTAGACTAAACGGGTTGCA

TGGGCAGATTCAGGCACAGTAAACGCCGGTGAGCGCAGAAATGACTCTCCCATCAGTACA  480
ACCCGTCTAAGTCCGTGTCATTTGCGGCCACTCGCGTCTTTACTGAGAGGGTAGTCATGT

AACGCAACATATTTGCCACGCAGCATCCAGACATCACGAAACGAATCCATCTTTATCGCA  540
TTGCGTTGTATAAACGGTGCGTCGTAGGTCTGTAGTGCTTTGCTTAGGTAGAAATAGCGT

TGTTCTGGCGGCGCGGGTTCCGTGCGTGGGACATAGCTAATAATCTGGCGGTTTTGCTGG  600
ACAAGACCGCCGCGCCCAAGGCACGCACCCTGTATCGATTATTAGACCGCCAAAACGACC

CGGAGCGGTTTCTTCATTACTGGCTTCACTAAACGCATATTAAAAATCAGAAAAACTGTA  660
GCCTCGCCAAAGAAGTAATGACCGAAGTGATTTGCGTATAATTTTTAGTCTTTTTGACAT

GTTTAGCCGATTTAGCCCCTGTACGTCCCGCTTTGCGTGTATTTCATAACACCGTTTCCA  720
CAAATCGGCTAAATCGGGGACATGCAGGGCGAAACGCACATAAAGTATTGTGGCAAAGGT

GAATAGTCTCCGAAGCGGGATCTGGCTGGTGGTCTATAGTTAGAGAGTTTTTTGACCAAA  780
CTTATCAGAGGCTTCGCCCTAGACCGACCACCAGATATCAATCTCTCAAAAAACTGGTTT

                                          M  S  Q  H  N  E  K  (7)
ACAGCGGCCCTTTCAGTAATAAATTAAGGAGACGAGTTCAATGTCGCAACATAACGAAAA  840
TGTCGCCGGGAAAGTCATTATTTAATTCCTCTGCTCAAGTTACAGCGTTGTATTGCTTTT
                           SD
```

```
  N  P  H  Q  H  Q  S  P  L  H  D  S  S  E  A  K  P  G  M  D   (27)
GAACCCACATCAGCACCAGTCACCACTACACGATTCCAGCGAAGCGAAACCGGGGATGGA  900
CTTGGGTGTAGTCGTGGTCAGTGGTGATGTGCTAAGGTCGCTTCGCTTTGGCCCCTACCT
                                 ---------GCT--------E21A→

  S  L  A  P  E  D  G  S  H  R  P  A  A  E  P  T  P  P  G  A   (47)
CTCACTGGCACCTGAGGACGGCTCTCATCGTCCAGCGGCTGAACCAACACCGCCAGGTGC  960
GAGTGACCGTGGACTCCTGCCGAGAGTAGCAGGTCGCCGACTTGGTTGTGGCGGTCCACG

  Q  P  T  A  P  G  S  L  K  A  P  D  T  R  N  E  K  L  N  S   (67)
ACAACCTACCGCCCCAGGGAGCCTGAAAGCCCCTGATACGCGTAACGAAAAACTTAATTC  1020
TGTTGGATGGCGGGGTCCCTCGGACTTTCGGGGACTATGCGCATTGCTTTTTGAATTAAG
-------AGC----------T50S→

  L  E  D  V  R  K  G  S  E  N  Y  A  L  T  T  N  Q  G  V  R   (87)
TCTGGAAGACGTACGCAAAGGCAGTGAAAATTATGCGCTGACCACTAATCAGGGCGTGCG  1080
AGACCTTCTGCATGCGTTTCCGTCACTTTTAATACGCGACTGGTGATTAGTCCCGCACGC

  I  A  D  D  Q  N  S  L  R  A  G  S  R  G  P  T  L  L  E  D   (107)
CATCGCCGACGATCAAAACTCACTGCGTGCCGGTAGCCGTGGTCCAACGCTGCTGGAAGA  1140
GTAGCGGCTGCTAGTTTTGAGTGACGCACGGCCATCGGCACCAGGTTGCGACGACCTTCT
                             SeqPriA→

  F  I  L  R  E  K  I  T  H  F  D  H  E  R  I  P  E  R  I  V   (127)
TTTTATTCTGCGCGAGAAAATCACCCACTTTGACCATGAGCGCATTCCGGAACGTATTGT  1200
AAAATAAGACGCGCTCTTTTAGTGGGTGAAACTGGTACTCGCGTAAGGCCTTGCATAACA

---------AAA---------->R111K
---------GCC---------->R111A

                         ---------GCT---------->H119A
                         ---------AAT---------->H119N
                                          ---------GCT---------R125A
                                          ---------AAA---------R125K

  H  A  R  G  S  A  A  H  G  Y  F  Q  P  Y  K  S  L  S  D  I   (147)
TCATGCACGCGGATCAGCCGCTCACGGTTATTTCCAGCCATATAAAAGCTTAAGCGATAT  1260
AGTACGTGCGCCTAGTCGGCGAGTGCCAATAAAGGTCGGTATATTTTCGAATTCGCTATA
                                              HindIII
-AAT--------H128N

  T  K  A  D  F  L  S  D  P  N  K  I  T  P  V  F  V  R  F  S   (167)
TACCAAAGCGGATTTCCTCTCAGATCCGAACAAAATCACCCCAGTATTTGTACGTTTCTC  1320
ATGGTTTCGCCTAAAGGAGAGTCTAGGCTTGTTTTAGTGGGGTCATAAACATGCAAAGAG

                                          ---------GCT---------R165A
                                          ---------AAA---------R165K

  T  V  Q  G  G  A  G  S  A  D  T  V  R  D  I  R  G  F  A  T   (187)
TACCGTTCAGGGTGGTGCTGGCTCTGCTGATACCGTGCGTGATATCCGTGGCTTTGCCAC  1380
ATGGCAAGTCCCACCACGACCGAGACGACTATGGCACGCACTATAGGCACCGAAACGGTG
                                        EcoRV
```

```
  K  F  Y  T  E  E  G  I  F  D  L  V  G  N  N  T  P  I  F  F  (207)
CAAGTTCTATACCGAAGAGGGTATTTTTGACCTCGTTGGCAATAACACGCCAATCTTCTT  1440
GTTCAAGATATGGCTTCTCCCATAAAAACTGGAGCAACCGTTATTGTGCGGTTAGAAGAA

  I  Q  D  A  H  K  F  P  D  F  V  H  A  V  K  P  E  P  H  W  (227)
TATCCAGGATGCGCATAAATTCCCCGATTTTGTTCATGCGGTAAAACCAGAACCGCACTG  1500
ATAGGTCCTACGCGTATTTAAGGGGCTAAAACAAGTACGCCATTTTGGTCTTGGCGTGAC
SeqPriB→

  A  I  P  Q  G  Q  S  A  H  D  T  F  W  D  Y  V  S  L  Q  P  (247)
GGCAATTCCACAAGGGCAAAGTGCCCACGATACTTTCTGGGATTATGTTTCTCTGCAACC  1560
CCGTTAAGGTGTTCCCGTTTCACGGGTGCTATGAAAGACCCTAATACAAAGAGACGTTGG

  E  T  L  H  N  V  M  W  A  M  S  D  R  G  I  P  R  S  Y  R  (267)
TGAAACTCTGCACAACGTGATGTGGGCGATGTCGGATCGCGGCATCCCCCGCAGTTACCG  1620
ACTTTGAGACGTGTTGCACTACACCCGCTACAGCCTAGCGCCGTAGGGGGCGTCAATGGC


  T  M  E  G  F  G  I  H  T  F  R  L  I  N  A  E  G  K  A  T  (287)
CACCATGGAAGGCTTCGGTATTCACACCTTCCGCCTGATTAATGCCGAAGGGAAGGCAAC  1680
GTGGTACCTTCCGAAGCCATAAGTGTGGAAGGCGGACTAATTACGGCTTCCCTTCCGTTG

         ---------AGT---------I274S
         ---------GCT---------I274A
         ---------GGT---------I274G
         ---------GTT---------I274V
         ---------TTT---------I274F
         ---------TGC---------I274C

  F  V  R  F  H  W  K  P  L  A  G  K  A  S  L  V  W  D  E  A  (307)
GTTTGTACGTTTCCACTGGAAACCACTGGCAGGTAAAGCCTCACTCGTTTGGGATGAAGC  1740
CAAACATGCAAAGGTGACCTTTGGTGACCGTCCATTTCGGAGTGAGCAAACCCTACTTCG

  Q  K  L  T  G  R  D  P  D  F  H  R  R  E  L  W  E  A  I  E  (327)
ACAAAAACTCACCGGACGTGACCCGGACTTCCACCGCCGCGAGTTGTGGGAAGCCATTGA  1800
TGTTTTTGAGTGGCCTGCACTGGGCCTGAAGGTGGCGGCGCTCAACACCCTTCGGTAACT

  A  G  D  F  P  E  Y  E  L  G  F  Q  L  I  P  E  E  D  E  F  (347)
AGCAGGCGATTTTCCGGAATACGAACTGGGCTTCCAGTTGATTCCTGAAGAAGATGAATT  1860
TCGTCCGCTAAAAGGCCTTATGCTTGACCCGAAGGTCAACTAAGGACTTCTTCTACTTAA
                                                      EcoRI

  K  F  D  F  D  L  L  D  P  T  K  L  I  P  E  E  L  V  P  V  (367)
CAAGTTCGACTTCGATCTTCTCGATCCAACCAAACTTATCCCGGAAGAACTGGTGCCCGT  1920
GTTCAAGCTGAAGCTAGAAGAGCTAGGTTGGTTTGAATAGGGCCTTCTTGACCACGGGCA
SeqPriC→         --------CTA--------P356L→

  Q  R  V  G  K  M  V  L  N  R  N  P  D  N  F  F  A  E  N  E  (387)
TCAGCGTGTCGGCAAAATGGTGCTCAATCGCAACCCGGATAACTTCTTTGCTGAAAACGA  1980
AGTCGCACAGCCGTTTTACCACGAGTTAGCGTTGGGCCTATTGAAGAAACGACTTTTGCT

  Q  A  A  F  H  P  G  H  I  V  P  G  L  D  F  T  N  D  P  L  (407)
ACAGGCGGCTTTCCATCCTGGGCATATCGTGCCGGGACTGGACTTCACCAACGATCCGCT  2040
TGTCCGCCGAAAGGTAGGACCCGTATAGCACGGCCCTGACCTGAAGTGGTTGCTAGGCGA
```

```
  L  Q  G  R  L  F  S  Y  T  D  T  Q  I  S  R  L  G  G  P  N  (427)
GTTGCAGGGACGTTTGTTCTCCTATACCGATACACAAATCAGTCGTCTTGGTGGGCCGAA  2100
CAACGTCCCTGCAAACAAGAGGATATGGCTATGTGTTTAGTCAGCAGAACCACCCGGCTT

                                  ----------GCT---------R422A
                                  ----------AAA---------R422K

         ---------GCC--------->F413A
         ---------TAC--------->F413Y
         ---------CAG--------->F413Q
         ---------GAG--------->F413E
         ---------AAA--------->F413K

  F  H  E  I  P  I  N  R  P  T  C  P  Y  H  N  F  Q  R  D  G  (447)
TTTCCATGAGATTCCGATTAACCGTCCGACCTGCCCTTACCATAATTTCCAGCGTGACGG  2160
AAAGGTACTCTAAGGCTAATTGGCAGGCTGGACGGGAATGGTATTAAAGGTCGCACTGCC

  M  H  R  M  G  I  D  T  N  P  A  N  Y  E  P  N  S  I  N  D  (467)
CATGCATCGCATGGGGATCGACACTAACCCGGCGAATTACGAACCGAACTCGATTAACGA  2220
GTACGTAGCGTACCCCTAGCTGTGATTGGGCCGCTTAATGCTTGGCTTGAGCTAATTGCT
SphI
----GCT--------->H449A
----AAT--------->H449N

  N  W  P  R  E  T  P  P  G  P  K  R  G  G  F  E  S  Y  Q  E  (487)
TAACTGGCCGCGCGAAACACCGCCGGGGCCGAAACGCGGCGGTTTTGAATCATACCAGGA  2280
ATTGACCGGCGCGCTTTGTGGCGGCCCCGGCTTTGCGCCGCCAAAACTTAGTATGGTCCT

  R  V  E  G  N  K  V  R  E  R  S  P  S  F  G  E  Y  Y  S  H  (507)
GCGCGTGGAAGGCAATAAAGTTCGCGAGCGCAGCCCATCGTTTGGCGAATATTATTCCCA  2340
CGCGCACCTTCCGTTATTTCAAGCGCTCGCGTCGGGTAGCAAACCGCTTATAATAAGGGT

  P  R  L  F  W  L  S  Q  T  P  F  E  Q  R  H  I  V  D  G  F  (527)
TCCGCGTCTGTTCTGGCTAAGTCAGACGCCATTTGAGCAGCGCCATATTGTCGATGGTTT  2400
AGGCGCAGACAAGACCGATTCAGTCTGCGGTAAACTCGTCGCGGTATAACAGCTACCAAA

  S  F  E  L  S  K  V  V  R  P  Y  I  R  E  R  V  V  D  Q  L  (547)
CAGTTTTGAGTTAAGCAAAGTCGTTCGTCCGTATATTCGTGAGCGCGTTGTTGACCAGCT  2460
GTCAAAACTCAATTGCTTTCAGCAAGCAGGCATATAAGCACTCGCGCAACAACTGGTCGA
-------GCT---------E530A
-------GAT---------E530D

  A  H  I  D  L  T  L  A  Q  A  V  A  K  N  L  G  I  E  L  T  (567)
GGCGCATATTGATCTCACTCTGGCCCAGGCGGTGGCGAAAAATCTCGGTATCGAACTGAC  2520
CCGCGTATAACTAGAGTGAGACCGGGTCCGCCACCGCTTTTTAGAGCCATAGCTTGACTG

  D  D  Q  L  N  I  T  P  P  P  D  V  N  G  L  K  K  D  P  S  (587)
TGACGACCAGCTGAATATCACCCCACCTCCGGACGTCAACGGTCTGAAAAAGGATCCATC  2580
ACTGCTGGTCGACTTATAGTGGGGTGGAGGCCTGCAGTTGCCAGACTTTTTCCTAGGTAG

  L  S  L  Y  A  I  P  D  G  D  V  K  G  R  V  V  A  I  L  L  (607)
CTTAAGTTTGTACGCCATTCCTGACGGTGATGTGAAAGGTCGCGTGGTAGCGATTTTACT  2640
GAATTCAAACATGCGGTAAGGACTGCCACTACACTTTCCAGCGCACCATCGCTAAAATGA
```

```
  N  D  E  V  R  S  A  D  L  L  A  I  L  K  A  L  K  A  K  G  (627)
TAATGATGAAGTGAGATCGGCAGACCTTCTGGCCATTCTCAAGGCGCTGAAGGCCAAAGG  2700
ATTACTACTTCACTCTAGCCGTCTGGAAGACCGGTAAGAGTTCCGCGACTTCCGGTTTCC

  V  H  A  K  L  L  Y  S  R  M  G  E  V  T  A  D  D  G  T  V  (647)
CGTTCATGCCAAACTGCTCTACTCCCGAATGGGTGAAGTGACTGCGGATGACGGAACGGT  2760
GCAAGTACGGTTTGACGAGATGAGGGCTTACCCACTTCACTGACGCCTACTGCCAAGCCA

  L  P  I  A  A  T  F  A  G  A  P  S  L  T  V  D  A  V  I  V  (667)
GTTGCCTATAGCCGCTACCTTTGCCGGTGCACCTTCGCTGACGGTCGATGCGGTCATTGT  2820
CAACGGATATCGGCGATGGAAACGGCCACGTGGAAGCGACTGCCAGCTACGCCAGTAACA

  P  C  G  N  I  A  D  I  A  D  N  G  D  A  N  Y  Y  L  M  E  (687)
CCCTTGCGGCAATATCGCGGATATCGCTGACAACGGCGATGCCAACTACTACCTGATGGA  2880
GGGAACGCCGTTATAGCGCCTATAGCGACTGTTGCCGCTACGGTTGATGATGGACTACCT

  A  Y  K  H  L  K  P  I  A  L  A  G  D  A  R  K  F  K  A  T  (707)
AGCCTACAAACACCTTAAACCGATTGCGCTGGCGGGTGACGCGCGCAAGTTTAAAGCAAC  2940
TCGGATGTTTGTGGAATTTGGCTAACGCGACCGCCCACTGCGCGCGTTCAAATTTCGTTG

  I  K  I  A  D  Q  G  E  E  G  I  V  E  A  D  S  A  D  G  S  (727)
AATCAAGATCGCTGACCAGGGTGAAGAAGGGATTGTGGAAGCTGACAGCGCTGACGGTAG  3000
TTAGTTCTAGCGACTGGTCCCACTTCTTCCCTAACACCTTCGACTGTCGCGACTGCCATC

  F  M  D  E  L  L  T  L  M  A  A  H  R  V  W  S  R  I  P  K  (747)
TTTTATGGATGAACTGCTAACGCTGATGGCAGCACACCGCGTGTGGTCACGCATTCCTAA  3060
AAAATACCTACTTGACGATTGCGACTACCGTCGTGTGGCGCACACCAGTGCGTAAGGATT

  I  D  K  I  P  A  *                                          (753)
GATTGACAAAATTCCTGCCTGATGGGAGCGCGCAATTGCGCCGCCTCAATGATTTACATA  3120
CTAACTGTTTTAAGGACGGACTACCCTCGCGCGTTAACGCGGCGGAGTTACTAAATGTAT

GTGCGCTTTGTTTATGCCGGATGCGCGTGAACGCCTTATCCGGCCTACAAAACTGTGCAA  3180
CACGCGAAACAAATACGGCCTACGCGCACTTGCGGAATAGGCCGGATGTTTTGACACGTT

ATTCAATATATTGCAGGAAACACGTAGGCCTGATAAGCGAAGCCATCAGGCAGTTTTGCG  3240
TAAGTTATATAACGTCCTTTGTGCATCCGGACTATTCGCTTCGGTAGTCCGTCAAAACGC

TTTGTCAGCAGTCTCAAGCGGCGGCAGTTACGCCGCCTTTGTAGGAATTAATCGCCGGAT  3300
AAACAGTCGTCAGAGTTCGCCGCCGTCAATGCGGCGGAAACATCCTTAATTAGCGGCCTA

GCAAGGTTCACGCCGATCTGGCAAACATCCTCACTTACACATCCCGATAACTCCCCAACC  3360
CGTTCCAAGTGCGGCTAGACCGTTTGTAGGAGTGAATGTGTAGGGCTATTGAGGGGTTGG

GATAACCACGCTGAGCGATAGCACCTTTCAACGACGCTGATGTCAACACATCCAGCTCCG  3420
CTATTGGTGCGACTCGCTATCGTGGAAAGTTGCTGCGACTACAGTTGTGTAGGTCGAGGC

TTAAGCGTGGGAAACAGTAAGCACTCTGACGGATAGTATTATCGAT                3466
AATTCGCACCCTTTGTCATTCGTGAGACTGCCTATCATAATAGCTA ClaI
```

Table 2.2. Oligonucleotides and *katE* restriction fragments used for site-directed mutagenesis of *katE*.

Mutant	Sequence change	Oligonucleotide[a]	Restriction fragment
R111A	(CGC→GCC)	TTTATTCTG**GCC**GAGAAAATC	*Pst*I-*Hin*dIII (1 - 1246)
R111K	(CGC→AAA)	TTTATTCTG**AAA**GAGAAAATC	*Pst*I-*Hin*dIII (1 - 1246)
H449A	(CAT→GCT)	GACGGCATG**GCT**CGCATGGGG	*Eco*RI-*Cla*I (1856 - 3466)
H449N	(CAT→AAT)	GACGGCATG**AAT**CGCATGGGG	*Eco*RI-*Cla*I (1856 - 3466)
H119A	(CAT→GCT)	CACTTTGAC**GCT**GAGCGCATT	*Pst*I-*Hin*dIII (1 - 1246)
H119N	(CAT→AAT)	CACTTTGAC**AAT**GAGCGCATT	*Pst*I-*Hin*dIII (1 - 1246)
F413A	(TTC→GCC)	GGACGTTTG**GCC**TCCTATACC	*Eco*RI-*Cla*I (1856 - 3466)
F413E	(TTC→GAG)	GGACGTTTG**GAG**TCCTATACC	*Eco*RI-*Cla*I (1856 - 3466)
F413K	(TTC→AAA)	GGACGTTTG**AAA**TCCTATACC	*Eco*RI-*Cla*I (1856 - 3466)
F413Q	(TTC→CAG)	GGACGTTTG**CAG**TCCTATACC	*Eco*RI-*Cla*I (1856 - 3466)
F413Y	(TTC→TAC)	GGACGTTTG**TAC**TCCTATACC	*EcoRI-ClaI* (1856 - 3466)
H128N/	(CAT→AAT	GGACGTTTG**AAT**TCCTATACC	*Pst*I-*Hin*dIII (1 - 1246)
F413Y	TTC→TAC)	GGACGTTTG**TAC**TCCTATACC	*Eco*RI-*Cla*I (1856 - 3466)
R111A/	(CGC→GCC	TTTATTCTG**GCC**GAGAAAATC	*Pst*I-*Hin*dIII (1 - 1246)
F413Y	TTC→TAC)	GGACGTTTG**TAC**TCCTATACC	*Eco*RI-*Cla*I (1856 - 3466)
R125A	(CGT→GCT)	ATTCCGGAA**GCT**ATTGTTCAT	*Pst*I-*Hin*dIII (1 - 1246)
R125K	(CGT→AAA)	ATTCCGGAA**AAA**ATTGTTCAT	*Pst*I-*Hin*dIII (1 - 1246)
R165A	(CGT→GCT)	GTATTTGTA**GCT**TTCTCTACC	*Hin*dIII-*Eco*RI (1246 - 1856)
R165K	(CGT→AAA)	GTATTTGTA**AAA**TTCTCTACC	*Hin*dIII-*Eco*RI (1246 - 1856)

R422A	(CGT→GCT)	CAAATCAGT**GCT**CTTGGTGGG	*Eco*RI-*Cla*I (1856 - 3466)
R422K	(CGT→AAA)	CAAATCAGT**AAA**CTTGGTGGG	*Eco*RI-*Cla*I (1856 - 3466)
I274A	(ATT→GCT)	GGCTTCGGT**GCT**CACACCTTC	*Hin*dIII-*Eco*RI (1246 - 1856)
I274G	(ATT→GGT)	GGCTTCGGT**GGT**CACACCTTC	*Hin*dIII-*Eco*RI (1246 - 1856)
I274V	(ATT→GTT)	GGCTTCGGT**GTT**CACACCTTC	*Hin*dIII-*Eco*RI (1246 - 1856)
I274C	(ATT→TGC)	GGCTTCGGT**TGC**CACACCTTC	*Hin*dIII-*Eco*RI (1246 - 1856)
I274S	(ATT→TCT)	GGCTTCGGT**TCT**CACACCTTC	*Hin*dIII-*Eco*RI (1246 - 1856)
E530A	(GAG→GCT)	TTCAGTTTT**GCT**TTAAGCAAA	*Eco*RI-*Cla*I (1856 - 3466)
E530D	(GAG→GAT)	TTCAGTTTT**GAT**TTAAGCAAA	*Eco*RI-*Cla*I (1856 - 3466)

[a] The sequence in bold is the codon that has been modified.

confirmation. Reconstructed, mutant *katE* clones were then transformed into UM255 for protein expression, purification and determination of enzyme activity. Visualization of protein from either whole cells or crude extracts was done by SDS-PAGE. Clones expressing significant levels of variant HPII protein were then grown in large scale batches (4-6 L) for purification and characterization.

2.4.3. DNA isolation and purification

Plasmid DNA was isolated according to Sambrook *et al.* (1989). Plasmid harbouring cells were grown in tubes containing 5 ml LB medium to stationary phase and were then pelleted by centrifugation and resuspended in 200 µl Tris-glucose-EDTA buffer (25 mM Tris-HCl, pH 8.0, 1% glucose, 10 mM Na-EDTA). Resuspended cells were lysed by addition of 400 µl 1% SDS (w/v), 0.2 M NaOH solution and gentle mixing. This was then neutralized by addition of 300 µl 6.2 M ammonium acetate, pH 5.9. After 10 min incubation on ice, the mixture was centrifuged twice to remove all precipitates. Plasmid DNA was then precipitated by addition of 550 µl isopropanol to the remaining supernatant followed by 15 min incubation at room temperature. Plasmid DNA was pelleted by centrifugation, washed twice with 70% (v/v) ice-cold ethanol, and then dried under vacuum or on table top. The DNA pellet was either stored in this condition at -20 ^{o}C or was resuspended in HPLC grade distilled water or TE buffer (10 mM Tris, pH 8.0, 1 mM Na-EDTA) prior to being stored at -20 ^{o}C until further use.

Preparation of single stranded template DNA for site-directed mutagenesis was carried out according to Vieira and Messing (1987). Plasmid harbouring cells were grown in a 5 ml LB culture to early exponential phase and then infected with 50 µl of helper phage

R408 and 50 µl of 1 M $MgSO_4$ and were grown overnight. After centrifuging 1.5 ml of culture in order to remove cells and debris, a solution of 300 µl of 1.5 M NaCl-20% PEG 6000 was added per ml of medium supernatant and mixed. This mixture was incubated for 15 min at room temperature and then centrifuged to pellet the phage particles. The pellet was then resuspended in TE buffer on ice and extracted first with an equal volume of buffer saturated phenol, followed by extraction with an equal volume of water-saturated chloroform. Single-stranded DNA was precipitated by addition of an equal volume of 7.5 M ammonium acetate, pH 7.5 and 4 volumes of ice-cold 95% ethanol followed by incubation at -20 ^{o}C for 20 mins. Single-stranded DNA was recovered by centrifugation and the pellet washed once with 95% (v/v) ethanol and 2 times with 70% (v/v) ethanol. The dried pellet was stored at -20 ^{o}C until further use.

2.4.4. Restriction endonuclease digestion of DNA

All restriction endonucleases and buffers used in this study were products of Invitrogen. Restriction digestions were carried out at 37 ^{o}C for 2-5 hours in total volumes of 10 µl, containing 1 µg RNAse, 1 µl of 10X appropriate buffer provided by the supplier, ~ 1-5 µg DNA, and 0.5-1 µl (50-2,000 U) of endonuclease. The 5'-phosphate groups of vector DNA obtained from single restriction digests were removed by 12.5-25 U of calf intestinal alkaline phosphate (Invitrogen) added during the cleavage reaction.

2.4.5. Agarose gel electrophoresis

Electrophoresis of restriction endonuclease digested DNA was performed according to Sambrook *et al.* (1989). Agarose gels prepared in TAE buffer (40 mM Tris-acetate and 1 mM EDTA, pH 8.0), containing 1% (w/v) agarose, and 0.1 µg/ml ethidium bromide was

cast in Bio-Rad Mini Sub Cell plexiglass horizontal electrophoresis trays (6.5 cm x 10 cm). Samples of 10 µl volumes were mixed with 2 µl Stop buffer (40% [v/v] glycerol, 10 mM EDTA pH 8.0, 0.25% [w/v] bromophenol blue). 1 kb DNA Ladder or 1 kb Plus DNA Ladder (Invitrogen) was used as molecular weight size standards. Electrophoresis was carried out at 45 mA constant current in 1X TAE buffer, usually until the bromophenol blue dye font had migrated two-thirds of the length of the gel. Following electrophoresis, DNA bands were visualised with ultraviolet light using a (Bio-Rad) Gel Doc 1000.

2.4.6. DNA Ligation

DNA fragments to be ligated were excised from agarose gels and purified using the Gene Clean DNA extraction kit (M Bio.) according to the instructions supplied by the manufacturer. Ligation of insert DNA was carried out according to Sambrook *et al.* (1989). Purified DNA was mixed in a ratio of 2-3 of insert to vector in 10 µl volumes, containing 1 unit of T4 DNA ligase (Invitrogen), and the manufacturer's supplied buffer. Ligation mixtures were incubated overnight at 15 ^{o}C. A sample with no insert DNA added was used as the control.

2.4.7. Transformation

Transformation of *E.coli* cells with the various plasmids was performed according to Chung *et al.* (1989). Cells grown in tubes containing 5 ml LB medium to exponential phase (2-4 hour) were harvested by centrifugation and made competent by resuspension in 500 µl ice-cold 0.1 M $CaCl_2$ for 30 minutes on ice. 2-10 µg DNA was usually added to 100 µl of this cell suspension, followed by a further 30 minutes incubation on ice, and a 90 second heat shock at 42 ^{o}C. LB medium (0.9 ml) was then added to the cell suspension and incubated at 37 ^{o}C for 60-90 minutes without aeration. The mixture was then either spread-

plated, or (in the case of ligation mixture transformations) mixed with 3 ml molten (50 ^{o}C) R-Top agar (0.125 g yeast extract, 1.25 g tryptone, 1 g NaCl, 1 g agar per 125 ml volume with 0.25 ml 1M $CaCl_2$ and 0.42 ml 30% glucose sterile solutions added for autoclaving) and poured onto ampicillin-containing LB plates.

2.4.8. DNA sequencing

At the beginning of the study DNA sequencing was carried out according to Sanger *et al.* (1977). Sequencing was carried out manually with double stranded DNA templates using primers annealing to the pKS vector or other primers as appropriate for the particular mutant of interest. To prepare the double stranded DNA template, 5 µg of plasmid DNA was resuspended and denatured in a 40 µl volume of 2 M freshly prepared NaOH. This mixture was incubated for 10 mins at 37 ^{o}C, and then precipitated by addition of 10 µl 3 M sodium acetate, pH 4.8 and 140 µl ice-cold 95% ethanol. Following incubation at -20 ^{o}C for 30 minutes, the DNA pellet was recovered by centrifugation and washed once with 1 ml 95% ice-cold ethanol, and twice with 70% ice-cold ethanol, and then evaporated to dryness under vacuum or at room temperature. Annealing and sequencing reactions were carried out using a T7 sequencing kit (USB Corporation, USA) according to the specifications of the supplier and using 5-15 µCi [S^{35}] dATP (NEN-Dupont). Reaction mixtures were separated and resolved on 8% (w/v) polyacrylamide vertical slab gels containing 7 M urea, 0.13 M Tris, 0.13 M boric acid, and 10 mM EDTA. Electrophoresis was carried out at 18-24 mA constant current in TBE buffer (90 mM Tris, 89 mM borate, 2.2 mM EDTA) for 1.5-5 h as required. Gels were mounted on 3 mm Whatman paper and dried at 80 ^{o}C for 1 hour in a slab gel vacuum dryer (Savant). Dried gels were exposed to X-ray film (Kodak X-OMAT AR) overnight or more in order to visualize the DNA bands.

In the later part of the study DNA sequencing was done with the automated Applied Biosystems 3130 Genetic Analyzer. The DNA to be sequenced was isolated as described above but the DNA pellet was resuspended in MQ water instead of TE buffer as recommended by the instructions of the BigDye Terminator v1.1 Cycle Sequencing Kit (Applied Biosystems). The sequencing reaction mixture contained approximately 200 ng of DNA with 3 pmol of the appropriate primer and sequencing was carried out according to the instructions in the BigDye Terminator v1.1 Cycle Sequencing Kit (Applied Biosystems) in a final volume of 20 µl. The PCR cycle program for the sequencing reaction included a preheat step at 96 ^{o}C for 1 minute followed by 25 cycles of denaturing, annealing, and extension steps at 96 ^{o}C for 10 seconds, 50 ^{o}C for 5 seconds, and 60 ^{o}C for 4 minutes respectively, followed by cooling at 4 ^{o}C. The DNA was then precipitated by adding 2 µl of 125 mM EDTA, 2 µl of 3 M sodium acetate, pH 4.8, and 60 µl of 95% ethanol and gentle mixing by inversion. After 15 minute incubation at RT, the DNA was pelleted by centrifugation at 4 ^{o}C for 15 minutes. The DNA pellet was washed with 60 µl of 70% ethanol by centrifugation at 4 ^{o}C for 15 minutes. The pellet was dried for 20 minutes at RT, and denatured with 20 µl of Hi-Dye formamide by vigorous vortexing and incubation at 94 ^{o}C for 5 minutes. The denatured sample was then loaded into the sample plate provided with the automated sequencer (Applied Biosystems) for sequencing.

2.5. Purification of HPII and its variants

For whole cell assay used in the determination of relative levels of protein expression and catalase activity, plasmid containing cells were grown in 30 ml of LB medium in 125 ml shaker flasks at 37 ^{o}C and 28 ^{o}C for 16-20 hours. Whole cell cultures and crude extracts were used for enzyme assay and protein visualization was carried out by electrophoresis on

sodium dodecyl sulfate polyacrylamide gels (SDS-PAGE). For crude extract assays, cells were pelleted by centrifugation at 10,000 rpm for 5 minutes and then resuspended in 1 ml 50 mM potassium phosphate buffer (KPi). Resuspended cells were then sonicated using a small probe with two 45 second pulses. Ruptured cells were again centrifuged to pellet cell debris and supernatant was used for enzyme assay and protein visualization.

For large scale protein preparations, UM255 cells over expressing the desired protein from the appropriate plasmid borne gene were grown in 4-6 L of LB medium, in 2 L shake flasks (500 ml LB per flask) supplemented with 100 µg/ml ampicillin for 20-22 hours at 28 ^{o}C or 16-20 hours at 37 ^{o}C with good aeration. Isolation of HPII proteins was done according to Loewen and Switala (1986) with modification.

Cells were harvested from the growth medium by centrifugation and the cell pellet was kept at -60 ^{o}C overnight. The cell pellet was then resuspended in 150-250 ml of 50 mM potassium phosphate buffer, pH 7.0, containing 2 mM EDTA. The cells were disrupted by passing through a French pressure cell at 20,000 psi. The unbroken cells and debris were removed by centrifugation, and to this crude extract was added streptomycin sulphate to a final concentration of 2.5% (w/v). The resulting precipitates were removed by centrifugation and discarded, solid ammonium sulphate was then added starting at a concentration of 30%, incrementally increasing by 10% up to 60% to the supernatant with gentle stirring at 4 °C to precipitate the desired protein. HPII and most of its variants were found to precipitate in ammonium sulphate at 50-60% saturation. The pellets from 50 and 60% ammonium sulphate precipitations were dissolved in 50 mM potassium phosphate buffer, pH 7.0, combined together and dialyzed against 2 L of 50 mM KPi, over night. The dialyzed fraction was then subjected to second round of ammonium sulphate precipitation and 50 and 60%

fractions were combined together and the mixture was heat treated at 50 ^{o}C for 15-20 min (only for variants which maintained activity after incubation at 50 ^{o}C for 15-20 min), centrifuged and dialyzed overnight as described above. The dialyzed sample was then centrifuged and loaded on to a 2.5 cm x 23 cm column of DEAE-cellufine A-500 (CHISSO Corporation, Japan) preequilibrated with 50 mM of KPi. The column was washed with an excess of 50 mM KPi until the OD_{280} reached ≤ 0.05. The protein of interest was then eluted with a linear gradient of 0 to 500 mM NaCl in 50 mM KPi. The appropriate fractions were collected, pooled together and concentrated under nitrogen using an Amicon YM-30 membrane in an Amicon (model 8050) protein concentrator to a volume of 5 ml. The concentrated protein was then dialyzed overnight against 1 L of 50 mM KPi overnight. The purity of the protein was analyzed both spectrophotometrically (A_{407}/A_{280}) and by SDS-PAGE. If the A_{407}/A_{280} ratio was found <0.7 and too many bands appeared on the SDS gel then the protein was loaded on to a 2.5 cm x 15 cm hydroxyapatite column (BioRad) pre-equilibrated with 5 mM KPi. Protein was eluted with a gradient of 5-400 mM KPi buffer, pH 7.0. Fractions were collected and analysed as described above. The purified protein was stored in small volumes at -60 ^{o}C until needed.

2.6. Sodium dodecyl sulphate-polyacrylamide gel electrophoresis (SDS-PAGE)

Denaturing SDS-PAGE was carried out according to Weber et al., 1972. Discontinuous 4% stacking and 8% separating polyacrylamide gels were cast as vertical slabs of dimensions 10 x 10 cm and 0.5 mm thickness. Samples were mixed with equal volumes of sample buffer (3.4 mg/ml NaH_2PO_4, 10.2 mg/ml Na_2HPO_4, 10 mg/ml SDS, 0.1 mM 2-mercaptoethanol, 0.36 g/ml Urea, and 0.15% bromophenol blue) and boiled for 3-5 minutes before loading onto the gel (between 2-10 µg of protein were used for loading).

Gels were run at a constant voltage of 150 V, until the dye reached the bottom, in a vertical BIORAD Mini-Protean II electrophoresis system using a running buffer containing 14 g/L glycine, 3 g/L Tris base, and 1 g/L SDS. Gels were stained with a solution containing 0.5 g/L Coomassie Brilliant Blue R-250, 30% ethanol, and 10% glacial acetic acid for 1 hour and destained with the destaining solution containing 15% methanol and 7% acetic acid until the background color of the gel was clear. The gels were then soaked in a solution containing 7% acetic acid and 1% glycerol for 20-30 minutes in order to fix the desired protein band on the gel. Then the gels were transferred to 3 mm Whatman paper, covered with clear plastic film and dried at 80 ^{o}C for 1 hour on a slab gel dryer (Savant).

2.7. Enzyme assay and protein quantification

Catalase activity was determined by the method of Rørth and Jensen (1967) in a Gilson oxygraph equipped with a Clark electrode. One unit of catalase is defined as the amount of enzyme that decomposes 1 µmol H_2O_2 in 1 minute in 60 mM H_2O_2 solution at 37 ^{o}C, pH 7.0.

A volume of 1.8 ml of 50 mM KPi buffer, pH 7.0 was added to the reaction chamber followed by addition of 50 µl H_2O_2 to a final concentration of 60 mM. After 0.5-1.0 minute incubation at 37 ^{o}C, appropriately diluted enzyme samples or cell cultures were added. Catalase activity was determined in U/ml from the slope of the plot representing oxygen evolution. Specific catalase activity was determined as U/mg protein for purified protein or as U/mg dry cell weight for whole cells. Specific activities were always determined as the average of three individual determinations. Protein concentration was determined by the method of Layne (1957).

2.8. Absorption spectrophotometry

Absorption spectra of the purified proteins were determined using Pharmacia Ultrospec 4000 or a Milton Roy MR3000 spectrophotometer. Spectra were obtained at ambient temperature in 1 ml quartz cuvettes with protein diluted in 50 mM KPi, pH 7.0 over the range from 250-750 nm. Buffer was used as the reference. Data was analyzed using SigmaPlot.

2.9. Heme extraction

Heme extraction was carried out according to Loewen et al., 1993. A 10-20 µl aliquot of protein sample was treated with 1 ml acetone-HCl (10 ml acetone, 13 µl concentrated HCl) for 1 minute at RT. The sample was centrifuged and supernatant was transferred to a fresh tube and neutralized by adding 8 µl 1 M Na_2CO_3, mixed and centrifuged. The absorbance spectrum was obtained and the data analyzed using SigmaPlot.

2.10. Effect of inhibitors on catalase activity

The effects of NaCN, NaN_3, and NH_2OH on the catalase activity of the HPII wild-type and its variants were studied. The appropriately diluted variant proteins were preincubated in 1.8 ml of 50 mM KPi buffer, pH 7.0 at 37 ^oC with different concentrations of inhibitors for 1 minute prior to H_2O_2 addition in the reaction chamber. Catalase specific activities were plotted against inhibitor concentration to determine the concentration at 50% inhibition.

2.11. Crystallization and structure determination

Crystals of HPII wild-type and its variants were obtained at room temperature (~22 ^oC) by the hanging drop vapour diffusion method at a protein concentration between 8-14

mg/ml over a reservoir solution containing 13-15% PEG 3350 (Carbowax), 1.2-1.8% LiCl (Fisher) and 0.1 M Tris-HCl pH 9.0.

X-ray diffraction data were collected using an in-house X-ray source (RIGAKU R-axis IV++) and/or synchrotron beam line CMCF 08ID-1 at the Canadian Light Source in Saskatoon, Canada from crystals flash-cooled in liquid nitrogen. Diffraction data were processed and scaled using programs MOSFLM and SCALA (CCP4 Suite, 1994). For some variants structure diffraction data were processed and scaled using d*TREK program (Pflugrath, 1999) from RIGAKU. Structure refinement was completed using program REFMAC (Murshudov et al., 1997) and manual modeling with the molecular graphics program COOT (Emsley and Cowtan, 2004). In all cases 5 % of the measured reflections were reserved for R_{free} monitoring during refinement. Figures were generated using PyMOL (DeLano, 2002).

3. ROLE OF RESIDUES AROUND THE CENTRAL CAVITY ON THE HEME PROXIMAL SIDE IN CATALASE HPII

3.1. Effect of Arg111 and His449 mutation on biochemical and structural properties of catalase HPII

3.1.1. Introduction

Catalase HPII of *Escherichia coli* has been the subject of study for three decades. After its first characterization (Claiborne et al., 1979) and 3-D structure determination (Bravo et al., 1995, 1999) several studies combining site-directed mutagenesis and X-ray crystallography have been carried out leading to the identification of key residues involved in enzyme catalysis and post-translational modifications including conversion of heme *b* into heme *d* and covalent linkage between His392 and conserved Tyr415 (Bravo et al., 1997).

One peculiar observation was a break in the molecular symmetry of four residues, including Arg111, Phe413, Thr416 and Asp417, upon addition of H_2O_2 to the inactive variant H128N. These changes occurred remote from the bound peroxide clustered around the central cavity of the tetramer and occurred in only two of the subunits (Melik-Adamyan et al., 2001). Inter-subunit contacts between His449 residues in adjacent subunits along the molecular axis in native HPII also require small departures from perfect molecular symmetry which could be the trigger of an asymmetric behaviour during catalysis. Arg is conserved at position 111 in the four structurally characterized large subunit clade 2 catalases, but His is not conserved at position 449 in other catalases. How H_2O_2 binding and movement of residues relate to the modulation of catalytic activity and structural organization is still a subject of conjecture. The aim of this study was to determine the role

of this group of residues, situated near the central cavity of catalase HPII, in the catalytic function of the enzyme.

3.1.2. Construction, purification and characterization of HPII and mutants

Arg111 was replaced by an alanine (R111A) and a lysine (R111K), while His449 was replaced by an alanine (H449A) and an asparagine (H449N). All variants were constructed and purified according to the protocol outlined in Chapter 2, and purified proteins were analyzed by SDS-PAGE as shown in Figure 3.1.1. The WT-HPII enzyme and the variants exhibit similar electrophoretic mobility with a predominant band at an apparent molecular mass of ~84 kDa. The absorption spectra of purified WT-HPII and variants are shown in Figure 3.1.2. No significant change in the position of Soret band was observed in the spectra of any of the variants and all spectra contained a strong peak at 590 nm confirming the presence of heme *d* as the predominant heme species. A small shoulder at 630 nm in the spectra of R111K and H449N (Figures 3.1.2 and Table 3.1.1) suggest the presence of a small amount of heme *b* in both variants. The A_{407}/A_{280} ratio or R_z is commonly used as a measure of protein purity and heme content. For native HPII, the R_z is usually in the 0.9 to 1.0 range, and the R_z values of the variants were just slightly lower. The values of the absorption maxima and R_z values are listed in Table 3.1.1 for comparison with WT-HPII.

Catalase specific activities of WT-HPII and its variants are listed in Table 3.1.1. No significant change in the specific activities was observed among the four variants compared to WT-HPII. The kinetics of the variants (Figure 3.1.3) revealed similar specificity for H_2O_2 with the k_{cat}/K_M values being similar to those of WT-HPII, but H449A and H449N did have lower apparent K_M and k_{cat} values (Table 3.1.2).

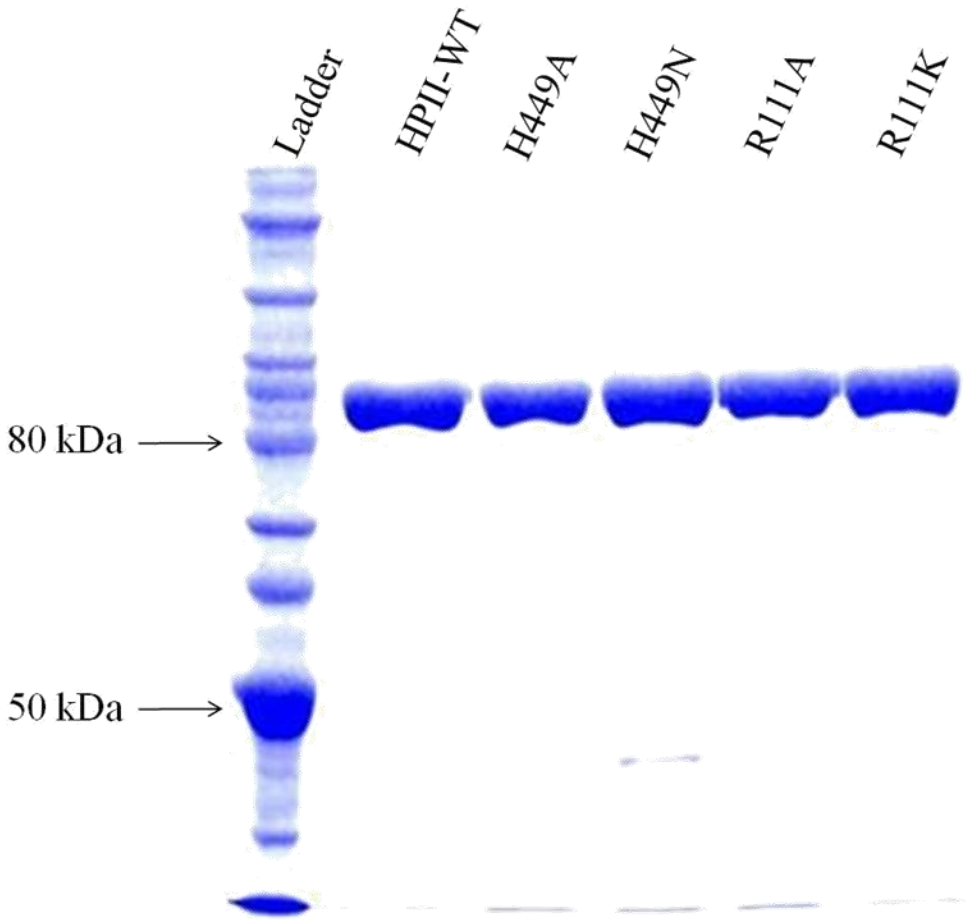

Figure 3.1.1. SDS-PAGE analysis of purified WT-HPII and its variants. Approximately 2.0 µg of protein were loaded on an 8% polyacrylamide gel and stained with Coomassie brilliant blue after electrophoretic separation.

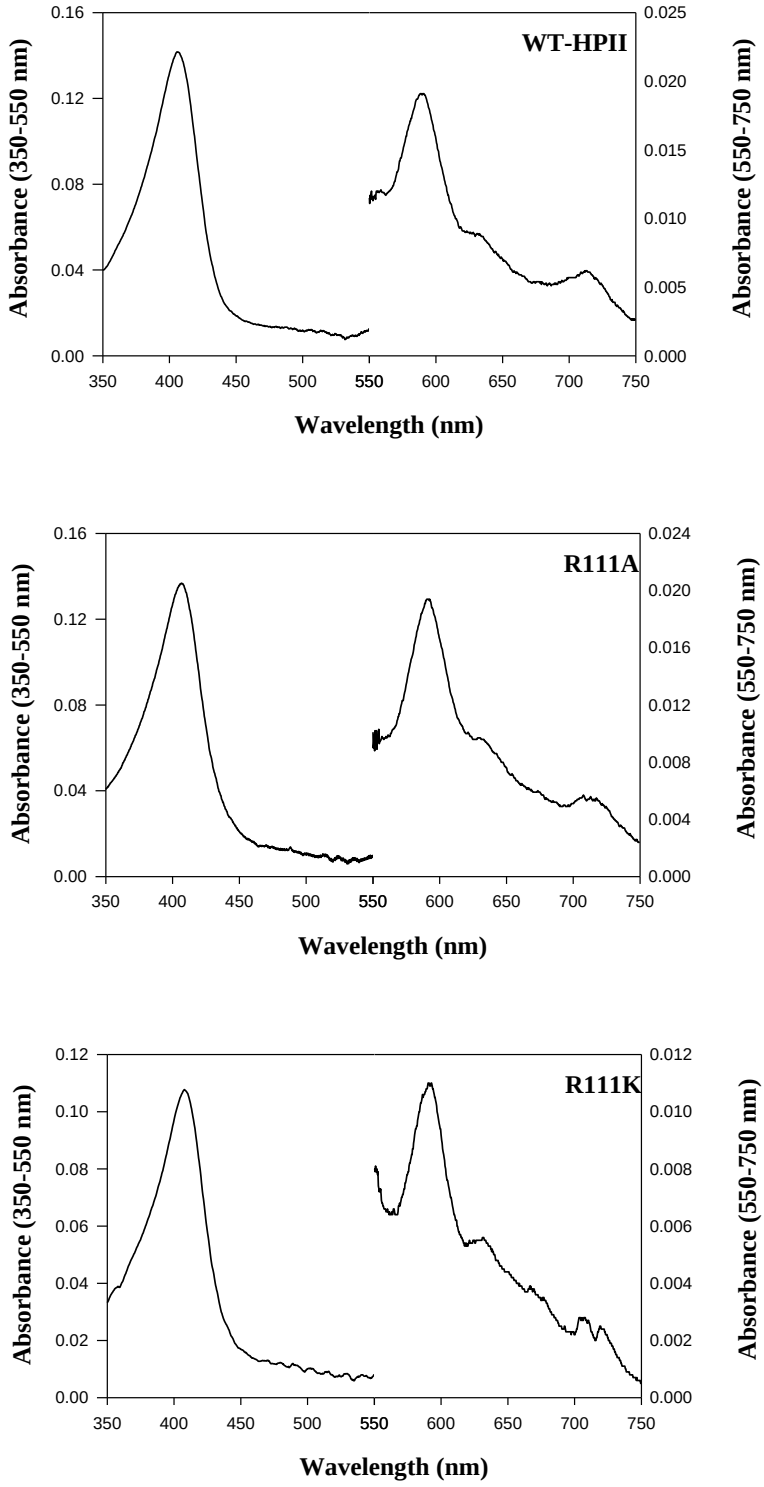

Figure 3.1.2. Absorption spectra of WT-HPII and its variants. The left axis corresponds to the absorbance values between wavelengths 350-550 nm and the right axis to the wavelength range between 550-750 nm.

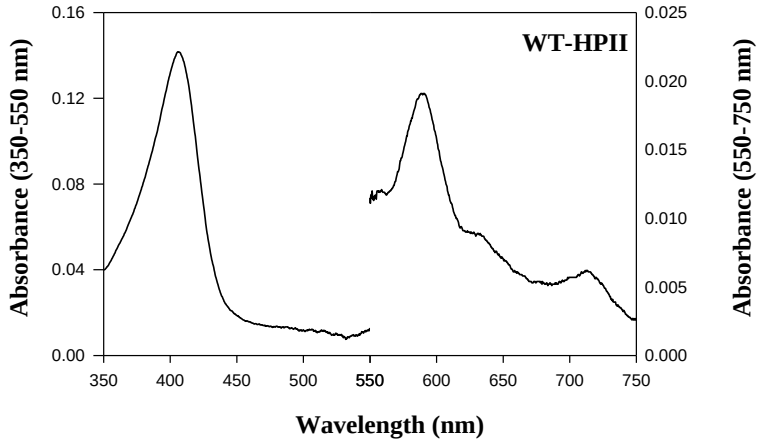

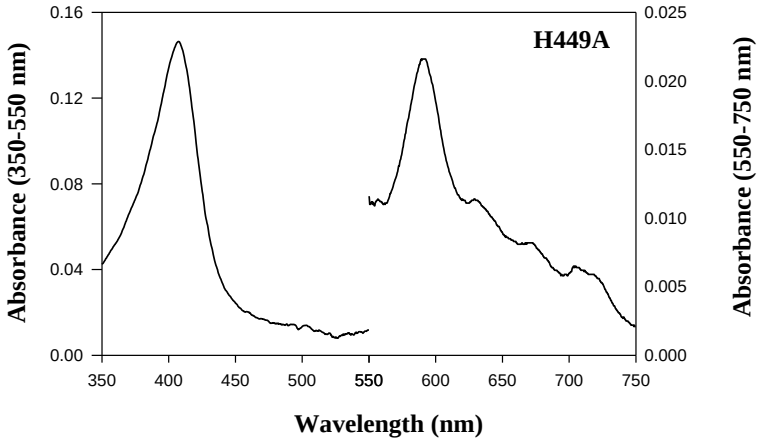

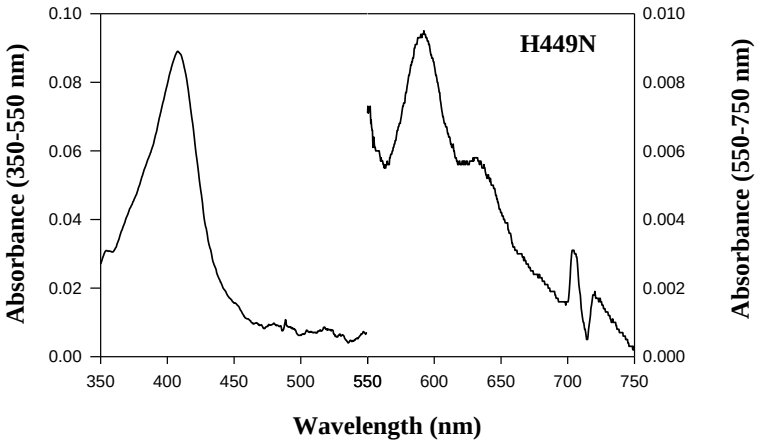

Figure 3.1.2. Continued...

Table 3.1.1. Comparison of observed absorbance maxima, A_{407}/A_{280} ratio and catalase specific activities of purified WT-HPII and its variants.

Variants	**Soret (nm)**	**R_z[a] (A_{407}/A_{280})**	**Specific activity (U/mg)**
WT-HPII	406	0.94	21000 ± 1400
R111A	407	0.88	19500 ± 1000
R111K	407	0.86	22000 ± 500
H449A	407	0.86	20500 ± 1400
H449N	408	0.82	21000 ± 2100

[a] The theoretical A_{407}/A_{280} ratio is 1.0.

Assays for determining specific activity were performed in triplicate and results were averaged.

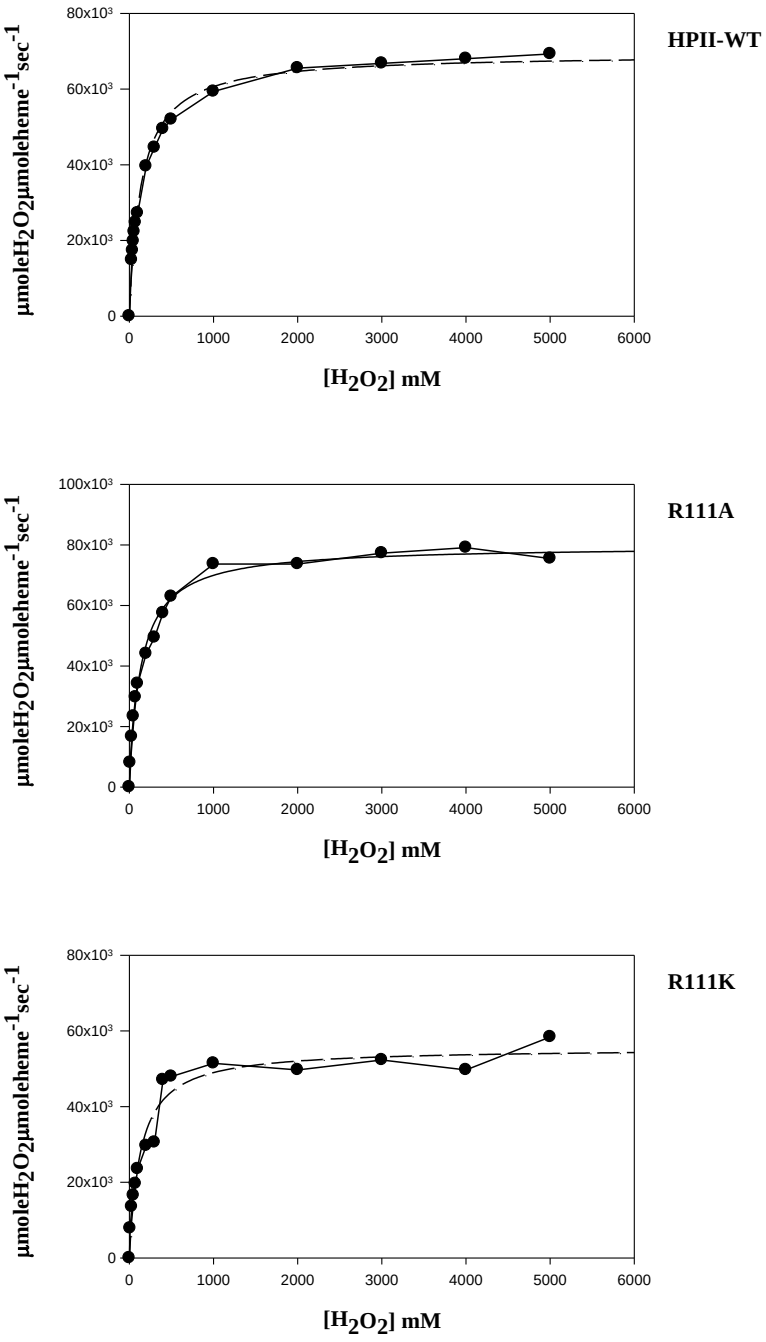

Figure 3.1.3. Effect of H_2O_2 concentration on reaction velocity of WT-HPII and its variants. In all panels the solid line represents the observed data and the dashed line represents the theoretical Michaelis-Menten curve calculated from constants determined at low H_2O_2 concentration (Table 3.1.2). Note the difference in the scales of Y-axis.

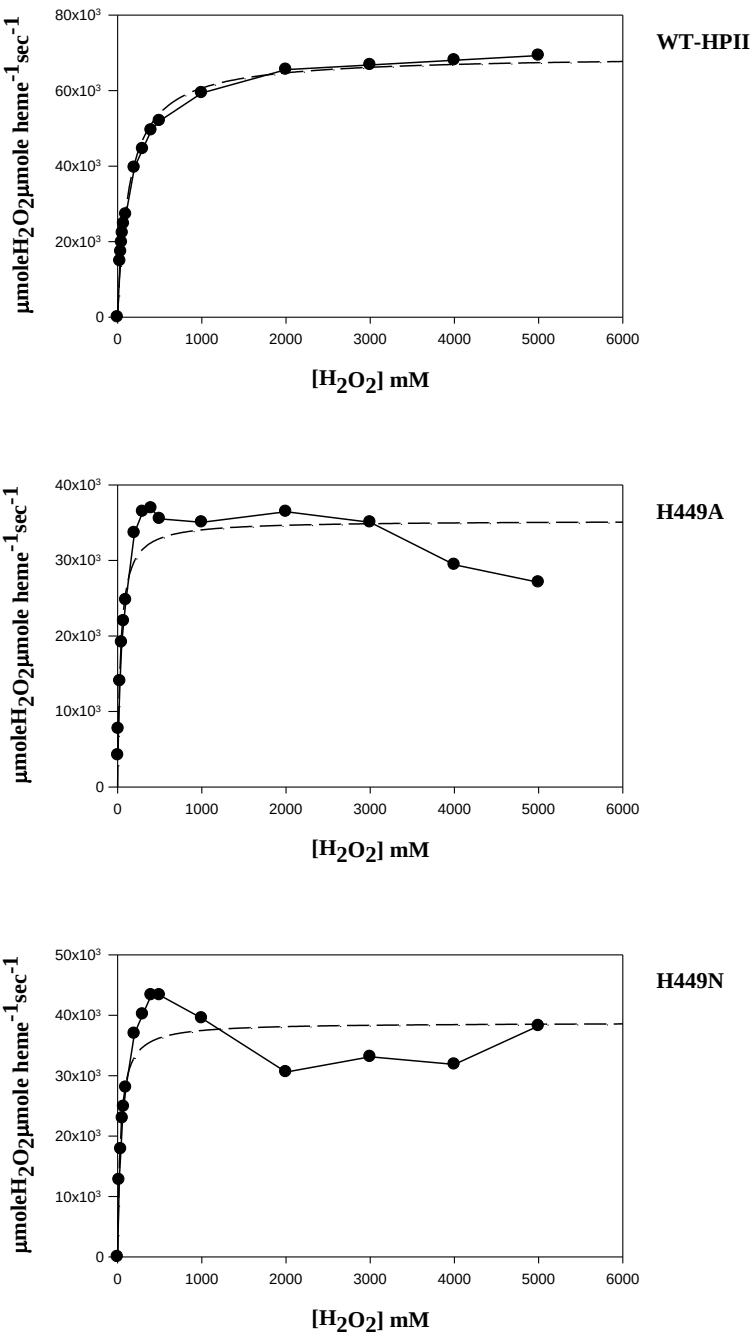

Figure 3.1.3. Continued…

Table 3.1.2. Comparison of the observed kinetic parameters of WT-HPII and its variants.

Variants	**Observed**		**k_{cat}/K_M ($M^{-1}sec^{-1}$)**
	k_{cat} (sec^{-1})	K_M (app)[a]	
WT-HPII	70000	145	0.5×10^6
R111A	80000	140	0.6×10^6
R111K	55470	132	0.4×10^6
H449A	35300	40	0.9×10^6
H449N	38800	35	1.1×10^6

[a] K_M (apparent), H_2O_2 concentration at $V_{max}/2$, mM.

3.1.3. Effect of catalase inhibitors on WT-HPII and variants

Heme catalases are sensitive to a number of small molecules including cyanide, azide and hydroxylamine. Concentrations of these inhibitors required for 50% inhibition varies considerably among catalases (Switala and Loewen, 2002), most likely because of differences in channel architecture, but also because of the nature of the complex and whether it is at the iron active site or elsewhere. To characterize further the variants and compare the changes, if any, from WT-HPII, the effect of these inhibitors on the catalase activity of variants R111A, R111K, H449A, and H449N was investigated (Figures 3.1.4, 3.1.5 and 3.1.6). The concentrations of inhibitors required for 50% reduction in catalytic activity are summarized in Table 3.1.3, and none of the variants differed substantially from WT-HPII except R111K, which requires twice the concentration of NH_2OH for 50% inhibition compared to WT enzyme. Thermostablity of these variants was also analyzed and compared with WT-HPII which has a T_m of 82 °C (Switala et al., 1999). The variants were incubated at 80 °C for different time periods and assayed for catalase activity, and the times required for 50% inactivation are listed in Table 3.1.3. All variants were less thermostable than WT-HPII (Figure 3.1.7).

3.1.4. Structural characterization of R111K and H449A

Crystallization of the four purified HPII variants was attempted according to the protocol outlined in Chapter 2. However, good quality diffracting crystals were successfully obtained only for R111K and H449A variants. Data sets for both R111K and H449A were collected using the in-house X-ray facility and refined to about 2.0 Å. Data collection for WT-HPII was carried out at the Canadian Light Source in Saskatoon, Canada using synchrotron beam line CMCF 08ID-1. The diffraction data set refined to 1.5 Å. Data

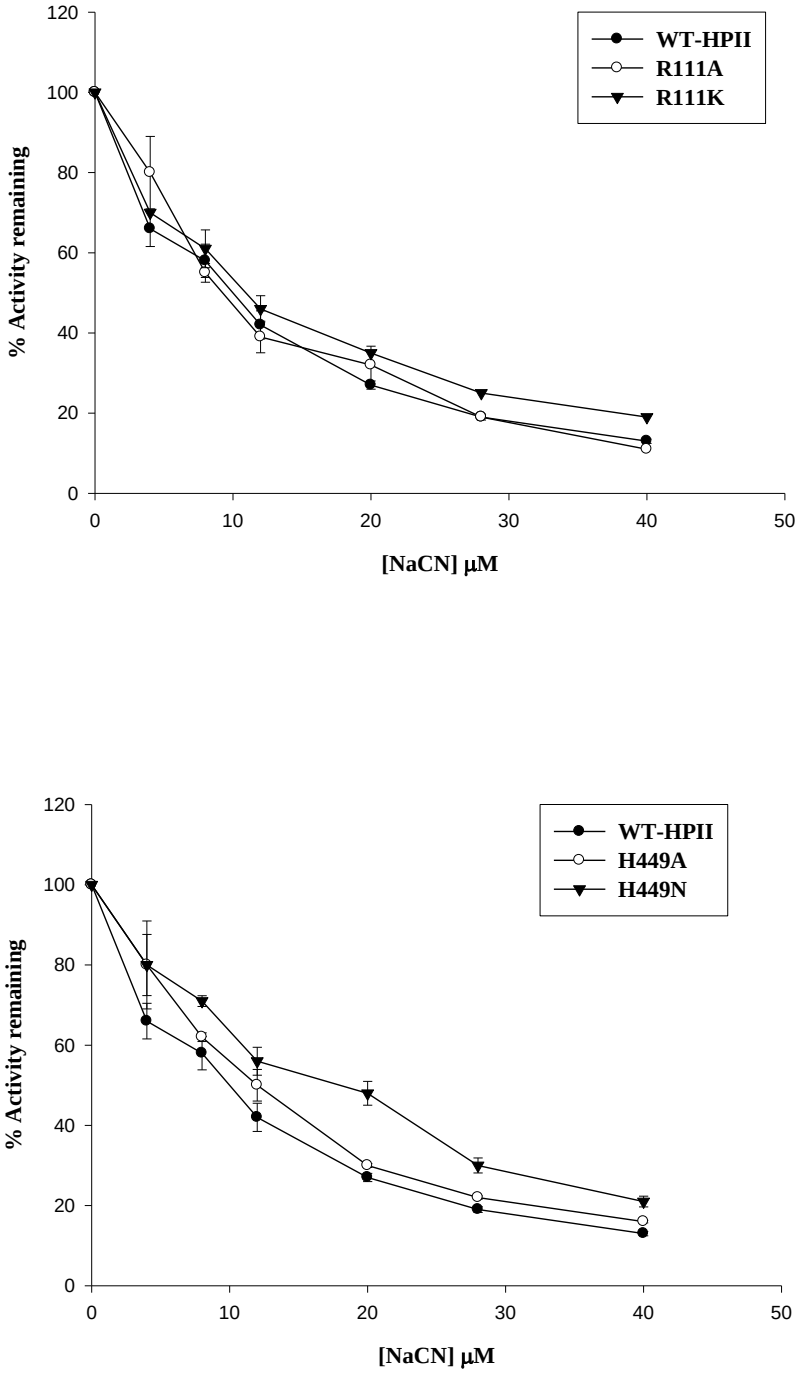

Figure 3.1.4. Effect of sodium cyanide (NaCN) on WT-HPII and its variants. Each enzyme was incubated with inhibitor for 1 minute in 50 mM KPi buffer at 37 °C before starting the reaction by adding H_2O_2. All assays were repeated in triplicate and the results were averaged.

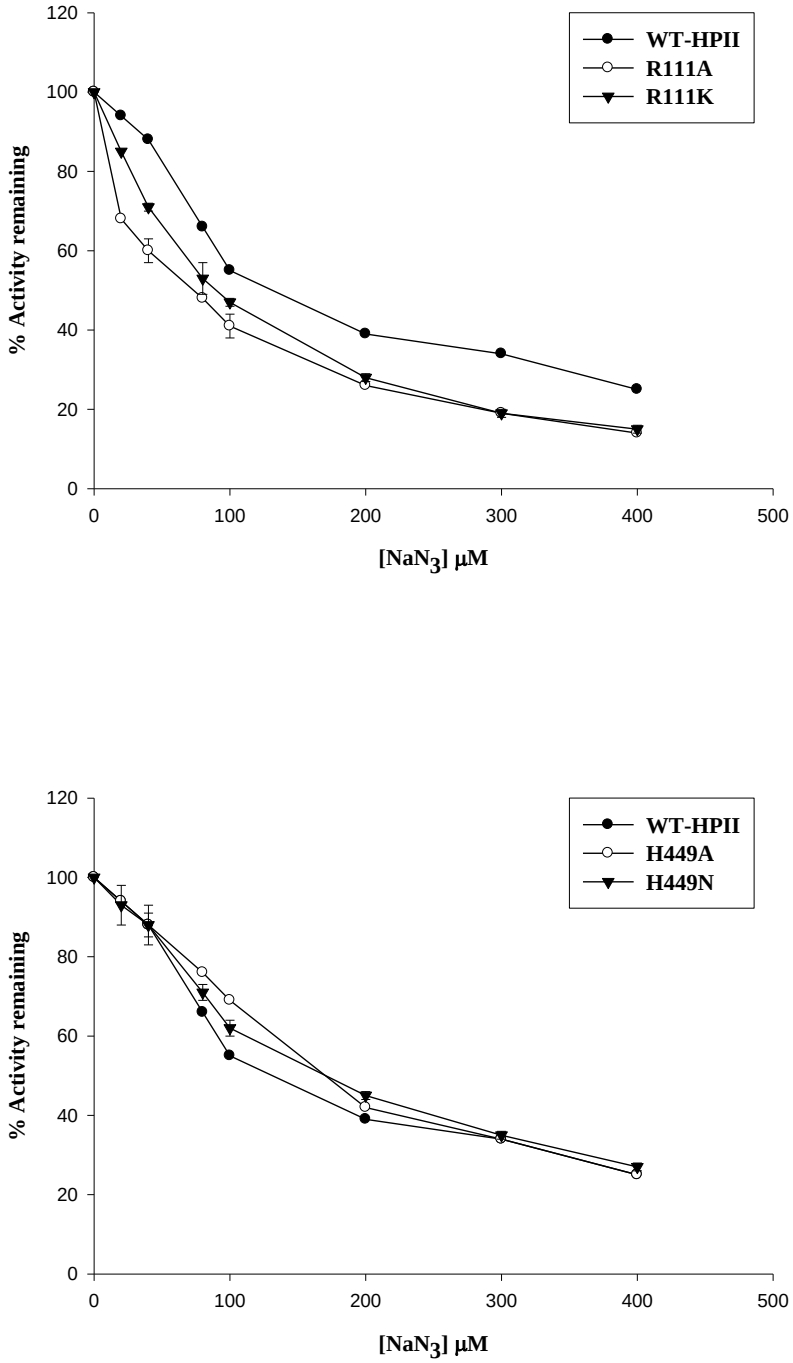

Figure 3.1.5. Effect of sodium azide (NaN_3) on WT-HPII and its variants. Each enzyme was incubated with inhibitor for 1 minute in 50 mM KPi buffer at 37 °C before starting the reaction by adding H_2O_2. All assays were repeated in triplicate and the results were averaged.

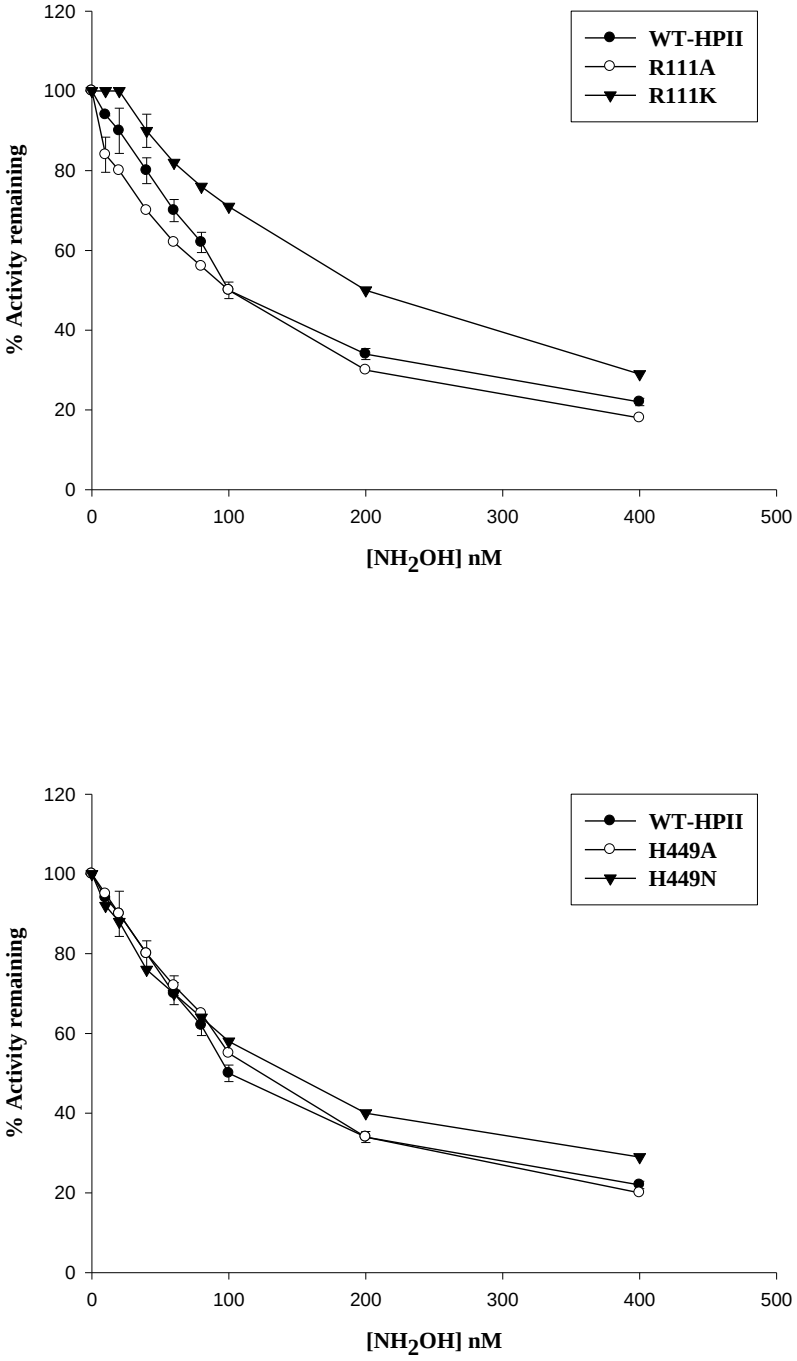

Figure 3.1.6. Effect of hydroxylamine (NH_2OH) on WT-HPII and its variants. Each enzyme was incubated with inhibitor for 1 minute in 50 mM KPi buffer at 37 °C before starting the reaction by adding H_2O_2. All assays were repeated in triplicate and the results were averaged.

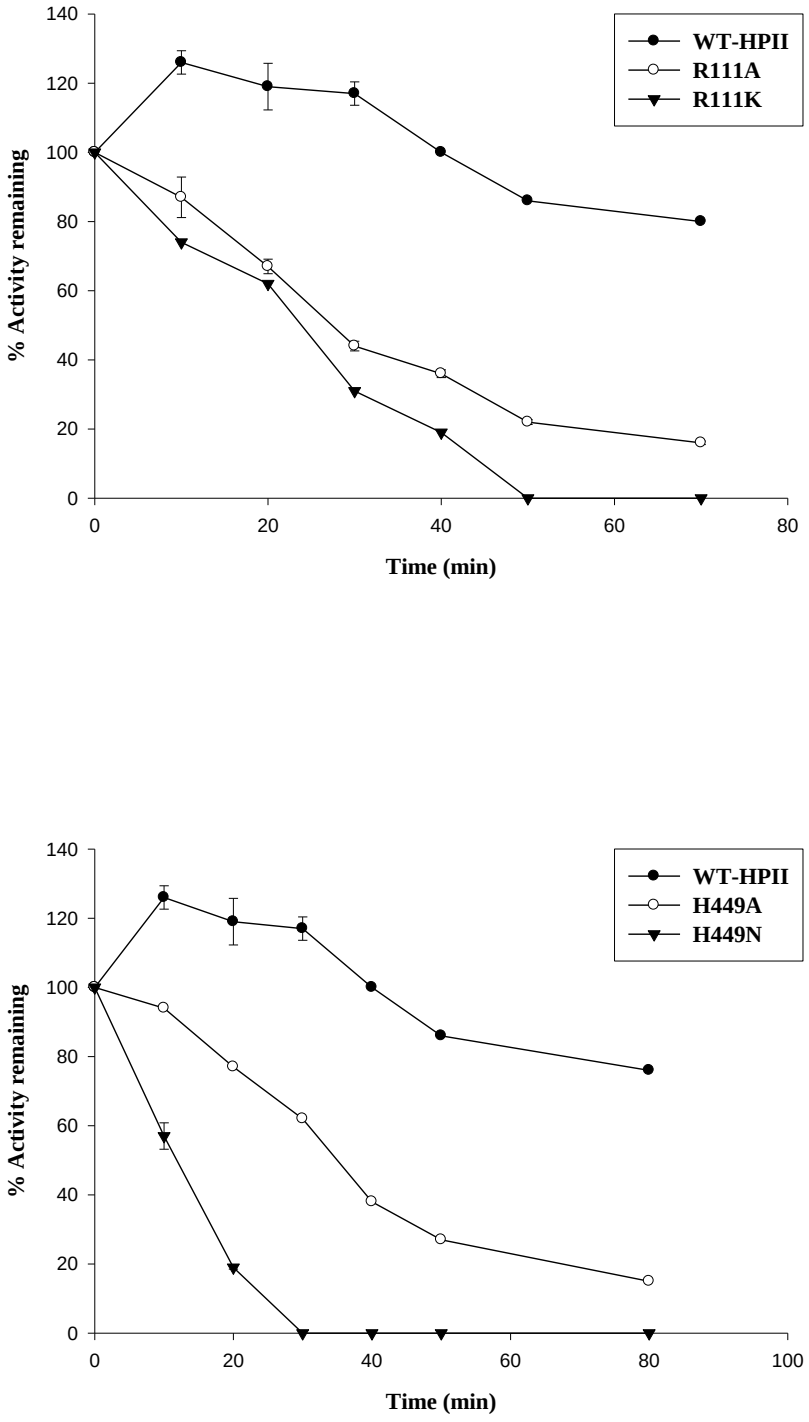

Figure 3.1.7. Comparison of thermostability at 80 °C of WT-HPII and its variants. Each enzyme was incubated at 80 °C for different time intervals and then assayed for catalase activity. All assays were repeated in triplicate and the results were averaged.

Table 3.1.3. Sensitivity of WT-HPII and its variants towards catalase inhibitors and incubation at 80 °C[*].

Variants	Inhibitor concentration at 50% inhibition[a]			Time to 50% inhibition at 80 °C (min)[b]
	NaCN (μM)	NaN_3 (μM)	NH_2OH (nM)	
WT-HPII	11 ± 1.0	140 ± 10	110 ± 10	> 80
R111A	10 ± 0.7	75 ± 5.0	105 ± 7	25 ± 0
R111K	11 ± 1.5	90 ± 7.0	200 ± 0	20 ± 0
H449A	12 ± 1.0	160 ± 15	120 ± 0	30 ± 0
H449N	16 ± 2.5	160 ± 15	160 ± 0	15 ± 0

[a] Enzyme was incubated with inhibitor for one minute before adding H_2O_2.

[b] Enzyme was incubated at 80 °C for different time intervals.

[*]All assays were repeated in triplicate and results were averaged.

Table 3.1.4. Data collection and structural refinements statistics of WT-HPII and its variants R111K and H449A.

	WT-HPII	H449A	R111K
A. Data collection statistics			
Space group	$P2_1$	$P2_1$	$P2_1$
Unit cell parameters			
a (Å)	93.53	93.37	93.37
b (Å)	132.78	133.02	132.93
c (Å)	122.13	122.11	122
α, β,ϒ (deg.)	90, 109.52, 90	90, 109.74, 90	90, 109.7, 90
Resolution range (Å)	29.38-1.54 (1.62-1.54)[a]	41.37-2.10 (2.21-2.10)	41.34-2.05 (2.16-2.05)
Total no. of reflections	1,534,237 (201,240)	353,272 (54,535)	303,128 (39,513)
Unique reflections	404,090 (56,801)	145,780 (23,290)	166,643 (23,095)
Completeness (%)	97.8 (94.3)	89.4 (97.7)	95.3 (90.5)
$\langle I/\sigma(I)\rangle$	15.9 (6.5)	14.5 (7.3)	5.3 (2.1)
R_{merge}[b]	0.056 (0.174)	0.040 (0.101)	0.101 (0.405)
B. Refinement statistics			
Resolution range (Å)	115.11-1.54	114.93-2.10	114.86-2.05
% age observed	97.7	89.2	95.0
R_{work}[c] (%)	13.65	13.59	15.12
R_{free}[d] (%)	16.96	20.24	21.82
No. of non-hydrogen atoms			
proteins	23,052	22,964	22,967
hemes	176	176	176
waters	3,508	3,133	3,027
rms deviations			
bond lengths (Å)	0.02	0.02	0.02
bond angles (deg.)	2.34	1.84	1.80
Average B factor ($Å^2$)			
main chain	12.16	14.51	15.80
side chain	14.30	15.34	16.90
water	25.30	22.80	23.30

[a] Values in parentheses correspond to the highest-resolution shell.

[b] $R_{merge} = \Sigma_{hkl} \Sigma_j |I_{hklj} - \langle I_{hkl}\rangle| / \Sigma_{hkl} \langle I_{hkl}\rangle$, where j extends to all the observed *hkl* symmetry related reflections.

[c] $R_{work} = \Sigma||F_{obs}|-|F_{calc}|| / \Sigma|F_{obs}|$.

[d] R_{free} is as for R_{work} but calculated for a test set,comprising 5% of reflections, that was not used in the refinement.

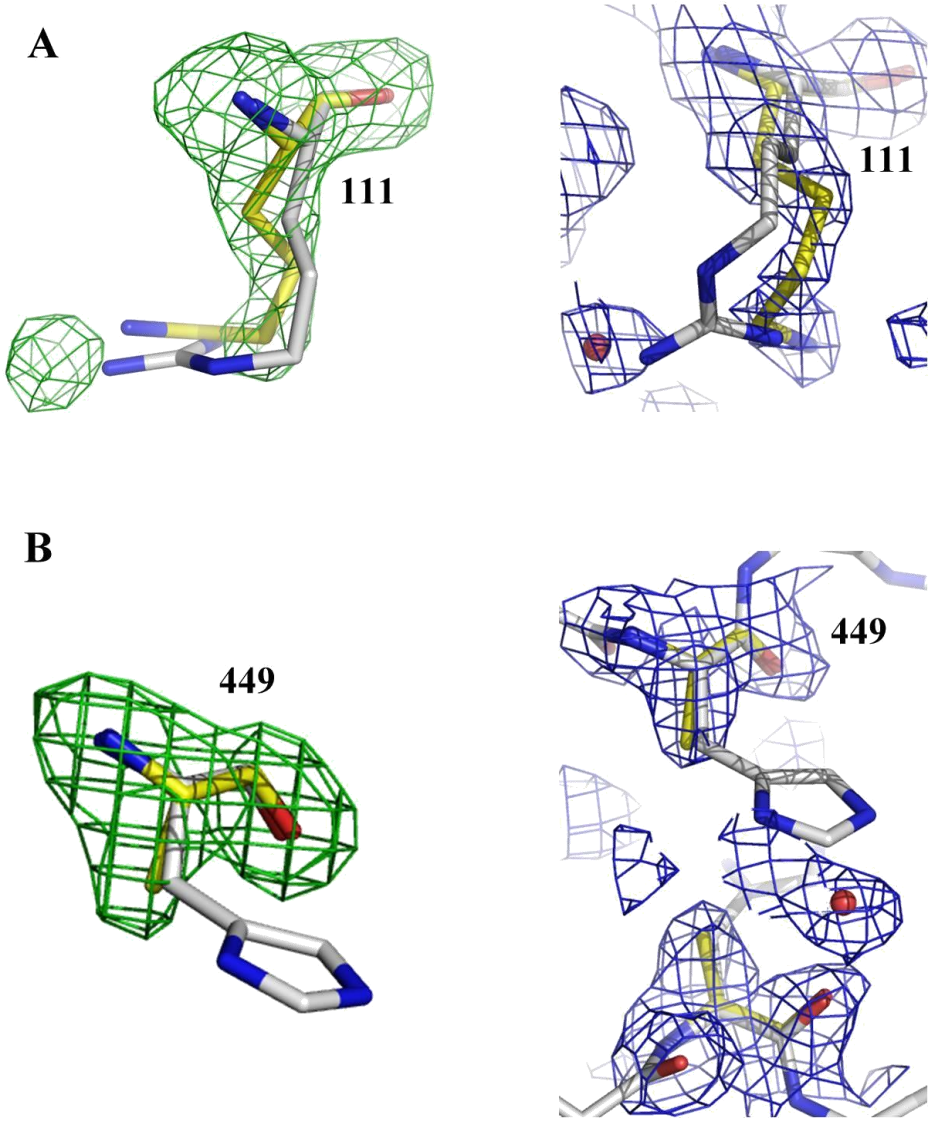

Figure 3.1.8. Stereoview of the F_o-F_c (green) and $2F_o$-F_c (blue) electron density maps of the site of mutation in the HPII variants R111K and H449A. F_o-F_c maps were generated without the respective atoms in the model. Panel A: F_o-F_c and $2F_o$-F_c electron density maps with sticks showing the residue at 111. Panel B: F_o-F_c and $2F_o$-F_c maps with sticks showing the residue at 449. Yellow sticks represent the mutated residues in the variants while gray sticks represent the residue in WT-HPII. The $2F_o$-F_c density is modelled at 1.0 σ and the F_o-F_c density at 3.0 σ. Waters are depicted as red spheres.

Table 3.1.5. Comparison of B values of arginine and lysine side chain atoms in WT-HPII and R111K variant, respectively in four subunits. A, B, C and D represents the individual subunits.

Atoms	**Arginine in native HPII**				**Lysine in R111K**			
	A	B	C	D	A	B	C	D
CA	6.27	4.31	6.18	4.48	10.38	10.81	10.61	9.89
CB	5.59	6.41	6.49	5.23	10.21	10.73	8.96	10.43
CG	7.21	6.81	7.84	6.07	18.75	18.16	15.78	18.01
CD	7.77	7.08	6.03	6.31	20.02	23.25	21.87	22.75
NE	7.02	7.97	6.79	5.64	-	-	-	-
CZ	8.73	6.62	8.01	7.28	-	-	-	-
NH1	8.78	7.34	7.42	9.16	-	-	-	-
NH2	7.32	8.16	7.55	8.02	-	-	-	-
CE	-	-	-	-	26.15	27.11	23.21	26.84
NZ	-	-	-	-	30.55	30.49	19.49	29.33

collection and refinement statistics are listed in Table 3.1.4.

The electron density maps clearly define the main chain and side chain atoms of 2904 amino acids, four heme groups and 3027-3508 waters in four subunits. As in the native structure, the N-terminal 28 residues are not visible, but the maps generally show complete continuity from Ser28 to Ala753 in all four subunits of R111K and H449A. No change in either the overall structure or distribution of water in the main channel was observed in either of the variants compared to WT-HPII. The electron density in the F_o-F_c omit maps calculated with the residues omitted from the model confirm the presence of the mutated residues, Lys111 and Ala449 (Figure 3.1.8). However, the maps and B-factors reveal that Lys111 is more disordered than Arg111 in WT-HPII (Figure 3.1.8 and Table 3.1.5). In both R111K and H449A, heme *d* is clearly evident and His392 is 100% covalently linked to Tyr415 (Figure not shown; refer to Murshudov et al., 1996 and Bravo et al., 1997) suggesting that the enzyme had undergone several rounds of the catalytic cycle to complete the two post-translational modifications.

3.2. Effect of changes to His119 at the core of subunit-subunit interactions in the central cavity

3.2.1. Introduction

Catalases in general and large subunit catalases in particular, display complex intersubunit interactions. The long N-terminal arm of each subunit passes through a loop formed by the wrapping domain of an adjacent subunit and leads to the heme pocket of another neighbouring subunit giving rise to a large number of interactions between the residues of the other subunits. The role of these complex intersubunit interactions, if anything beyond that of structure stabilization, is not well understood. Furthermore interactions between residues within the range of hydrogen bonding distance near or around the heme could be influential in modulating enzyme catalysis, protein stability and even heme modification and orientation in the case of *E. coli* HPII.

His119 is located towards the central cavity of the molecule about 11 Å away from the heme. In addition, His119 of subunit A in the WT-HPII is 2.74 and 2.77 Å, respectively from Ser421 and Asp417 of subunit D and makes hydrogen or ionic bond interactions with these residues (Figure 3.2.1). Also Asp417 of subunit D is in close association with Asp118 of subunit A (2.4 Å) both of which are the part of a bridge between hemes in the adjacent subunits that includes the following components (where the superscript letters denote the subunit identity):

$$Heme^{A}\text{-}S414^{A}\text{-}D118^{D}\text{-}D417^{A}\text{-}H_2O\text{-}D417^{B}\text{-}D118^{C}\text{-}S414^{B}\text{-}Heme^{B}$$

Because of its close proximity to the reaction center and to these structurally and functionally important residues, the role of His119 was investigated.

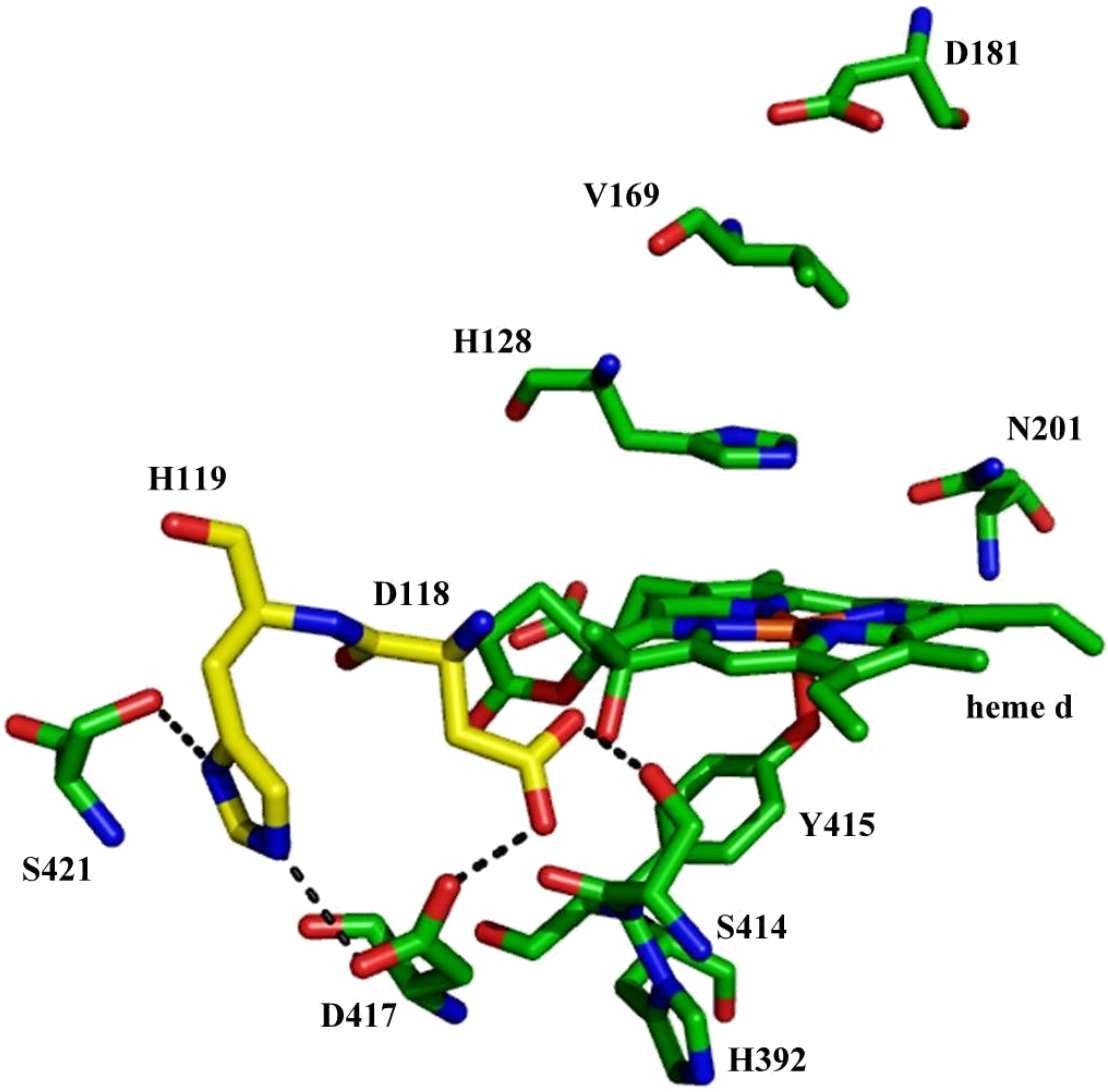

Figure 3.2.1. View of the region showing interaction of His119 with the residues of other subunits adjacent to the heme. Green sticks represent the residues from subunit A whereas yellow sticks represent residues from subunit D. Interactions between residues are shown with black dashed lines.

3.2.2. Construction and characterization of H119 variants

Two variants of HPII, H119A and H119N, were constructed and purified as outlined in Chapter 2. Both variants accumulated as fully folded protein and revealed similar electrophoretic mobilities on the SDS-PAGE giving a predominant band with an apparent molecular mass of ~ 84 kDa (Figure 3.2.2). An additional thin band at ~ 40 kDa in H119A was attributed to glycerol kinase which is notoriously difficult to remove from HPII preparations.

A comparison of absorption spectra of WT-HPII and the variants H119A and H119N is contained in Figure 3.2.3. and characterization data are summarized in Table 3.2.1. No major change in the Soret band was observed for either H119A and H119N compared to WT-HPII and the spectra of both variants contained the strong band at 590 nm characteristic of heme *d*, albeit with a small shoulder at 630 nm indicating the presence of a small amount of heme *b*. The R_z of H119A is slightly lower compared to WT-HPII and H119N which is attributable to the small amount of glycerol kinase.

The specific activities of H119A and H119N are similar to that of WT-HPII (Table 3.2.1) and the V vs [S] plots reveal only minor differences compared to WT-HPII (Figure 3.2.4) that suggested H119A is more sensitive to the damaging effects of H_2O_2. The kinetic data for the WT enzyme and variants H119A and H119N are listed in Table 3.2.2 for comparison. Variant H119A exhibited reduced turnover compared to WT-HPII, whereas H119N exhibited a two times higher turnover with similar affinity for H_2O_2 in comparison to WT-HPII.

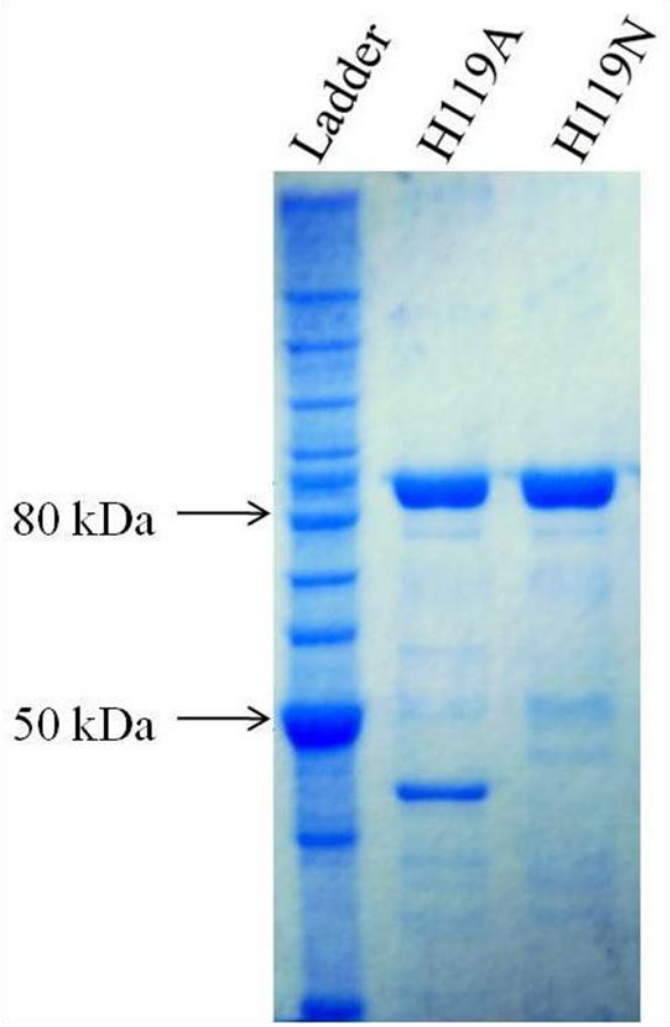

Figure 3.2.2. SDS -PAGE analysis of purified WT-HPII and its variants. Approximately 2.0 µg of protein were loaded on an 8% polyacrylamide gel and stained with Coomassie brilliant blue after electrophoretic separation.

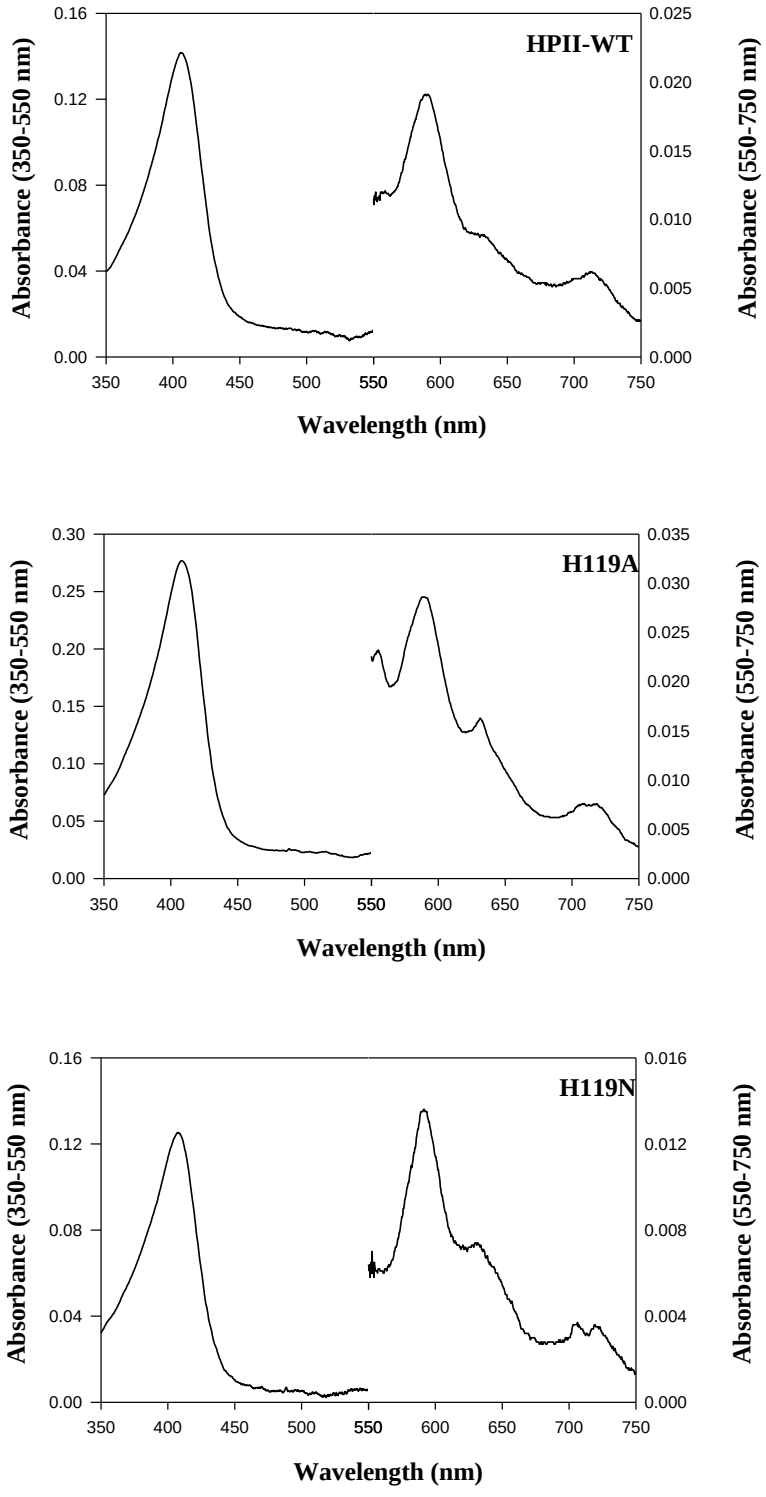

Figure 3.2.3. Absorption spectra of WT-HPII and its variants. The left axis corresponds to the absorbance values between wavelengths 350-550 nm and the right axis to the wavelength range between 550-750 nm.

Table 3.2.1. Comparison of observed absorbance maxima, A_{407}/A_{280} ratio and catalase specific activities of purified WT-HPII and its variants.

Variants	**Soret (nm)**	**R_z[a] (A_{407}/A_{280})**	**Specific activity (U/mg)**
WT-HPII	406	0.94	21000 ± 1400
H119A	408	0.80	18500 ± 220
H119N	408	0.86	23750 ± 1760

[a] The theoretical A_{407}/A_{280} ratio is 1.0.

Assays for determining specific activity were performed in triplicate and results were averaged.

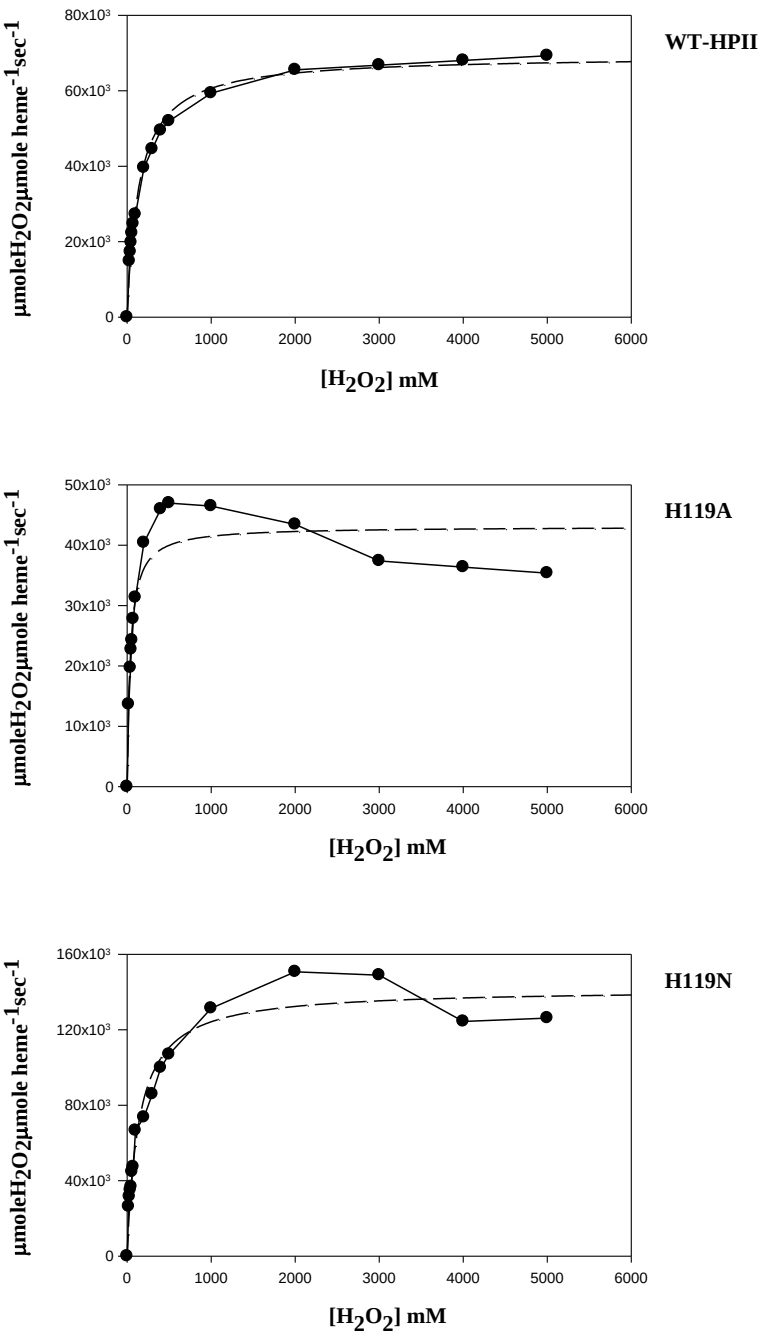

Figure 3.2.4. Effect of H_2O_2 concentration on reaction velocity of WT-HPII and its variants. In all panels the solid line represents the observed data and the dashed line represents the theoretical Michaelis-Menten curve calculated from constants determined at low H_2O_2 concentration (Table 3.1.2).

Table 3.2.2. Comparison of the observed kinetic parameters of WT-HPII and its variants.

Variants	**Observed**		**k_{cat}/K_M ($M^{-1}sec^{-1}$)**
	k_{cat} (sec^{-1})	K_M (app)[a]	
WT-HPII	70000	145	0.5×10^6
H119A	43100	40	1.0×10^6
H119N	141680	141	1.0×10^6

[a] K_M (apparent), H_2O_2 concentration at $V_{max}/2$, mM.

3.2.3. Effect of inhibitors

The concentrations of inhibitor required for 50% inhibition and the length of time required for 50% inactivation at 80 °C are included in Table 3.2.3. Comparison of kinetics of inactivation for WT-HPII and variants H119A and H119N (Figures 3.2.5 and 3.2.6) reveals a broad range in concentrations required for 50% inhibition. Both H119A and H119N are less sensitive to cyanide and hydroxylamine than is WT-HPII, but they exhibit similar sensitivity to azide. In addition, H119A and H119N suffer more rapid inactivation at 80 °C (Table 3.2.3 and Figure 3.2.6).

3.2.4. Structure of H119A and H119N variants

To investigate in more detail the differences in biochemical properties between the variants and WT-HPII, their crystal structures were determined. The diffraction data for the crystals of H119A and H119N were collected using synchrotron beam line CMCF 08ID-1 at the Canadian Light Source in Saskatoon, Canada. Data collection and structure refinement statistics are outlined in Table 3.2.4. The diffraction data sets of H119A and H119N refined to 1.5 and 1.7 Å respectively. The electron density maps defined the main chain and side chain atoms of 2904 amino acids, four heme groups, one in each subunit, and 3634 and 3188 water molecules in H119A and H119N respectively. The maps showed clear continuity in each of the four subunits over the complete length from Ser28 to Ala753. The F_o-F_c omit electron density maps confirmed the presence of the expected mutation at position 119 in both variants (Figures 3.2.7 A and 3.2.8 A).

In both H119A and H119N the major change is observed in the vicinity of the site of mutation. The histidine side chain at 119 in the WT-HPII is replaced by an alanine and three water molecules in H119A (Figure 3.2.7 A). The side-chain of Ser421 in the vicinity of

A

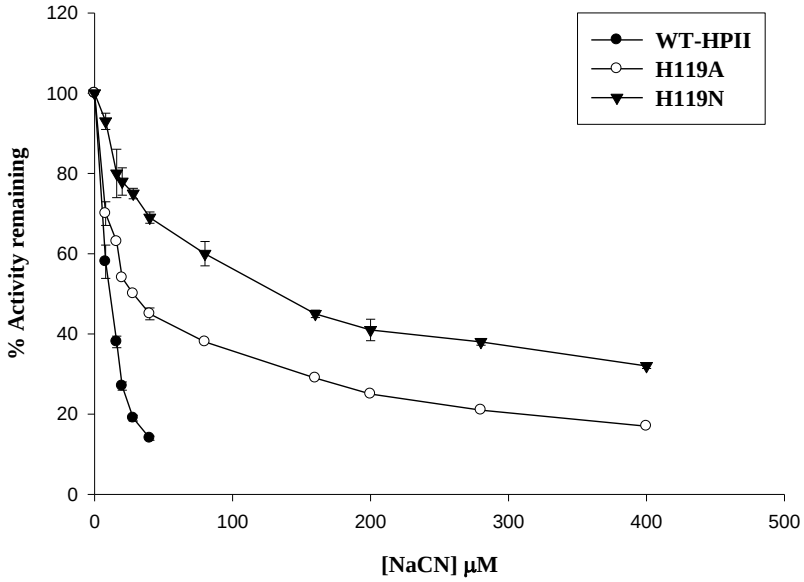

B

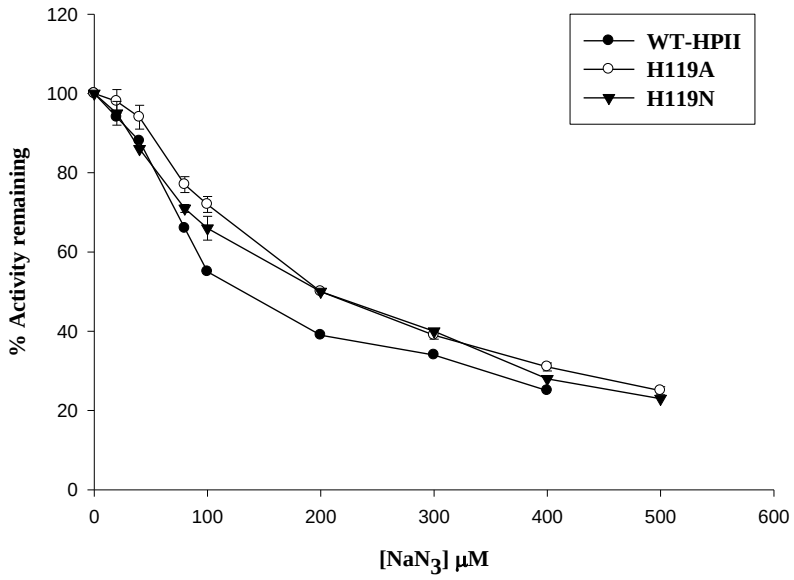

Figure 3.2.5. Effect of NaCN (A) and NaN_3 (B) on WT-HPII and its variants. Each enzyme was incubated with the inhibitor for 1 minute in 50 mM KPi buffer at 37 °C before starting the reaction by adding H_2O_2. All assays were repeated in triplicate and the results were averaged.

A

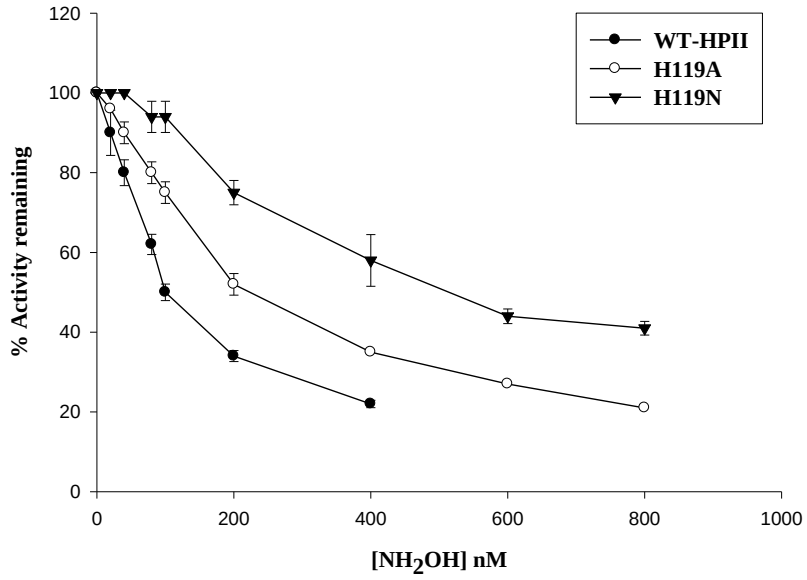

B

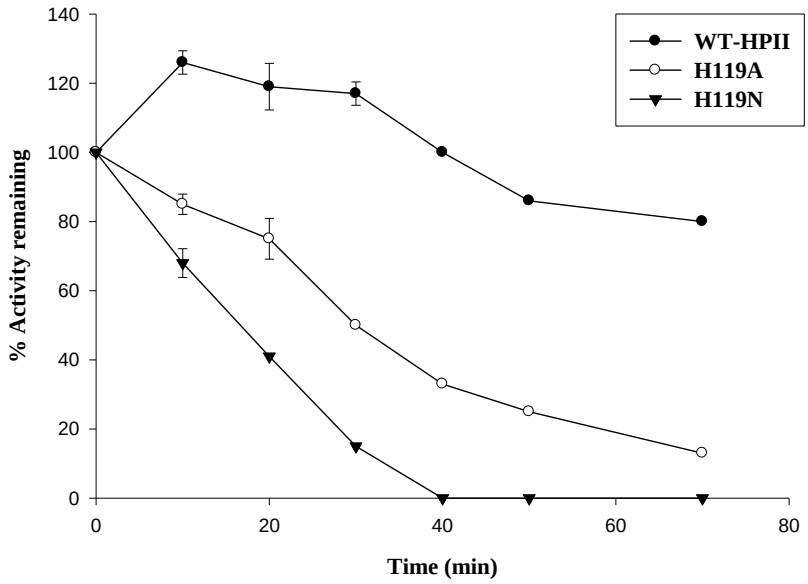

Figure 3.2.6. Effect of NH_2OH (A) on and comparison of thermostability at 80 °C (B) of WT-HPII and its variants. In A, each enzyme was incubated with inhibitor for 1 min in 50 mM KPi at 37 °C before adding H_2O_2. In B, the enzymes were incubated at 80 °C for different time intervals. All assays were repeated in triplicate and the results averaged.

Table 3.2.3. Sensitivity of WT-HPII and its variants towards catalase inhibitors and incubation at 80 °C[*].

Variants	**Inhibitor concentration at 50% inhibition[a]**			**Time to 50% inhibition at 80°C (min)[b]**
	NaCN (μM)	NaN_3 (μM)	NH_2OH (nM)	
WT-HPII	11 ± 1.0	140 ± 10	110 ± 10	>80
H119A	30 ± 2.0	200 ± 0	210 ± 7.0	35 ± 0
H119N	120 ± 14	200 ± 0	470 ± 20	18 ± 3

[a] Enzyme was incubated with inhibitor for one minute before adding H_2O_2.

[b] Enzyme was incubated at 80 °C for different time intervals.

[*]All assays were repeated in triplicate and results were averaged.

Table 3.2.4. Data collection and structural refinement statistics for HPII variants H119A and H119N.

	H119A	H119N
A. Data collection statistics		
Space group	$P2_1$	$P2_1$
Unit cell parameters		
a (Å)	93.49	93.40
b (Å)	132.91	133.03
c (Å)	122.29	122.63
α, β, ϒ (deg.)	90, 109.51, 90	90, 109.42, 90
Resolution range (Å)	37.22-1.54 (1.63-1.54)[a]	37.03-1.70 (1.79-1.70)
Total no. of reflections	1,524,628 (212,108)	634,231 (74,768)
Unique reflections	407,796 (58,448)	277,117 (37,820)
Completeness (%)	99.4 (97.8)	90.0 (84.2)
$\langle I/\sigma(I)\rangle$	9.8 (3.9)	7.5 (2.8)
R_{merge}	0.080 (0.262)	0.075 (0.214)
B. Refinement statistics		
Resolution range (Å)	132.91-1.54	133.03-1.70
% age observed	99.4	89.5
R_{work} (%)	13.77	13.97
R_{free} (%)	17.05	18.38
No. of non-hydrogen atoms		
proteins	23,019	23,097
hemes	172	172
waters	3,634	3,188
rms deviations		
bond lengths (Å)	0.02	0.02
bond angles (deg.)	2.37	2.06
Average B factor ($Å^2$)		
main chain	11.59	16.54
side chain	13.54	18.36
water	24.0	27.2

[a] Values in parentheses correspond to the highest-resolution shell.

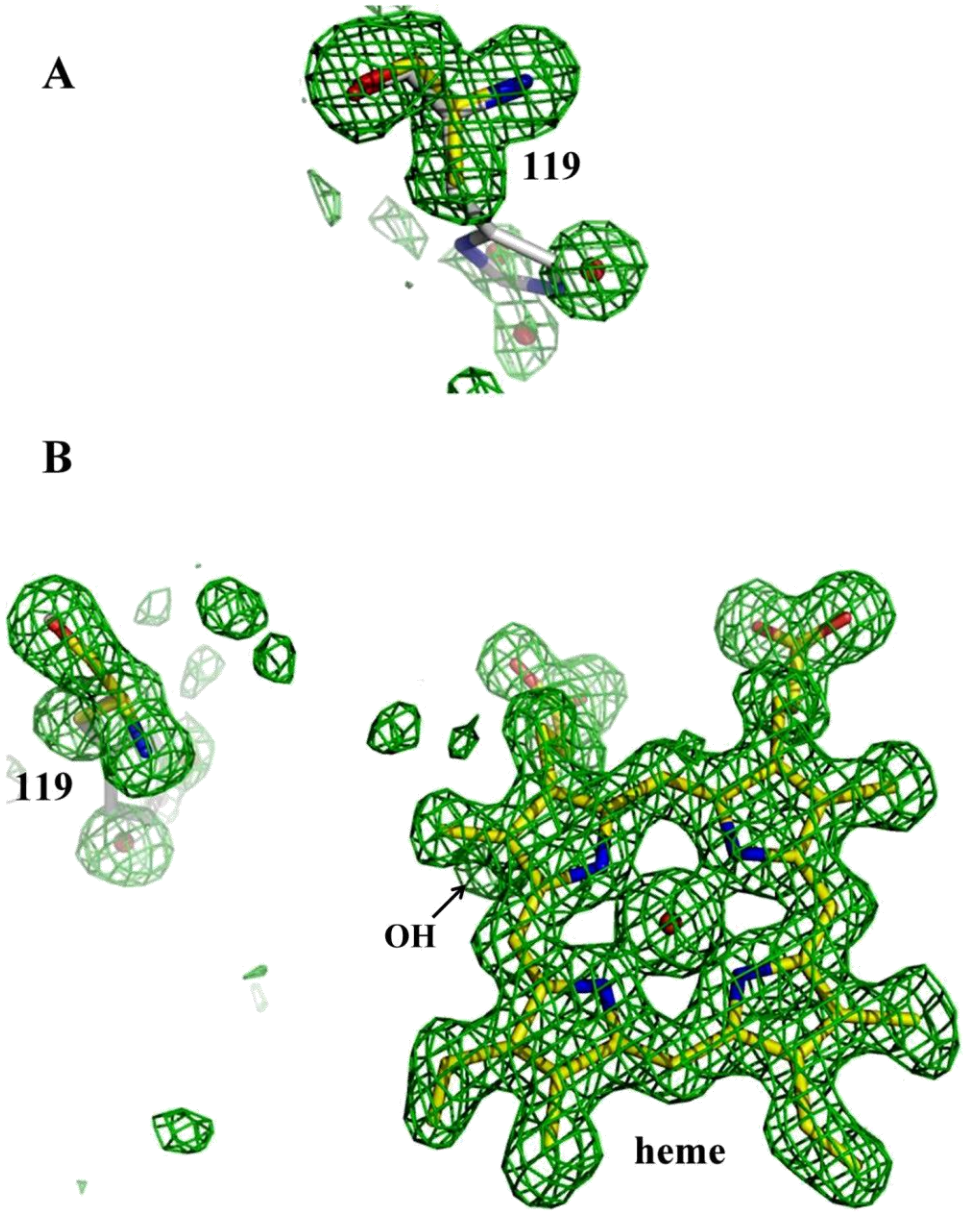

Figure 3.2.7. View of the F_o-F_c (green) electron density maps of the region around Ala119 and heme calculated without the respective atoms in the model, and the appropriate model was superimposed for illustration Panel A: F_o-F_c electron density map around Ala119. Panel B: F_o-F_c electron density map illustrating heme species. Waters are depicted as red spheres. Yellow sticks represent the residues of variant H119A whereas grey sticks represent the residues of WT-HPII. F_o-F_c electron density maps were modeled at 3.0 σ.

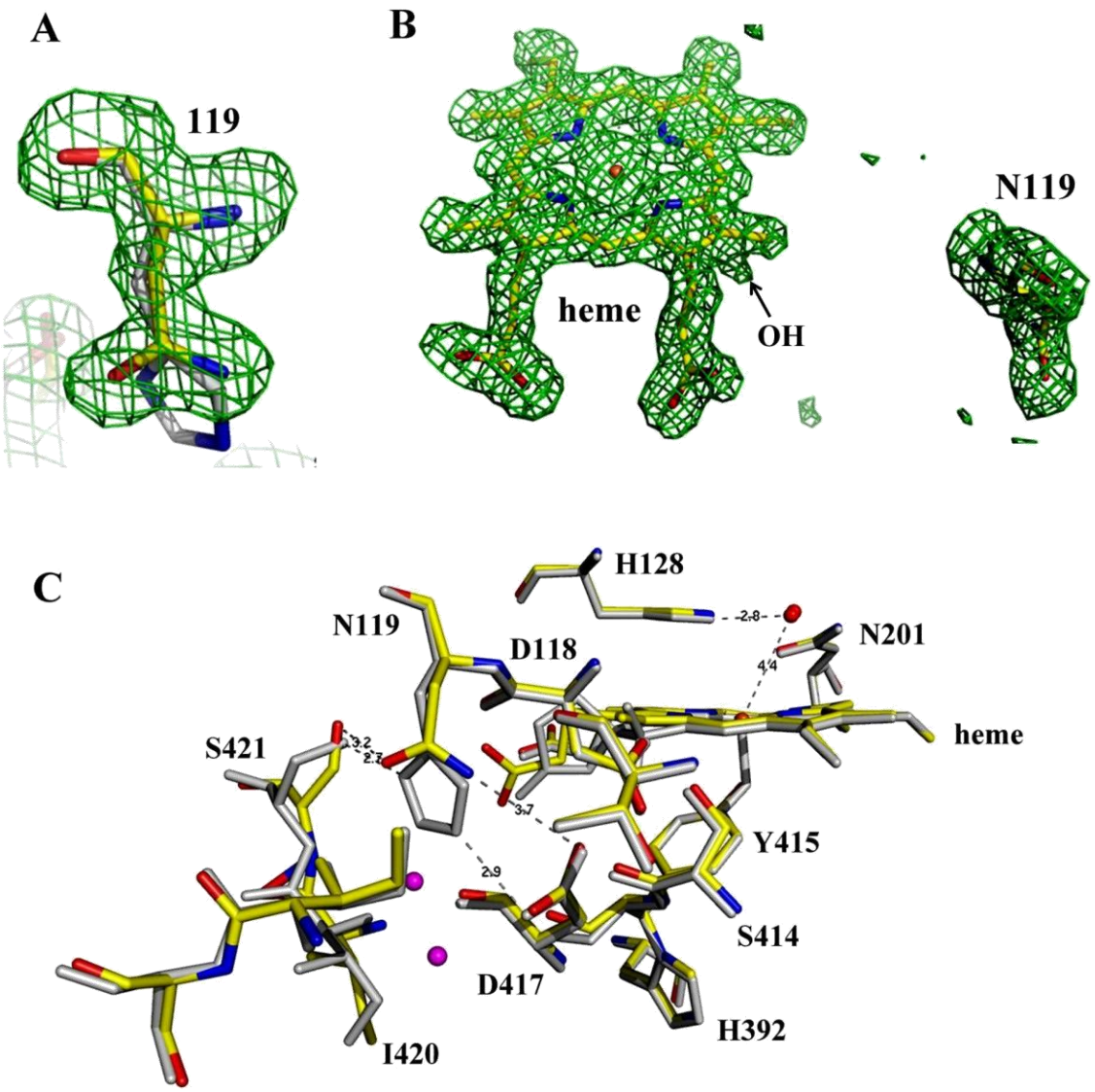

Figure 3.2.8. View of the F_o-F_c (green) electron density maps of the region around Asn119 and heme calculated without the respective atoms in the model, and the appropriate model was superimposed for illustration. Panel A: F_o-F_c electron density around Asn119. Panel B: F_o-F_c electron density around heme and Asn119. Panel C: superimposed residues of WT-HPII (grey sticks) and variant H119N (yellow sticks) in the vicinity of the site of mutation. Conserved waters are depicted as red spheres while new waters in the variant H119N are depicted as magenta spheres. Dotted black lines depict the interactions between residues at the site of mutation. F_o-F_c electron density maps were modeled at 3.0 σ.

Table 3.2.5. Comparison of average B values for the side chain atoms of residues in the vicinity of 119 in WT-HPII and variants H119A and H119N.

Residues in the vicinity of 119	**Average B values of side chains in four subunits**		
	WT-HPII	H119A	H119N
D118	6.08	7.58	11.68
D417	6.90	10.58	16.98
Q419	8.70	10.53	18.65
I420	9.18	20.50	28.40
S421	8.25	17.80	24.83

His119 is either modified or has become more mobile in both H119A and H119N, possibly because of the loss of hydrogen bond interaction with His119 as in WT-HPII. In H119N the Ser421 side chain has a different orientation compared to its orientation in WT-HPII and two new water molecules appears in the region of mutation (Figure 3.2.8 C). In both H119A and H119N, the side chains of Gln419, Ile420 and Ser421 are more mobile as is evident from their B values (Table 3.2.5) and from the presence of two conformations of Gln419. The asparagine side chain in H119N is shifted away from both Asp417 and Ser421side chains (3.7 and 3.2 Å respectively) (Figure 3.2.8 C). F_o-F_c electron density in the region of heme indicates mixtures of heme *b* and heme *d* in both H119A and H119N (Figure 3.2.7 B and Figure 3.2.8 B). Finally, the covalent linkage between His392 and Tyr415 is formed normally and there is no change in the distribution of solvent molecules in the main channel of either variant compared to WT-HPII.

3.3. Discussion

Site-directed mutagenesis of residues located far from the active site around the central cavity on the proximal side of the heme caused no change in the overall biochemical properties of the enzyme. Replacing His449 involved in breaking the molecular symmetry in the native enzyme with either alanine (H449A) and asparagine (H449N) and Arg111 which was shown to break molecular symmetry upon peroxide binding with either alanine or similarly charged lysine did not result in any change in catalase specific activity (Table 3.1.1) or overall structure suggesting that changes in the locations of specific residues caused by substrate binding that break the symmetry do not have an important role in catalysis.

At least three channels have been described in catalase HPII: a main channel, a lateral channel, and a third channel leading from the proximal side of the heme towards the central cavity. This channel has been postulated to be the access path for the substrate required for heme *b* to heme *d* conversion (Murshudov et al., 1996) and formation of the His-Tyr bond (Bravo et al., 1997). Thus enlarging the access channel maintains easy access for substrate used in heme modification ensuring 100% conversion to heme *d* in the variants. An unexpected change was the reduced turnover rate and this may reflect poorer containment of substrate in the active site making the catalytic process more difficult (Dominguez et al., 2010).

Replacement of the histidine side chain at position 119 with either alanine or asparagine resulted in minor structural changes mainly localized in the vicinity of the mutated residue. The imidazole ring in H119A is replaced by three water molecules, which are hydrogen bonded to Ser421 and Asp417 but the hydrogen bond network between the residues are lost in H119N because of the shorter side chain of asparagine at 119 and different conformation of Ser421 both of which increases the distance between them (Figure 3.2.8 C), suggesting the importance of hydrogen bond interactions at this location. Inefficient heme *b* to *d* conversion could also be related to this change. Previous work had suggested a close link between heme oxidation and His–Tyr bond formation in HPII, and a concerted mechanism was proposed (Bravo et al., 1999). Variants containing unoxidized heme *b* with His-Tyr bond had been characterized and it was proposed that compound I is sufficient to promote the formation of the His–Tyr bond, but not heme oxidation and that the energy barrier for His–Tyr bond formation is lower than for heme oxidation (Melik-Adamyan et al., 2001). In this case it seems that the hydrogen bonding network between

His119, Asp417 and Ser420 in close proximity of heme is important for maintaining the appropriate energy barrier for complete conversion of heme *b* to heme *d*.

Whether the reduced sensitivity of H119A and H119N towards cyanide and hydroxylamine is a result of heme *b* or the change in the interactions among the residues at the site of mutation is still a matter of conjecture. Co-crystallization of these variants with inhibitors may be planned as a future direction.

4. EFFECT OF F413 MUTATION ON CATALASE HPII

4.1. Introduction

Although catalase HPII of *E. coli* belongs to the large subunit clade 2 of catalase phylogeny, its core is similar in sequence to other catalases including the conservation of several residues that have been implicated as playing a catalytic role, His128, Asn201, Ser167 and Tyr415. These residues are located in the vicinity of the heme on its distal and proximal sides, but there are also conserved residues far from the heme on its proximal side that have not had their function investigated. Phe413, located about 13 Å from the heme, is one such residue which is well conserved in catalases from bacteria to higher eukaryotes including thirteen of the fourteen structurally known catalases (Figure 4.1).

It first came to notice in a structural analysis of the inactive H128N variant of HPII where the addition of H_2O_2 caused a conformation change of Phe413 compared to WT-HPII in subunits C and D, but not A and B. Along with this change in Phe413, a conformational change in the nearby Arg111 of subunits A and B was also noted (as discussed in Chapter 3). Other residues in close proximity to Phe413 in HPII include two threonines at 115 and 416, neither of which are conserved, and aspartate 417 which is highly conserved. These changes in conformation were intriguing and their appearance in the presence of substrate suggested a possible role in catalysis. To investigate this possibility, a structure-function study of Phe413 was undertaken.

```
CAT-3   387 YSYLDTQLNR HRGPNFEQLP INRPVS.GVH N.NHRDGQGQ AW.IHKNIHH YSPSYLNKGY  443
CAT-1   377 FSYFDTQISR LGV.NFQELP INRPVC.PVM N.FNRDGAMR HT.ISRGTVN YYPNRFD..A  430
PVC     348 FSYLDTQLNR HGGPNFEELP IDRPRA.PIH D.DDRDGAGE MF.IPLDPLA YSPNTEDSGS  404
HPII    413 FSYTDTQISR LGGPNFHEIP INRPTC.PYH N.FQRDGMHR MG.IDTNPAN YEPNSINDNW  469
PMC     335 FSYGDAHRYR LGV.NHHQIP VNAPKC.PFH N.YHRDGAMR VDGNSGNGIT YEPNSGG..V  389
PSCF    330 FSYADTQMYR LGA.NGLSLP VNQPKV.AVN N.GNQDGALN TG.HTTSGVN YEPSRLE..P  383
VSC     334 FAYGDAQRYR LG.VNHQHIP VNAPRC.PVH S.YHRDGAMR VDGNFGSTLG YEPND..QGQ  388
HPC     337 FSYGDTHRYR LG.VNYPQIP VNKPRC.PFH S.SSRDGYMQ NG.YYGSLQN YTPSS..LPG  390
EFC     335 FAYGDAHRHR VGA.NSHQLP INQAKA.PVN N.YQKDGNMR FN.NGNSEIN YEPNS..YTE  388
EOC     337 FSYSDTQRHR IGP.NYQQLP INCPFA.QVN N.YQRDGAMP FK.QQTSSVN YEPNRYQD.E  391
MLC     336 FAYHDAQLYR VGA.HVNQLP VNRPKN.AVH N.YAFEGQMW YD.HTGDRST YVPNSNG..D  389
SCCA    339 FSYADAHRYR LGP.NFHQIP VNCPYASKFF NPAIRDGPMN VNGNFGSEPT YL.ANDK..S  394
BLC     355 FAYPDTHRHR LGP.NYLQIP VNCPYRARVA N.YQRDGPMC MMDNQGGAPN YYPNSFS..A  410
HEC     356 FAYPDTHRHR LGP.NYLHIP VNCPYRARVA N.YQRDGPMC MQDNQGGAPN YYPNSFG..A  411
```

Figure 4.1. Amino acid sequence alignment of fourteen structurally known heme catalases. The conserved phenylalanine at position 413 (*E. coli* numbering) is indicated in bold red.

4.2. Results

4.2.1. Construction and characterization of F413 variants

For a comprehensive investigation of residue 413 in WT-HPII, variants F413A, F413Y, F413E, F413K, F413Q, F413Y/R111A and F413Y/H128N were constructed and purified as described in Chapter 2. This group of variants included basic, acidic, neutral polar, and non-polar residues while the double mutants introduced changes to nearby residues and the loss of activity. With the exception of F413Y and F413Y/R111A, all of the variants resembled WT-HPII in presenting a single band at ~84 kDa. By contrast, F413Y and F413Y/R111A presented two bands at ~84 kDa and ~74 kDa suggesting the two variants containing the F413Y mutation may have suffered proteolysis (Figure 4.2), leading to the conclusion that the inclusion of tyrosine at position 413 seems to facilitate chain fragmentation.

To investigate further the proteolytic event involving Tyr413, the F413Y variant was purified in the presence of the protease inhibitor PMSF added to the resuspension buffer at concentrations between 0.5 and 1.0 mM prior to cell lysis by French Press. Surprisingly, protein cleavage was still evident suggesting that it must have taken place inside the cell during growth. This was substantiated when protein from cells grown in small cultures in the presence of 0.5 to 2 mM PMSF presented less of the 74 kDa band (Figure 4.3). In fact, PMSF only provided partial, never complete, protection against protein cleavage, and a large scale preparation of F413Y from cells grown in the presence of PMSF still contained a small amount of the cleaved protein, similar in amount to that observed in F413Y/R111A. Preparations of both F413Y and F413Y/R111A also contained larger amounts of apparently cross linked tetramer migrating at ~320 kDa (Figure 4.2 and 4.3) suggesting enhanced

reactivity among subunits. Very significantly, the inactive variant F413Y/H128N did not exhibit any protein cleavage suggesting that catalytic turnover was necessary.

Cells were also grown under partial anaerobic conditions to see whether reduced production of peroxide or reactive species affected cleavage. While, the expression of protein was poor under these conditions and other proteins interfered with the purification, it was evident that a smaller fraction of the protein was cleaved. Thus, lower levels of ROS evidently reduced protein cleavage. Cleavage of the protein in vitro was also attempted with protein being treated with different concentrations of H_2O_2, glucose-glucose oxidase (to constantly purge the protein with H_2O_2) and xanthine-xanthine oxidase (which generates superoxide ion) for up to 24 hours. After separation on SDS-PAGE, it was evident that no further cleavage had taken place (Data not shown).

Mass spectrometry analysis of the trypsin digested peptides extracted from bands of F413Y separated on SDS-PAGE was performed using MALDI-TOF to identify the missing peptides. The ~74 kDa protein band from the gel was excised, extracted and digested according to Shevchenko et al., 2006. Digested samples were mixed with an equal volume of matrix (2,5-dihydroxybenzoic acid) and deposited on a metal plate that fits into a MALDI QqTOF mass spectrometer (Loboda et al., 2000). Spectra were acquired and analysed using software developed in the time-of-flight laboratory in the Department of Physics and Astronomy. Output data were submitted online to MASCOT, the peptide search engine of MATRIX Science (http://www.matrixscience.com). Tandem mass spectra were analysed manually. About 130 N-terminal residues could not be identified in the peptide search when compared with WT-HPII peptides (Figure 4.5 and Figure 4.6) consistent with protein cleavage having occurred in the N-terminal 110-130 residues.

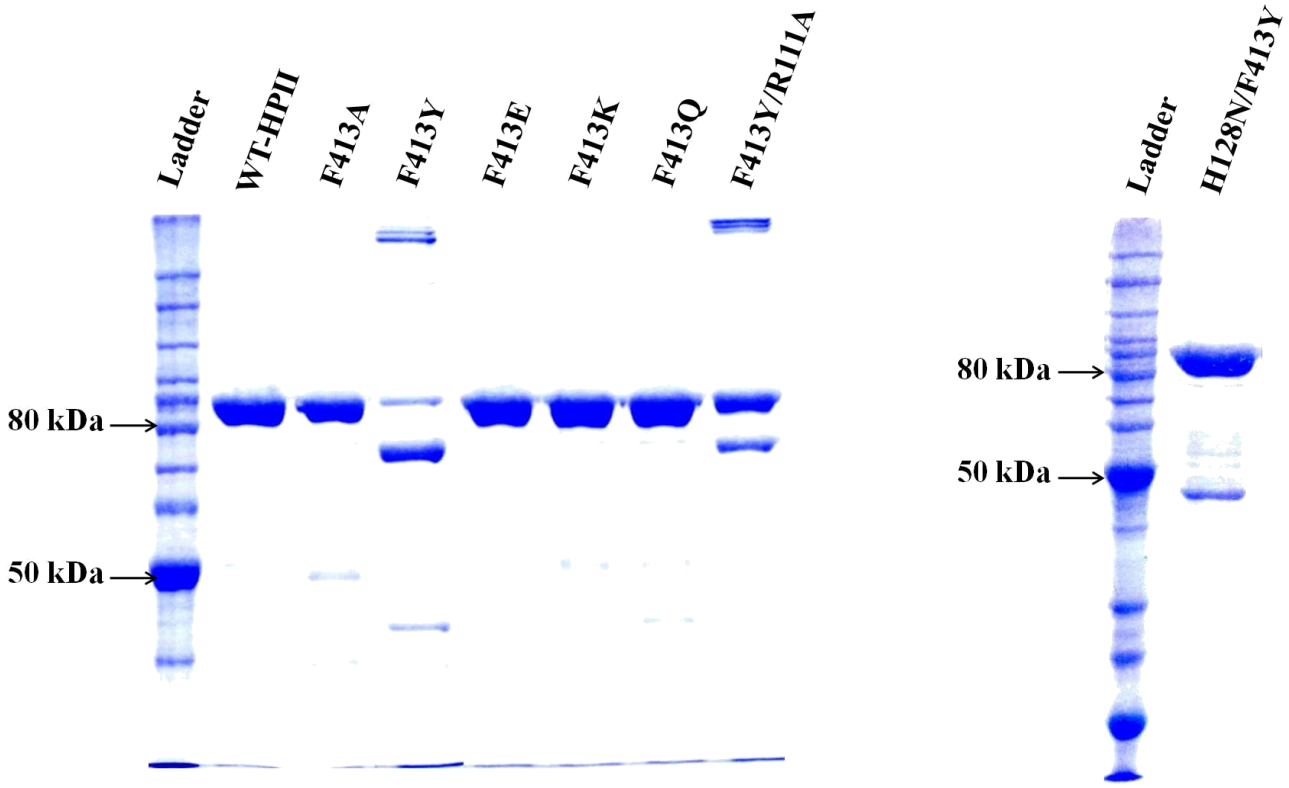

Figure 4.2. SDS-PAGE analysis of purified WT-HPII and its variants. Approximately 2.0 µg of protein were loaded on an 8% polyacrylamide gel and stained with Coomassie brilliant blue after electrophoretic separation.

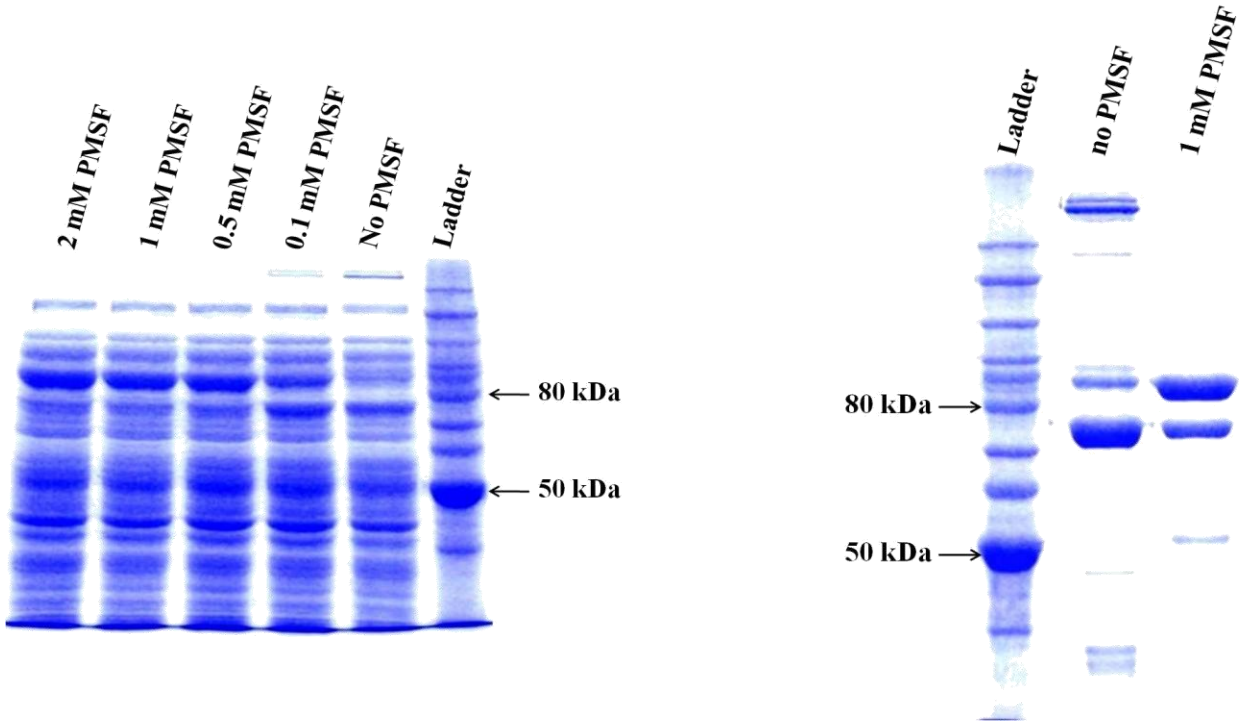

Figure 4.3. SDS-PAGE analysis of F413Y protein. On the left is the SDS-PAGE of crude extract from the cells expressing F413Y grown with varying concentration of PMSF at 37 °C for 16 hrs. Approximately 10.0 µg of protein were loaded on an 8% polyacrylamide gel. On the right is the SDS-PAGE gel of F413Y (purified from cells grown with 1 mM PMSF). Approximately 2.0 µg of protein were loaded on an 8% polyacrylamide gel. The gels were stained with Coomassie brilliant blue after electrophoretic separation.

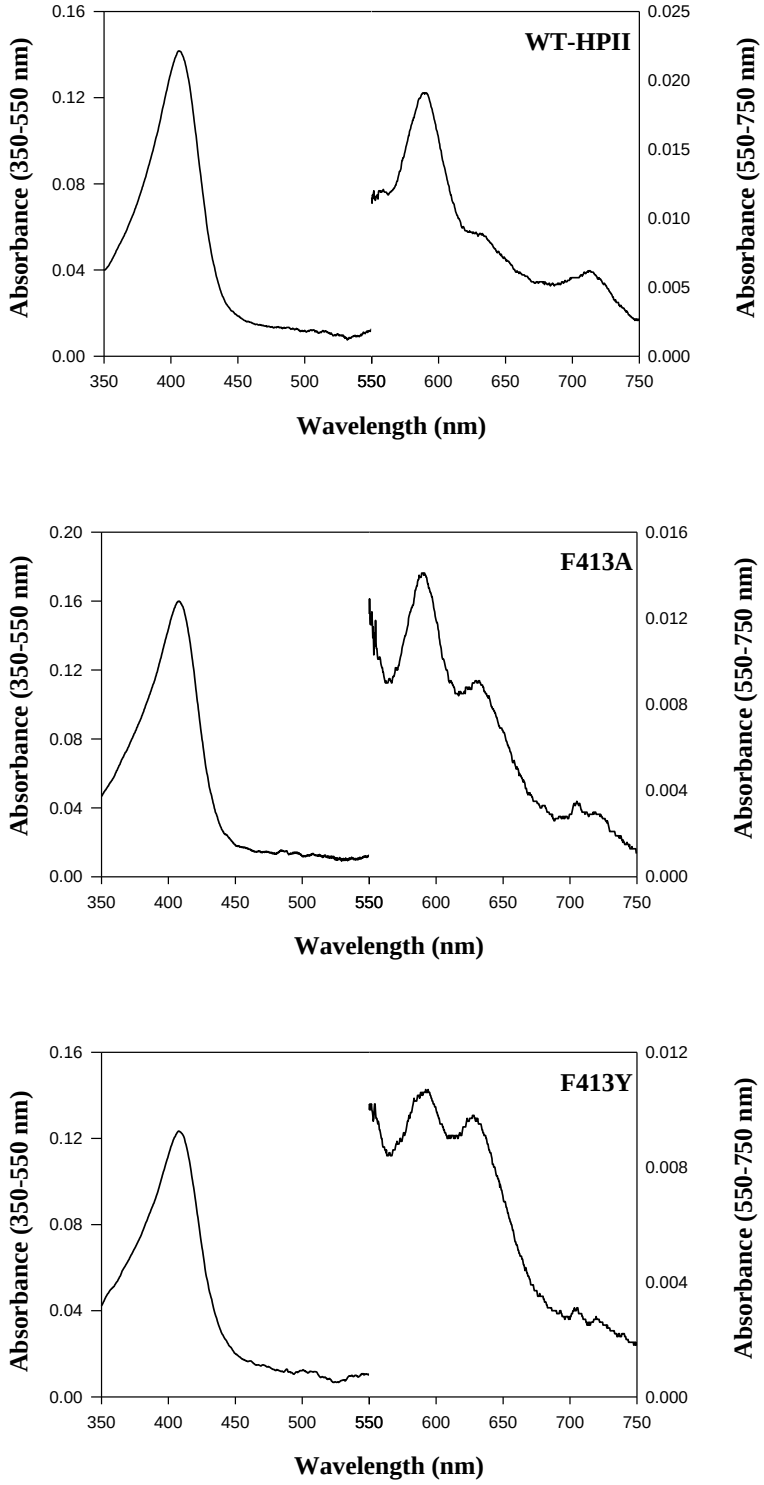

Figure 4.4. Absorption spectra of WT-HPII and its variants. The left axis corresponds to the absorbance values between wavelengths 350-550 nm and the right axis to the wavelength between 550-750 nm.

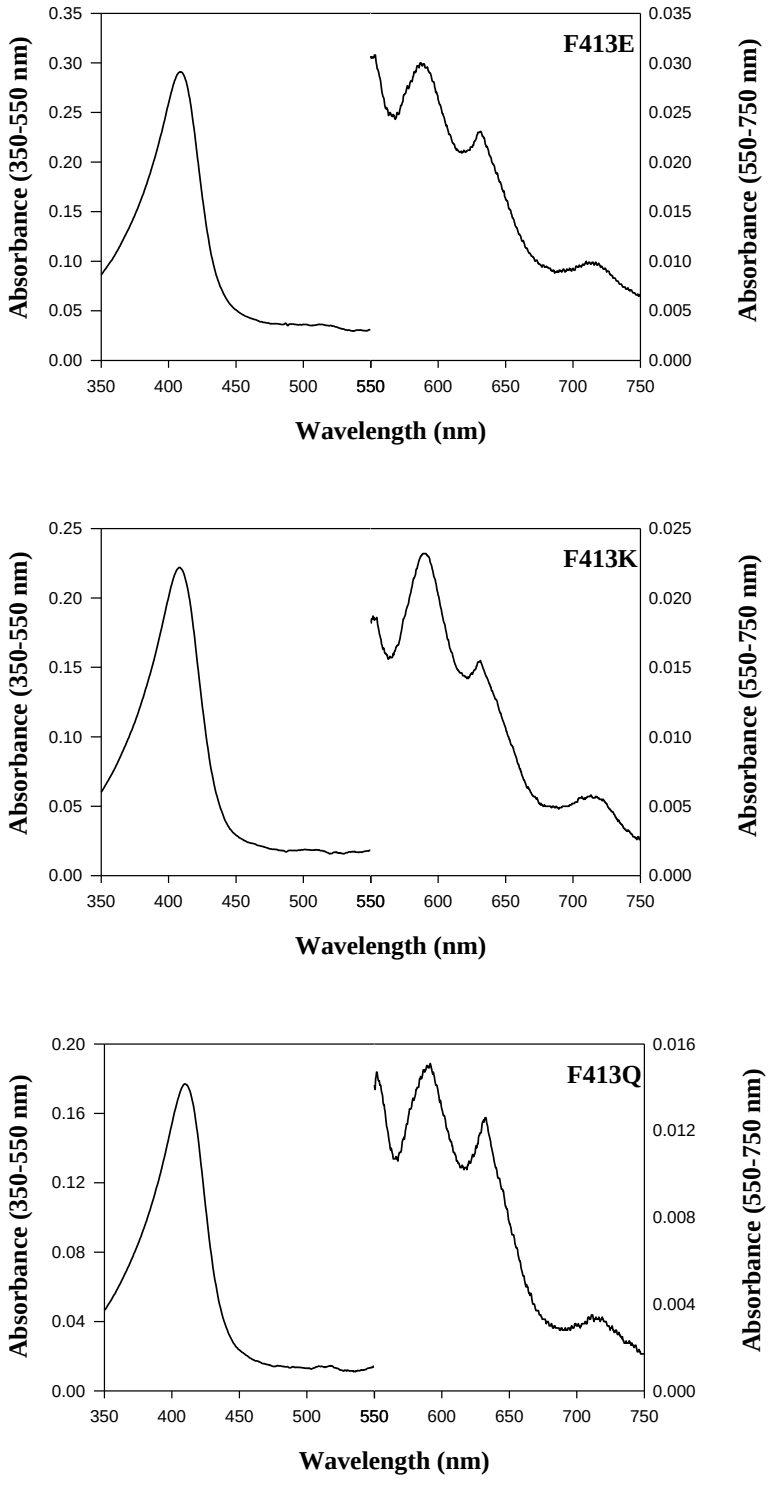

Figure 4.4. Continued...

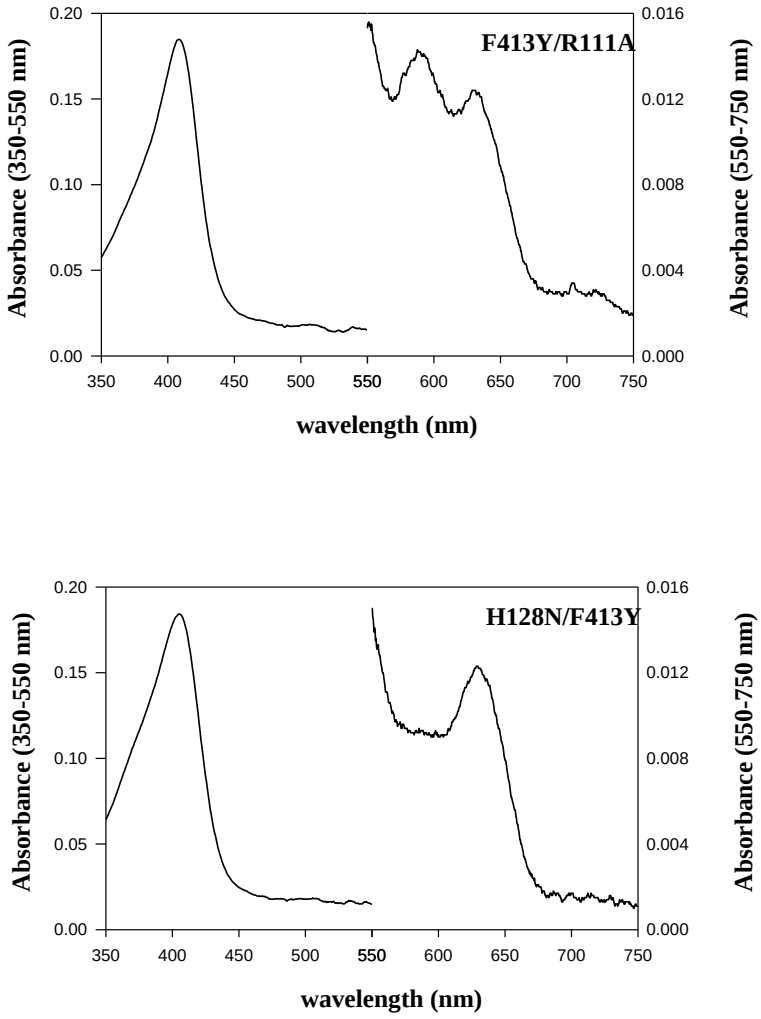

Figure 4.4. Continued...

Table 4.1. Comparison of observed absorbance maxima, A_{407}/A_{280} ratio and catalase specific activities of purified WT-HPII and its variants.

Variants	**Soret (nm)**	**R_z[a] (A_{407}/A_{280})**	**Specific activity (U/mg)**
WT-HPII	406	0.94	21000 ± 1400
F413A	408	0.96	16000 ± 160
F413Y	408	0.90	16000 ± 1400
F413E	409	0.90	16800 ± 640
F413K	408	0.82	13400 ± 160
F413Q	409	0.86	11300 ± 280
R111A/F413Y	408	0.94	15000 ± 500
H128N/F413Y	405	0.72	No activity

[a] The theoretical A_{407}/A_{280} ratio is 1.0.

Assays for determining specific activity were performed in triplicate and results were averaged.

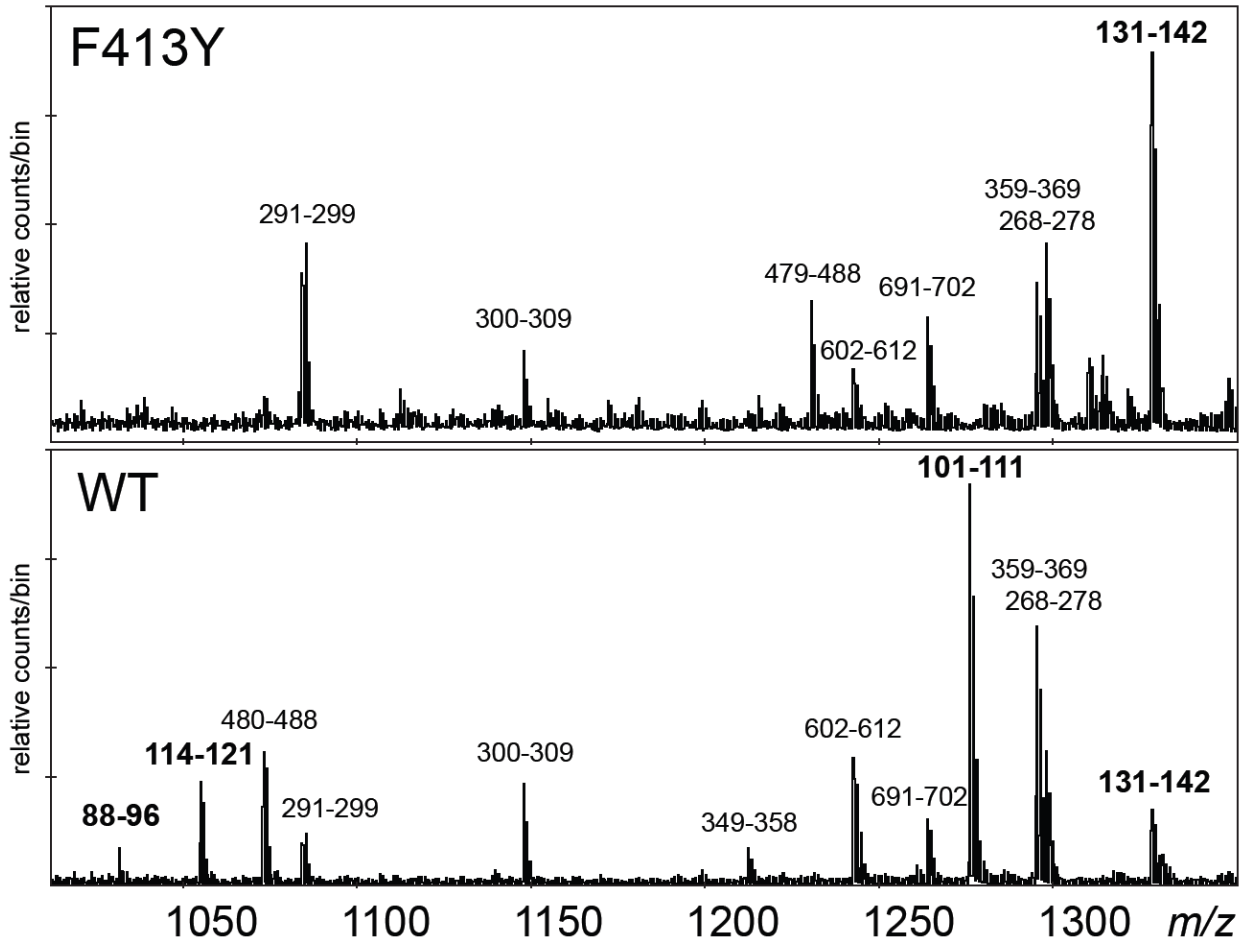

Figure 4.5. MALDI spectra of the digested F413Y and WT-HPII. The ions are labelled with the sequence identity rather than the m/z values for describing the proteins. The ones in larger font and bold are the ions which are confirmed by MS-MS. No ions matching the first 130 amino acids were found in F413Y.

WT-HPII

```
1     MSQHNEKNPH QHQSPLHDSS EAKPGMDSLA PEDGSHRPAA EPTPPGAQPT
51    APGSLKAPDT RNEKLNSLED VRKGSENYAL TTNQGVRIAD DQNSLRAGSR
101   GPTLLEDFIL REKITHFDHE RIPERIVHAR GSAAHGYFQP YKSLSDITKA
151   DFLSDPNKIT PVFVRFSTVQ GGAGSADTVR DIRGFATKFY TEEGIFDLVG
201   NNTPIFFIQD AHKFPDFVHA VKPEPHWAIP QGQSAHDTFW DYVSLQPETL
251   HNVMWAMSDR GIPRSYRTME GFGIHTFRLI NAEGKATFVR FHWKPLAGKA
301   SLVWDEAQKL TGRDPDFHRR ELWEAIEAGD FPEYELGFQL IPEEDEFKFD
351   FDLLDPTKLI PEELVPVQRV GKMVLNRNPD NFFAENEQAA FHPGHIVPGL
401   DFTNDPLLQG RLFSYTDTQI SRLGGPNFHE IPINRPTCPY HNFQRDGMHR
451   MGIDTNPANY EPNSINDNWP RETPPGPKRG GFESYQERVE GNKVRERSPS
501   FGEYYSHPRL FWLSQTPFEQ RHIVDGFSFE LSKVVRPYIR ERVVDQLAHI
551   DLTLAQAVAK NLGIELTDDQ LNITPPPDVN GLKKDPSLSL YAIPDGDVKG
601   RVVAILLNDE VRSADLLAIL KALKAKGVHA KLLYSRMGEV TADDGTVLPI
651   AATFAGAPSL TVDAVIVPCG NIADIADNGD ANYYLMEAYK HLKPIALAGD
701   ARKFKATIKI ADQGEEGIVE ADSADGSFMD ELLTLMAAHR VWSRIPKIDK
751   IPA
```

F413Y

```
1     MSQHNEKNPH QHQSPLHDSS EAKPGMDSLA PEDGSHRPAA EPTPPGAQPT
51    APGSLKAPDT RNEKLNSLED VRKGSENYAL TTNQGVRIAD DQNSLRAGSR
101   GPTLLEDFIL REKITHFDHE RIPERIVHAR GSAAHGYFQP YKSLSDITKA
151   DFLSDPNKIT PVFVRFSTVQ GGAGSADTVR DIRGFATKFY TEEGIFDLVG
201   NNTPIFFIQD AHKFPDFVHA VKPEPHWAIP QGQSAHDTFW DYVSLQPETL
251   HNVMWAMSDR GIPRSYRTME GFGIHTFRLI NAEGKATFVR FHWKPLAGKA
301   SLVWDEAQKL TGRDPDFHRR ELWEAIEAGD FPEYELGFQL IPEEDEFKFD
351   FDLLDPTKLI PEELVPVQRV GKMVLNRNPD NFFAENEQAA FHPGHIVPGL
401   DFTNDPLLQG RLYSYTDTQI SRLGGPNFHE IPINRPTCPY HNFQRDGMHR
451   MGIDTNPANY EPNSINDNWP RETPPGPKRG GFESYQERVE GNKVRERSPS
501   FGEYYSHPRL FWLSQTPFEQ RHIVDGFSFE LSKVVRPYIR ERVVDQLAHI
551   DLTLAQAVAK NLGIELTDDQ LNITPPPDVN GLKKDPSLSL YAIPDGDVKG
601   RVVAILLNDE VRSADLLAIL KALKAKGVHA KLLYSRMGEV TADDGTVLPI
651   AATFAGAPSL TVDAVIVPCG NIADIADNGD ANYYLMEAYK HLKPIALAGD
701   ARKFKATIKI ADQGEEGIVE ADSADGSFMD ELLTLMAAHR VWSRIPKIDK
751   IPA
```

Figure 4.6. Protein sequence of WT-HPII and F413Y. In red are the peptides found in database search after mass spectrometry analysis and in bold red are peptides further confirmed by MS-MS. Note the unidentified peptides in F413Y.

Visible absorption spectra of the variants are shown in Figure 4.4 for comparison with WT-HPII. The values of absorption maxima, A_{407}/A_{280} ratio, and catalase specific activities are listed in Table 4.1. All the variants except that of H128N/F413Y exhibited two shoulders in the charge transfer region, one at 590 nm similar to WT-HPII and another at 630 nm indicating the presence of both heme *b* and heme *d*. The spectrum of F413Y/H128N exhibited a single peak at 630 nm consistent with the inactive variant containing only heme *b* consistent with earlier work (Melik-Adamyan et al, 2001). All variants revealed R_z values similar to WT-HPII except for H128N/F413Y which exhibited a lower R_z, probably a result of contaminating glycerol kinase (evident in the band at ~45 kDa in Figure 4.2). Variants F413A, F413Y, and F413E exhibited near WT activity, while variants F413K, F413Q and double variant F413Y/R111A retained 65%, 55% and 70% of WT activity respectively. As expected the double variant F413Y/H128N was inactive like the H128N variant.

Kinetic constants for the catalase reaction of WT-HPII and F413 variants were determined by titrating the enzymes with different concentrations of H_2O_2 (Figure 4.7) and the kinetic constants are summarized in Table 4.2. All the variants presented observed k_{cat}, apparent K_M, and k_{cat}/K_M values similar to those of WT-HPII except the variant F413A. F413A exhibited a much lower k_{cat} and K_M (Figure 4.7 and Table 4.2). This was unexpected, as Phe413 does not form part of any channel and is not located in the heme active site. Also, all the variants were very sensitive to heat treatment at 80 °C (Figure 4.9 and Table 4.3) and exhibited reduced sensitivity towards various inhibitors especially to cyanide and hydroxylamine (Figure 4.8, 4.9 and Table 4.3).

4.2.2. Structure of F413Y and H128N/F413Y

Good quality diffracting crystals of F413Y (prepared with and without PMSF) and inactive double mutant H128N/F413Y were obtained by the hanging drop vapour diffusion method as described in Chapter 2. Diffraction data for the crystals were collected at Canadian Light Source in Saskatoon, Canada using synchrotron beam line CMCF 08ID-1 that refined to between 1.6-1.9 Å. Data collection and refinement statistics are listed in Table 4.4. The electron density maps in the variants show complete continuity from Ser28 to Ala753 in all four subunits, except for two locations which will be described below. The tyrosine side chain in F413Y at residue 413 is not evident in the F_o-F_c electron density maps calculated without the side chain in the model for protein prepared without PMSF (Figure 4.10 A). However, the tyrosine side chain is evident in crystals prepared from F413Y protein prepared with PMSF, albeit with low occupancy, and in F413Y/H128N, at high occupancy (Figure 4.10 B and C). The expected glutamine side chain at 128 in H128N/F413Y is also clearly evident (Figure not shown). Electron density in the region of heme is indicative of 100% heme *b* in F413Y (both PMSF and non PMSF purified proteins) and H128N/F413Y. The second covalent modification in the HPII heme cavity linking His392 and Tyr415 is present in both preparations of F413Y but not in F413Y/H128N.

4.2.3. Structural changes in the vicinity of 413 in F413Y

Besides the missing electron density of tyrosine side chain in F413Y prepared without PMSF, the density for the side chains of other residues in the vicinity of 413

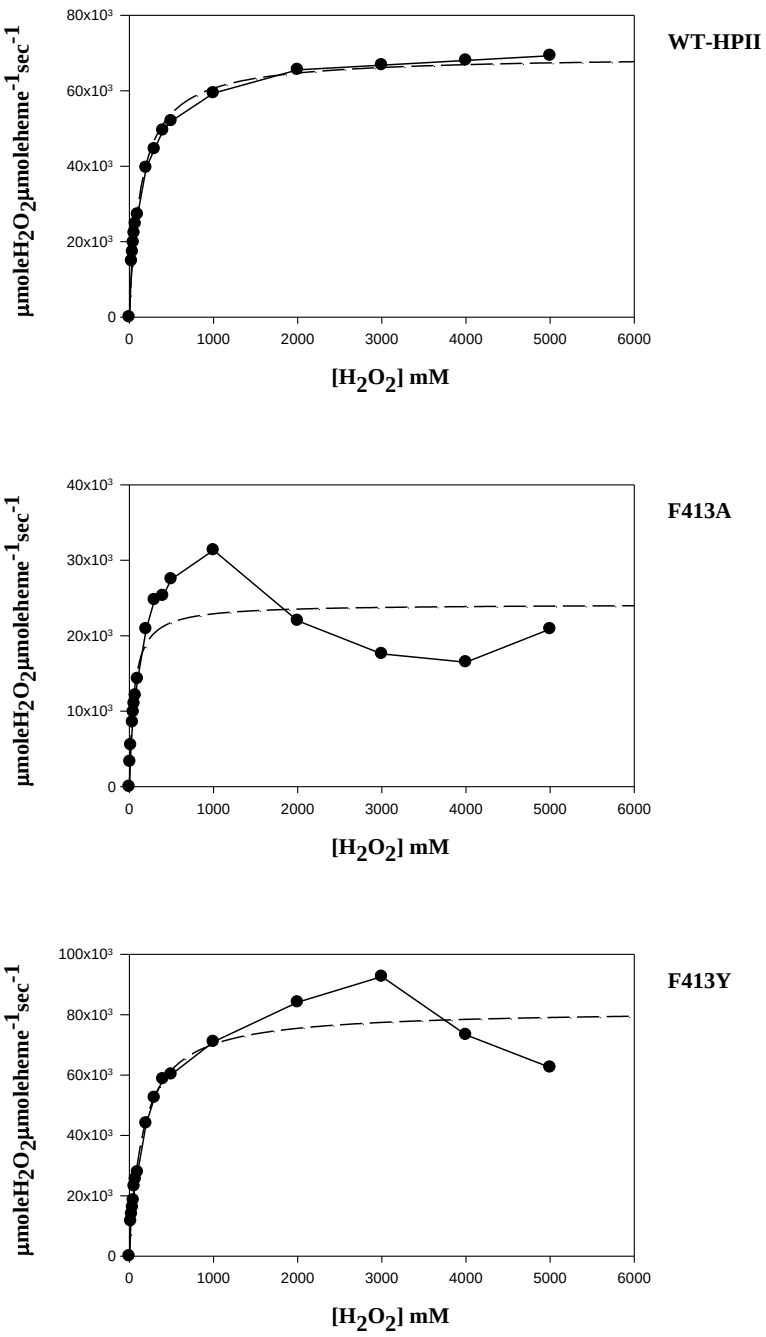

Figure 4.7. Effect of H_2O_2 concentration on reaction velocity of WT-HPII and its variants. In all panels the solid line represents the observed data and the dashed line represents the theoretical Michaelis-Menten curve calculated from constants determined at low H_2O_2 concentration (Table 3.1.2). Note the difference in the scales of Y-axis.

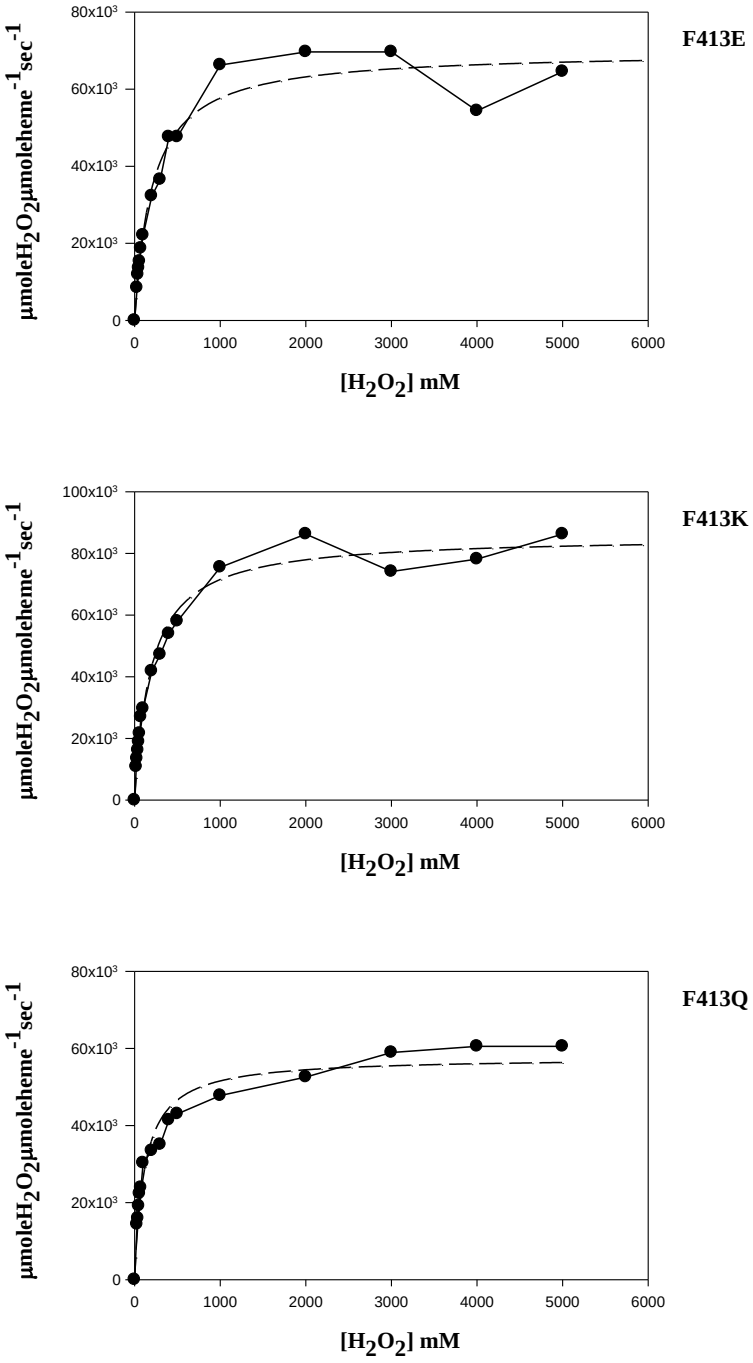

Figure 4.7. Continued...

Table 4.2. Comparison of the observed kinetic parameters of WT-HPII and its variants.

Variants	**Observed**		**k_{cat}/K_M ($M^{-1}sec^{-1}$)**
	k_{cat} (sec^{-1})	K_M (app)[a]	
WT-HPII	70000	145	0.5×10^6
F413A	24200	56	0.4×10^6
F413Y	81640	160	0.5×10^6
F413E	69800	200	0.3×10^6
F413K	85560	196	0.4×10^6
F413Q	57700	120	0.5×10^6

[a] K_M (apparent), H_2O_2 concentration at $V_{max}/2$, mM.

A

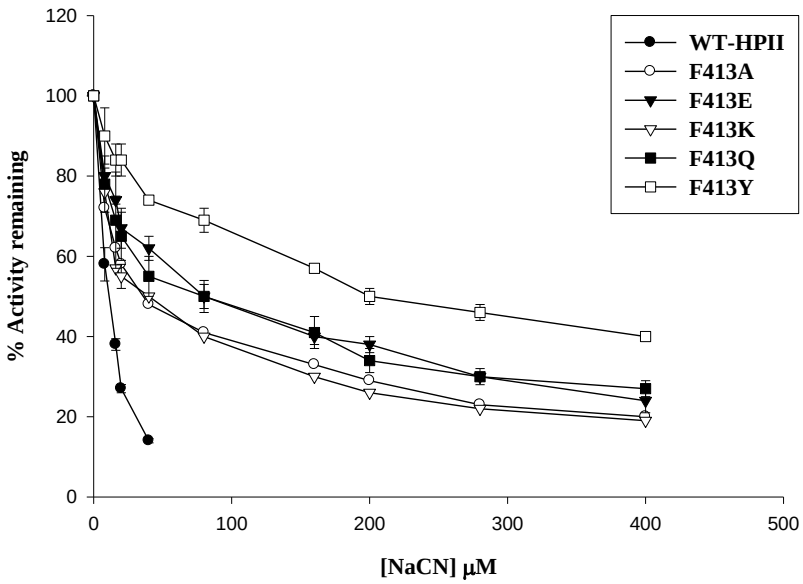

B

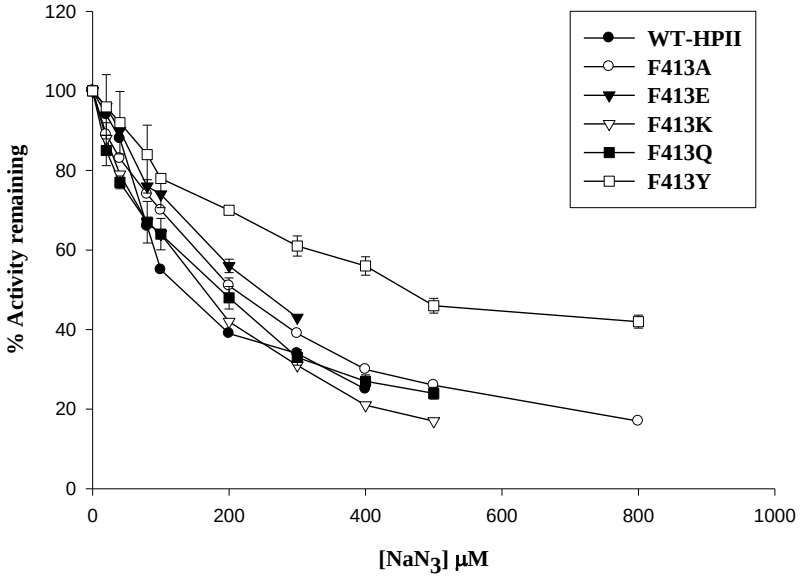

Figure 4.8. Effect of NaCN (A) and NaN_3 (B) on WT-HPII and its variants. Each enzyme was incubated with inhibitor for 1 minute in 50 mM KPi buffer at 37 °C before starting the reaction by adding H_2O_2. All assays were repeated in triplicate and the results were averaged.

A

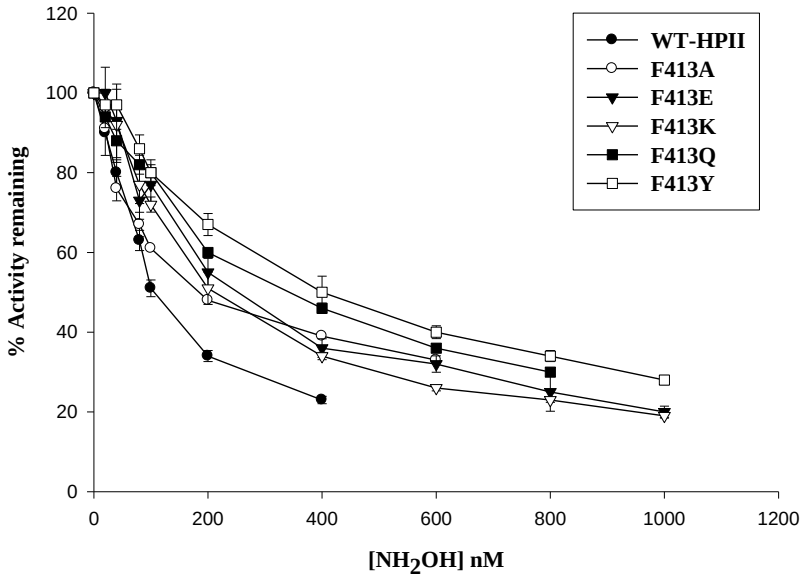

B

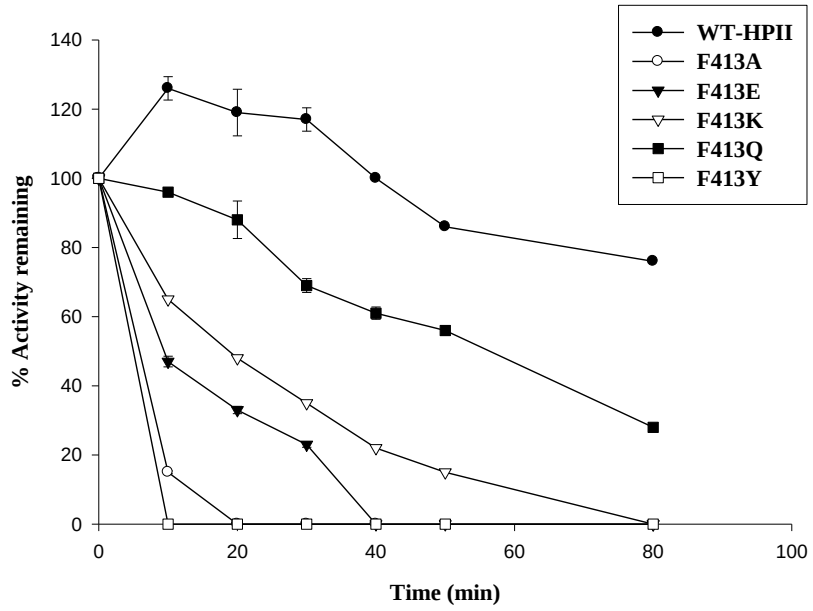

Figure 4.9. Effect of NH_2OH (A) on and comparison of thermostability at 80 °C (B) of WT-HPII and its variants. In panel A, each enzyme was incubated with inhibitor for 1 minute in 50 mM KPi buffer at 37 °C before starting the reaction by adding H_2O_2. In panel B, each enzyme was incubated at 80 °C for different time intervals. All assays were repeated in triplicate and the results were averaged.

Table 4.3. Sensitivity of WT-HPII and its variants towards catalase inhibitors and incubation at 80 °C[*].

Variants	Inhibitor concentration at 50% inhibition[a]			Time to 50% inhibition at 80 °C (min)[b]
	NaCN (μM)	NaN_3 (μM)	NH_2OH (nM)	
WT-HPII	11 ± 1.0	140 ± 10	110 ± 10	>80
F413A	50 ± 10	200 ± 0	200 ± 0	5 ± 0
F413Y	180 ± 20	420 ± 25	425 ± 35	<1
F413E	100 ± 15	280 ± 30	280 ± 30	5 ± 0
F413K	50 ± 10	175 ± 15	220 ± 20	15 ± 0
F413Q	100 ± 15	200 ± 0	375 ± 35	60 ± 0

[a] Enzyme was incubated with inhibitor for one minute before adding H_2O_2.

[b] Enzyme was incubated at 80 °C for different time intervals.

[*]All assays were repeated in triplicate and results were averaged.

Table 4.4. Data collection and structural refinement statistics of HPII variants F413Y and H128N/F413Y.

	F413Y		H128N/F413Y
	with PMSF	without PMSF	
A. Data collection statistics			
Space group	$P2_1$	$P2_1$	$P2_1$
Unit cell parameters			
a (Å)	93.54	93.56	93.62
b (Å)	133.21	133.33	132.96
c (Å)	122.30	122.16	122.67
α, β, ϒ (deg.)	90, 109.57, 90	90, 109.58, 90	90, 109.39, 90
Resolution range (Å)	27.12-1.60 (1.69-1.60)[a]	29.38-1.58 (1.67-1.58)	41.39-1.89 (2.0-1.89)
Total no. of reflections	1,379,565 (188,507)	1,626,247 (223,239)	733,532 (76,557)
Unique reflections	369,488 (53,330)	376,939 (54,792)	189,038 (21,370)
Completeness (%)	99.7 (98.8)	98.9 (98.6)	84.3 (65.5)
$\langle I/\sigma(I)\rangle$	7.8 (2.3)	7.3 (2.3)	14.9 (5.1)
R_{merge}	0.112 (0.484)	0.121 (0.564)	0.062 (0.214)
B. Refinement statistics			
Resolution range (Å)	133.21-1.60	115.10-1.58	115.71-1.89
% age observed	99.73	98.75	84.30
R_{work} (%)	14.67	15.89	14.03
R_{free} (%)	18.52	19.54	19.43
No. of non-hydrogen atoms			
proteins	23,050	22,979	22,983
hemes	172	172	172
waters	3,464	3,019	3,141
rms deviations			
bond lengths (Å)	0.02	0.02	0.02
bond angles (deg.)	2.16	2.06	1.90
Average B factor ($Å^2$)			
main chain	11.55	13.63	14.19
side chain	13.52	16.33	15.47
water	23.6	26.2	23.3

[a] Values in parentheses correspond to the highest-resolution shell.

suggests that they have also been modified, and the modifications are more extensive in the protein prepared without PMSF. The modified residues include Arg111, Thr115, Asp417, Ile420, and Ser421. No changes were evident in the electron density of Tyr413 side chain or the side chains of residues in its vicinity in the merged data sets of early and late images suggesting that the changes are not caused by the X-ray damage. In addition, there is a break in the electron density of the main chain atoms between Arg111 and Glu112 and between Thr115 and His116 at 1.5 σ in the $2F_o$-F_c maps (not shown) and at 4.0 σ in the F_o-F_c maps (Figure 4.11). By comparison, the electron density for the adjacent main chain atoms remains strong. This suggestion of main chain cleavage is consistent with the size of the protein fragments observed on SDS-PAGE and the missing peptides in the mass spectrometric analysis of the smaller band.

4.2.4. Structure of F413E and F413K

Crystals of F413E and F413K were also grown and X-ray diffraction data were collected at Canadian Light Source in Saskatoon, Canada using synchrotron beam line CMCF 08ID-1 that refined to 1.6 and 1.7 Å respectively. Data collection and refinement statistics are listed in Table 4.5. The electron density maps defined the main chain and side chain atoms of 2904 amino acids, four heme groups, one in each subunit, and 3292 and 3348 water molecules in F413E and F413K respectively. The maps show clear continuity in each of the four subunits over the complete length from Ser28 to Ala753. The F_o-F_c omit and $2F_o$-F_c electron density maps confirmed the presence of the expected replacements at position 413 in both variants (Figure 4.12 A & B). Both the glutamate and lysine side chains exhibit greater mobility than that of the phenylalanine side chain in WT-HPII; this is evident in the

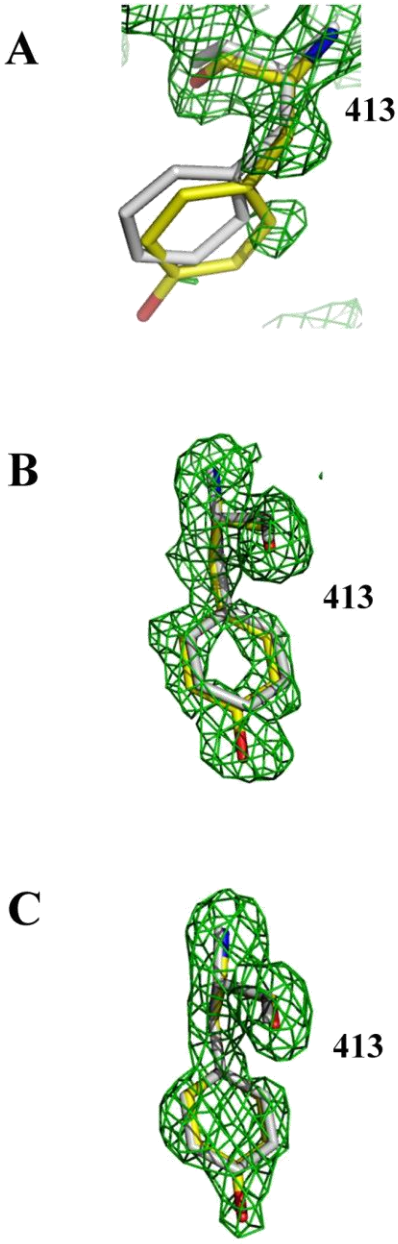

Figure 4.10. F_o-F_c electron density maps around 413. Maps were calculated without the side chain in the model and the appropriate model was superimposed for illustration. Panel A: region of 413 in F413Y prepared without PMSF, Panel B: region of 413 in F413Y prepared with PMSF, Panel C: region of 413 in H128N/F413Y. Yellow and grey stick represents the residue in the mutant and WT-HPII respectively. The F_o-F_c electron density map was modelled at $\sigma = 3.0$.

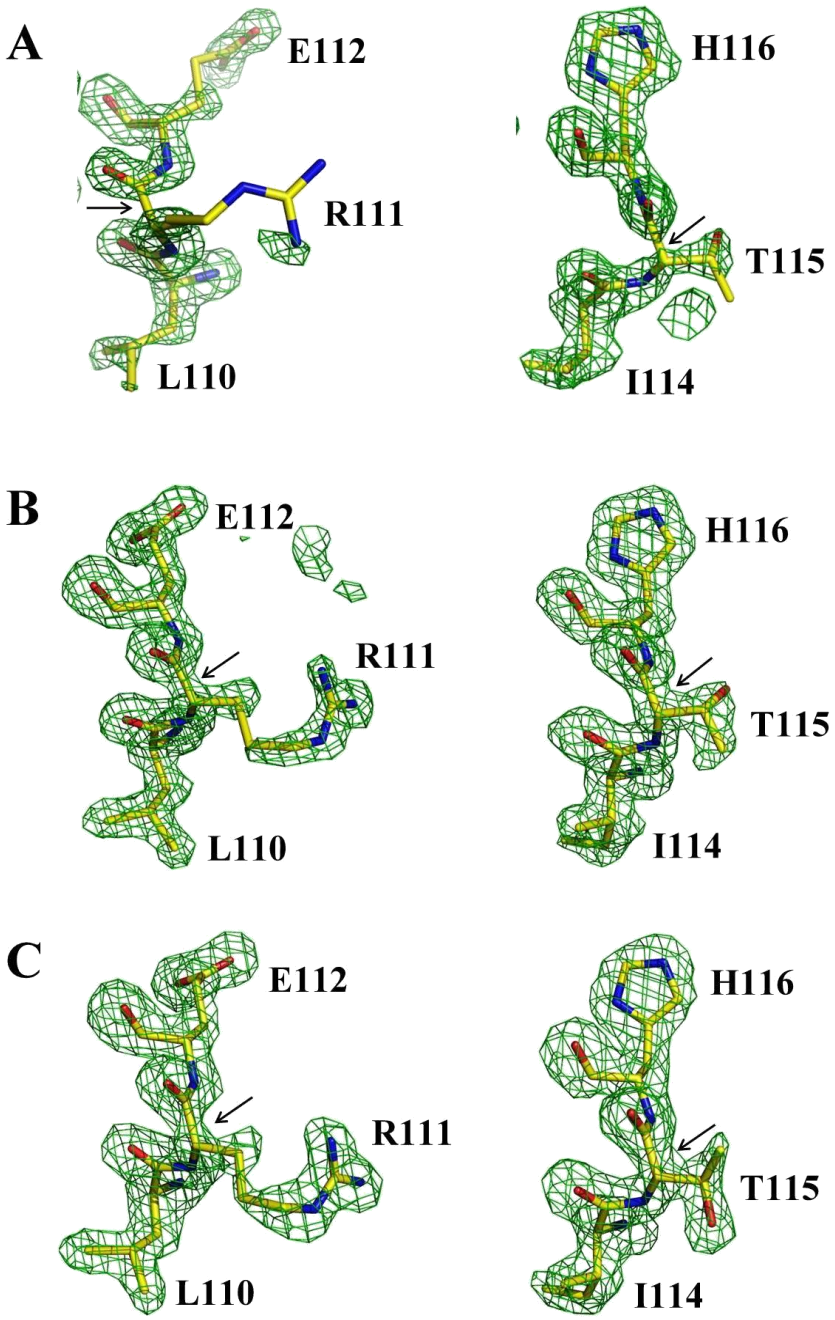

Figure 4.11. F_o-F_c electron density maps corresponding to the region between 110-112 and 114-116 of F413Y prepared without PMSF (Panel A), F413Y prepared with PMSF (Panel B) and H128N/F413Y (Panel C). Maps were calculated without the residues in the model and the appropriate model was superimposed for illustration. F_o-F_c electron density maps were modeled at 4.0 σ. Predicted site of the lesion is indicated with arrows.

Table 4.5. Data collection and structural refinement statistics of HPII variants F413E and F413K.

	F413E	F413K
A. Data collection statistics		
Space group	$P2_1$	$P2_1$
Unit cell parameters		
a (Å)	93.49	93.50
b (Å)	132.85	132.96
c (Å)	122.68	122.03
α, β, ϒ (deg.)	90, 109.36, 90	90, 109.69, 90
Resolution range (Å)	31.27-1.62 (1.71-1.62)[a]	35.18-1.74 (1.83-1.74)
Total no. of reflections	1,130,971 (157,606)	1,024,623 (125,281)
Unique reflections	311,384 (46,552)	278,274 (37,423)
Completeness (%)	87.1 (89.3)	97.2 (89.8)
$\langle I/\sigma(I)\rangle$	9.2 (2.0)	9.7 (2.9)
R_{merge}	0.085 (0.581)	0.106 (0.458)
B. Refinement statistics		
Resolution range (Å)	115.74-1.62	114.89-1.74
% age observed	87.10	97.04
R_{work} (%)	15.47	14.22
R_{free} (%)	20.4	18.64
No. of non-hydrogen atoms		
proteins	23,046	22,987
hemes	172	172
waters	3,292	3,348
rms deviations		
bond lengths (Å)	0.02	0.02
bond angles (deg.)	2.14	2.03
Average B factor ($Å^2$)		
main chain	15.50	12.48
side chain	17.43	14.14
water	28.0	24.0

[a] Values in parentheses correspond to the highest-resolution shell.

higher B values (> 30 $Å^2$) and is probably the result of nearby negatively and positively charged residues. In both F413E and F413K, the arginine at 111 in all subunits is oriented in a different conformation compared to WT-HPII, while glutamine at 419 exist in two conformation as opposed to single conformation in WT-HPII (Figure 4.14).

Structural analysis of the heme environment revealed mixtures of heme *b* and heme *d* in both F413E and F413K which is consistent with the absorption spectra (Figure 4.4), but the percentage of heme *b* is higher compared to heme *d* (~80% and ~20% respectively) in both F413E and F413K. No other changes are observed and the overall structure is similar to that of WT-HPII.

4.3. Discussion

Phe413 is a highly conserved hydrophobic amino acid located ~13 Å from the active site on the proximal side of the heme in HPII. Its conserved nature among catalases suggests a possible structural or functional significance and the study reported here was undertaken to investigate this possibility.

Replacement of the large hydrophobic phenyl ring side chain of Phe413 with either a small hydrophobic methyl side chain of alanine (F413A) or neutral (F413Y and F413Q) and charged residues (F413E and F413K) did not result in significant loss of catalytic activity or change in reaction velocities suggesting that phenylalanine at 413 (in HPII) does not have a significant catalytic role. All the variants including the double variant F413/R111A retained activity ranging from 55% to 75% of WT activity (Table 4.1) and also exhibited similar kinetic constants as WT-HPII with similar specificity towards the substrate H_2O_2 (Table 4.2).

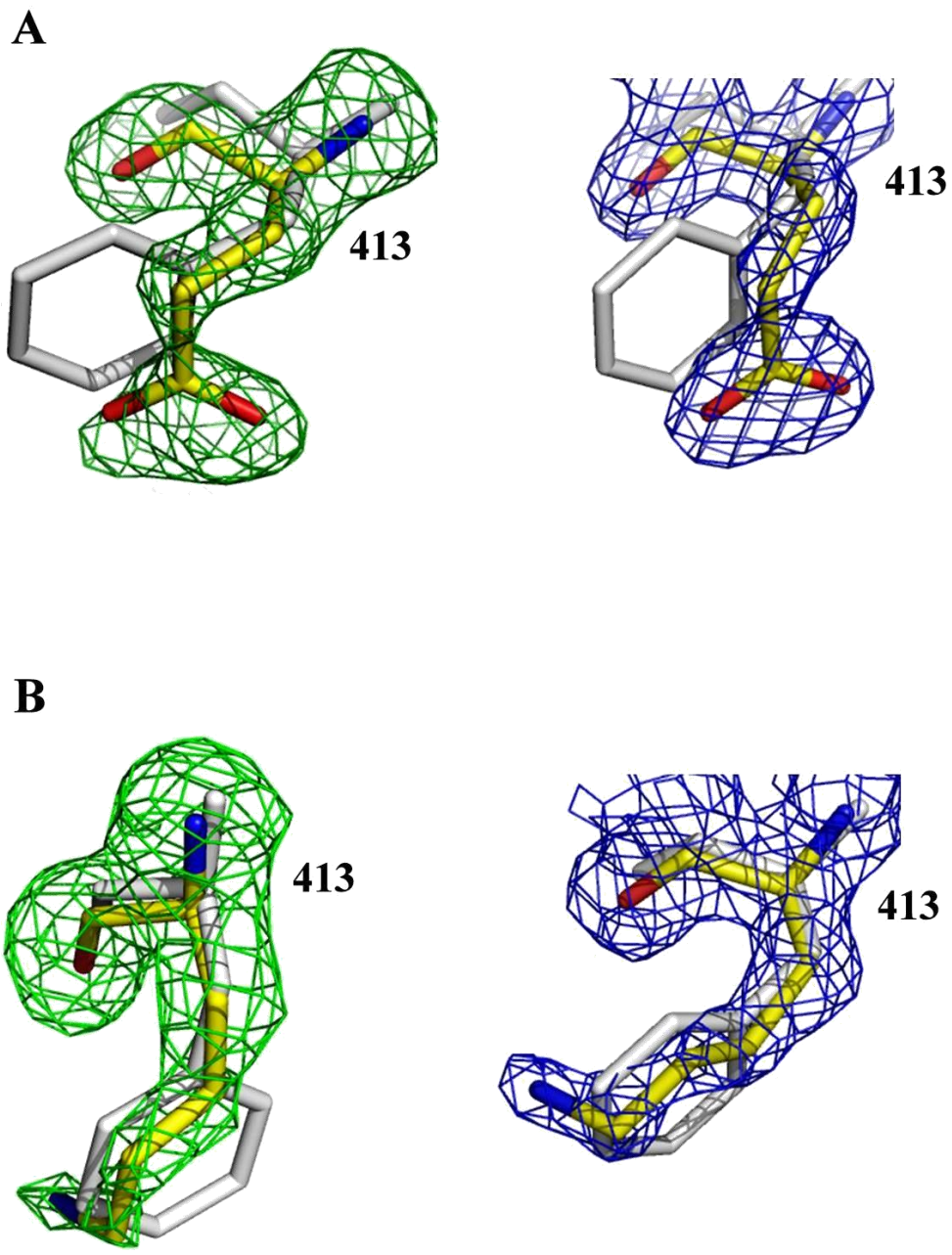

Figure 4.12. F_o-F_c (green) and $2F_o$-F_c (blue) electron density maps corresponding to the region of mutation at 413 in F413E (A) and F413K (B). F_o-F_c maps were calculated without the residues in the model and the appropriate model was superimposed. Yellow and grey stick represents the residue in the mutant and WT-HPII respectively. The Fo-Fc and $2F_o$-F_c electron density maps were modelled at $\sigma = 3.0$ and $\sigma = 1.0$ respectively.

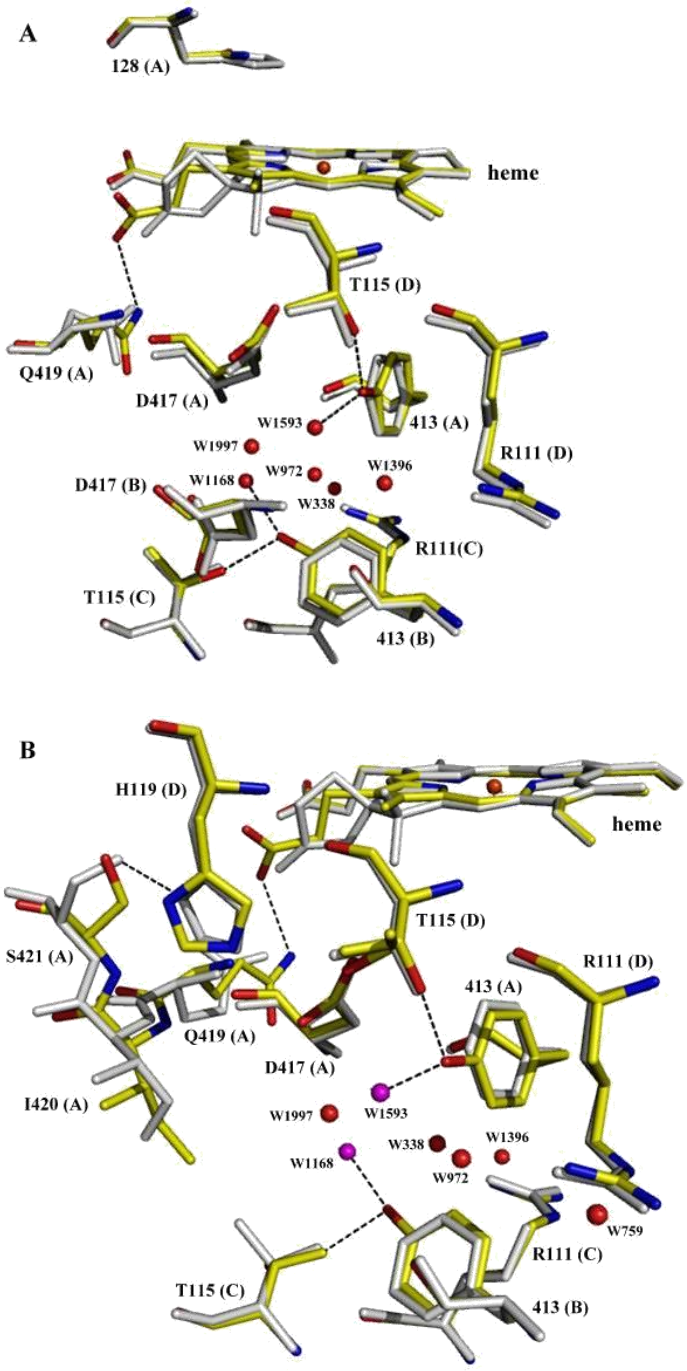

Figure 4.13. View of the heme proximal side residues and solvent organization in the vicinity of site of mutation at 413 in H128N/F413Y (A) and in F413Y with residues that are affected due to tyrosine replacement (B). Yellow and grey sticks represent residues of mutants and WT-HPII respectively. Letters in bracket represents residues of respective subunits. Solvent molecules are represented as red spheres. Magenta spheres (B) represents the solvent molecules conserved in H128N/F413Y and WT-HPII but absent in F413Y.

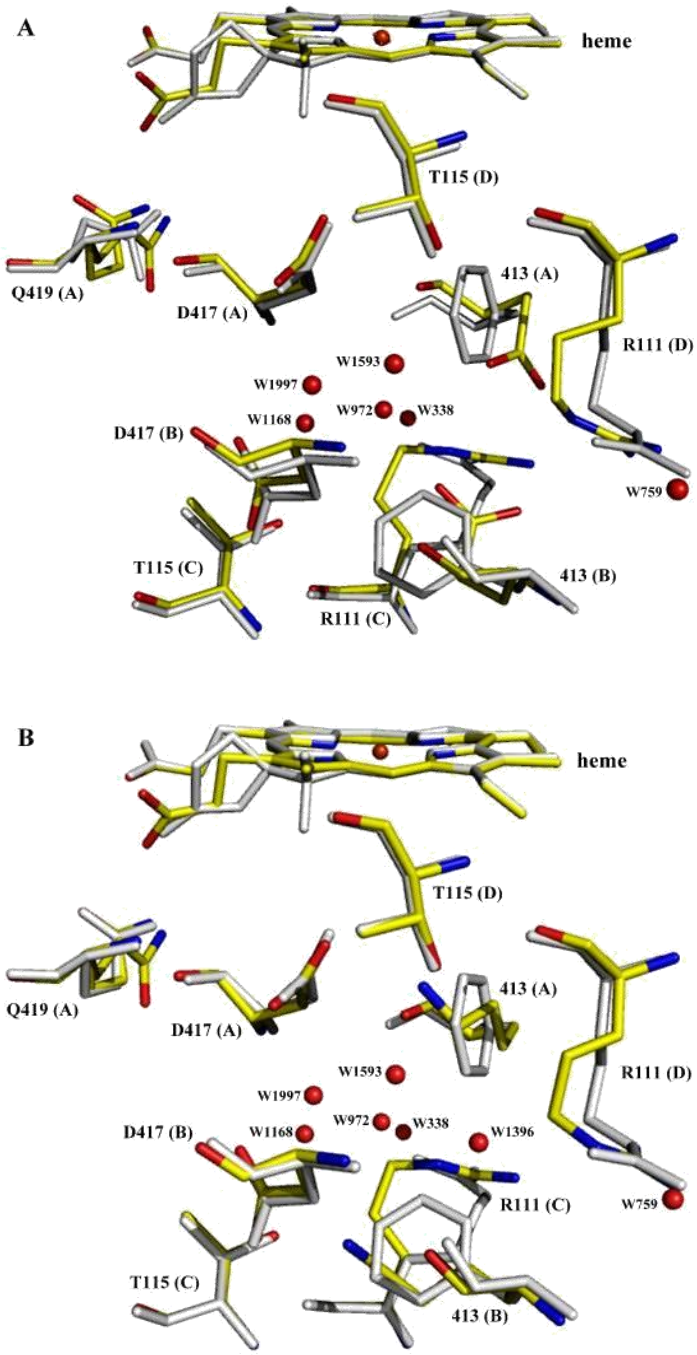

Figure 4.14. View of the heme proximal side residues and solvent organization in the vicinity of site of mutation at 413 in F413E (A) and in F413K (B). Yellow and grey sticks represents residues of mutants and WT-HPII respectively. Solvent molecules are represented as red spheres. All the waters including W1168 and W1593 are conserved in both WT-HPII and all F413 variants except in F413Y. Arg111 has a different conformation compared to WT-HPII and Gln419 occupies two conformations (A) and (B).

For reasons that cannot be fully explained, the variants show increased resistance to inhibitors compared to WT-HPII despite there being no change in the active site or access channel. Usually the reactivity and binding efficiencies of different enzymes towards these inhibitors vary based on differences in channel architecture, nature of the complex they form with the enzyme and also whether the binding is at the iron active site or elsewhere. Since no change in the channel architecture is observed in any mutants compared to WT-HPII, the reduced sensitivity towards inhibitors cannot be attributed to the reduced access of inhibitors into the active site. This is consistent with the similar catalytic turnover rates exhibited by the variants and the WT-HPII and is also supported by *Proteus mirabilis* and *Pseudomonas aeruginosa* catalases being respectively insensitive and sensitive to inhibitors despite similar access channels (Switala and Loewen, 2002). The differences in sensitivities of the variants towards inhibitors in comparison to WT-HPII might therefore be attributed either to a difference in the binding location or to the type of complex they form. Unfortunately, structures of the variants in complex with the inhibitors are not available, making it impossible to properly explain the observations.

Whereas there were only minor structural changes in the vicinity of the mutations in F413E and F413K, major structural changes are evident in the vicinity of the tyrosine in F413Y (Figure 4.13 and Figure 4.14). Not only are the side chains of a number of residues, including Tyr413 modified, but there are breaks in the main chain evident between residues 111 and 112, and 115 and 116. The common location of the side chain modifications and chain cleavage suggest that the changes are part of the same process and related to reactions occuring as part of the catalytic process rather than being caused by proteases

Numerous examples of the use of hydroxyl radical-generating systems for the modification and cleavage of protein (Rana et al., 1991 and Heilek et al., 1995), including side chain modification, crosslinking, and backbone scission have been described in the literature. In particular, exposure of peptides to hydroxyl radical is known to effect backbone cleavage, although the mechanism is not fully understood. Furthermore, tyrosyl residues have been shown to form relatively stable radicals in proteins (Marsh and Neil, 1995) including in catalases such as BLC (Ivancich et al., 1996) and PMC (Andreoletti et al., 2001), horseradish peroxidase (Miller et al., 1995), catalase-peroxidases (Ivancich et al., 2001, 2003; Chouchane et al., 2002; Ranguelova et al., 2007) and allene oxide synthase (Wu et al., 2003) where the tyrosine is located far from the active site heme. Therefore, one explanation for the structural changes observed in F413Y lies in the formation of a tyrosyl radical leading to a reactive center in the protein. The close proximity of Tyr413 to the heme and, in particular, the proximal ligand Tyr415 is consistent with this explanation. Catalytic turnover is required for heme modification and for creation of the His-Tyr cross link most likely involving a radical mechanism (Bravo et al., 1997). Thus, catalytic turnover may also produce a radical on Tyr413 that leads to other reactions in its vicinity. Consistent with this conclusion is the absence of any modifications in the vicinity of Tyr413 in the inactive variant F413Y/H128N. Furthermore, tyrosine radical formation is favored in tyrosines situated in an ionic environment which is created by the nearby Arg111.

Explaining how PMSF reduces the extent of modification in the vicinity of Tyr413 is more challenging. It is unlikely that it is acting in its normal role of a protease inhibitor, particularly during cell growth at 37 °C. Two possibilities seem likely. The first is that a degradation product of PMSF acts as a radical scavenger reducing the likelihood of radical

based reactions. The second is that a PMSF degradation product or a trace contaminant of fluoride might be inhibiting the enzyme in vivo reducing the extent of catalytic turnover and, therefore, modification. Further experimentation would be required to draw firm conclusions.

5. EFFECT OF CHANGES TO ILE274 AT THE ENTRANCE TO THE LATERAL CHANNEL ON CATALASE HPII

5.1. Introduction

Heme-containing monofunctional catalases catalyze the degradation of H_2O_2 utilizing the hydroperoxide as both an oxidant of the heme (reaction 8, Chapter 1) and a reductant of the intermediate oxoferryl heme species (reaction 9, Chapter 1), both being energetically favourable reactions. Several features of catalases have been identified as being important for catalysis, including specific residues and topographical features such as access channels. For example, a His and an Asn (Fita et al., 1986; Loewen et al., 1993; Melik-Adamyan et al., 2001) in the distal side heme pocket and an Asp 12 Å (Chelikani et al., 2003) from the heme in the main channel are essential for or greatly enhance the catalytic process. The dimensions of the access channels, as determined by the residues lining them are similarly important (Putnam et al., 2000). For example, removal of an Arg-Glu pair in the lateral channel enhanced activity almost 3 fold (Sevinc et al., 1999), presumably because the enlarged channel allowed easier movement of substrate H_2O_2 and products, O_2 and H_2O.

Modifications to amino acids and the heme, usually arising from oxidations, are common in catalases. In addition to there being two different heme orientations among the catalases, some large subunit or clade 2 catalases contain heme *d*, in which one propionate is converted to a hydroxylated spirolactone (Loewen et al., 1993 and Murshudov et al., 1996). In *Escherichia coli* KatE (also HPII), the proximal ligand Tyr415 is covalently linked to the nearby His392 (Bravo et al., 1997), while in *Neurospora crassa* Cat1, the Tyr-His linkage is replaced by a Tyr-Cys link (Diaz et al., 2004). Catalases generally have a small number of

cysteines, but their modification in KatE has been reported (Sevinc et al., 1995). Surprisingly, none of these modifications are required for or significantly affect activity, but they may protect the enzyme against further oxidation and, by providing increased rigidity, may enhance the enzyme's heat and protease resistance (Switala et al., 1999 and Chelikani et al., 2003).

Among the 14 catalase structures so far determined, a small number of residues are found with unfavorable backbone geometry, but the location of one residue with backbone angles, $\psi \approx -60°$ and $\varphi \approx 70°$ has been conserved across representatives from all three phylogenetic clades of the enzyme. The conserved location is near the heme edge at the opening to the lateral channel (Figure 5.1), an access route to the heme cavity that also parallels an electron transfer route between NADPH and the heme in some clade 3 enzymes (Olson et al., 1995 and Sicking et al., 2008). Only five different amino acids are found at the location among all catalases, including Val (62%), Ser (32%), Gly (3%), Ile (2%) and Ala (1%), with Ile being found only in large subunit clade 2 catalases, including Ile274 in *E. coli* KatE. Ser at the location has been assigned a role in electron transfer from NADPH to heme (Sicking et al., 2008) and the slow turnover rates of large subunit catalases have been correlated, in part, with the presence of Ile blocking the entrance to the lateral channel (Sevinc et al., 1999 and Switala and Loewen, 2002).

To define more clearly the role of this residue adjacent to the heme, whether catalytic, structural or both, a series of variants of *E. coli* KatE mutated at position 274 were constructed and characterized.

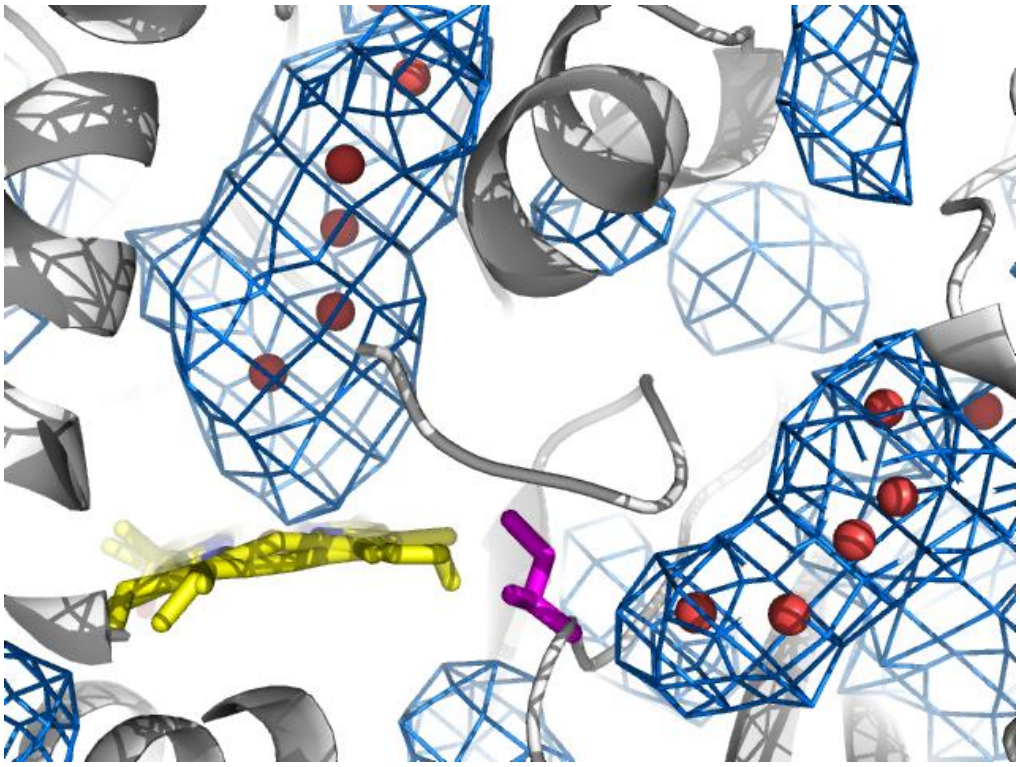

Figure 5.1. View of the heme cavity in HPII in relation to the main and lateral access channels based on the coordinates in 1GGE. The heme is shown in yellow and the side chain of I274 is colored magenta. The periphery or surface of the channels is indicated by the blue mesh and the red spheres within the mesh mark the locations of waters in the channels. The main channel is perpendicular to the plane of the heme and the lateral channel extends to the right with the I274 side chain situated at its end.

5.2. Results

5.2.1. Construction, purification and characterization of variants

Residue Ile274 in HPII is situated adjacent to the heme edge at the entrance to the lateral channel and, like residues at the same position in other catalases, it possesses unfavorable main chain geometry. To investigate the integrity of this residue in the catalytic function of the enzyme, it was mutated to residues found at the same location in other catalases. HPII mutants I274G, I274A, I274V, and I274S were constructed along with I274C to provide a sulfhydryl group for the introduction of non-standard amino acid side chains, and I274F to insert a large aromatic group.

Despite repeated attempts, no protein was ever obtained from the I274S- or I274F-encoding systems. This was most likely the result of aberrant folding that allowed proteolysis to occur before a protease resistant structure was formed (Sevinc et al., 1998). While not a big surprise in the case of I274F, where the large phenyl ring would have occluded heme packing and interfered with protein folding, the outcome with I274S was puzzling because Ser is common at this location among catalases, is similar in size to the Cys in I274C and is smaller than the β-branched I274V and native I274, all of which accumulated normal amounts of protein along with I274G and I274A.

The variants I274A, I274G, I274V, and I274C exhibited similar electrophoretic mobilities as the WT-HPII on the SDS-PAGE gel (Figure 5.2). All the four variants revealed differences in the UV-vis spectra compared to WT-HPII indicating the presence of a mixture of heme *b* and heme *d* (Figure 5.3). Extraction of heme from the variants by acetone-HCl followed by HPLC analysis revealed predominantly heme *d* but with amounts of heme *b* that varied among the variants and even among different batches of the same variant. I274C was

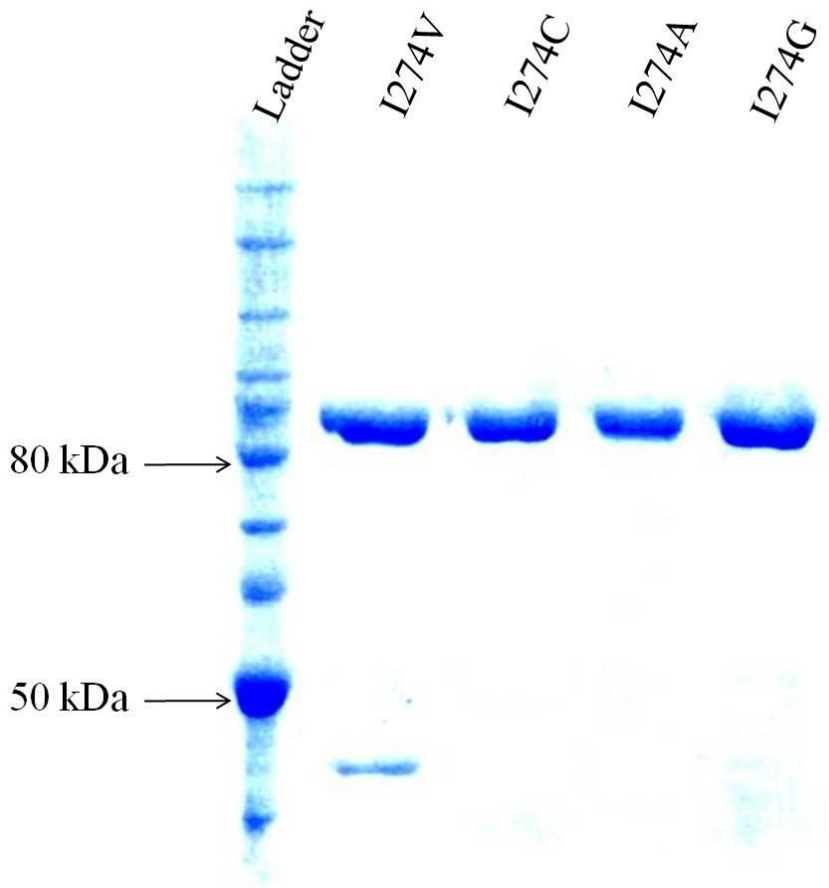

Figure 5.2. SDS-PAGE analysis of the purified WT-HPII and its variants. Approximately 2 µg of proteins were loaded and run on the 8% polyacrylamide gel. The gel was stained with Coomassie brilliant blue after electrophoretic separation.

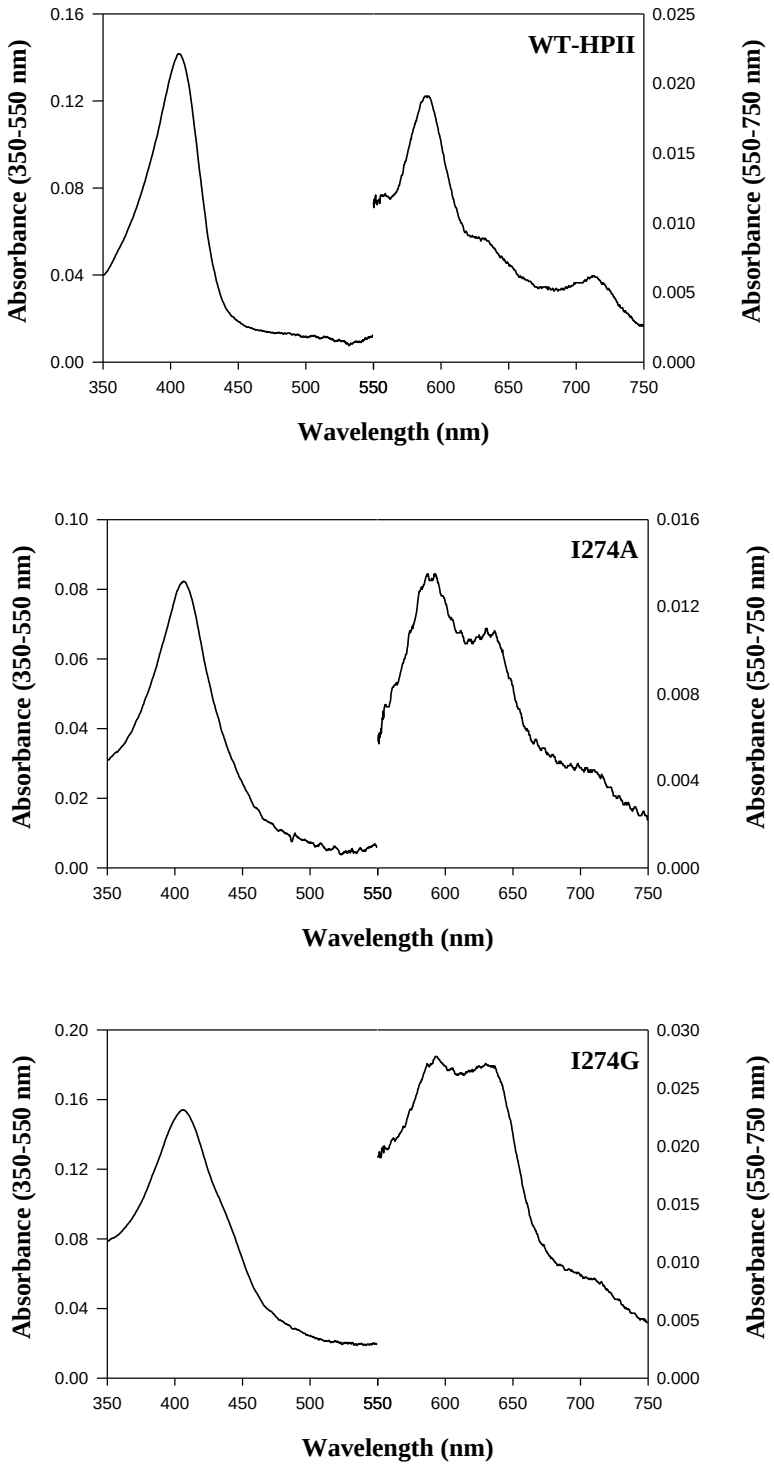

Figure 5.3. Absorption spectra of purified WT-HPII and its variants. The left axis corresponds to the absorbance values between 350-550 nm while the right axis corresponds to the absorbance values between 550-750 nm.

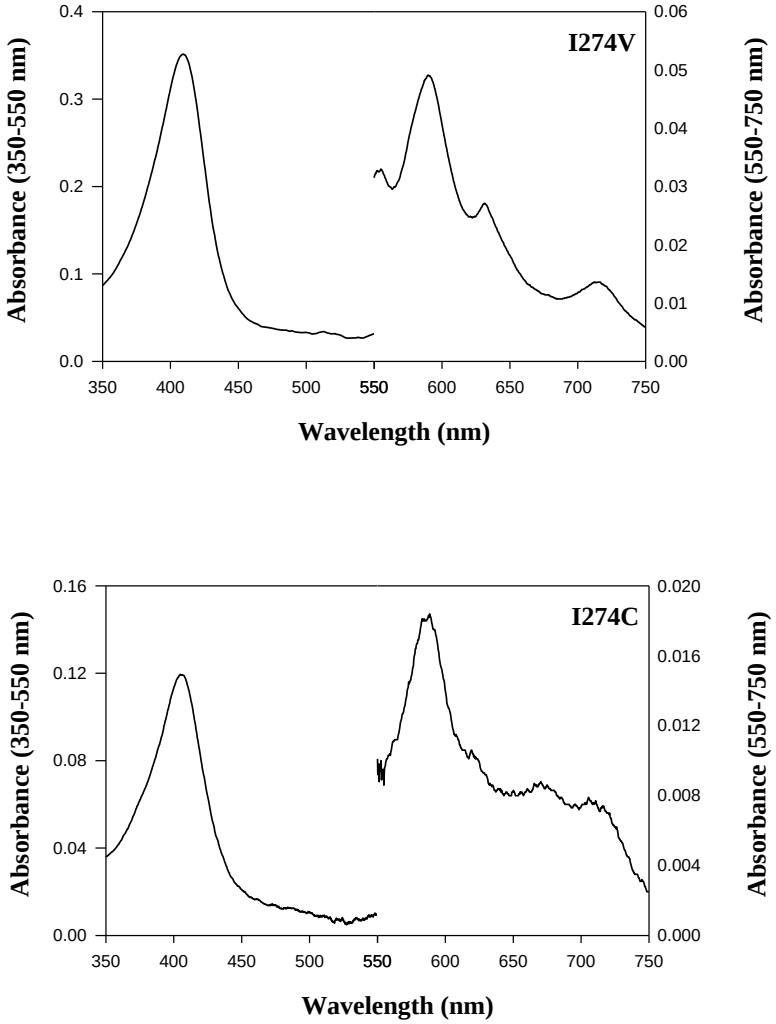

Figure 5.3. Continued...

unique in yielding no extractable heme either by acetone-HCl extraction (Figure 5.4) or during mass spectrometry analysis (Figure 5.5 and 5.6) suggesting that its heme was covalently linked to the protein.

The R_z values exhibited by I274A, I274G and I274C are much lower, in the range of 0.5 to 0.6 similar to what has previously been reported for the Cpd I/II derivative of WT-HPII (Chelikani et al., 2005). Two explanations for such low values, impure protein or low heme content, are inconsistent with the > 95% purity as judged by SDS-PAGE and the integrity of the heme in the core of the enzyme that precludes protein folding in its absence. In the case of I274C, an additional charge transfer band at 670 is evident suggesting a change in heme chemistry.

The kinetic parameters of the Gly, Ala and Val variants reveal reduced turnover rates and decreased affinities for H_2O_2 (higher apparent K_M values) (Table 5.1), leading to a correlation of lower activity with smaller residues at position 274, just the opposite of what was expected for a less obstructed entrance to the lateral channel. The Cys variant also exhibits a slower turnover rate and differed only in presenting a reduced apparent K_M, which may be related to cysteine-specific reactions described below.

5.2.2. Crystal structure analysis of the I274 variants

To determine what changes in structure might be responsible for the catalytic and spectral differences observed among the I274 variants, their structures were determined by X-ray crystallography. Crystals of I274G, I274A, I274V and I274C were prepared and used to collect X-ray diffraction data sets that refined to between 1.9 and 1.5 Å (Table 5.2). The electron density maps clearly defined the main chain and side chain atoms of 2904 amino acids, four heme groups and 3200-3500 waters in four subunits. The maps show complete

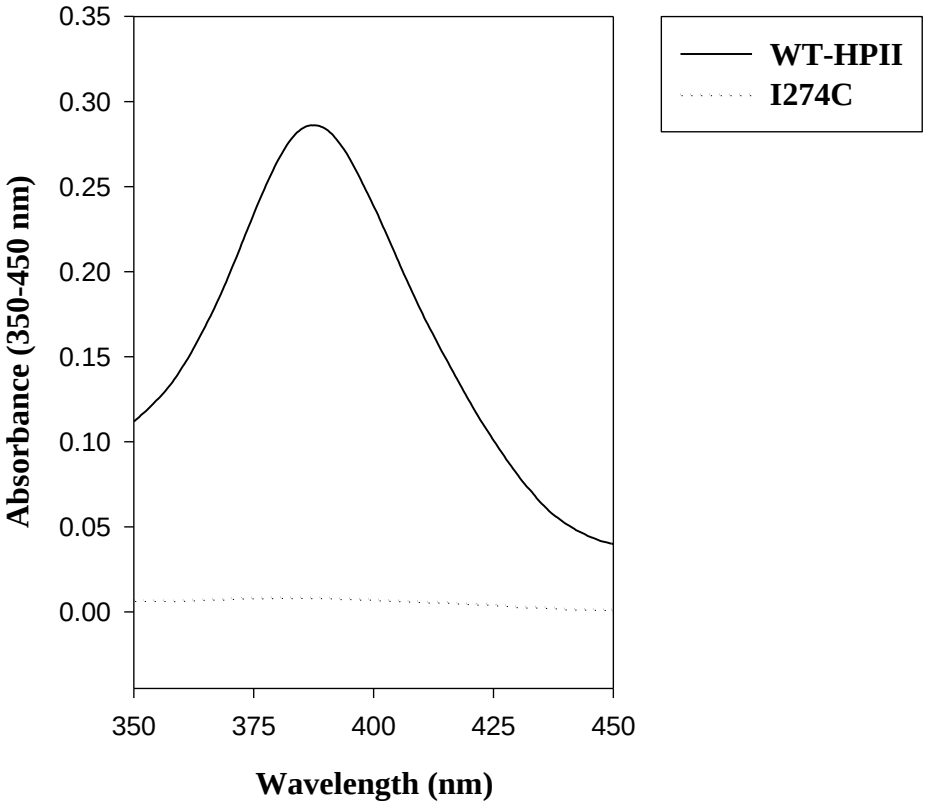

Figure 5.4. Absorption spectra of heme extracted from WT-HPII and variant I274C with acetone-HCl at RT.

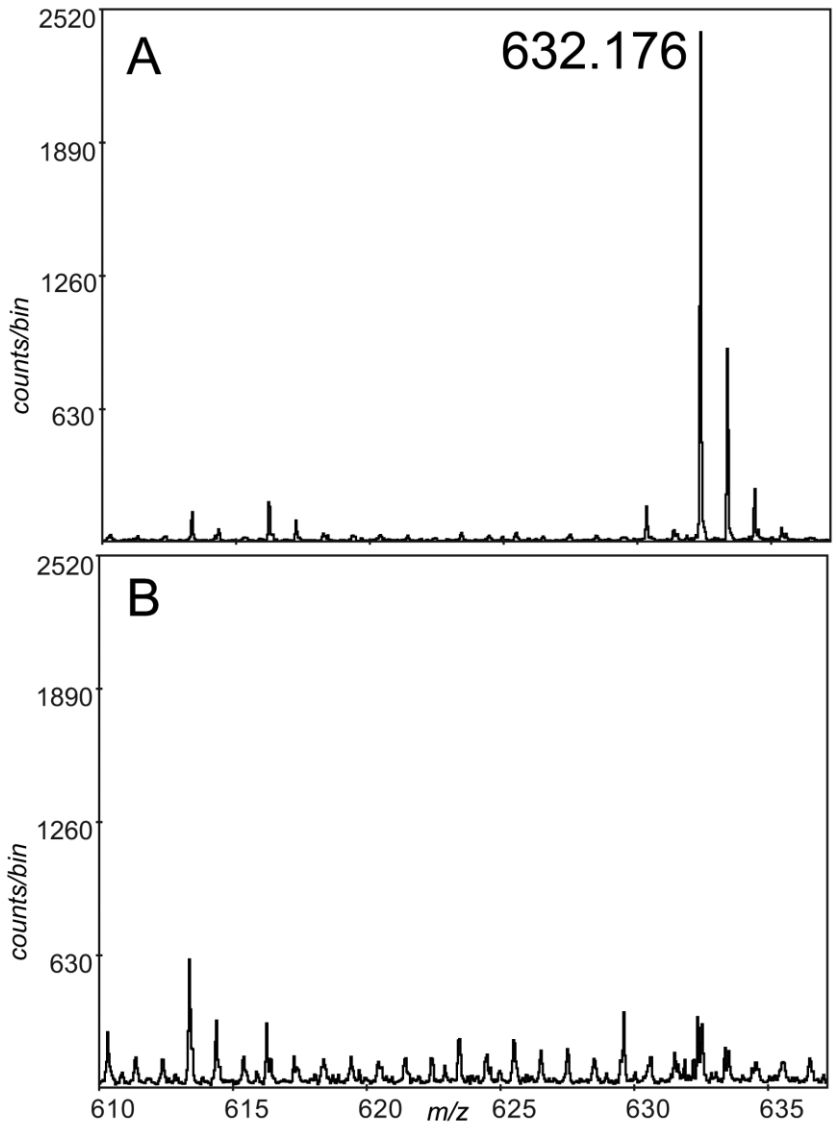

Figure 5.5. Mass analysis by electrospray mass spectrometry of denatured HPII (A) and its I274C variant (B) in the 610 to 640 Da region. Protein was dialysed into 5 mM ammonium acetate, diluted to 10 μM protein in 50% methanol, 1% acetic acid. Spectra were obtained by electrospray ionization on a mass spectrometer built and maintained at the University of Manitoba by Drs. K. G. Standing and W. Ens (Kozlovski et al., 2005). Using a declustering voltage of 180 V in both samples to facilitate heme release from the protein, significant heme was released only from HPII and not from the I274C variant. The time of ion accumulation in B was twice as long as in A, but no significant ions at 616 Da (heme *b*) and 632 Da (heme *d*) were evident.

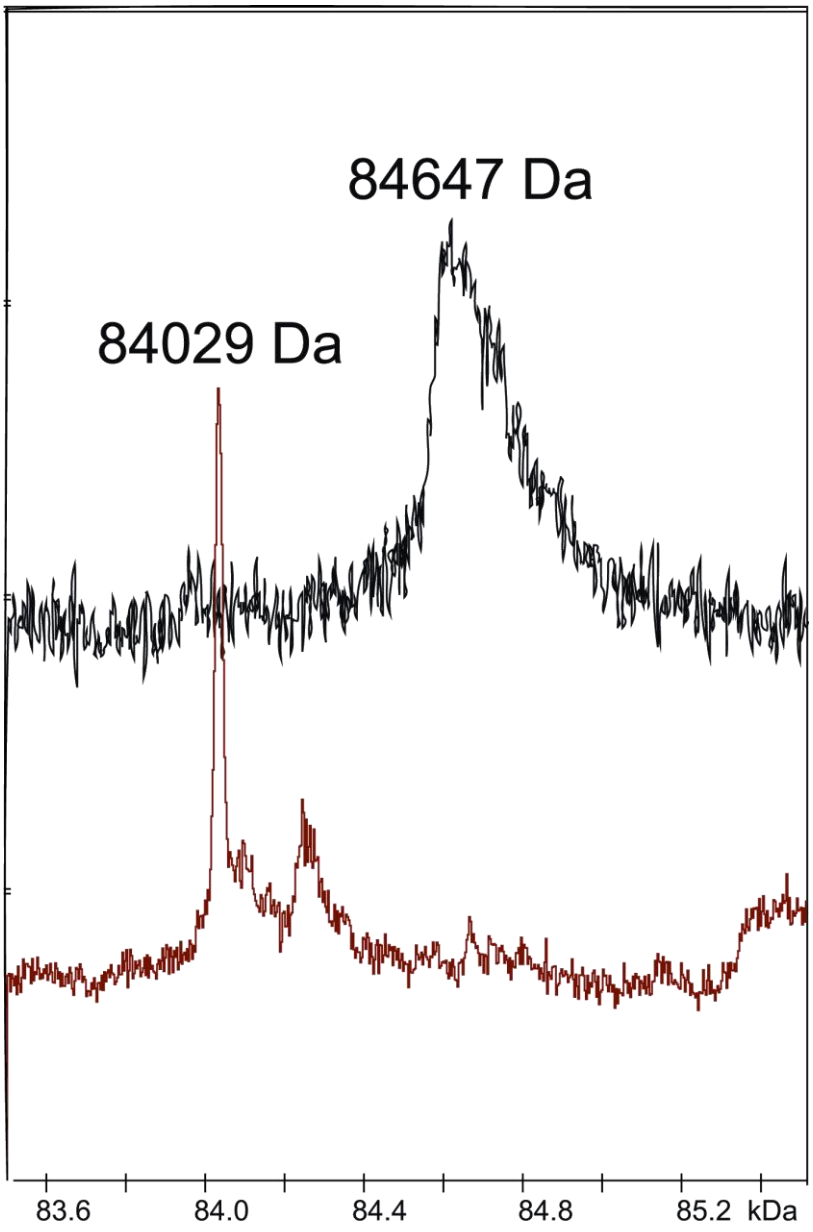

Figure 5.6. Mass analysis by electrospray mass spectrometry of denatured HPII (red) and its I274C variant (black) in the 84-85 kDa region. The samples were treated as described in Figure 5.4. The mass of the variant is larger than that of the native enzyme by the approximate mass of a heme 616 to 634 Da consistent with it not being released from the protein. The larger size envelope of the I274C variant was observed in all preparations and cannot be fully explained although it may in part be due to a mixture of heme *b* and heme *d* attached to the protein.

Table 5.1. Comparison of A_{407}/A_{280} ratio, catalase specific activities and kinetic constants for purified WT-HPII and its variants.

Variants	**R_z (A_{407}/A_{280})**	**Specific activity (U/mg)**	**Observed**		**k_{cat}/K_M ($M^{-1}sec^{-1}$)**
			k_{cat} (sec^{-1})	K_M (app)[a]	
WT-HPII	0.94	21000 ± 1400	70000	145	0.5×10^6
I274A	0.74	7700 ± 490	20900	500	0.4×10^5
I274G	0.52	4300 ± 710	13700	1000	0.1×10^5
I274V	0.90	18000 ± 1400	53000	500	0.1×10^6
I274C	0.52	4560 ± 600	19300	80	0.2×10^6

[a] K_M apparent, represents H_2O_2 concentration at $V_{max}/2$, mM.

Table 5.2. Data collection and structural refinement statistics for I274 variants of HPII.

	I274G	I274A	I274V	I274C
A. Data collection statistics				
Space group	$P2_1$	$P2_1$	$P2_1$	$P2_1$
Unit cell parameters				
a (Å)	93.41	93.56	93.5	93.66
b (Å)	133.18	133.17	132.82	133.02
c (Å)	122.74	122.81	122.59	122.59
α, β,γ (deg.)	90, 109.21, 90	90, 109.24, 90	90, 109.47, 90	90, 109.60, 90
Resolution[a]	35.20-1.90 (2.00-1.90)	31.30-1.90 (2.00-1.90)	29.40-1.50 (1.58-1.50)	35.20-1.48 (1.52-1.48)
Unique reflections	221,203 (31,939)	197,718 (23,877)	426,044 (58,221)	429,958 (54,412)
Completeness %	99.4 (98.7)	88.9 (74.0)	95.0 (89.1)	91.8 (79.7)
R_{merge}	0.139 (0.533)	0.097 (0.284)	0.119 (0.590)	0.081 (0.483)
$\langle I/\sigma(I)\rangle$	8.7 (2.9)	7.5 (3.1)	7.0 (1.9)	8.4 (2.0)
Multiplicity	3.8 (3.7)	2.8 (2.2)	3.7 (3.1)	3.1 (2.7)
B. Refinement statistics				
No. of reflections	210,008 (11,178)	187,606 (9,959)	404,546 (26,760)	408,282 (25,943)
R_{work} (%)	13.6 (21.4)	14.1 (21.7)	14.8 (29.7)	14.2 (26.2)
R_{free} (%)	18.6 (27.0)	19.4 (28.0)	18.4 (33.2)	17.6 (33.0)
Non-hydrogen atoms	26,229	26,183	26,643	26,838
Water molecules	3,222	3,204	3,283	3,512
Average B factor (Å^2)				
proteins	12.3	6.5	10.5	9.4
hemes	10.5	6.3	4.3	8.2
waters	22.1	14.9	22.2	19.7
rms deviations				
bond lengths (Å)	0.023	0.022	0.027	0.029
bond angles (deg.)	1.86	1.97	2.35	2.35

[a] Values in parantheses correspond to the highest resolution shell.

continuity from Ser28 to Ala753 in all four subunits. The expected side chains at position 274 were evident for each of I274A, I274G and I274V (Figure 5.7) and the unfavourable geometry of the residue was retained in each. A new water in the cavity created by the missing side chain was evident in I274G, coordinated between the main chain carbonyl oxygens of Thr203 (2.9 Å) and Phe272 (3.5 Å) (Figure 5.7 C). In all three cases, the covalent linkage between the side chains of Tyr415 and His392 was fully formed confirming that the variants had gone through several rounds of catalysis prior to purification (Loewen et al., 1993). In addition, the crystal structures of the variants reveal distal side waters coordinated with the heme iron at higher occupancy in I274A, I274C and I274G than in I274V or the native enzyme (Figure 5.8).

5.2.2a. Heme heterogeneity

The heme of catalases is either heme *b* or heme *d* and is found in one or the other of two orientations that are 'flipped' along the vinyl-propionate axis relative to one another. In WT-HPII a mixture of heme *b* and *d* is always found with heme *d* or *b* predominating (> 80%) in cells grown aerobically (Mate et al., 1999) or anaerobically (Loewen et al., 1993), respectively. In WT-HPII and catalase CatF from *Pseudomonas syringae* (Carpena et al., 2003), the heme is oriented with ring IV overlapping or stacked (3.4 Å) with the imidazole ring of the essential histidine (His128 in HPII), the His-IV orientation. The opposite or flipped orientation with ring III stacked with the essential histidine (His-III) is found in clade 3 enzymes (Fita et al., 1986; Putnam et al., 2000; Mate et al., 1999 and Loewen et al., 2004). It was therefore surprising to find a mixture of approximately equal proportions of both orientations in I274V and a greater proportion of the flipped, His-III, orientation in I274A (Figure 5.9). The orientation and relative amounts were estimated based on satisfactory

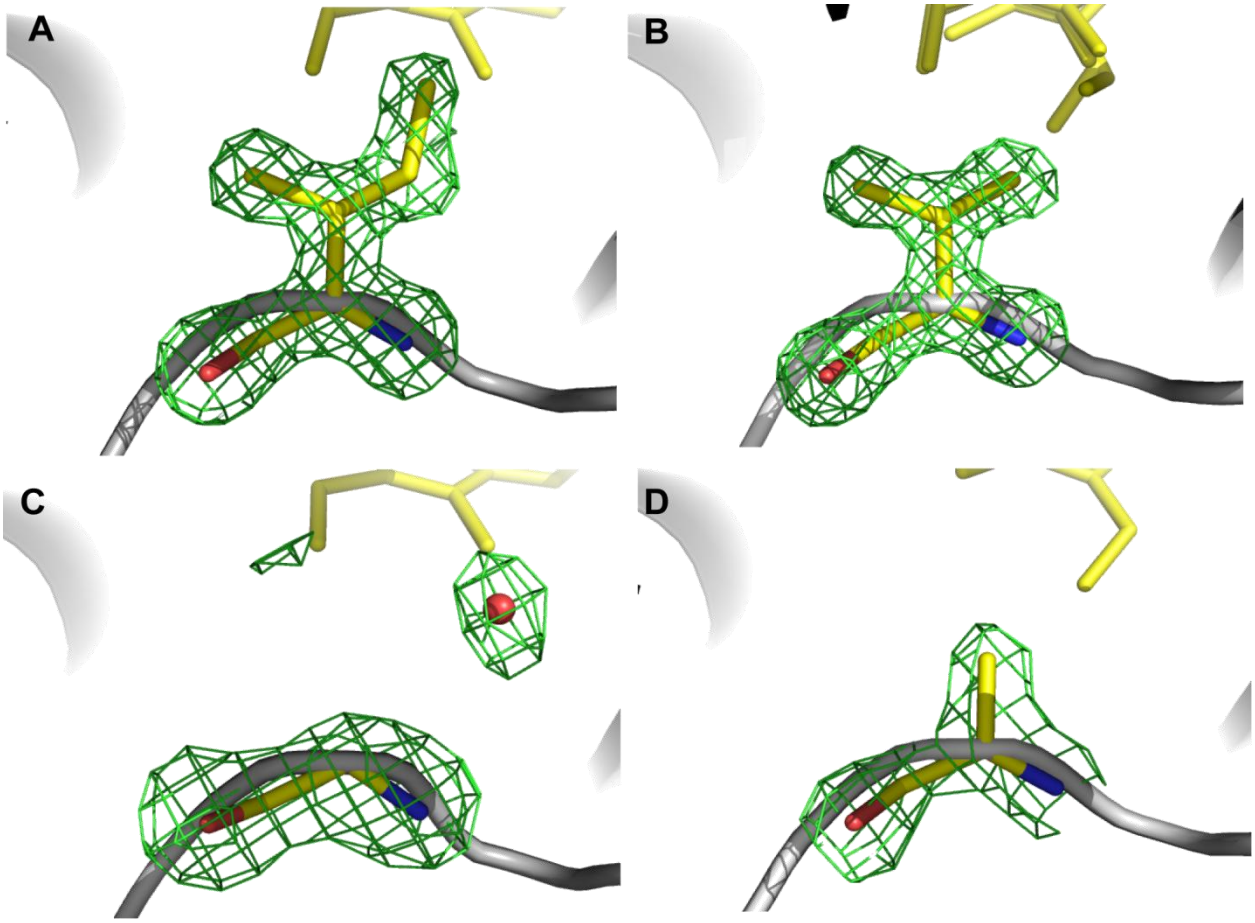

Figure 5.7. F_o-F_c electron density maps corresponding to the side chains of Ile274 (A), Val274 (B), Gly274 (C) and Ala274 (D). The F_o-F_c electron density maps, drawn in green at $\sigma = 3.0$, were calculated without the side chain in the model and the appropriate models are superimposed for illustration.

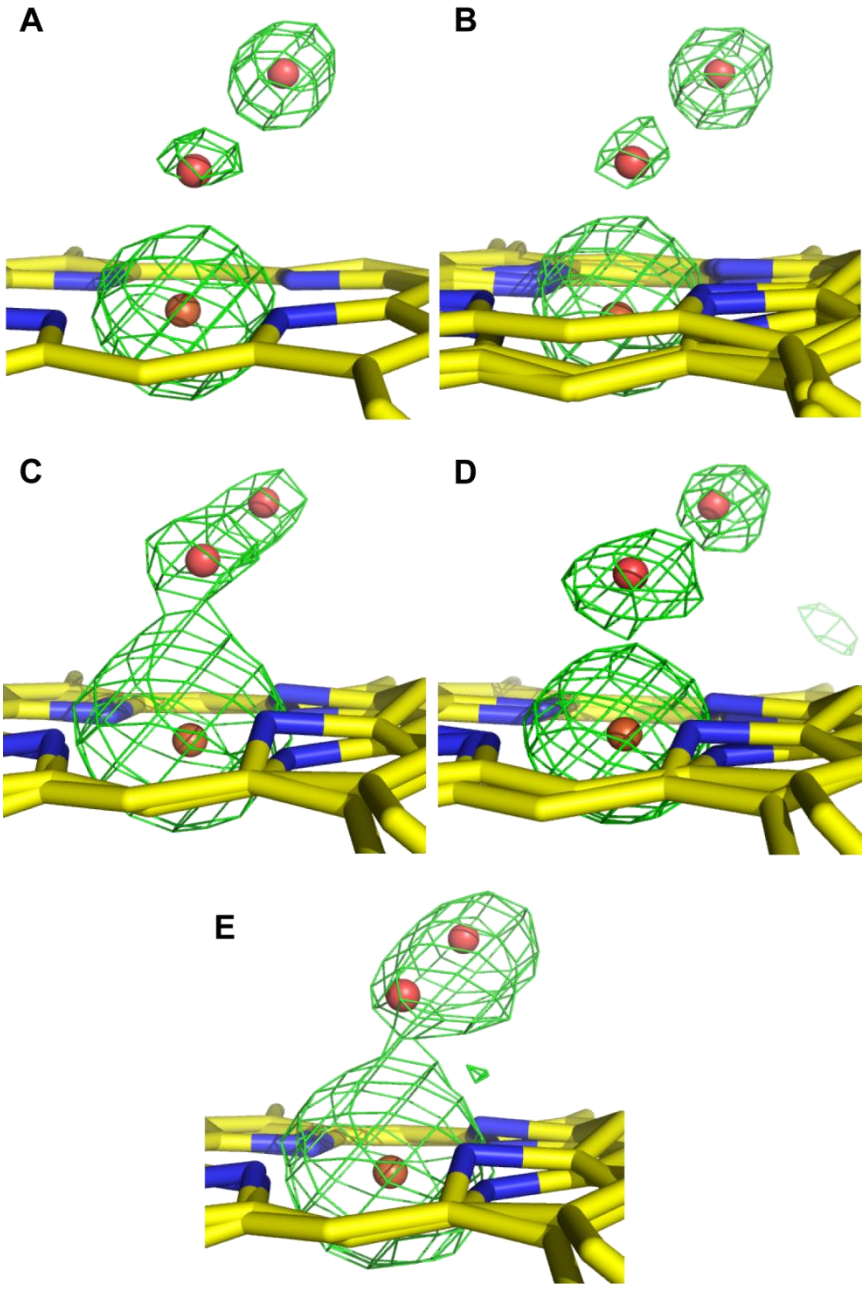

Figure 5.8. Electron density maps showing the heme iron and distal side waters in the native enzyme (A), I274V (B), I274A (C), I274C (D) and I274G (E). The F_o-F_c electron density maps, drawn in green at $\sigma = 3.0$, were calculated without iron or oxygen in the model and the orange sphere for iron and red sphere for oxygen are superimposed for illustration. The multiplicity of different heme orientations is also included.

refinements with partial occupancies of the two orientations and on the B factors for the vinyl C_βs being similar to those of the nearby heme atoms. The presence of predominantly His-IV orientation in I274G breaks the apparent correlation of more His-III orientation with smaller side chains, but this discrepancy might be explained by the water apparently replacing the side chain (Figure 5.7 C). In this location, it is 3.6 Å from the ring I methyl in the His-IV orientation and would make contact with a vinyl at that location in the His-III orientation. Thus while the identity of residue 274 in close proximity to the heme vinyl groups does influence heme orientation, chain size is not the only determinant. I274A also presents an unusual modification on the vinyl, possibly a result of hydroxylation (Figure 5.9 D). A water refines nicely at this location about 1.7 Å from the vinyl carbon, but confirmatory data are needed.

The heme complement in I274V includes both orientations of both heme *d* and heme *b*, estimated to be in equal proportions based on a comparison of B factors of the spirolactone and unmodified propionate atoms. This would have arisen from heme *b* initially binding in both orientations, each of which would have been oxidized stereospecifically to generate the two different isomers of heme *d*. In the native His-IV orientation, carbons 12 and 13 of ring III are modified to the 12(S)-hydroxy-13(R)-cis-spirolactone porphyrin, whereas in the flipped His-III orientation, carbons 17 and 18 of ring IV are modified to an 18(S)-hydroxy-17(R)-cis-spirolactone porphyrin (Figure 5.9 E and F). The subtlety of these stereochemical differences is illustrated by the fact that the initial structural assignment of heme *d* from HPII based on NMR was as 12(R)-hydroxy-13(S)-cis-spirolactone (32), and this was later revised by the X-ray structure to the 12(S)-13(R) isomer in both HPII and *Penicillium vitale* catalase (Murshudov et al., 1996). The native crystal (Figure 5.9 A) also

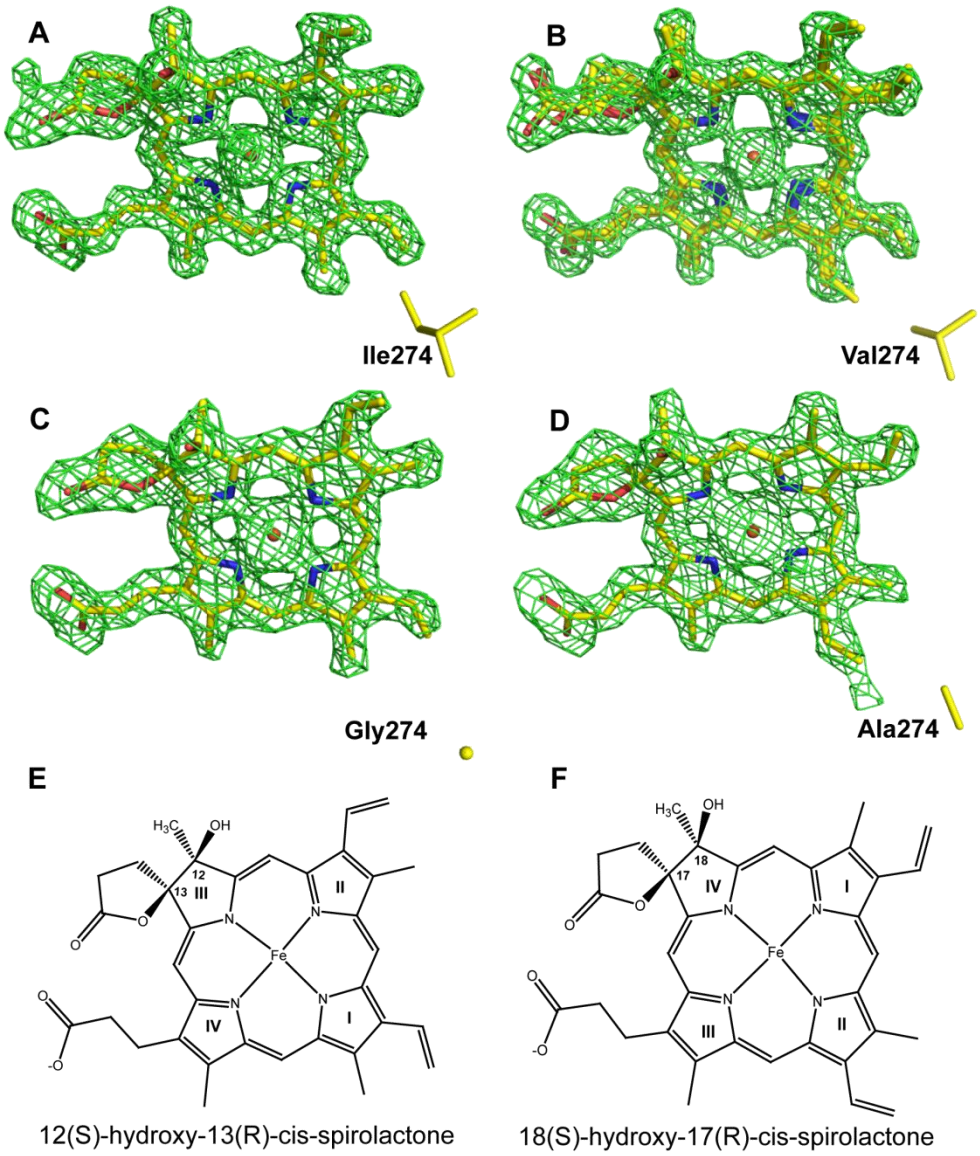

Figure 5.9. Heme composition in the WT-HPII (A), I274V (B), I274G (C) and I274A (D). The side chain of the different residues are shown at the bottom right of each panel for orientation. The F_o-F_c electron density maps, drawn in green at $\sigma = 3.0$, were calculated without heme in the model and the appropriate models are superimposed for illustration. The native enzyme (A) and I274G variant (C) contain predominantly the His-IV orientation. The I274V variant (B) contains a mixture of both heme *b* and heme *d* in both the native His-IV and His-III orientations while the I274A variant contains predominantly (~70%) of heme *d* in the 'flipped' His-III orientation. The stereochemistry of the heme *d* isomers are shown for the native His-IV orientation in panel E and the 'flipped' His-III orientation in panel F.

shows evidence of a small amount of the heme *b*, confirming that the extent of heme *b* to heme *d* conversion is batch specific and must be determined by subtle differences in growth conditions.

5.2.2b. X-ray irradiation causes changes in the structure of I274C

Analysis of the I274C diffraction data was presumably complicated by chemical changes associated with a striking colour change in the crystal from the normal dark brown-green to bright green that occurred rapidly on exposure to an X-ray beam (Figure 5.10). Fortunately, the chemical changes causing the color change did not affect the diffraction quality of the crystals, which routinely diffracted to above 1.6 Å (Table 5.2).

The electron density maps reveal only heme *d*, but with approximately equal proportions of the two orientations. Unlike the I274G, I274A and I274V variants, which produced electron density maps that were readily satisfied by the expected side chains in the model, a cysteine side chain presents only a partial solution for residue 274 in I274C. The F_o-F_c omit maps present four unusual features including (i) the presence of weak density corresponding to C_β, (ii) a sphere of density close to but only weakly linked to either the heme vinyl or the C_β of residue 274, (iii) a nearby isolated sphere of density and (iv) density between the heme vinyl and the side chain of Asn201 (Figure 5.11 A). Whereas Figure 5.11 A shows no obvious electron density linking the vinyl (in the His-III orientation) and Cys274, the maps in Figure 5.11 B (the orientation is rotated to that in Figure 5.9) calculated from a data set of early images (see below) reveal density linking the protein with the vinyl of the heme, although both bonds are somewhat stretched at 1.9 Å for C_β-S and 1.7 Å for heme-S. The unlinked sulfur is situated approximately 2.5 Å from the heme vinyl (in the His-IV orientation) and 2.2 Å from the C_β methylene group, too far in both cases for a

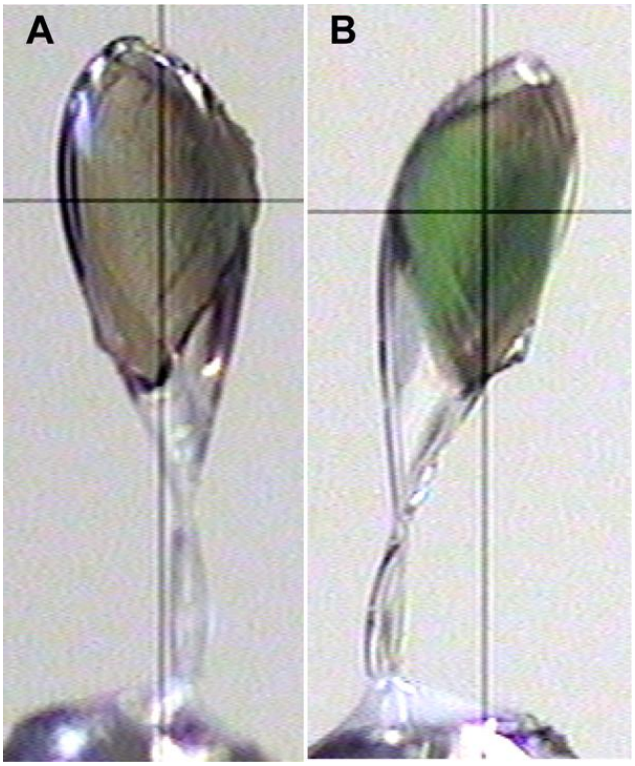

Figure 5.10. The colour change in a crystal of I274C before (A) and after (B) X-ray irradiation. The crystal shown was used to collect 160 images involving 5 hours of exposure time.

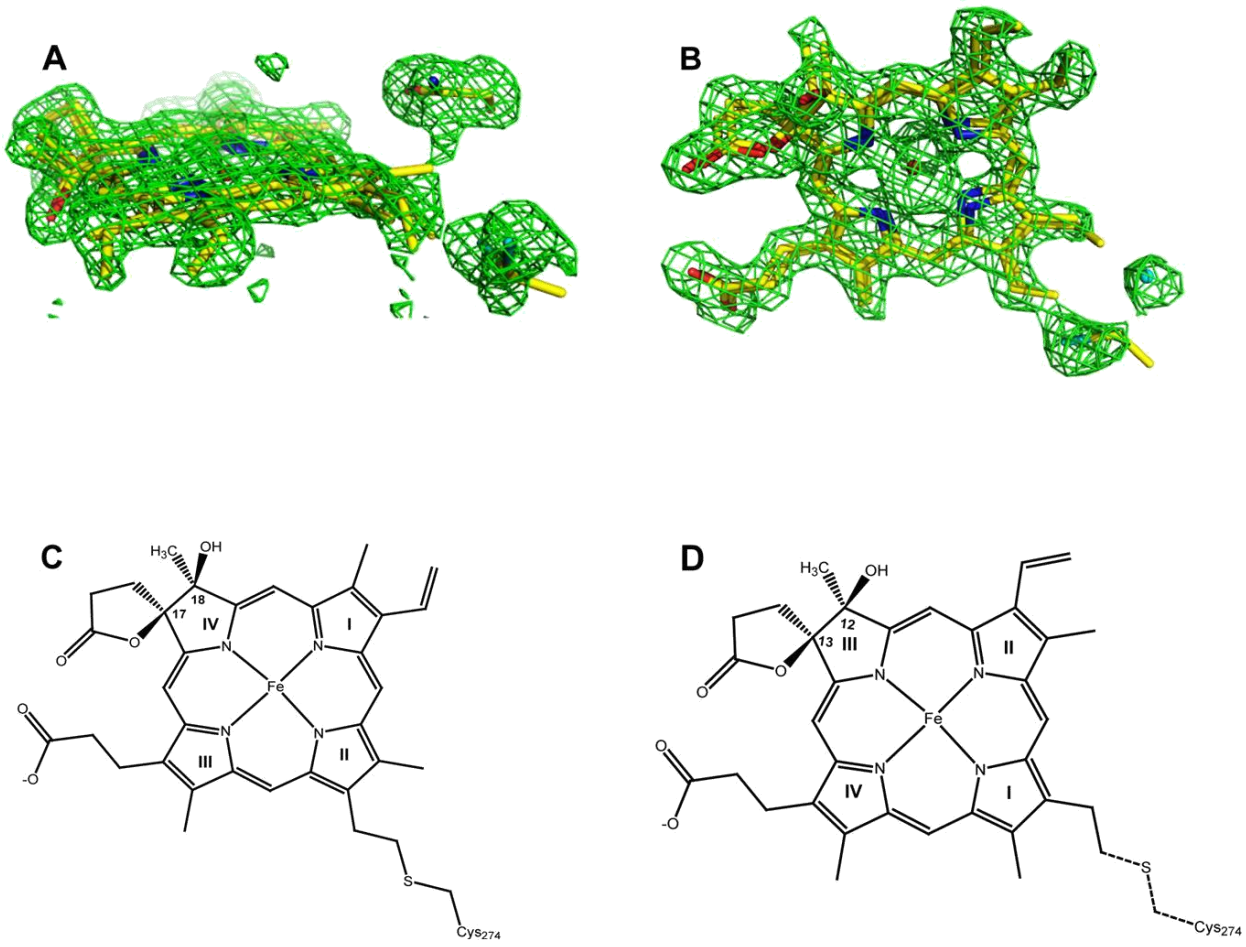

Figure 5.11. Electron density maps illustrating the residual heme-protein crosslink in I274C. The F_o-F_c electron density maps, drawn in green at $\sigma = 3.0$, were calculated without heme in the model and the appropriate models are superimposed for illustration. Two different views are shown in panels A and B. The electron density maps in panel A are calculated from a complete data set and reveal the absence of density between the heme and Cys side chains. In addition, the weak density approaching the distal side Asn201 is evident. The maps in panel B were calculated from a merged data set of the first six images (1 to 6) from 33 crystals and are shown in the same orientation as in Figure 5.9 for comparison with the other variants. Panels C and D show the structures of the two different heme-Cys cross links arising from the presence of two heme *d* isomers. The structure in panel D is shown with dashed bonds because the linkage has been completely destroyed by irradiation whereas there is weak electron density evidence for the structure in panel E.

covalent bond. Given that the heme is 100% covalently attached to the protein before X-ray exposure, these maps suggest that the covalent bonds between the Cys-S and the nearby vinyl groups, 50% in each orientation, are very sensitive to X-ray irradiation. The covalent bond that would have existed between what has become the unlinked sulfur and the heme is more sensitive than between the residual Cys and the heme, for which there is stronger density. Another unusual and unexpected feature evident in the electron density maps is the presence of weak density linking the heme and the distal side asparagine (N201) (Figure 5.11 A).

The rapid color change caused by X-ray irradiation suggested that changes in heme chemistry were occurring within the first one or two exposures to the X-ray beam whereas the fragmented model evident in the refined structure (Figure 5.11 A) was initially based on a data set of 180 sequential images. In an attempt to gain a better picture of the molecule before X-ray damage had occurred, images from 33 different crystals were merged in blocks of six (images 1 to 6, 7 to 12, 13 to 18, etc). There was more evidence of the Cys-heme crosslink in the electron density maps calculated from the first six images (Figure 5.12 A), but there is still considerable breakage evident, particularly around the unlinked sulfur atom. Further degradation of the Cys-heme bond is evident as exposure times increase until there is no further bond evident after 30 exposures (Figure 5.12). In addition the density between the heme and Asn201 is not evident at short exposure times indicating that it is a result of longer X-ray exposure.

5.2.2c. I274C is isolated as oxoferryl intermediate

As documented in Table 5.1, the R_z values of the I274G, I274A and I274C variants are low suggesting a lower than expected extinction coefficient for the Soret absorbance.

The crystal structures of the variants provided no evidence of a heme modification (aside from the fragmented cross link in I274C) that might be responsible for the change in Soret band, but they did reveal significant differences in the distal side waters which are present with much higher occupancy in I274A and I274G and in I274V and the native enzyme (Figure 5.8). In addition, the models refined from the merged data set of early images do present a subtle but significant difference from the model refined from a single continuous image set. Specifically, the oxygen atom in close coordination with the heme iron is subtly closer in the earliest image set (2.26 Å compared to 2.39 Å) and has a smaller B value (12.6 $Å^2$ compared to 20.8 $Å^2$). Comparing the different merged data sets reveals a gradual change in B value for the oxygen from 12.6 $Å^2$ to 24.6 $Å^2$ (image set 1-6 compared to image set 37-42) while the distance increases slightly from 2.26 Å to 2.41Å (Table 5.3). The B factor of the water adjacent to the coordinated oxygen changes only slightly over the same period (Table 5.3 C). A striking visual confirmation of this change is evident in the electron density maps, wherein continuous density between the iron and oxygen in the earliest image set becomes broken in the later image sets, (Figure. 5.13). These changes in oxygen occupancy and association with the heme iron are reminiscent of the changes observed in horseradish peroxidase (Berglund et al., 2002) and cytochrome c peroxidase (Meharenna et al., 2010) as the oxoferryl compound I suffers reduction by X-ray irradiation.

5.3. Discussion

Changing the side chain of Ile274 in HPII, a residue with unusual main chain geometry located in the heme cavity at the entrance to the lateral channel, elicits a number of changes in the activity and structure of the enzyme, including reduced turnover rates, a mixture of heme orientations and heme crosslinking to the protein in the Cys variant.

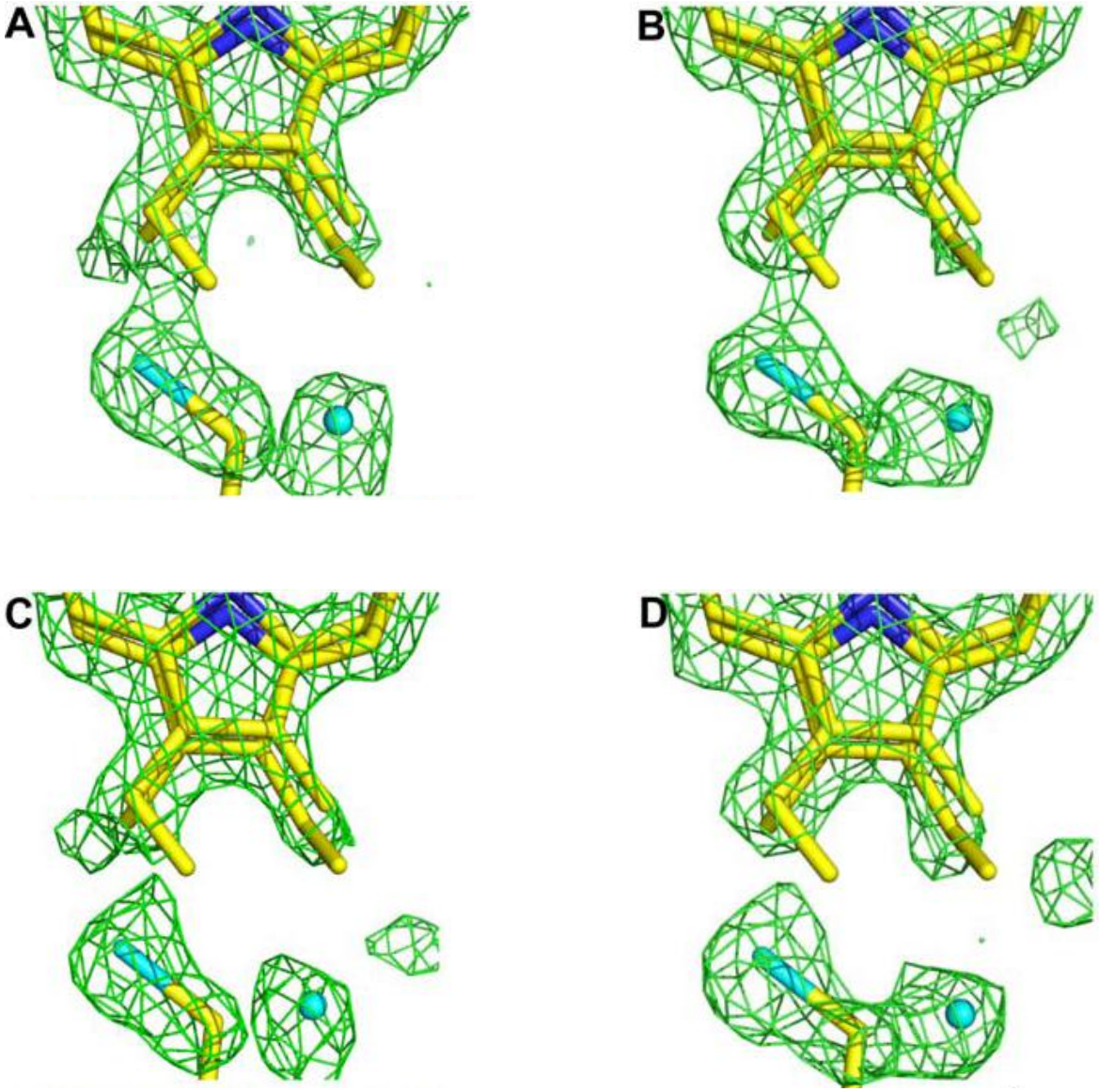

Figure 5.12. Electron density maps showing the changes around residue 274 and the adjacent heme edge in the variant I274C with increasing times of X-ray exposure. The F_o-F_c electron density maps, drawn in green at $\sigma = 3.0$, were calculated without heme or residue 274 side chain in the model. The heme, Cys-SH and S are added to the figure for illustration. The maps were calculated from data sets composed of images 1 to 6 (A), images 13 to 18 (B), images 25 to 30 (C) and images 37 to 42 (D) from 33 different crystals.

Table 5.3. Fe-O distance and B factors of coordinated oxygen and adjacent water in I274C.

Image set	Subunit				
	A	B	C	D	Average
A - *Fe-O distance (Å)*					
1-6	2.16	2.26	2.31	2.31	2.26
7-12	2.17	2.31	2.41	2.34	2.31
13-18	2.17	2.28	2.43	2.4	2.32
19-24	2.30	2.20	2.46	2.43	2.35
25-30	2.29	2.40	2.50	2.46	2.41
31-36	2.18	2.27	2.46	2.39	2.33
37-42	2.27	2.25	2.49	2.34	2.34
B - *B factor (Å^2) of coordinated O*					
1-6	14.32	13.97	9.54	12.45	12.57
7-12	16.87	19.38	17.84	15.85	17.49
13-18	23.43	26.78	17.81	20.98	22.25
19-24	22.57	26.06	17.92	22.52	22.27
25-30	22.95	25.24	22.81	23.06	23.52
31-36	22.14	28.79	23.63	24.09	24.66
37-42	23.65	26.62	22.94	24.78	24.50
C - *B factor (Å^2) of adjacent distal heme cavity water*					
1-6	18.21	18.72	27.52	24.31	22.19
7-12	23.54	28.17	28.76	23.80	26.07
13-18	26.63	27.57	25.79	26.93	26.73
19-24	26.04	24.02	23.30	26.38	24.94
25-30	20.31	27.60	24.00	22.26	23.54
31-36	22.89	29.40	22.14	25.76	25.05
37-42	28.63	29.34	27.46	26.03	27.87

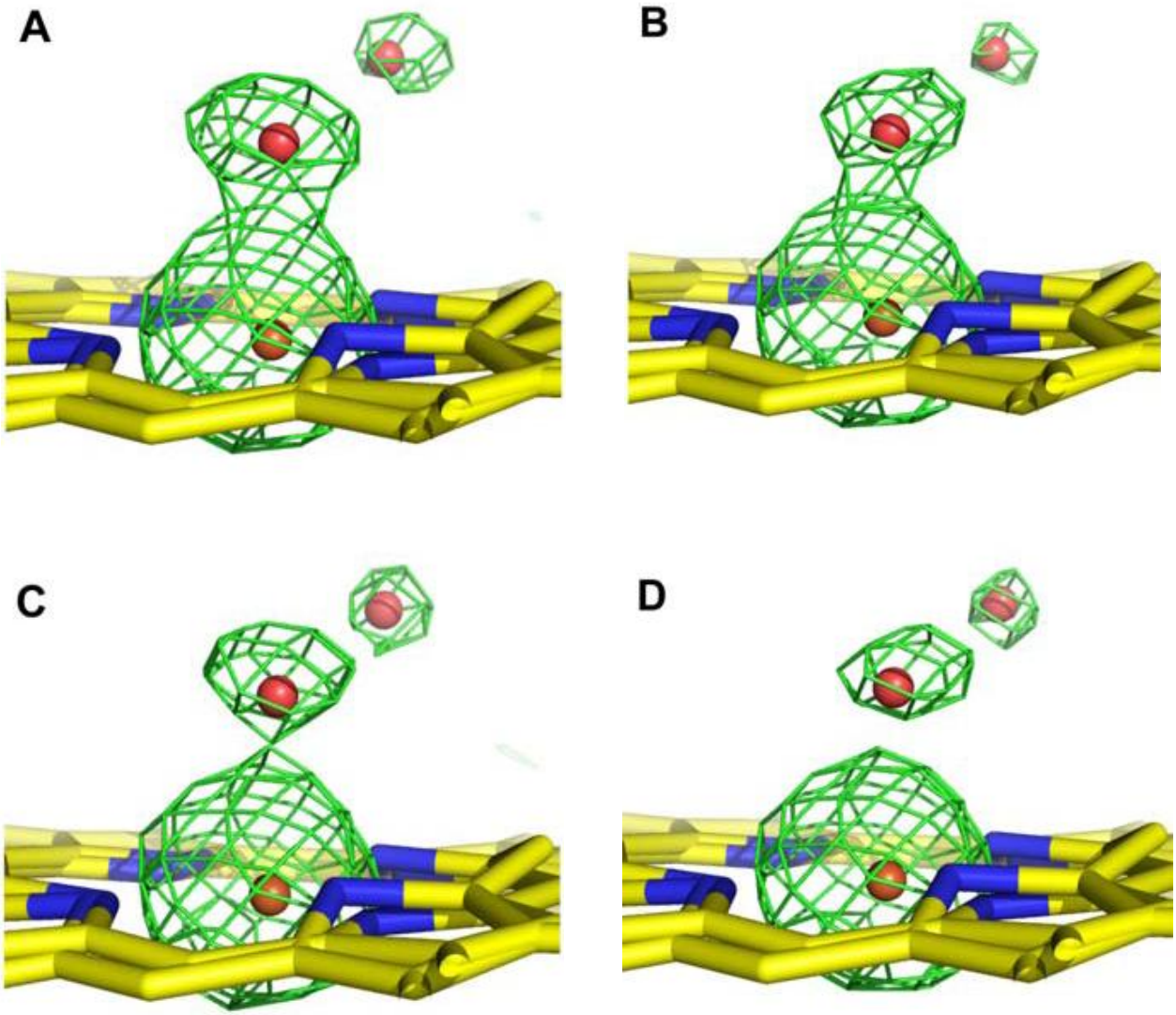

Figure 5.13. Electron density maps showing the changes around the coordinated heme iron and oxygen atom with increasing times of X-ray exposure in I274C. The F_o-F_c electron density maps, drawn in green at $\sigma = 3.0$, were calculated without iron or oxygen in the model and the orange sphere for iron and red sphere for oxygen are superimposed for illustration. The adjacent water in hydrogen bonding distance is included for reference. The maps were calculated from data sets composed of images 1 to 6 (A), images 13 to 18 (B), images 25 to 30 (C) and images 37 to 42 (D) from 40 different crystals.

Previous work had demonstrated that enlarging the middle section of the lateral channel led to an increase in activity (Sevinc et al., 1999) leading to the hypothesis that opening the entrance to the lateral channel would also enhance activity. In fact, just the opposite is observed, with catalytic efficiency decreasing as the channel is opened and an explanation may lie in the recent prediction arising from a computational study that the heme cavity has evolved to restrict efflux of H_2O_2, thereby extending its residency time in the cavity (Domínguez et al., 2010). Thus, the bulky isoleucine in the native enzyme restricts movement of H_2O_2 out of the cavity via the lateral channel, and the longer occupancy in the cavity increases its chances of participating in the reaction. Conversely, opening the lateral channel (with smaller side chains at residue 274) facilitates H_2O_2 diffusion out of the cavity leading to a shorter residency time, poorer substrate binding and a slower reaction. The elevated apparent K_M values for H_2O_2 exhibited by the I274G, I274A and I274V variants suggest that higher substrate concentrations are required for equivalent turnover rates and are consistent with this explanation. The slower turnover rate of I274C may also be influenced by heme oxidation inherent in the Cys-heme crosslink, which may affect the reduction potentials of the heme and its Cpd I intermediate.

The increased heme heterogeneity cannot be so easily rationalized. Reducing the size of the side chain from isobutyl (I274) to isopropyl (I274V) or methyl (I274A) seems to remove a determinant that restricts heme binding to the orientation with the essential histidine stacked above ring IV of the heme found in WT-HPII. Approximately, equal proportions of the native His-IV and flipped His-III orientations of heme are found in I274V and a predominance of the flipped orientation is evident in I274A. I274G breaks the apparent correlation of smaller subunit with the flipped His-III orientation, possibly a result

of a water occupying the enlarged cavity. Partial conversion of heme *b* to heme *d*, a result of small changes in growth conditions, and not the type of mutation, results in an even more complex heme composition with the different heme types in two different orientations. Furthermore, whereas heme *b* is identical in both orientations, the flipped orientations of heme *d* are actually stereochemically distinct isomers, 12(S)-hydroxy-13(R)-cis-spirolactone in the native His-IV orientation and 18(S)-hydroxy-17(R)-cis-spirolactone in the flipped His-III orientation.

The covalent crosslink between the cysteine and heme in I274C is reminiscent of the outcome from the mutation of Val169 to Cys at the entrance of the main channel into the heme cavity which resulted in a Cys169-His128 crosslinked structure (Mate et al., 1999). In both cases, the strategy of chemically introducing groups by sulfhydryl modification had to be abandoned because of the highly oxidative environment of the heme active site. The color change in the crystal after just seconds of exposure and the fact that images after six exposures show only limited evidence of the crosslink speak to its hypersensitivity to X-ray irradiation. Such extreme sensitivity is surprising in light of the similar protein-heme crosslinks found in myeloperoxidase (Kooter et al., 1997; Blair-Johnson et al., 2001), cytochrome c (Ochi et al., 1983) and cytochrome P460 (Pearson et al., 2007) where they are stable to X-ray irradiation. Possible explanations for the sensitivity lie in strained stereochemistry, evident in the slightly stretched nature of the bonds in the refined model, and in the involvement of heme *d* rather than heme *b*.

The enhanced stability of the oxoferryl species allowing it to survive through isolation and prolonged incubation for crystallization is unexpected. However, two observations support the conclusion that the Gly, Cys and Ala variants are isolated as their

oxoferryl derivatives. The first is the X-ray induced change in the electron density associated with the oxygen atom in close coordination with the iron. Both a decrease in occupancy and an increase in separation from the iron are similar to the changes in compound I/II of both horseradish peroxidase (Berglund et al., 2002) and cytochrome c peroxidase (Meharenna et al., 2010) during X-ray irradiation. The second is the reduced intensity of the Soret band, responsible for the low R_z values of the purified variants, never observed previously among any of the other 100 or so purified variants of KatE except upon heme oxidation where reduced intensity of the Soret band and the main charge transfer band at 590 nm with no shift in wavelength is observed (Chelikani et al., 2005). Unlike heme *b* containing catalases, there are no other spectral changes that permit the differentiation between Cpd I and Cpd II oxoferryl species KatE, and the rapid degradation of the Fe-O structure evident even in the earliest images precludes a crystallographic definition of the initial state. Since, the oxoferryl species of HPII is EPR silent; Mossbauer spectra are probably the only option to study the nature of such species. Experiments to investigate the feasibility of a Mossbauer application are being planned.

6. ROLE OF ARGININES IN THE VICINITY OF HEME IN HPII

6.1. Introduction

Three arginines (residues 125, 165 and 422 in HPII) near the heme propionate are conserved in all known catalase sequences. The conservation is illustrated in the alignment of the sequences of the 14 catalases for which structures have been determined (Figure 6.1). Arg125 is sandwiched equidistant between Arg165 and Arg422 interacting with the heme propionate through ionic bonds (Figure 6.2). The structural and functional significance of these arginines has never been investigated in any catalase and a mutational analysis was therefore carried out in HPII.

6.2. Results

6.2.1. Construction and characterization of arginine variants

The three arginines Arg125, Arg165, and Arg422 were replaced by an alanine and a lysine and the variants R125A, R125K, R165A, R165K, R422A and R422K were expressed and purified according to the protocol outlined in the Materials and Methods. None of the alanine variants accumulated properly folded protein under any growth temperatures tested, as was evident from the lack of activity in the whole cell assay and absence of a band on the SDS-PAGE. Surprisingly no protein accumulated from the R165K variant either suggesting a significant disruption in the interaction with the heme even with this very conservative mutation possibly a result of Arg165 having the closest association with the propionate on pyrolle ring IV.

```
CAT-3   91  FDHERIPERV VH.ARGAGAH GIFTSYGDWS NITAASFL.G AKDKQTPVFV RFSTVAGSRG  148
CAT-1   81  FDHERIPERV VH.ARGSGAF GKFKVYESAS DLTMAPVL.T DTSRETPVFV RFSTVLGSRG  138
PVC     52  FDHERVPERA VH.ARGTGAH GTFVSYGDWS NLTAASFL.S AEGKQTPMFT RFSTVAGSRG  109
HPII   117  FDHERIPERI VH.ARGSAAH GYFQPYKSLS DITKADFL.S DPNKITPVFV RFSTVQGGAG  174
PMC     43  FDREVIPERR XH.AKGSGAF GTFTVTHDIT KYTRAKIF.S EVGKKTEMFA RFSTVAGERG  100
PSCF    41  FDRERIPERV VH.ARGTGVK GEFTASADIS DLSKATVF.. KSGEKTPVFV RFSSVVHGNH  97
VSC     42  FDREVIPERR MH.AKGSGAY GTFTVTHDIT KYTKAKIF.S DIGKKTDMFA RFSTVAGERG  99
HPC     45  FDRERIPERV VH.AKGSGAY GTFTVTKDIT KYTKAKIF.S KVGKKTECFF RFSTVAGERG  102
EFC     43  FNRERVPERV VH.AKGAGAH GIFKVSQSMA QYTKADFL.S EVGKETPLFA RFSTVAGELG  100
EOC     45  FDRERVPERV VH.ARGFGAH GVFKVKNSMK KYTKAAFL.Q EEGTEVPVFA RFSTVIHGTH  102
MLC     45  FNRMNIPERR PH.AKGSGAF GEFEVTEDVS KYTKALVF.. QPGTKTETLL RFSTVAGELG  101
SCCA    45  FNRENIPQRN PH.AHGSGAF GYFEVTDDIT DICGSAMF.S KIGKRTKCLT RFSTVGGDKG  102
BLC     63  FDRERIPERV VH.AKGAGAF GYFEVTHDIT RYSKAKVF.E HIGKRTPIAV RFSTVAGESG  120
HEC     64  FDRERIPERV VH.AKGAGAF GYFEVTHDIT KYSKAKVF.E HIGKKTPIAV RFSTVAGESG  121

CAT-3   387 YSYLDTQLNR HRGPNFEQLP INRPVS.GVH N.NHRDGQGQ AW.IHKNIHH YSPSYLNKGY  443
CAT-1   377 FSYFDTQISR LGV.NFQELP INRPVC.PVM N.FNRDGAMR HT.ISRGTVN YYPNRFD..A  430
PVC     348 FSYLDTQLNR HGGPNFEELP IDRPRA.PIH D.DDRDGAGE MF.IPLDPLA YSPNTEDSGS  404
HPII    413 FSYTDTQISR LGGPNFHEIP INRPTC.PYH N.FQRDGMHR MG.IDTNPAN YEPNSINDNW  469
PMC     335 FSYGDAHRYR LGV.NHHQIP VNAPKC.PFH N.YHRDGAMR VDGNSGNGIT YEPNSGG..V  389
PSCF    330 FSYADTQMYR LGA.NGLSLP VNQPKV.AVN N.GNQDGALN TG.HTTSGVN YEPSRLE..P  383
VSC     334 FAYGDAQRYR LG.VNHQHIP VNAPRC.PVH S.YHRDGAMR VDGNFGSTLG YEPND..QGQ  388
HPC     337 FSYGDTHRYR LG.VNYPQIP VNKPRC.PFH S.SSRDGYMQ NG.YYGSLQN YTPSS..LPG  390
EFC     335 FAYGDAHRHR VGA.NSHQLP INQAKA.PVN N.YQKDGNMR FN.NGNSEIN YEPNS..YTE  388
EOC     337 FSYSDTQRHR IGP.NYQQLP INCPFA.QVN N.YQRDGAMP FK.QQTSSVN YEPNRYQD.E  391
MLC     336 FAYHDAQLYR VGA.HVNQLP VNRPKN.AVH N.YAFEGQMW YD.HTGDRST YVPNSNG..D  389
SCCA    339 FSYADAHRYR LGP.NFHQIP VNCPYASKFF NPAIRDGPMN VNGNFGSEPT YL.ANDK..S  394
BLC     355 FAYPDTHRHR LGP.NYLQIP VNCPYRARVA N.YQRDGPMC MMDNQGGAPN YYPNSFS..A  410
HEC     356 FAYPDTHRHR LGP.NYLHIP VNCPYRARVA N.YQRDGPMC MQDNQGGAPN YYPNSFG..A  411
```

Figure 6.1. Amino acid sequence alignment of 14 structurally characterized monofunctional heme catalases. The first four are large subunit catalases and the remainder are small subunit catalases. Conserved arginines in the vicinity of heme ring III and IV are highlighted in bold red.

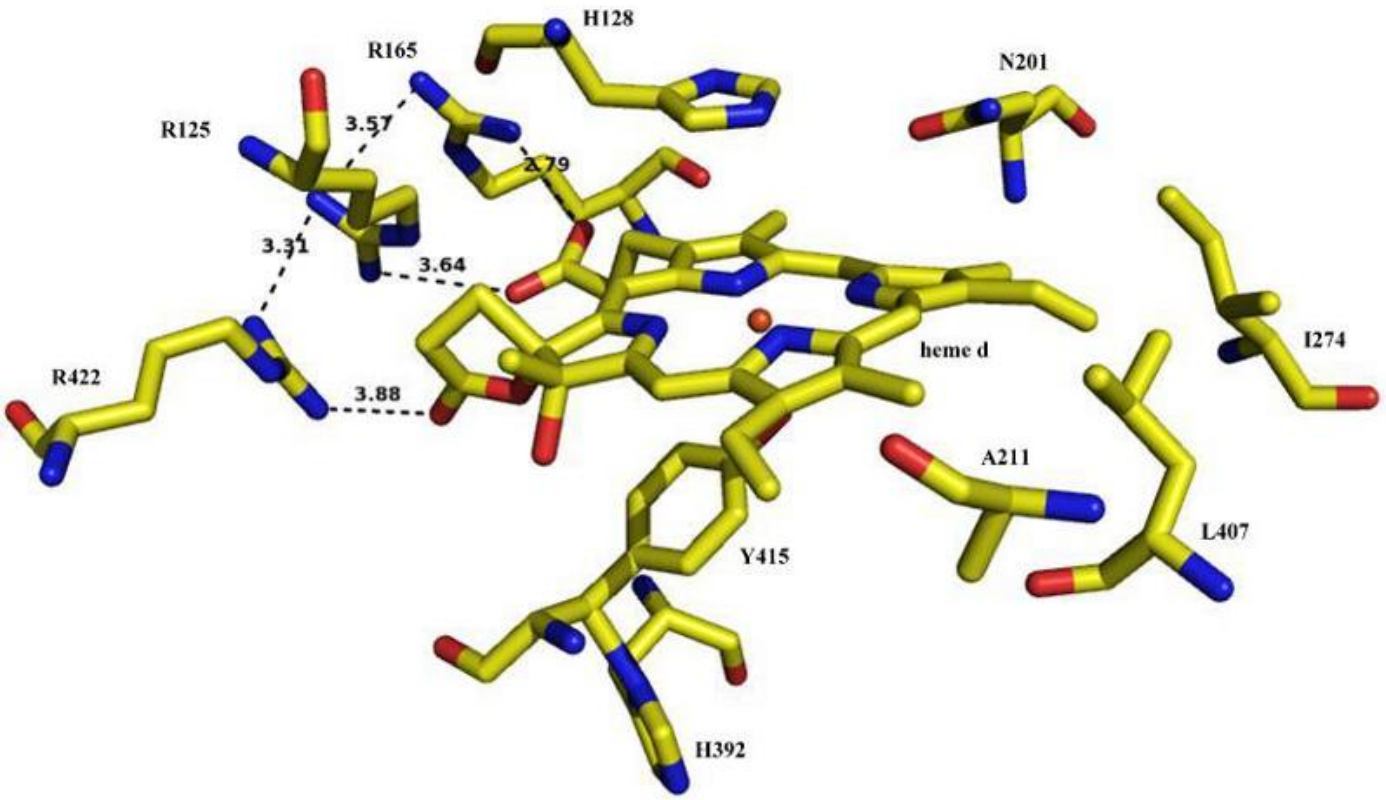

Figure 6.2. Amino acid residues around the heme in HPII. Interaction of the three arginines with heme propionates are indicated with dashed lines. Distances are in Å. The figure is based on HPII (PDB 1GGE).

Active and folded protein was obtained for variants R125K and R422K which migrated on SDS gel similar to the WT-HPII giving predominant band with an apparent molecular mass of ~ 84 kDa (Figure 6.3.).

Only minor differences were observed in the absorption spectra of the variants compared to WT-HPII (Figure 6.4). In all cases a strong Soret band was present at 407 nm and a predominant band in the charge transfer region was present at 590 nm, characteristic of heme *d*. However, both R125K and R422 exhibited low R_z values compared to WT-HPII (Table 6.1.), indicating some change in the heme electronic environment. To identify whether the low R_z value was due to cross-linking between the protein and the heme as was observed in case of I274C mutant, heme extraction and analysis was successfully carried out revealing that the heme was not covalently linked to the protein (Figure 6.5). While, R125K retained WT levels of activity, R422K exhibited only 45% of activity compared to WT-HPII (Table 6.1).

The kinetic constants for velocity variation as a function of substrate concentration were determined revealing only minor differences compared to the WT-HPII (Figure 6.6). The k_{cat} and apparent K_M constants for R125K were essentially the same as those of WT-HPII as was the apparent K_M for R422K. Only the k_{cat} exhibited by R422K was reduced to about 50% of the native enzyme (Table 6.2).

The effect of various inhibitors and heat sensitivity at 80 °C on the variants was investigated. Both variants showed similar sensitivity towards cyanide, azide and hydroxylamine as WT-HPII (Figure 6.7 and 6.8) but the variants were very sensitive towards heat (Figure 6.8). The concentrations of inhibitors and time required for 50% inactivation upon incubation at 80 °C are summarized in Table 6.3.

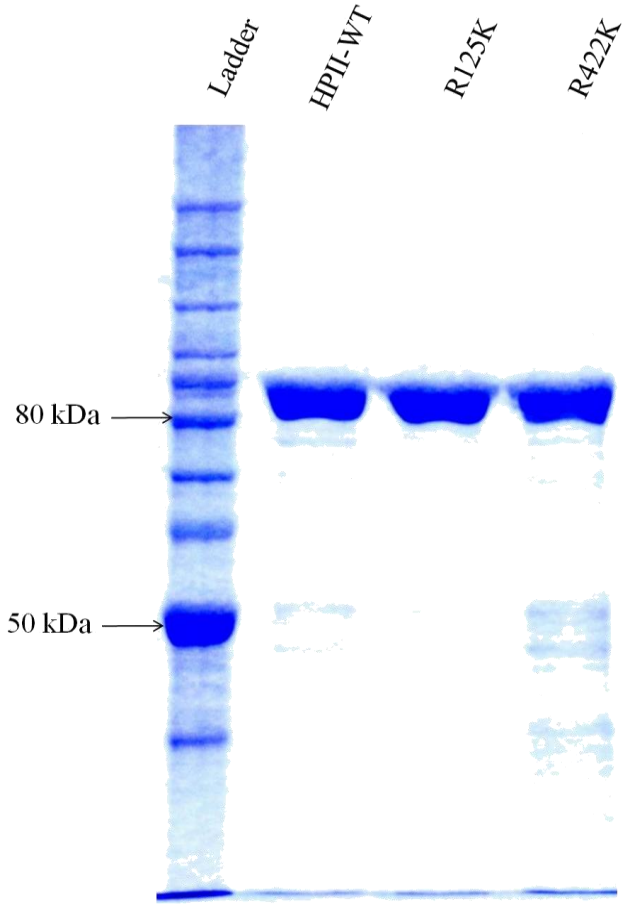

Figure 6.3. SDS-PAGE analysis of the purified WT-HPII and its variants. Approximately 2 µg of proteins were loaded and run on the 8% polyacrylamide gel. The gel was stained with Coomassie brilliant blue after electrophoretic separation.

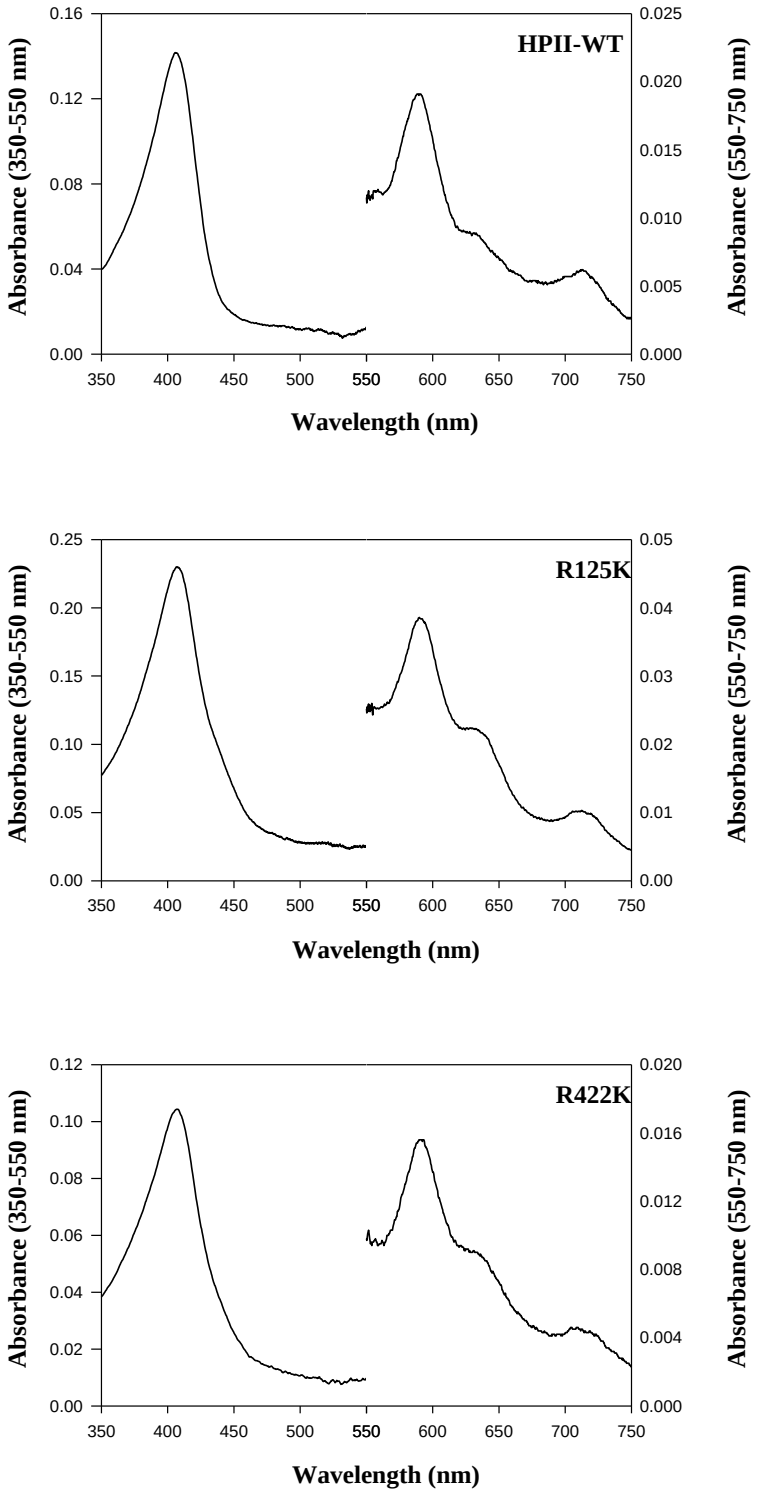

Figure 6.4. Absorption spectra of purified WT-HPII and its variants. The left axis corresponds to the absorbance values between 350-550 nm while the right axis corresponds to the absorbance values between 550-750 nm.

Table 6.1. Comparison of observed absorption spectra, A_{407}/A_{280} ratio, and catalase specific activities for purified WT-HPII and its variants.

Enzymes	**Soret (nm)**	**R_z (A_{407}/A_{280})[a]**	**Specific activity (U/mg)**
WT-HPII	406	0.94	21000 ± 1400
R125A[b]	ND[c]	ND	ND
R125K	406	0.72	16400 ± 1300
R165A[b]	ND	ND	ND
R165K[b]	ND	ND	ND
R422A[b]	ND	ND	ND
R422K	407	0.49	9200 ± 400

[a] The theoretical A_{407}/A_{280} ratio is 1.0.

[b] Protein was not obtained for these variants

[c] ND Not determined.

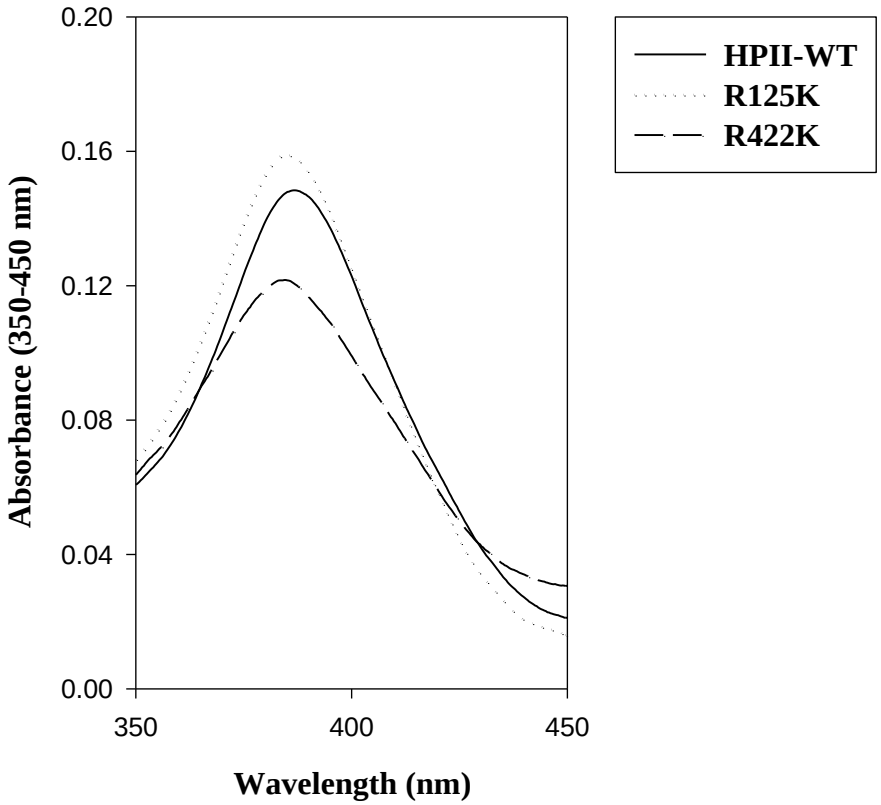

Figure 6.5. Absorption spectra of heme extracted from WT-HPII and variants R125K and R422K with acetone-HCl at RT.

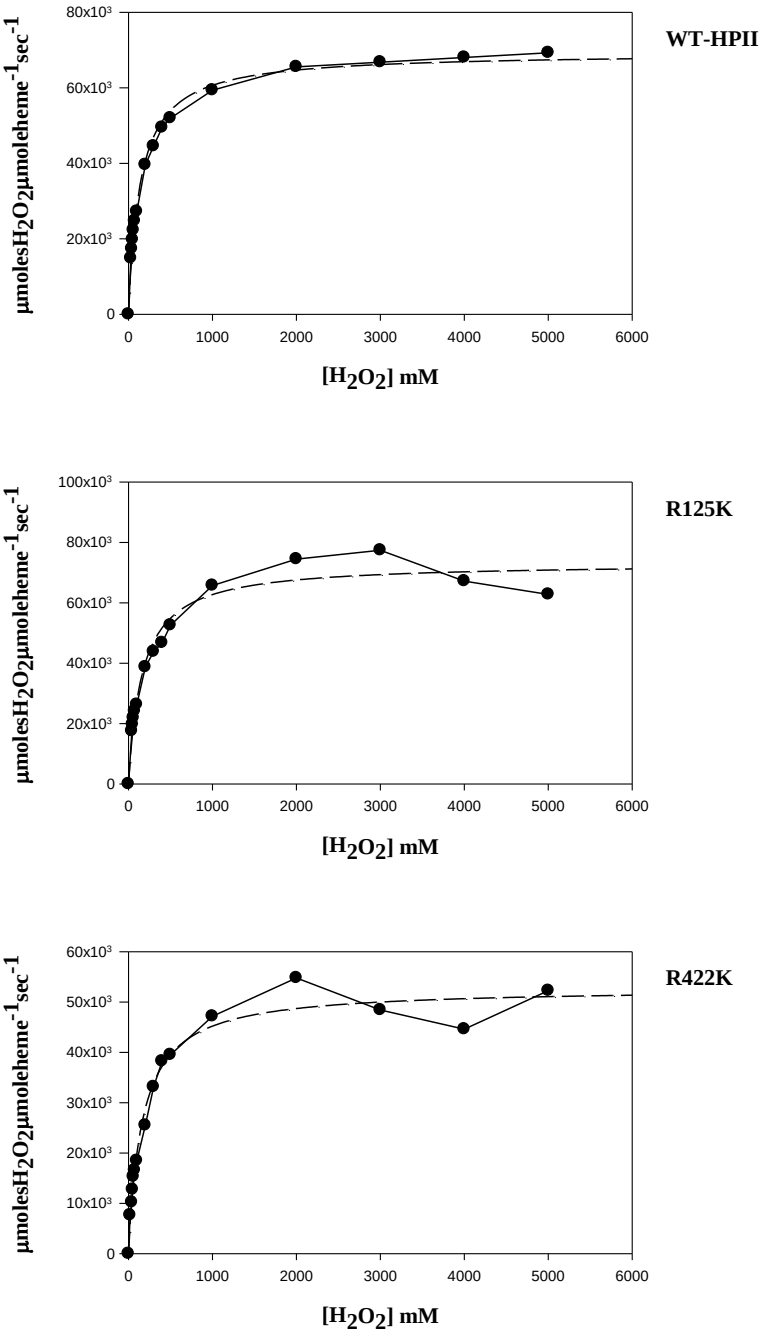

Figure 6.6. Effect of H_2O_2 concentration on reaction velocity of WT-HPII and its variants. In all panels the solid lines represent the observed data and the dashed lines represent the theoretical Michaelis-Menten curve calculated from constants determined at low H_2O_2 concentration (Table 6.2). Note the differences in the scales on the Y-axis.

Table 6.2. Comparison of the observed kinetic parameters of the WT-HPII and its variants R125K and R422K.

Variants	**Observed**		**k_{cat}/K_M ($M^{-1}sec^{-1}$)**
	k_{cat} (sec^{-1})	K_M (app)[a]	
WT-HPII	70000	145	0.5×10^6
R125K	73200	165	0.4×10^6
R422K	52800	170	0.3×10^6

[a] K_M apparent, represents H_2O_2 concentration at $V_{max}/2$, mM

6.2.2. Structure of R125K and R422K

Crystals of R125K and R422K were obtained under similar conditions as used for WT-HPII. X-ray diffraction data sets were collected using synchrotron beam line CMCF 08ID-1 at the Canadian Light Source in Saskatoon, Canada that refined to 1.8 and 1.7 Å respectively. The data quality of R422K variant is not very good, as is evident from the high R_{merge} values. The electron density maps were used to confirm the mutation. The diffraction data and structure refinement statistics are summarized in Table 6.4. The electron density maps clearly defined the main chain and side chain atoms of 2904 amino acids, four heme groups and 3153-3393 waters in four subunits. The maps show clear continuity from Ser28 to Ala753 in all four subunits. The electron density maps in the region of residue 125 in R125K and residue 422 in R422K are consistent with the lysine side chain being present (Figure 6.9 A and C). A new water molecule in variant R125K occupies the space that is occupied by the guanidinium group in the WT-HPII structure (Figure 6.9 A and B) and makes hydrogen bond contact with the amino group of lysine. In both cases heme *b* is modified to heme *d* although a small amount of unmodified heme *b* is evident in the structure of variant R422K (Figure 6.9 C and D). Also in both variants, the covalent linkage between Tyr415 and His392 is fully formed confirming that the variants had undergone several rounds of catalysis prior to purification. Otherwise, the solvent organization on the heme distal and proximal side in both variants is very similar to that of WT-HPII and the global structure of the proteins remained unchanged.

6.3. Discussion

Mutational analysis of three structurally conserved arginines near heme revealed that the presence of positive charge in the vicinity of the heme is important for heme binding and

A

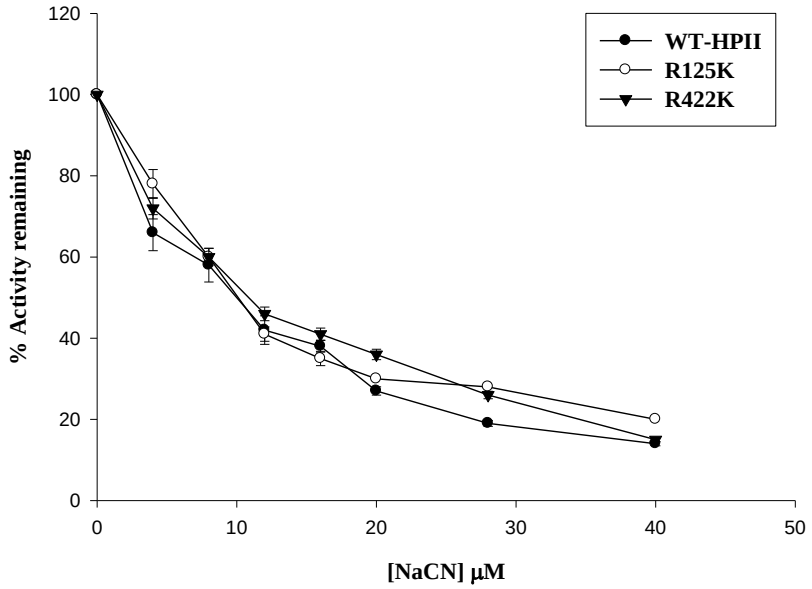

B

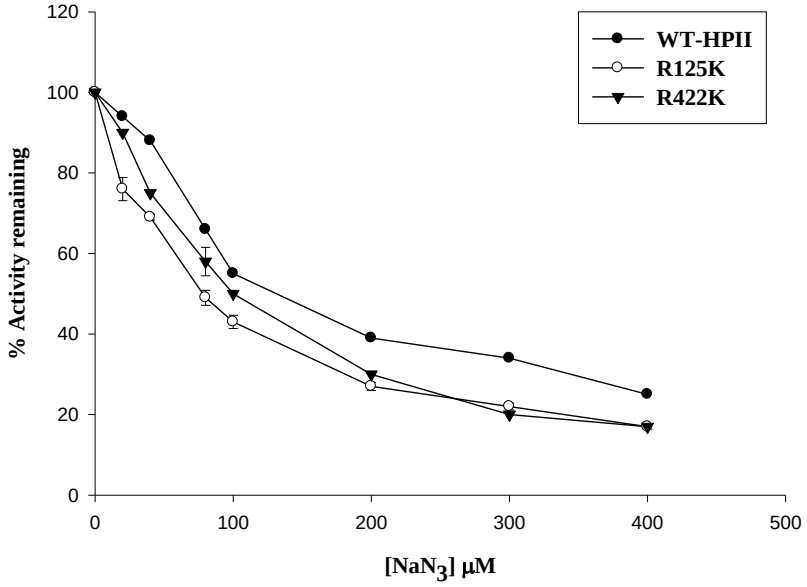

Figure 6.7. Effect of NaCN (A) and NaN_3 (B) on WT-HPII and variants R125K and R422K. Each enzyme was incubated with inhibitor for 1 min in 50 mM KPi at 37 °C before adding H_2O_2. All assays were repeated in triplicate and the results averaged.

A

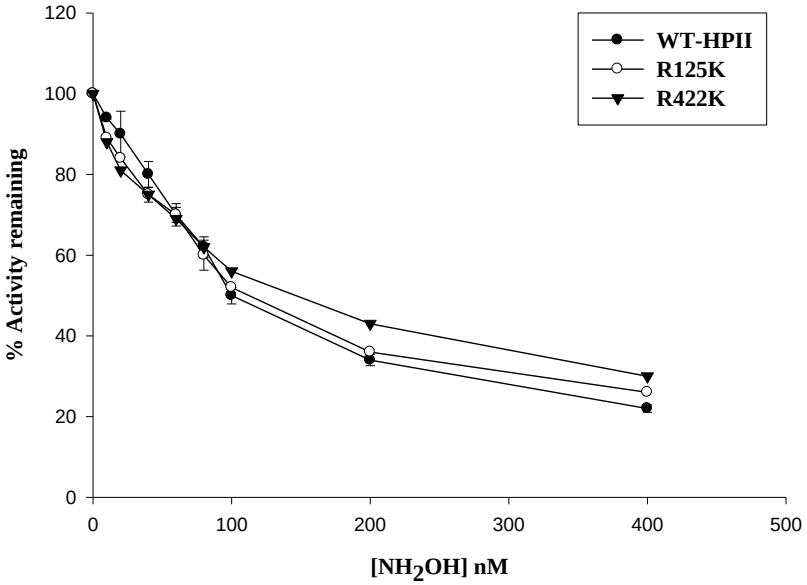

B

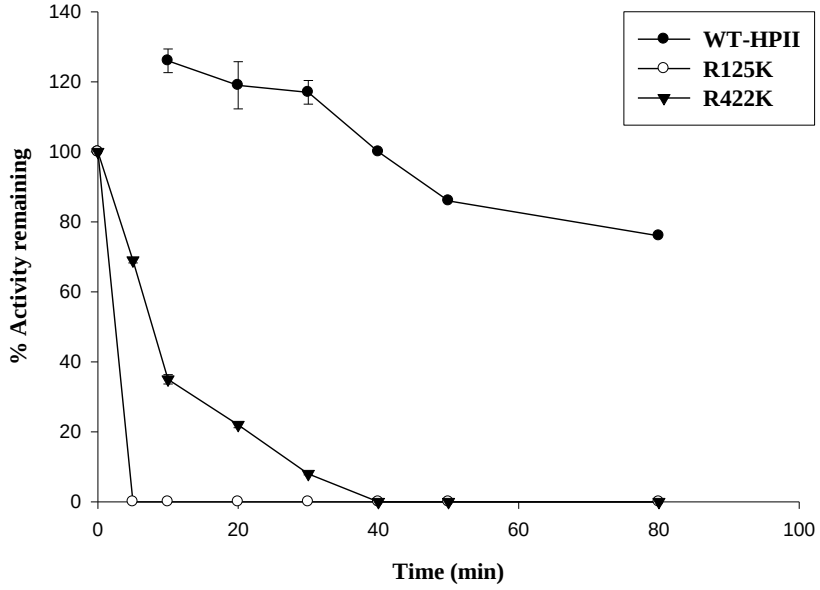

Figure 6.8. Effect of NH_2OH (A) on and sensitivity to incubation at 80 °C (B) of WT-HPII and variants R125K and R422K. In A, each enzyme was incubated with inhibitor for 1 min in 50 mM KPi at 37 °C before adding H_2O_2. In B, the enzymes were incubated at 80 °C for different time intervals. All assays were repeated in triplicate and the results averaged.

Table 6.3. Sensitivity of WT-HPII and its variants to various inhibitors and heat treatment at 80 °C[*]

Variants	**Inhibitor concentration at 50% inhibition[a]**			**Time to 50% inhibition at 80 °C (min)[b]**
	NaCN (μM)	NaN_3 (μM)	NH_2OH (nM)	
WT-HPII	11 ± 1.0	140 ± 10	110 ± 10	> 80
R125K	11 ± 1.5	85 ± 7.0	100 ± 0	< 1
R422K	11 ± 1.0	100 ± 0	125 ± 15	5 ± 0

[a] Enzyme was incubated with inhibitor for one minute before adding H_2O_2.

[b] Enzyme was incubated at 80 °C for different time intervals.

[*]All assays were repeated in triplicate and results were averaged.

Table 6.4. Data collection and structural refinement statistics for HPII variants R125K and R422K.

	R125K	R422K
A. Data collection statistics		
Space group	$P2_1$	$P2_1$
Unit cell parameters		
a (Å)	93.62	93.11
b (Å)	132.84	132.50
c (Å)	122.91	121.68
α, β,ϒ (deg.)	90, 109.09, 90	90, 109.66, 90
Resolution range (Å)	29.21-1.80 (1.90-1.80)[a]	26.98-1.70 (1.79-1.70)
Total no. of reflections	557,241 (66,088)	1,169,024 (168,388)
Unique reflections	202,239 (26,494)	304,162 (44,383)
Completeness (%)	77.30 (69.60)	100 (100)
$\langle I/\sigma(I)\rangle$	8.7 (2.2)	3.4 (2.1)
R_{merge}	0.082 (0.475)	0.312 (0.538)
B. Refinement statistics		
Resolution range (Å)	116.15-1.80	114.58-1.70
% age observed	77.16	99.90
R_{work} (%)	14.18	16.85
R_{free} (%)	19.51	21.48
No. of non-hydrogen atoms		
proteins	22,987	22,982
hemes	176	176
waters	3,153	3,393
rms deviations		
bond lengths (Å)	0.02	0.02
bond angles (deg.)	1.89	1.98
Average B factor ($Å^2$)		
main chain	15.34	11.22
side chain	16.68	13.00
water	25.36	22.88

[a] Values in parentheses correspond to the highest-resolution shell.

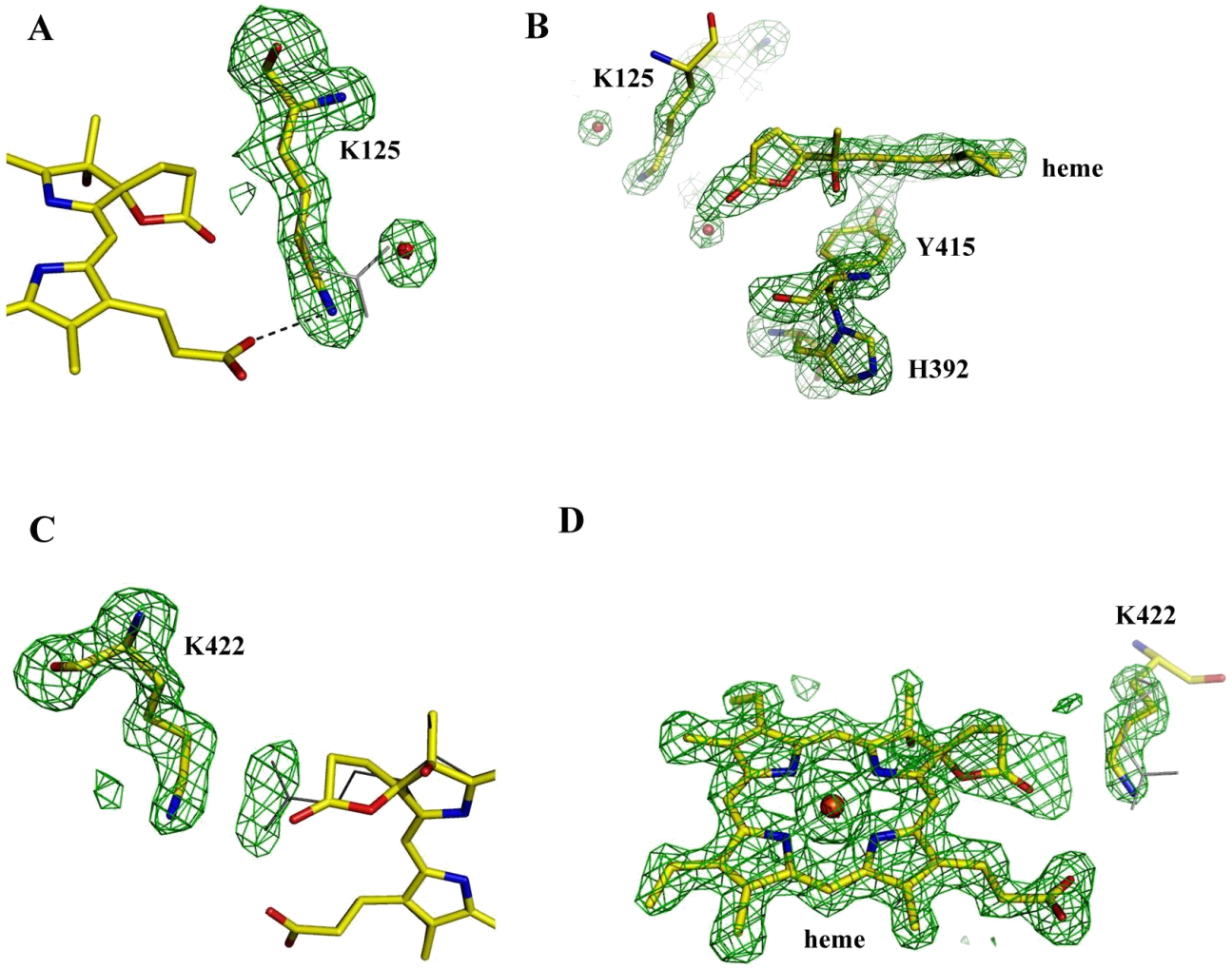

Figure 6.9. View of F_o-F_c electron density maps corresponding to the side chains of Lys125 (A) and Lys422 (C), and the environments of the heme in variants R125K (B) and R422K (D). Note the small fraction of heme *b* in R422K. Electron density maps were calculated without the respective atoms in the model and the appropriate models are superimposed for illustration. The maps were modelled at $\sigma = 3.0$. The covalent bond between His392-Tyr415 is fully formed in both variants but shown only for R125K (B). Water molecules are indicated as red spheres.

consequently for proper folding of the protein. Replacing the guanidinium side chain of arginines at 125, 165 and 422 with the methyl side chain of alanine in HPII mutants R125A, R165A and R422A so adversely affected the folding of the protein that none accumulated. Similarly, and somewhat surprisingly, even replacing Arg165 with Lys also adversely affected protein folding and no protein accumulated revealing that the precise location of the positive charge is critical. The location of this arginine is closest to the propionate of heme ring IV compared to the arginines at 125 and 422 (Figure 6.10 A) and disruption of this interaction must be responsible for the improper orientation and binding of the heme into the protein during folding. However, replacement of Arg125 and Arg422 with Lys allowed accumulation of active protein with similar characteristics to WT-HPII.

The replacements only marginally modified the local structure, as evidenced by the same orientation of each arginine or lysine side chain (Figure 6.10 A, B and C). However, the distances of the three residues with respect to each other and with respect to heme has changed and the low R_z values in R125K and R422K might be associated with the change in heme microenvironment as a result of changed interactions (Figure 6.10 A, B and C). Although variant R422K retained only 45% activity and exhibited slightly slower reaction velocity compared to WT-HPII its sensitivity towards inhibitors remained similar to WT-HPII suggesting that neither Arg125 nor Arg422 regulate either the binding or reactivity of inhibitors to the enzyme. Both R125K and R422K mutants lost thermostability after incubation at 80 °C (Figure 6.7 & Table 6.3) most likely because of the loss of important ionic and hydrogen bond interactions.

Together, the data suggest that the three conserved arginines have more of a structural than a functional role. The precise positioning of Arg165 suggests that it is the

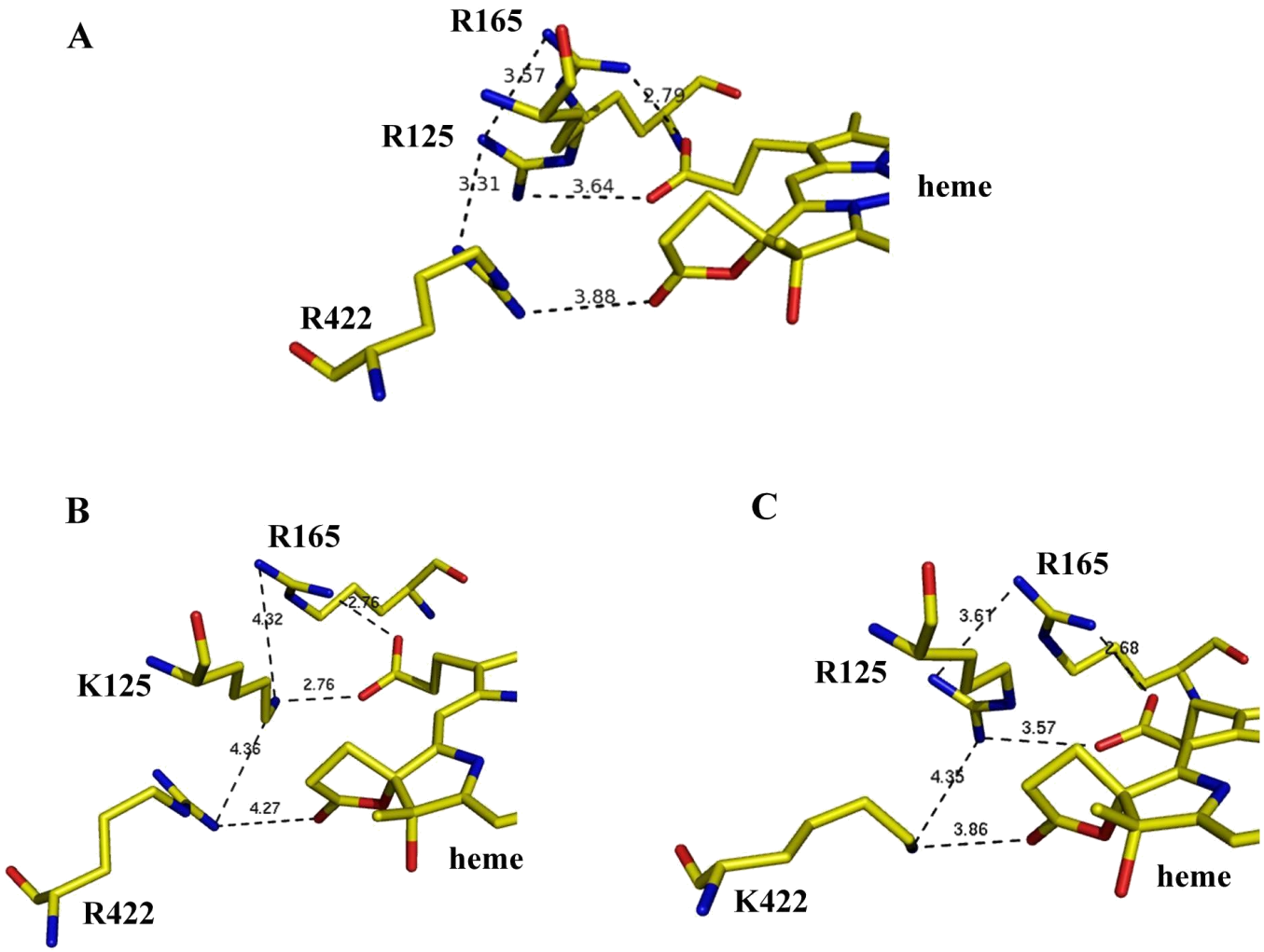

Figure 6.10. Arrangement of arginine and lysine residues in WT-HPII and variants R125K and R422K. Panel A: three arginines near heme in WT-HPII. Panel B: two arginines and a lysine in R125K. Panel C: two arginines and a lysine in R422K. Note the changes in the distance between the residues and the heme.

most important of the three residues in orienting and positioning the heme into the core of the protein. While the precise locations of the positively charged side chains at residues 125 and 422 are not as important, the positive charge itself is clearly important for stabilizing the heme interaction and protein folding.

7. CONCLUSIONS

The work described in this thesis has extended an ongoing structure-function study into the role of specific residues in catalase HPII of *E. coli*. The conclusions are as follows:

1. Breaks observed in the molecular symmetry of HPII in the native enzyme and after binding of H_2O_2 do not appear to have a functional significance. Mutations of the residues involved caused little change in catalytic, biochemical or structural properties of the enzyme.

2. Inter-subunit interactions involving His119 with Ser421 and Asp417 do not affect catalytic properties but do affect the heme *b* to *d* conversion suggesting that His119 is important to the environment for heme conversion. A rationale for why the modification of His119 should enhance resistance to cyanide and azide is not clear.

3. The mutation in F413Y introduces a reactive center into the protein that leads to main chain cleavage at two locations and the loss or modification of three side chains.

4. Other changes to residue 413 (F413A, F413E, F413K and F413Q) all exhibit poor heme *b* to *d* conversion suggesting that this residue is important to the environment needed for heme modification.

5. The bulky side chain of I274 at the entrance to the lateral channel enhances catalytic activity by retaining the substrate in the active site.

6. Changes to the side chain of residue 274 also affects the heme orientation, but a clear correlation between side chain size and heme orientation did not arise.

7. The Cys274 variant contained a covalent link between the heme vinyl and the Cys-S which was hypersensitive to X-ray irradiation.

8. The group of arginines including R125, R165 and R422 adjacent to the heme propionates is critical for heme binding and proper folding of the protein.

APPENDIX A

STRUCTURAL CHARACTERIZATION OF E530A AND E530D VARIANTS OF HPII

A.1. Introduction

The side chain of Glu530 which is located in the upper part of the major channel in HPII is situated about 2.7 Å from hydroxyl group of Ser234 and is hydrogen bonded to two water molecules (Bravo et al., 1999). A direct connection between the main channels of the two subunits (A and D) originating from Glu530 towards the active site has been noted (Nicholls et al., 2001) and the importance of this residue was suggested by its interaction with H_2O_2 in the inactive variant H128N (Melik-Adamyan et al., 2001).

A site-directed mutagenesis study of Glu530 had previously been conducted by Chelikani (Chelikani PhD thesis, 2003) in which the variants E530A, E530D, E530I, and E530Q were constructed. All of the variants exhibited reduced specific activites, reduced affinity for the substrate (higher apparent K_M values) and, except for E530D, slightly different spectra compared to WT-HPII. The E530 variants were not characterized structurally in this earlier study, and the structure analyses of E530A and E530D were undertaken as part of the current study with the object of explaining the changed kinetic properties.

A.2. Construction, purification and biochemical characterization of E530A and E530D variants

Variants E530A and E530D were expressed and purified according to the protocol outlined in Chapter 2. The purified proteins showed similar electrophoretic mobilities as WT-HPII on the SDS-PAGE gel revealing a single band of approximately 84 kDa (Figure A.1). The absorbance spectra were similar to those reported in the previous study with

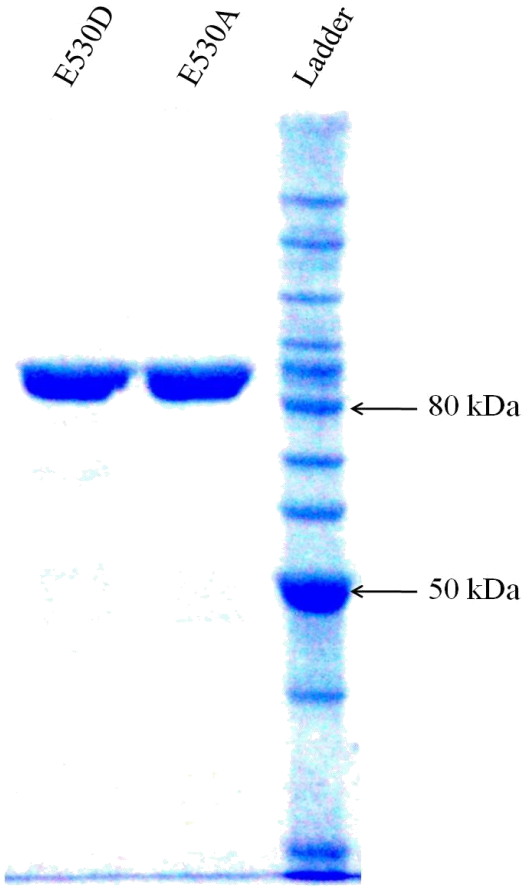

Figure A.1. SDS-PAGE analysis of the purified E530A and E530D. Approximately 2 µg of proteins were loaded and run on the 8% polyacrylamide gel. The gel was stained with Coomassie brilliant blue after electrophoretic separation.

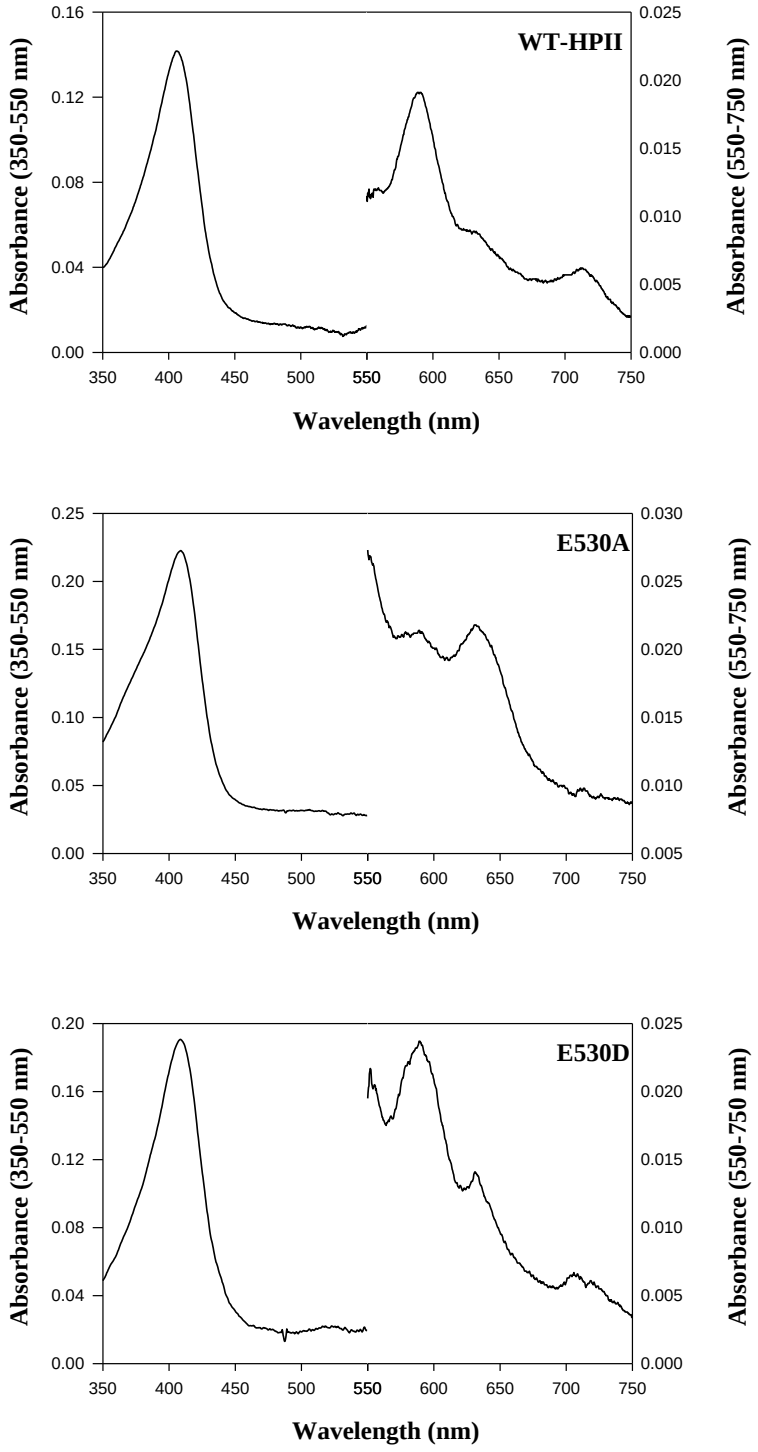

Figure A.2. Absorption spectra of purified WT-HPII and its variants. The left axis corresponds to the absorbance values between 350-550 nm while the right axis corresponds to the absorbance values between 550-750 nm.

variant E530A exhibiting a predominant peak at 630 nm suggesting that heme *b* is the major heme species and E530D exhibiting a spectrum similar to that of WT-HPII (Figure A.2). Both variants exhibited slightly reduced specific activities but both were capable of higher reaction velocities at higher substrate concentrations (Table A.1).

A.3. Sensitivity towards inhibitors and heating at 80 °C

Variants E530A and E530D were assayed to determine their sensitivity towards various inhibitors and to heat treatment at 80 °C which was not done in the previous study. The 50% inhibitory concentrations of cyanide, azide and hydroxylamine are summarized in Table A.2. Surprisingly, E530A requires eight times more cyanide than WT-HPII for 50% inhibition, whereas both variants are more sensitive to azide than WT-HPII (Figure A.3). In addition, both variants are more sensitive to heat treatment at 80 °C than WT-HPII with E530A being even more sensitive than E530D (Figure A.4 and Table A.2) most likely the result of loss of proper hydrogen bonding network with Ser234 and water molecules.

A.4. Structure determination of E530A and E530D

Crystals of variants E530A and E530D were grown by hanging drop vapour diffusion method as described in Chapter 2. X-ray diffraction data sets were collected using synchrotron beam line CMCF 08ID-1 at the Canadian Light Source in Saskatoon, Canada that refined to 1.5 and 1.9 Å respectively. The diffraction data and structure refinement statistics are summarized in Table A.3. The expected alanine and aspartate side chains at residue 530, in E530A and E530D respectively, are evident in the F_o-F_c electron density maps calculated without the side chain in the model (Figure A.5). Minor structural changes with respect to WT-HPII, including heme *b* rather than heme *d*, and a few changes in solvent

Table A.1. Comparison of A_{407}/A_{280} ratio, catalase specific activities and kinetic constants for purified WT-HPII and variants E530A and E530D.

Variants	**R_z (A_{407}/A_{280})**	**Specific activity (U/mg)**	**Observed**		**k_{cat}/K_M ($M^{-1}sec^{-1}$)**
			k_{cat} (sec^{-1})	K_M (app)[a]	
WT-HPII	0.94	21000 $\pm$ 1400	70000	145	0.5×10^6
E530A	0.87	16000 $\pm$ 800	201730	510	0.4×10^6
E530D	0.86	12000 $\pm$ 750	114740	420	0.3×10^6

[a]K_M apparent, represents H_2O_2 concentration at $V_{max}/2$, mM.

A

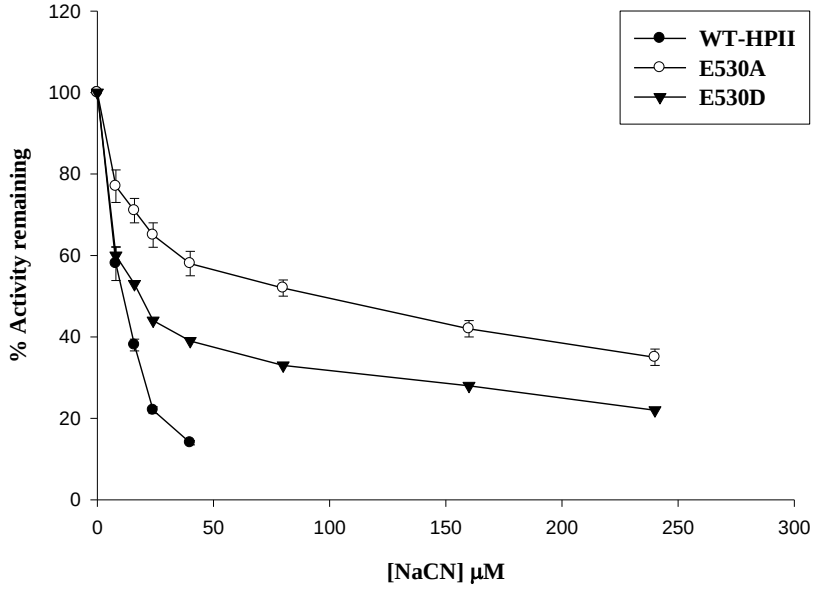

B

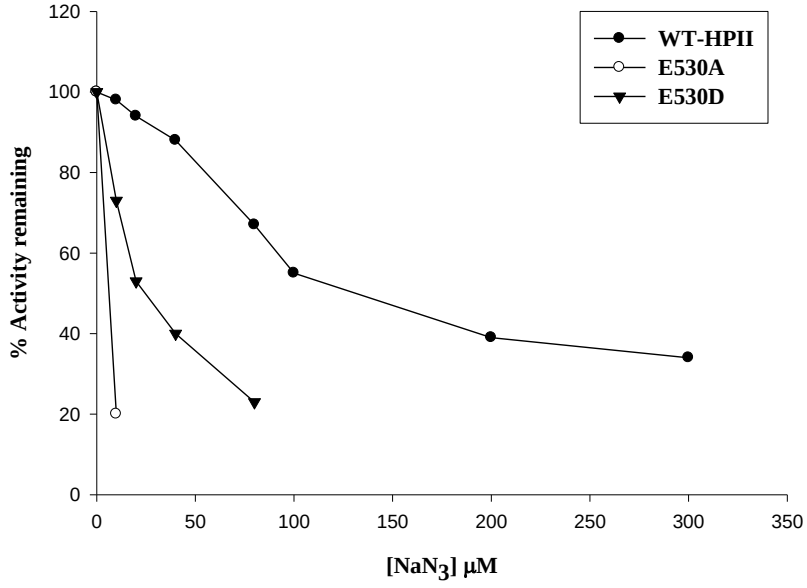

Figure A.3. Effect of NaCN (A) and NaN_3 (B) on WT-HPII and variants E530A and E530D. Each enzyme was incubated with inhibitor for 1 min in 50 mM KPi at 37 °C before adding H_2O_2. All assays were repeated in triplicate and the results averaged.

A

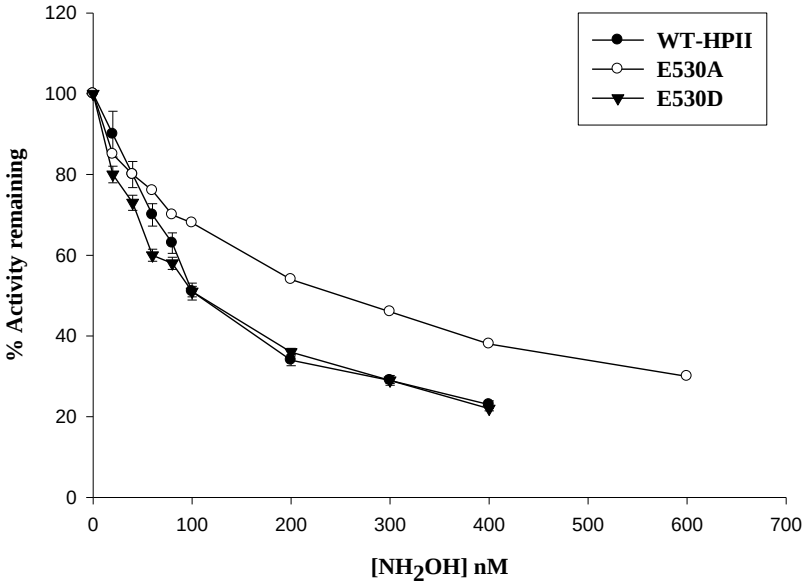

B

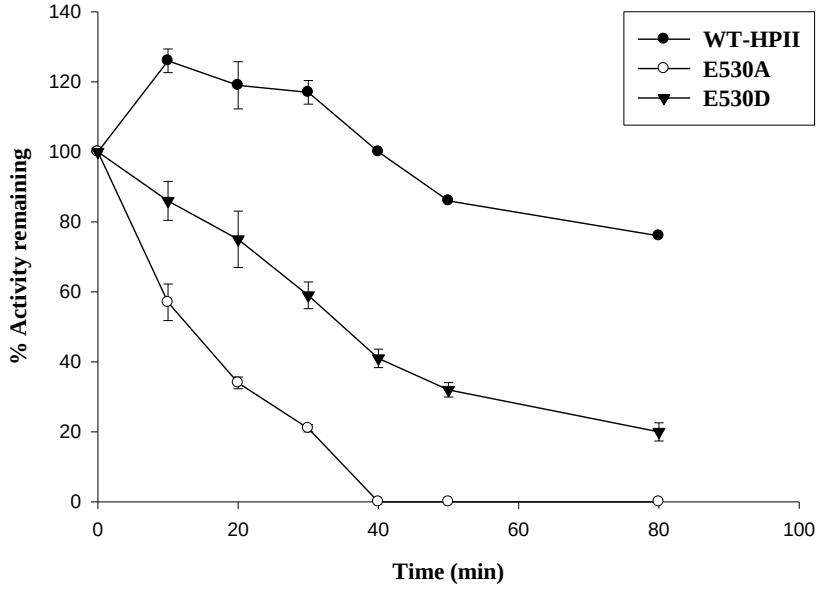

Figure A.4. Effect of NH_2OH (A) on and sensitivity to incubation at 80 °C (B) of WT-HPII and variants E530A and E530D. In A, each enzyme was incubated with inhibitor for 1 min in 50 mM KPi at 37 °C before adding H_2O_2. In B, the enzymes were incubated at 80 °C for different time intervals. All assays were repeated in triplicate and the results averaged.

Table A.2. Sensitivity of WT-HPII and its variants to various inhibitors and heat treatment at 80 °C*

Variants	**Inhibitor concentration at 50% inhibition[a]**			**Time to 50% inhibition at 80 °C (min)[b]**
	NaCN (μM)	NaN_3 (μM)	NH_2OH (nM)	
WT-HPII	11 ± 1.0	140 ± 10	110 ± 10	> 80
E530A	100 ± 15	4 ± 0.7	260 ± 15	15 ± 3.0
E530D	25 ± 5.0	20 ± 0	110 ± 10	35 ± 3.0

[a] Enzyme was incubated with inhibitor for one minute before adding H_2O_2.

[b] Enzyme was incubated at 80 °C for different time intervals.

*All assays were repeated in triplicate and results were averaged.

location are evident in maps of E530A. For example, two waters approximately replace the glutamate carboxylate oxygens (Figure A.5 A) suggesting the existence of a hydrogen bonding network at this location. In addition, only one water is found in the distal side heme pocket compared to two in WT-HPII (Figure A.6) suggesting a diminished stability of the water matrix in the access channel and heme pocket. By contrast, E530D contains heme *d* and the water matrix in the lower part of the channel is similar to that in WT-HPII.

A.5. Discussion

Glu530 in HPII is located about 20 Å from the active site perpendicular to the plane of heme. Previous mutagenesis experiments at this location had shown that variants E530A and E530D both exhibit reduced affinity for the substrate, evident in their higher apparent K_M values. The structure of E530D does not present any significant structural changes compared to WT-HPII aside from minor changes in solvent location in the vicinity of the mutation. These adjustments restore or maintain the hydrogen bond matrix around D530 and S234. On the other hand, E530A presents structural changes both in the vicinity of the mutation and in the more distant heme cavity. In particular, two solvents replace the carboxylate oxygens and only one water is found in the lower part of the access channel and heme cavity compared to three in WT-HPII. While it is possible to rationalize the reduced affinity for H_2O_2 in E530A as being due to the loss of hydrogen bonding capability in the channel, this argument cannot be applied to E530D. In addition, because both E530A and E530D have similar properties, participation in an electrical potential gradient as proposed for Asp181 is not a reasonable explanation. The observation of higher turnover rates at higher [H_2O_2] than even WT-HPII suggests the alternative explanation that the more open channel fails to contain H_2O_2 as effectively in the heme cavity. The concept of catalases

Table A.3. Data collection and structural refinement statistics for HPII variants E530A and E530D.

	E530A	E530D
A. Data collection statistics		
Space group	$P2_1$	$P2_1$
Unit cell parameters		
a (Å)	93.33	93.38
b (Å)	133.11	133.09
c (Å)	122.74	122.34
α, β,ϒ (deg.)	90, 109.41, 90	90, 109.68, 90
Resolution range (Å)	35.24-1.50 (1.58-1.50)[a]	41.40-1.90 (2.00-1.90)
Unique reflections	449,780 (65,633)	419,420 (60,027)
Completeness (%)	99.9 (100.0)	92.4 (90.5)
$\langle I/\sigma(I)\rangle$	9.4 (3.9)	9.0 (3.0)
R_{merge}	0.079 (0.288)	0.065 (0.245)
B. Refinement statistics		
Resolution range (Å)	133.11-1.50	115.19-1.90
No. of reflections	427,199	194,502
R_{work} (%)	14.29	15.74
R_{free} (%)	17.03	21.04
No. of non-hydrogen atoms		
proteins	23,136	22,875
hemes	172	176
waters	3,376	3,230
rms deviations		
bond lengths (Å)	0.02	0.02
bond angles (deg.)	2.37	1.88
Average B factor ($Å^2$)		
proteins	16.03	15.05
hemes	9.07	9.35
water	22.10	14.90

[a] Values in parentheses correspond to the highest-resolution shell.

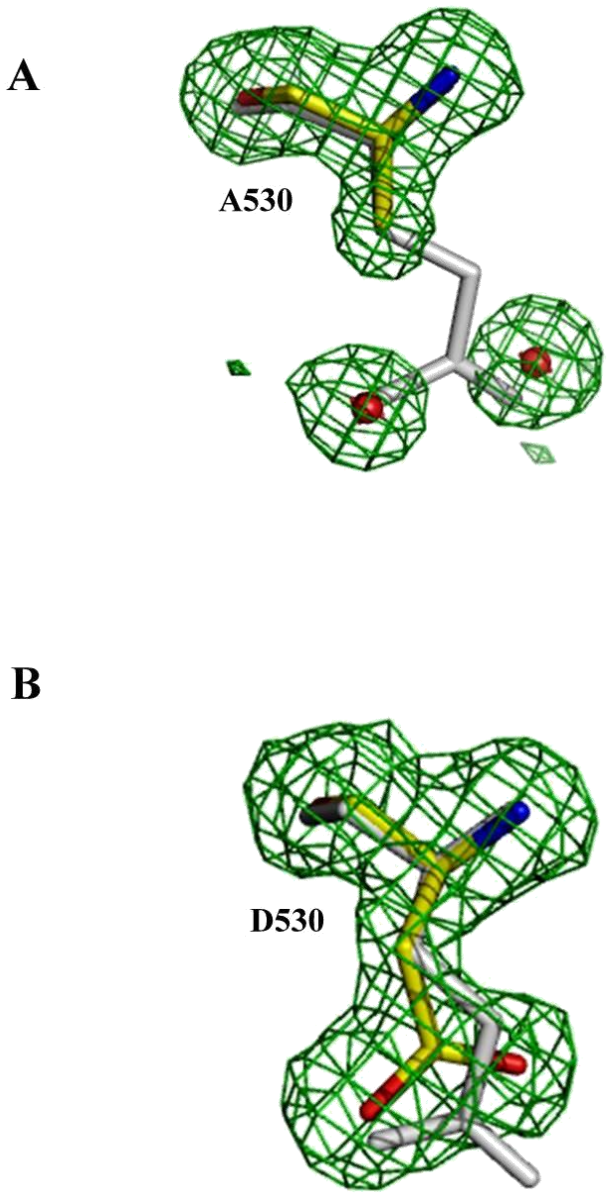

Figure A.5. F_o-F_c electron density maps corresponding to the side chains of Ala530 (A) and Asp530 (B). In panel A, F_o-F_c maps of two water molecules replacing the carboxylate oxygens of glutamate in WT-HPII are shown. The F_o-F_c electron density maps, drawn in green at $\sigma = 3.0$, were calculated without the side chain (A and B) and waters (A) in the model and the appropriate models are superimposed for illustration.

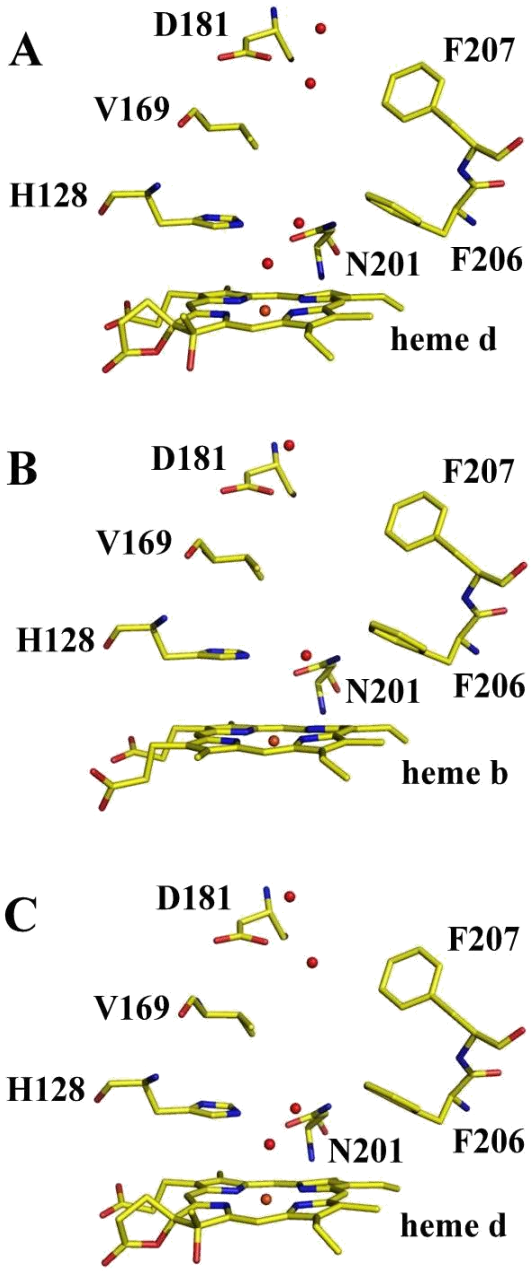

Figure A.6. View of solvent organization on the heme distal side in WT-HPII (A), variant E530A (B), and variant E530D (C). WT-HPII and variant E530D contain heme *d* and two solvent molecules in the heme pocket whereas E530A contains unmodified heme *b* and one solvent molecule. The solvent molecules are indicated as red spheres.

having evolved to concentrate or contain substrate H_2O_2 in the heme cavity has recently been proposed (Domínguez et al., 2010). Thus, a higher [H_2O_2] is required to achieve similar turnover rates (higher apparent K_M). In addition, the more open channel lacking H-bonding interactions presented by E530A may provide easier access for higher concentrations of H_2O_2 thereby allowing the turnover rate to exceed that of WT-HPII. The differences in sensitivity to azide and cyanide contribute to the puzzle that is not completely solved.

APPENDIX B

FUTURE STUDIES

The results obtained from the study opens up the scope for some future experimentation. Both biochemical and structural characterization of F413 variants suggested that the introduction of only tyrosine at this location leads to main chain cleavage located in the vicinity of mutation. It is proposed that Tyr introduces a reactive center into the protein which leads to the back bone cleavage. However, the exact mechanism behind this phenomenon is still not understood. Further site-directed mutagenesis of the nearby residues could be undertaken to strengthen the observation. Besides this, other replacements at 413 resulted in variants altered in heme *b* to heme *d* modification and reduced sensitivity towards catalase inhibitors. Similarly, mutations at other locations also resulted in some variants, for example, H119A, H119N, E530A and E530D, with altered heme modification and inhibitor sensitivity. Co-crystallization of these variants with inhibitors would be required to make claims about the mode of inhibition and role of these residues.

I274 variant proteins exhibit reduced intensity of the Soret band and low R_z values. Structural investigation suggests that the variants are isolated as stable oxoferryl species which might be responsible for low R_z values. However, exact picture is not yet clear. Since, the oxoferryl species of HPII is EPR silent, Mossbauer spectroscopy experiment can be carried out to identify the nature of compound or the changes associated with the heme environment.

8. REFERENCES

Alfonso-Prieto, M., Biarnes, X., Vidossich, P. and Rovira, C. (2009). The molecular mechanism of the catalase reaction. *J. Am. Chem. Soc.* **131:** 11751-11761.

Alfonso-Prieto, M., Vidossich, P., Rodriguez-Fortea, A., Carpena, X., Fita, I., Loewen, P.C. and Rovira, C. (2008). Electronic state of the molecular oxygen released by catalase. *J. Phys. Chem. A* **112:** 12842-12848.

Alfonso-Prieto, M., Borovik, A., Carpena, X., Murshudov, G., Melik-Adamyan, W., Fita, I., Rovira, C. and Loewen, P.C. (2007). The structures and electronic configuration of compound I intermediates of *Helicobacter pylori* and *Penicillium vitale* catalases determined by X-ray crystallography and QM/MM density functional theory calculations. *J. Am. Chem. Soc.* **129:** 4193-4205.

Allgood, G.S. and Perry, J.J. (1986). Characterization of a manganese-containing catalase from the obligate thermophile *Thermophilum album*. *J. Bacteriol.* **168:** 563-567.

Amo, T., Atomi, H. and Imanaka, T. (2002). Unique Presence of a Manganese Catalase in a Hyperthermophilic Archaeon, *Pyrobaculum calidifontis* VA1. *J. Bacteriol.* **184(12):** 3305-3312.

Andreoletti, P., Gambarelli, S., Sainz, G., Stojanoff, V., White, C., Desfonds, G., Gagnon, J., Gaillard, J. and Jouve, H.M. (2001). Formation of a tyrosyl radical intermediate in *Proteus mirabilis* catalase by directed mutagenesis and consequences for nucleotide reactivity. *Biochemistry* **40:** 13734-13743.

Andrews, S.C., Robinson, A.K. and Rodriguez-Quinones, F. (2003). Bacterial iron homeostasis. *FEMS Microbiol. Rev.* **27:** 215-237.

Antonyuk, S. V., Melik-Adamyan, V.R., Popov, A.N., Lamzin, V.S., Hempstead, P.D., Harrison, P.M., Artymyuk, P.J. and Barynin, V.V. (2000). Three-dimensional structure of the enzyme dimanganese catalase from *Thermus thermophilus* at 1 Å resolution. *Crystallography Rep.* **45:** 105–116.

Aslund, F., Zheng, M., Beckwith, J. and Storz, G. (1999). Regulation of the OxyR transcription factor by hydrogen peroxide and the cellular thiol-disulfide status. *Proc. Natl. Acad. Sci. USA* **96:** 6161-6165.

Aslund, F, Berndt, K.D. and Holmgren, A. (1997). Redox potentials of glutaredoxins and other thiol-disulfide oxidoreductases of the thioredoxin superfamily determined by direct protein-protein redox equilibria. *J. Biol. Chem.* **272:** 30780-30786.

Ausubel, F.M., Brent, R., Kingston, R.E., Moore, D.D., Seidman, J.G., Smith, J.A. and Strunhl, K. (1989). *Current protocols in molecular biology*. Green Publishing-Weiley Interscience. New York.

Baker, R.D., Cook, C.O. and Goodwin, D.C. (2004). Properties of catalase-peroxidase lacking its C-terminal domain. *Biochem. Biophys. Res. Commun.* **320:** 833-839.

Barynin, V. V., Whittaker, M.M., Antonyuk, S.V., Lamzin, V.S., Harrison, P.M., Artymiuk, P.J. and Whittaker, J.W. (2001). Crystal structure of manganese catalase from *Lactobacillus plantarum*. *Structure* **9:** 725–738.

Barynin, V. V., Hempstead, P.D., Vagin, A.A., Antonyuk, S.V., Melik-Adamyan, W.R., Lamzin, V.S., Harrison, P.M. and Artymiuk, P.J. (1997). The three-dimensional structure of the di-Mn catalase and the environment of the di-Mn sites in different redox states. *J. Inorg. Biochem.* **67:** 196.

Benov, L.T. and Fridovich, I. (1994). *E.coli* expresses a copper and zinc containing superoxide dismutase. *J. Biol. Chem.* **269:** 25310-25314.

Berglund, G. I., Carlsson, G. H., Smith, A. T., Szöke, H., Henriksen, A. and Hajdu, J. (2002). The catalytic pathway of horseradish peroxidase at high resolution. *Nature* **417:** 463-468.

Bertrand, T., Eady, N.A.J., Jones, J.N., Jesmin, J.M., Nagy, J.M., Jamart-Gregoire, B., Raven, E.L. and Brown, K.A. (2004). Crystal structure of *Mycobacterium tuberculosis* catalase-peroxidase. *J. Biol. Chem.* **279:** 38991-38999.

Blair-Johnson, M., Fiedler, T. and Fenna, R. (2001). Human myeloperoxidase: structure of a cyanide complex and its interaction with bromide and thiocyanate substrates at 1.9 Å resolution. *Biochemistry 40,* 13990-13997.

Bougdour, A. and Gottesman, S. (2007). ppGpp regulation of RpoS degradation via anti-adaptor protein IraP. *Proc. Natl. Acad. Sci. USA* **104:** 12896-12901.

Bougdour, A., Wickner, S. and Gottesman, S. (2006). Modulating RssB activity: IraP, a novel regulator of σs stability in *Escherichia coli*. *Genes Dev.* **20:** 884-897.

Bravo, J., Mate, M.J., Schneider, T., Switala, J., Wilson, K., Loewen, P.C. and Fita, I. (1999). Structure of catalase HPII from *Escherichia coli* at 1.9 Å resolution. *Proteins* **34:** 155-166.

Bravo, J., Fita, I., Ferrer, J., Ens, W., Hillar, A., Switala, J. and Loewen, P.C. (1997). Identification of a novel bond between a histidine and the essential tyrosine in catalase HPII of *Escherichia coli*. *Protein Sci.* **6:** 1016-1023.

Bravo, J., Verdaguer, N., Tormo, J., Betzel, C., Switala, J., Loewen, P.C. and Fita, I. (1995). Crystal structure of catalase HPII from *Escherichia coli*. *Structure* **3:** 491-502.

Brioukhanov, A.L. and Netrusov, A.I. (2004). Catalase and superoxide dismutase: distribution, properties, and physiological role in cells of strict anaerobes. *Biochemistry (Moscow)* **69:** 949-962.

Buettner, G.R. and Jurkiewicz, B.A. (1996). Catalytic metals, ascorbate and free radicals: Combinations to avoid. *Radiat. Res.* **145:** 532-541.

Cabiscol, E., Tamarit, J. and Ros, J. (2000). Oxidative stress in bacteria and protein damage by reactive oxygen species. *Internatl. Microbiol.* **3:** 3-8.

Carpena, X., Wiseman, B., Deemagarn, T., Herguedas, B., Ivancich, A., Singh, R., Loewen, P.C. and Fita, I. (2006). Roles for Arg426 and Trp111 in the modulation of NADH oxidase activity of the catalase-peroxidase KatG from *Burkholderia pseudomallei* inferred from pH-induced structural changes. *Biochemistry* **45:** 5171-5179.

Carpena, X., Wiseman, B., Deemagarn, T., Singh, R., Switala, J., Ivancich, A., Fita, I. and Loewen, P.C. (2005). A molecular switch and electronic circuit modulate catalase activity in catalase-peroxidases. *EMBO Reports* **6:** 1156-1162.

Carpena, X., Melik-Adamyan, W., Loewen, P.C. and Fita, I. (2004). Structure of the C-terminal domain of the catalase-peroxidase KatG from *Escherichia coli*. *Acta Cryst.* **D60:** 1824-1832.

Carpena, X., Loprasert, S., Mongkolsuk, S., Switala, J., Loewen, P.C. and Fita, I. (2003). Catalase-peroxidase KatG of *Burkholderia pseudomallei* at 1.7 Å resolution. *J. Mol. Biol.* **327:** 475-489.

Carpena, X., Soriano, M., Klotz, M.G., Duckworth, H.W., Donald, L.J., Melik-Adamyan, W., Fita, I. and Loewen, P.C. (2003). Structure of the clade 1 catalase, CatF from *Pseudomonas syringae* at 1.8 Å resolution. *Proteins* **50:** 423-436.

Campbell, N.A. and Reese, J.B. (2005). Biology, 7th Edition, San Francisco: Pearson-Benjamin Cummings.

Candeias, L.P. and Steenken, S. (1993). Electron transfer in di(deoxy)nucleoside phosphates in aqueous solution: rapid migration of oxidative damage (via adenine) to guanine. *J. Am. Chem. Soc.* **115:** 2437–40

Chan, E. and Weiss, B. (1987). Endonuclease IV of *Escherichia coli* is induced by paraquat. *Proc. Natl. Acad. Sci. USA* **84:** 3189–93.

Chelikani, P., Carpena, X., Perez-Luque, R., Donald, L. J., Duckworth, H. W., Switala, J., Fita, I. and Loewen, P. C. (2005). Characterization of a large subunit catalase truncated by proteolytic cleavage. *Biochemistry* **44:** 5597-5605.

Chelikani, P., Fita, I. and Loewen, P.C. (2004). Diversity of structures and properties among catalases. *Cell Molec. Life Sci.* **61:** 192-208.

Chelikani, P., Carpena, X., Fita, I. and Loewen, P. C. (2003). An electrical potential in the access channel of catalases enhances catalysis. *J. Biol. Chem.* **278:** 31290-31296.

Chelikani, P., Donald, L. J., Duckworth, H. W. and Loewen, P. C. (2003). Hydroperoxidase II of *Escherichia coli* exhibits enhanced resistance to proteolytic cleavage compared to other catalases. *Biochemistry* **42:** 5729-5735.

Chen, L., Keramati, L. and Helmann, J.D. (1995). Coordinate regulation of Bacillus subtilis peroxide stress genes by hydrogen peroxide and metal ions. *Proc. Natl. Acad. Sci. USA* **92:** 8190-8194.

Chiu, J. T., Loewen, P. C., Switala, J., Gennis, R. B. and Timkovich, R. (1989). Proposed structure for the prosthetic group of the catalase HPII from *Escherichia coli*. *J. Am. Chem. Soc.* **111:** 7046-7050.

Choi, H., Kim, S., Mukhopadhyay, P., Cho, S., Woo, J., Storz, G. and Ryu, S. (2001). Structural basis of the redox switch in the OxyR transcription factor. *Cell* **105:** 103-113.

Chouchane, S., Girotto, S., Shengwei, Y. and Magliozzo, R.S. (2002). Identification and characterization of tyrosyl radical formation in *Mycobacterium tuberculosis* catalase-peroxidase (KatG). *J. Biol. Chem.* **277:** 42633-42638.

Chung, C.T., Niemala, S.L. and Miller, R.H. (1989). One step preparation of competent *Escherichia coli*: transformation and storage of bacterial cells in the same solution. *Proc. Natl. Acad. Sci. USA* **86:** 2172-2175.

Claiborne, A. and Fridovich, I. (1979). Purification of the o-dianisidine peroxidase from *Escherichia coli* B. Physicochemical characterization and analysis of its dual catalatic and peroxidatic activities. *J. Biol. Chem.* **254:** 4245-4252.

Collaborative Computational Project, Number 4. (1994). The CCP4 Suite: Programs for protein crystallography. *Acta Crystallog.* **D50:** 760-763.

Compan, I. and Touati, D. (1993). Interaction of six global transcription regulators in the expression of manganese superoxide dismutase in *E.coli* K-12. *J. Bacteriol.* **175:** 1687-1696.

Cyrne, L., Martins, L., Fernandes, L. and Marinho, H.S. (2003). Regulation of antioxidant enzymes gene expression in the yeast *Saccharomyces cerevisiae* during stationary phase. *Free Radic. Biol. Med.* **34:** 385-393.

Das, K.C. and Das, C.K. (2000). Thioredoxin, a singlet oxygen quencher and hydroxyl radical scavenger: redox independent functions. *Biochem. Biophys. Res. Commun.* **277:** 443-447.

Davies, K.J. (1995). Oxidative stress: the paradox of aerobic life. *Biochem Soc Symp.* **61:** 1–31.

Deemagarn, T., Wiseman, B., Carpena, X., Ivancich, A., Fita, I. and Loewen, P.C. (2007). Two alternative substrate paths for Compound I formation and reduction in catalase-peroxidase KatG from *Burkholderia pseudomallei*. *Proteins* **66:** 219-228.

Deemagarn, T., Carpena, X., Singh, R., Wiseman, B., Fita, I. and Loewen, P.C. (2005). Structural characterization of the Ser324Thr variant of the catalase-peroxidase (KatG) from *Burkholderia pseudomallei. J. Mol. Biol.* **345:** 21-28.

DeLano, W.L. (2002). The PyMOL Molecular Graphics System on World Wide Web http://www.pymol.org.

Demple, B. (1991). Regulation of bacterial oxidative stress genes. *Annu. Rev. Genet.* **25:** 315-337.

Díaz, A., Valdés, V.J., Rudiño-Piñera, E., Horjales, E. and Hansberg, W. (2009). Structure-function relationships in fungal large-subunit catalases. *J. Mol. Biol.* **386:** 218-232.

Díaz, A., Horjales, E., Rudino-Pinera, E., Arreola, R. and Hansberg, W. (2004). Unusual Cys-Tyr covalent bond in a large catalase. *J. Mol. Biol.* **342:** 971-985.

Ding, H. and Demple, B. (1997). In vivo kinetics of a redox-regulated transcriptional switch. *Proc. Natl. Acad. Sci. USA* **94:** 8445-8449.

Dizdaroglu, M. (1992). Measurement of radiation-induced damage to DNA at the molecular level. *Int. J. Radiat. Biol.* **61:** 175-183.

Dominguez, L., Sosa-Peinado, A. and Hansberg, W. (2010). Catalase evolved to concentrate H_2O_2 at its active site. *Arch. Biochem. Biophys.* **500:** 82-91.

Donald, L.J., Krokhin, O.V., Duckworth, H.W., Wiseman, B., Deemagarn, T., Singh, R., Switala, J., Carpena, X., Fita, I. and Loewen, P.C. (2003). Characterization of the catalase-peroxidase KatG from *Burkholderia pseudomallei* by mass spectrometry. *J. Biol. Chem.* **278:** 35687-35692.

Dos Santos, W.G., Pacheco, I., Liu, M.Y., Teixeira, M., Xavier, A.V. and LeGall, J. (2000). Purification and characterization of an iron superoxide dismutase and a catalase from the sulphate-reducing bacterium *Desulfovibrio gigas*. *J. Bacteriol.* **182:** 796-804.

Duarte, T.L. and Lunec, J. (2005). From dietary antioxidants to regulators in cellular signalling and gene expression. *Free Rad. Res.* **39:** 671-686.

Emsley, P. and Cowtan, K. (2004). *Coot: model-building tools for molecular graphics. Acta Crystallog.* **D60:** 2126-2132.

Esterbauer, E., Schaur, R.J. and Zollner, H. (1991). Chemistry and biochemistry of 4-hydroxynonenal, malonaldehyde and related aldehydes. *Free Rad. Biol. Med.* **11:** 81-128.

Faguy, D.M. and Doolittle, W.F. (2000). Horizontal transfer of catalase-peroxidase genes between Archaea and pathogenic bacteria. *Trends Genet.* **16:** 196-197.

Fita, I. and Rossmann, M.G. (1985). The active center of catalase. *J. Mol. Biol.***185:** 21-37.

Flint, D.H., Tuminello, J.F. and Emptage, M.H. (1993). The inactivation of Fe-S cluster containing hydro-lyases by superoxide. *J. Biol. Chem.* **268:** 22369–76.

Fowler, R.G. and Schaaper, R.M. (1997). The role of *mut*T gene of *Escherichia coli* in maintaining replication fidelity. *FEMS Microbiol. Rev.* **21:** 43–54.

Fridovich, I. (1995). Superoxide radical and superoxide dismutases**.** *Annu. Rev. Biochem.* **64:** 97-112.

Fucci, L., Oliver, C.N., Coon, M. and Stadtman, E.R. (1983). Inactivation of key

metabolic enzymes by mixed function oxidation reactions: possible implication in protein turnover and ageing. *Proc. Natl. Acad. Sci. USA* **80:** 1521-1525.

Gaetani, G.F., Ferraris, A.M., Sanna, P. and Kirkman, H.N. (2005). A novel NADPH: (bound) $NADP^+$ reductase and NADH: (bound) $NADP^+$ transhydrogenase function in bovine liver catalase. *Biochem. J.* **385:** 763-768.

Galagan, J.E., Calvo, S.E., Borkovich, K.A., Selker, E.U., Read, N.D., Jaffe, D et al. (2003). Genome sequence of the filamentous fungus *Neurospora crassa*. *Nature* **422:** 859-868.

Gentry, D.R., Hernandez, V.J., Nguyen, L.H., Jensen, D.B. and Cashel, M. (1993). Synthesis of the stationary phase sigma factor σ^s is positively regulated by ppGpp. *J. Bacteriol.* **175:** 7982-7989.

Ghiladi, R.A., Knudsen, G.M., Medzihradszky, K.F. and Ortiz de Montellano, P.R. (2005). The Met-Tyr-Trp cross-link in *Mycobacterium tuberculosis* catalase-peroxidase (KatG): autocatalytic formation and effect on enzyme catalysis and spectroscopic properties. *J. Biol. Chem.* **280:** 22651-22663.

Godon, C., Lagniel, G., Lee, J., Buhler, J.M., Kieffer, S. and Perrot, M. (1998). The H_2O_2 stimulon in *Saccharomyces cerevisiae*. *J. Biol. Chem.* **273:** 22480-22489.

Gonzalez-Flecha and Demple, B. (1995). Metabolic sources of hydrogen peroxide in aerobically growing *Escherichia coli*. *J. Biol. Chem.* **270:** 13681-13687.

Gouet, P., Jouve, H.M. and Dideberg, O. (1995). Crystal structure of *Proteus mirabilis* PR catalase with and without bound NADPH. *J. Mol. Biol.* **249:** 933-954.

Grimsrud, P.A., Xie, H., Griffin, T.J. and Bernlohr, D.A. (2008). Oxidative stress and covalent modification of protein with bioactive aldehydes. *J. Biol. Chem.* **283:** 21837-21841.

Håkansson, K.O., Brugna, M. and Tasse, L. (2004). The three-dimensional structure of catalase from *Enterococcus faecalis*. *Acta Crystallogr.* **D60:** 1374-1380**.**

Halliwell, B. and Gutteridge, J.M.C. (1999). Free radicals in biology and medicine. Oxford: Oxford University Press.

Hara, I., Ichise, N., Kojima, K., Kondo, H., Ohgiya, S., Matsuyama, H. and Yumoto, I. (2007). Relationship between the size of the bottleneck 15 Å from iron in the main channel

and the reactivity of catalase corresponding to the molecular size of substrates. *Biochemistry* **46:** 11-22

Helmann, J.D., Winston Wu, M.F., Gaballa, A., Kobel, P.A., Morshedi, M.M., Fawcett, P. and Paddon, C. (2003). The global transcriptional response of *Bacillus subtilis* to peroxide stress is coordinated by three transcription factors. *J. Bacteriol.* **185:** 243-253.

Hengge-Aronis, R. (2000). The general stress response in *Escherichia coli*, In Storz G, Hengge-Aronis R (Eds.), Bacterial stress response. *ASM Press, Washington DC* 161-178.

Heilek, G.M., Marusak, R., Meares, C.F. and Noller, H.F. (1995). Directed hydroxyl radical probing of 16S rRNA using Fe(II) tethered to ribosomal protein S4. *Proc. Natl. Acad. Sci. USA* **92:** 1113-1116.

Hillar, A, Peters, B., Pauls, R., Loboda, A., Zhang, H., Mauk, A.G. and Loewen, P.C. (2000). Modulation of the activities of catalase-peroxidase HPI of *Escherichia coli* by site-directed mutagenesis. *Biochemistry* **39:** 5868-5875.

Hillar, A. and Nicholls, P. (1992). A mechanism for NADPH inhibition of catalase compound II formation. *FEBS Lett.* **314:** 179-182.

Hirsch, M. and Elliott, T. (2005). Fis regulates transcriptional induction of RpoS in *Salmonella enterica*. *J. Bacteriol.* **187:** 1568-1580.

Hirsch, M. and Elliott, T. (2005). Stationary-phase regulation of RpoS translation in *Escherichia coli*. *J. Bacteriol.* **187:** 7204-7213.

Hirsch, M. and Elliott, T. (2002). Role of ppGpp in *rpo*S stationary-phase regulation in *Escherichia coli*. *J. Bacteriol.* **184:** 5077-5087.

Imlay, J.A. (2008). Cellular defences against superoxide and hydrogen peroxide. *Annu. Rev. Biochem.* **77:** 755-776.

Imlay, J.A. and Storz, G. (1999). Oxidative stress. *Curr. Opin. Microbiol.* **2:** 188-194.

Ivancich, A., Jakopitsch, C., Auer, M., Un, S. and Obinger, C. (2003). Protein based radicals in the catalase-peroxidase *Synechocystis* PCC 6803: a multifrequency EPR investigation of wild-type and variants on the environment of the heme active site. *J. Am. Chem. Soc.* **125:** 14093-14102.

Ivancich, A., Dorlet, P., Goodin, D.B. and Un, S. (2001). Multifrequency high-field EPR study of the tryptophanyl and tyrosyl radical intermediates in wild-type and the W191G mutant of cytochrome c peroxidase. *J. Am. Chem. Soc.* **123:** 5050-5058.

Jakopitsch, C., Vlasits, J., Wiseman, B., Loewen, P.C. and Obinger, C. (2007). Redox intermediates in the catalase cycle of catalase-peroxidases from *Synechocystis* PCC 6803, *Burkholderia pseudomallei*, and *Mycobacterium tuberculosis*. *Biochemistry* **46:** 1183-1193.

Jakopitsch, C., Kolarich, D., Petutschnig, G., Furtmuller, P.G. and Obinger, C. (2003). Distal side tryptophan, tyrosine and methionine in catalase-peroxidases are covalently linked in solution. *FEBS Lett.* **552:** 135-140.

Jakopitsch, C., Auer, M., Ivancich, A., Ruker, F., Furtmuller, P.G. and Obinger, C. (2003). Total conversion of bifunctional catalase-peroxidase to monofunctional peroxidase by exchange of a conserved distal side tyrosine. *J. Biol. Chem.* **278:** 20185-20191.

Jakopitsch, C., Auer, M., Regelsberger, G., Jantschko, W., Furtmuller, P.G., Ruker, F. and Obinger, C. (2003). Distal side aspartate is essential in the catalase activity of catalase-peroxidases. *Biochemistry* **42:** 5292-5300.

Jakopitsch, C., Regelsberger, G., Furtmuller, P.G., Ruker, F., Peschek, G.A. and Obinger, C. (2001). Catalase-peroxidase from *Synechocystis* is capable of chlorination and bromination reactions. *Biochem. Biophys. Res. Commun.* **287:** 682-687.

Jamet, A., Sigaud, S., Van de Sype, G., Puppo, A. and Herouart, D. (2003). Expression of the bacterial catalase genes during *Sinorhizobium meliloti-Medicago sativa* symbiosis and their crucial role during the infection process. *Mol. Plant Microbe Interac.* **16:** 217-225.

Jamieson, D.J., Rivers, S.L. and Stephen, D.W.S. (1994). Analysis of *Saccharomyces cerevisiae* proteins induced by peroxide and superoxide stress. *Microbiology* **140:** 3277-3283.

Jang, S. and Imlay, J.A. (2006). Micromolar intracellular hydrogen peroxide disrupts metabolism by damaging iron-sulfur enzymes. *J. Biol. Chem.* **282:** 929-937.

Jones, D.P. (2006). Redefining oxidative stress. *Antioxid. Redox Signaling* **8:** 1865-1879.

Jung, I.L. and Kim, I.G. (2003). Transcription of *ahpC*, *katG*, and *katE* genes in *Escherichia coli* is regulated by polyamines: polyamine-deficient mutant sensitive to H_2O_2-induced oxidative damage. *Biochem. Biophys. Res. Commun.* **301:** 915-922.

Justino, M.C., Almeida, C.C., Teixeira, M. and Saraiva, L.M. (2007). *Escherichia coli* Di-iron YtfE protein is necessary for the repair of stress damaged iron-sulfur clusters. *J. Biol. Chem.* **282:** 10352-10359.

Kagawa, M., Murakoshi, N., Nishikawa, Y., Matsumoto, G., Kurata, Y., Mizobata, T., Kawata, Y. and Nagai, J. (1999). Purification and cloning of a thermostable manganese catalase from a thermophilic bacterium. *Arch. Biochem. Biophys.* **362:** 346-355.

Keyer, K. and Imlay, J.A. (1996). Superoxide accelerates DNA damage by elevating free-iron levels. *Proc. Natl. Acad. Sci. USA* **93:** 13635–13640.

Kiley, P.J. and Storz, G. (2004). Exploiting thiol modifications. *PLoS Biol.* **2:** 1714-1717.

Kirkman, H.N., Rolfo, M., Ferraris, A.M. and Gaetani, G.F. (1999). Mechanisms of protection of catalase by NADPH. *J. Biol. Chem.* **274:** 13908-13914.

Kirkman, H.N., Galiano, S. and Gaetani, G.F. (1987). The function of catalase-bound NADPH. *J. Biol. Chem.* **262:** 660-666.

Klauck, E., Lingnau, M. and Hengge-Aronis, R. (2001). Role of the response regulator RssB in σ^S recognition and initiation of σ^S proteolysis in *Escherichia coli*. *Mol. Microbiol.* **40:** 1381-1390.

Klotz, M.G. and Loewen, P.C. (2003). The molecular evolution of catalytic hydroperoxidases: evidence for lateral transfer of genes between prokaryota and from bacteria into eukaryota. *Mol. Biol. Evol.* **20:** 1098-1112.

Klotz, M.G., Klassen, G.R. and Loewen, P.C. (1997). Phylogenetic relationships among prokaryotic and eukaryotic catalases. *Mol. Biol. Evol.* **14:** 951-958.

Ko, T.P., Day, J., Malkin, A.J. and McPherson, A. (1999). Structure of orthorhombic crystals of beef liver catalase. *Acta Crystallog.* **D55:** 1383-1394.

Kono, Y. and Fridovich, I. (1983). Isolation and characterization of the pseudocatalase of *Lactobacillus plantarum*: a new manganese containing enzyme. *J. Biol. Chem.* **258:** 6015-6019.

Kono, Y. and Fridovich, I. (1983). Inhibition and reactivation of Mn-catalase: Implications for valence changes at the active site manganese. *J. Biol. Chem.* **258:** 13646-13648.

Kooter, I. M., Pierik, A. J., Merkx, M., Averill, B. A., Moguilevsky, N., Bollen, A. and Wever, R. (1997). Difference Fourier transform infrared evidence for ester bonds linking

the heme group in myeloperoxidase, lactoperoxidase, and eosinophil peroxidase. *J. Am. Chem. Soc.* **119:** 11542-11543.

Kozlovski, V.I., Donald, L.J., Collado, V.M., Spicer, V., Loboda, A.V., Chernushevich, I.V., Ens, W. and Standing, K.G. (2011). A TOF mass spectrometer for the study of noncovalent complexes. *International Journal of Mass Spectrometry*. under revision.

Kunkel, T. A., Roberts, J. D. and Zakour, R. A. (1987). Rapid and efficient site-specific mutagenesis without phenotypic selection. *Meth. Enzymol.* **154:** 367-382.

Lacour, S. and Landini, P. (2004). σ^S -dependent gene expression at the onset of stationary phase in *Escherichia coli*: function of σ^S-dependent genes and identification of their promoter sequences. *J. Bacteriol.* **186:** 7186-7195.

Lange, R.and Hengge-Aronis, R. (1994). The cellular concentration of the sigma S subunit of RNA polymerase in *Escherichia coli* is controlled at the levels of transcription, translation, and protein stability. *Genes Dev.* **8:** 1600-1612.

Layne, E. (1957). Spectrophotometric and turbidimetric methods for measuring proteins. *Meth. Enzymol.* **3:** 447-454.

Lei, B., Wei, C.J. and Tu, S.C. (2000). Action mechanism of antitubercular isoniazid: activation by *Mycobacterium tuberculosis* KatG, isolation and characterization of InhA inhibitor. *J. Biol. Chem.* **275:** 2520-2526.

Loboda, A.V., Krutchinsky, A.N., Bromirski, M., Ens, W. and Standing, K.G. (2000). A tandem quadrupor/time-of-flight mass spectrometer with a matrix-assisted laser desorption/ionization source: design and performance. *Rapid Communications in Mass Spectrometry* **14:** 1047-1057.

Loew, O. (1901). Catalase, A new enzyme of general occurrence with special reference to the tobacco plant. *U.S. Dept. Agr.Rep.* **68:** 47.

Loewen, P.C., Carpena, X., Rovira, C., Ivancich, A., Perez-Luque, R., Haas, R., Odenbreit, S., Nicholls, P. and Fita, I. (2004). Structure of *Helicobacter pylori* catalase, with and without formic acid bound, at 1.6 Å resolution. *Biochemistry* **43:** 3089-3103.

Loewen, P.C., Hu, B., Strutinsky, J. and Sparling, R. (1998). Regulation in the RpoS regulon of *Escherichia coli*. *Can. J. Microbiol.* **44:** 707-717.

Loewen, P.C. (1997). Bacterial catalases. In: *Oxidative Stress and the Molecular Biology of Antioxidant Defenses*, 273-308. Cold Spring Harbor Laboratory Press, Cold Spring Harbor NY.

Loewen, P.C. and Hengge-Aronis, R. (1994). The role of the sigma factor σ^s (KatF) in bacterial global regulation. *Annu. Rev. Microbiol.* **48:** 53-80.

Loewen, P.C., Switala, J., von Ossowski, I., Hillar, A., Christie, A., Tattrie, B. and Nicholls, P. (1993). Catalase HPII of *Escherichia coli* catalyzes the conversion of protoheme to cis-heme d. *Biochemistry* **32:** 10159-10164.

Loewen, P.C. and Switala, J. (1986). Purification and characterization of catalase HPII from *Escherichia coli*. *Biochem. Cell Biol.* **64:** 638-646.

Loewen, P.C., Switala, J. and Triggs-Raine, B.L. (1985). Catalases HPI and HPII in *Escherichia coli* are induced independently. *Arch. Biochem. Biophys.* **243:** 144-149.

Loewen, P.C. and Triggs, B.L. (1984). Genetic mapping of *katF*, a locus that with *katE* affects the synthesis of a second catalase species in *Escherichia coli*. *J. Bacteriol.* **160:** 668-675.

Lushchack, V.I. (2001). Oxidative stress and mechanisms of protection against it in bacteria. *Biochemistry (Moscow)* **66:** 476-489.

Manchado, M., Micha, K. and Pueyo, C. (2000). Hydrogen peroxide activates the soxRS regulon in vivo. *J. Bacteriol.* **182:** 6842-6844.

Margit, B., Zamocky, M., Furtmuller, P.G., Peschek, G.A. and Obinger, C. (2009). Occurrence, phylogeny, structure, and function of catalases and peroxidases in cyanobacteria. *J. Experimental Botany* **60:** 423-440.

Marsh, E.N. (1995). A radical approach to enzyme catalysis. *Bioessays* **17:** 431-441.

Mate, M.J., Zamocky, M., Nykyri, L.M., Herzog, C., Alzari, P.M., Betzel, C., Koller, F. and Fita, I. (1999). Structure of catalase-A from *Saccharocyces cerevisiae*. *J. Mol. Biol.* **286:** 135-149.

Mate, M.J., Sevinc, M.S., Hu, B., Bujons, J., Bravo, J., Switala, J., Ens, W., Loewen, P.C. and Fita, I. (1999). Mutants that alter the covalent structure of catalase hydroperoxidase II from *Escherichia coli*. *J. Biol. Chem.* **274:** 27717-27725.

Mead, D.A., Skorupa, E.S. and Kemper, B. (1985). Single-stranded DNA SP6 promoter plasmids for engineering mutant RNAs and proteins: synthesis of a 'stretched' preproparathyroid hormone. *Nucl. Acids Res.* **13:** 1103-1118.

Meharenna, Y. T., Doukov, T., Li, H., Soltis, S. M. and Poulos, T. L. (2010). Crystallographic and single-crystal spectral analysis of the peroxidase ferryl intermediate. *Biochemistry* **49:** 2984-2986.

Melik-Adamyan, W.R., Bravo, J., Carpena, X., Switala, J., Maté, M. J., Fita, I. and Loewen, P. C. (2001). Substrate flow in catalases deduced from the crystal structures of active site variants of HPII from *Escherichia coli*. *Proteins* **44:** 270-281.

Miller, V.P., Goodin, D.B., Friedman, A.E., Hartmann, C. and Ortiz de Montellano, P.R. (1995). Horseradish peroxidase Phe172-->Tyr mutant. Sequential formation of compound I with a porphyrin radical cation and a protein radical. *J. Biol. Chem.* **270:** 18413-18419.

Molina-Navarro, M.M., Castells-Roca, L., Belli, G., Garcia-Martinez, J., Marin-Navarro, J., Moreno, J., Perez-Ortin, J.E. and Herrero, E. (2008). Comprehensive transcriptional analysis of the oxidative response in yeast. *J. Biol. Chem.* **283:** 17908-17918.

Muffler, A., Fischer, D., Altuvia, S., Storz, G. and Hengge-Aronis, R. (1996). The response regulator RssB controls stability of the σ^S subunit of RNA polymerase in *Escherichia coli*. *EMBO J.* **15:** 1333-1339.

Mulvey, M.R., Switala, J., Borys, A. and Loewen, P.C. (1990). Regulation of transcription of *katE* and *kat*F in *Escherichia coli. J. Bacterial.* **172:** 6713-6720.

Mulvey, M.R. Sorby, P.A, Triggs-Raine, B.L. and Loewen, P.C. (1988). Cloning and physical characterization of *katE* and *katF*, required for catalase HPII expression in *E. coli*. *Gene* **73:** 337-345.

Murshudov, G.N., Grebenko, A.I., Brannigan, J.A., Antson, A.A., Barynin, V.V., Dodson, G.G., Dauter, Z., Wilson, K.S. and Melik-Adamyan, W.R. (2002). The structures of *Micrococcus lysodeikticus* catalase, its ferryl intermediate (compound II) and NADPH complex. *Acta Crystallog.* **D58:** 1972-1982.

Murshudov, G. N., Vagin, A. A. and Dodson, E. J. (1997). Refinement of macromolecular structures by the maximum-likelihood method. *Acta Crystallog.* **D53:** 240-255.

Murshudov, G. N., Grebenko, A. I., Barynin, V., Dauter, Z., Wilson, K. S., Vainshtein, B. K., Melik-Adamyan, W., Bravo, J., Ferrán, J. M., Ferrer, J. C., Switala, J., Loewen,

P. C. and Fita, I. (1996). Structure of the heme d of *Penicillium vitale* and *Escherichia coli* catalases. *J. Biol. Chem.* **271:** 8863-8868.

Murshudov, G.N., Melik-Adamyan, W.R., Grebenko, A.I., Barynin, V.V., Vagin, A.A., Vainshtein, B.K., Dauter, Z. and Wilson, K.S. (1982). Three dimensional structure of catalase from *Micrococcus lysodeikticus* at 1.5 Å resolution. *FEBS Lett.* **312:** 127-131.

Nadler, V., Goldberg, I. and Hochman, A. (1986). Comparative study of bacterial catalases. *Biochim. Biophys. Acta* **882:** 234-241.

Nathan, C. and Shiloh, M.U. (2000). Reactive oxygen and nitrogen intermediates in the relationship between mammalian hosts and microbial pathogens. *Proc. Natl. Acad. Sci. USA* **97:** 8841-8848.

Nicholls, P., Fita, I. and Loewen, P.C. (2001). Enzymology and structure of catalases. *Adv. Inorg. Chem.* **51:** 51-106.

Niederhoffer, E.C., Naranjo, C.M. and Bradley, K.L. (1990). Control of *E.coli* superoxide dismutase (*sod*A and *sod*B) genes by the ferric uptake regulation (*fur*) locus. *J.Bacteriol.* **172:** 1930-1938.

Ochi, H., Hata, Y., Tanaka, N., Kakudo, M., Sakurai, T., Aihara, S. and Morita, Y. (1983). Structure of rice ferricytochrome c at 2.0 Å resolution. *J. Mol. Biol.* **166:** 407-418.

Olson, L. P. and Bruice, T. C. (1995). Electron tunneling and *ab initio* calculations related to the one-electron oxidation of NAD(P)H bound to catalase. *Biochemistry* **34:** 7335-7347.

Paris, S., Wysong, D., Debeaupuis, J.P., Shibuya, K., Philippe, B., Diamond, R.D. and Latge, J.P. (2003). Catalases of *Aspergillus fumigatus*. *Infect. Immun.* **71:** 3551-3562.

Parsonage, D., Youngblood, D.S., Sarma, G.N., Wood, Z.A., Karplus, P.A. and Poole, L.B. (2005). Analysis of the link between enzymatic activity and oligomeric state in AhpC, a bacterial peroxiredoxin. *Biochemistry* **44:** 10583-10592.

Passardi, F., Theiler, G., Zamocky, M., Cosio, C., Rouhier, N., Teixera, F., Margis-Pinheiro, M., Loannidis, V., Penel, C., Falquet, L. and Dunand, C. (2007). PeroxiBase: the peroxidase database. *Phytochemistry* **68:** 1605-1611.

Passardi, F., Zamocky, M., Favet, J., Jakopitsch, C., Panel, C., Obinger, C. and Dunand, C. (2007). Phylogenetic distribution of catalase-peroxidases: are there patches of order in chaos? *Gene* **397:** 101-113.

Patten, C.L., Kirchhof, M.G., Schertzberg, M.R., Morton, R.A. and Schellhorn, H.E. (2004). Microarray analysis of RpoS-mediated gene expression in *Escherichia coli* K-12**.** *Mol. Genet. Genomics* **272:** 580-591.

Pearson, A. R., Elmore, B. O., Yang, C., Ferrara, J. D., Hooper, A. B. and Wilmot, C. M. (2007). The crystal structure of cytochrome P460 of *Nitrosomonas europaea* reveals a novel cytochrome fold an heme-protein cross-link. *Biochemistry* **46:** 8340-8349.

Pflugrath, J.W. (1999). The finer things in X-ray diffraction data collection. *Acta Crystallog.* **D55:** 1718-1725.

Pomposiello, P.J., Koutsolioutsou, A., Carrasco, D. and Demple, B. (2003). SoxRS-regulated expression and genetic analysis of the *yggX* gene of *Escherichia coli*. *J. Bacteriol.* **185:** 6624-6632.

Putnam, C.D., Arvai, A.S., Bourne, Y. and Tainer, J.A. (2000). Active and inhibited human catalase structures: ligand and NADPH binding and catalytic mechanism. *J. Mol. Biol.* **296:** 295-309.

Rana, T.M. and Meares, C.F. (1991). Iron chelate mediated proteolysis: protein structure dependence. *J. Am. Chem. Soc.* **113:** 1859-1861.

Rana, T.M. and Meares, C.F. (1991). Transfer of oxygen from an artificial protease to peptide carbon during proteolysis. *Proc. Natl. Acad. Sci. USA* **88:** 10578-10582.

Ranguelova, K., Girotto, S., Gerfen, G.J., Yu, S., Suarez, J., Metlitsky, L. and Magliozzo, R.S. (2007). Radical sites in *Mycobacterium tuberculosis* KatG identified using electron paramagnetic resonance spectroscopy, the three-dimensional crystal structure, and electron transfer couplings. *J. Biol. Chem.* **282:** 6255-6264.

Regelsberger, G., **Jakopitsch, C., Ruker, F., Krois, D., Peschek, G.A. and Obinger, C.** (2000). Effect of distal cavity mutations on the formation of compound I in catalase-peroxidases. *J. Biol. Chem.* **275:** 22854-22861.

Rhee, S.G. (2006). Cell signaling. H_2O_2, a necessary evil for cell signaling. *Science* **312:** 1882-1883.

Rhee, S.G. (2000). Redox signaling: hydrogen peroxide as intracellular messenger. *Exp. Mol. Med.* **31:** 53-59.

Riise, E.K., Lorentzen, M.S., Helland, R., Smalas, A.O., Leiros, H.K.S. and Willassen, N.P. (2007). The first structure of a cold-active catalase from *Vibrio salmonicida* at 1.96 Å reveals structural aspects of cold adaptation. *Acta Crystallog.* **D63:** 135-148.

Rocha, E.R. and Smith, C.J. (2004). Transcriptional regulation of the *Bacteroides fragilis* ferritin gene (*ftn*A) by redox stress. *Microbiology* **150:** 2125-2134.

Rørth, H. M. and Jensen, P. K. (1967). Determination of catalase activity by means of the Clark oxygen electrode. *Biochim. Biophys. Acta* **139:** 171-173.

Rovira, C. (2005). Structure, protonation state and dynamics of catalase compound II. *Chem. Phys. Chem***. 6:** 1820-1826.

Sambrook, J., Fritsch, E.F. and Maniatis, T. (1989). *Molecular cloning: A Laboratory Manual*. Cold Spring Harbour Laboratory. Cold Spring Harbour Press. New York.

Sanger, F. S., Nicklen, S. and Coulson, A. R. (1977). DNA sequencing with chain-terminating inhibitors. *Proc. Natl. Acad. Sci. USA* **74:** 5463-5467.

Sayre, L.M., Lin, D., Yuan, Q., Zhu, X. and Tang, X. (2006). Protein adducts generated from products of lipid oxidation: focus on HNE and ONE*. *Drug Metabolism Reviews* **38:** 651-675.

Sayre, L.M., Smith, M.A. and Perry, G. (2001). Chemistry and biochemistry of oxidative stress in neurodegenerative disease. *Current Medicinal Chemistry* **8:** 721-738.

Schellhorn, H.E. and Hassan, H.M. (1988). Transcriptional regulation of *katE* in *Escherichia coli* K-12. *J. Bacteriol*. **170:** 4286-4292.

Schweder, T., Lee, K.H., Lomovskaya, O. and Matin, A. (1996). Regulation of *Escherichia coli* starvation sigma factor (σ^S) by ClpXP protease. *J. Bacteriol.* **178:** 470-476.

Seaver, L.C. and Imlay, J.A. (2001*).* Alkyl hydroperoxide reductase is the primary scavenger of endogenous hydrogen peroxide in *Escherichia coli*. *J. Bacteriol.* **183:** 7182-7189.

Sevinc, M. S., Maté, M. J., Switala, J., Fita, I. and Loewen, P. C. (1999). Role of the lateral channel in catalase HPII of *Escherichia coli*. *Prot. Sci.* **8:** 490-498.

Sevinc, M. S., Switala, J., Bravo, J., Fita, I. and Loewen, P. C. (1998). Truncation and heme pocket mutations reduce production of functional catalase HPII in *Escherichia coli*. *Protein Eng.* **11:** 549-555.

Sevinc, M. S., Ens, W. and Loewen, P. C. (1995). The cysteines of catalase HPII of *Escherichia coli*, including Cys438 which is blocked, do not have a catalytic role. *Eur. J. Biochem.* **230:** 127-132.

Shevchenko, A, Tomas, H, Havlis, J., Olsen, J.V. and Mann, M. (2006). In-gel digestion for mass spectrophotometric characterization of proteins and proteomes. *Nature Protocols* **1:** 2856- 2860.

Sies H. (1997). Oxidative stress: Oxidants and antioxidants. *Experimental physiol.* **82:** 291-295.

Sies, H. (1993). Strategies of antioxidant defense. *Eur. J. Biochem.* **215:** 213-219.

Sies, H. and Menck, C.F. (1992). Singlet oxygen induced DNA damage. *Mutat. Res.* **275:** 367-375.

Shima, S., Sordel-Klippert, M., Brioukhanov, A., Netrusov, A., Linder, D. and Thauer, R.K. (2001). Characterization of a heme-dependent catalase from *Methanobrevibacter arboriphilus*. *Appl. Environ. Microbiol.* **67:** 3041-3045.

Sicking, W., Korth, H.-G., de Groot, H. and Sustmann, R. (2008). On the functional role of a water molecule in clade 3 catalases: a proposal for the mechanism by which NADPH prevents the formation of Compound II. *J. Am. Chem. Soc.* **130:** 7345-7356.

Singh, R., Wiseman, B., Deemagarn, T., Jha, V., Switala, J. and Loewen, P.C. (2008). Comparative study of catalase-peroxidases (KatGs). *Arch. Biochem. Biophys.* **471:** 207-214.

Singh, R., Switala, J., Loewen, P.C. and Ivancich, A. (2007). Two [Fe(IV)=O Trp·] intermediates in *M. tuberculosis* catalase-peroxidase discriminated by multifrequency (9-285 GHz) EPR spectroscopy: reactivity towards isoniazid. *J. Am. Chem. Soc.* **129:** 15954-15963.

Singh, R., Wiseman, B., Deemagarn, T., Donald, L.J., Duckworth, H.W., Carpena, X., Fita, I. and Loewen, P.C. (2004). Catalase-peroxidases (KatG) exhibit NADH oxidase activity. *J. Biol. Chem.* **279:** 43098-43106.

Smirnoff, N. (2005 Edition). Antioxidants and reactive oxygen species in plants, Blackwell Publishing.

Smith, C.D., Carney, J.M., Tatsumo, T., Stadtman, E.R., Floyd, R.A. and Markesbery, W.R. (1992). Protein oxidation in aging brain. *Ann. N.Y. Acad. Sci.* **663:** 110-119.

Smulevich, G., Jakopitsch, C., Droghetti, E. and Obinger, C. (2006). Probing the structure and bifunctionality of catalase-peroxidase (KatG). *J. Inorg. Biochem.* **100:** 568-585.

Spira, B. and Yagil, E. (1998). The relation between ppGpp and the PHO regulon in *Escherichia coli*. *Mol. Gen. Genet.* **257:** 469-477.

Stadtman, E.R. (1993). Oxidation of free amino acids and amino acid residues in proteins by radiolysis and by metal-catalyzed reactions. *Annu. Rev. Biochem.* **62:** 797-821.

Stadtman, E.R. (1990). Metal ion-catalyzed oxidation of proteins: biochemical mechanism and biological consequences. *Free Rad. Biol. Med.* **9:** 315-325.

Stern, K.G. (1936). The constitution of the prosthetic group of catalase. *J. Biol. Chem.* **112:** 661-669.

Storey, K.B. (1996). Oxidative stress: animal adaptations in nature. *Brazilian Journal of Medical Biology Research* **29:** 1715-1733.

Storz, G., Tartagila, L.A. and Ames, B.N. (1990). Transcriptional regulation of oxidative stress inducible genes: direct activation by oxidation. *Science* **248:** 189-194.

Suarez, J., Ranguelova, K., Jarzecki, A.A., Manzerova, J., Krymov, V., Zhao, X., Yu, S., Metlitsky, L., Gerfen, G.J. and Magliozzo, R.S. (2009). An oxyferrous heme/protein-based radical intermediate is catalytically competent in the catalase reaction of *Mycobacterium tuberculosis* catalase-peroxidase (KatG). *J. Biol. Chem.* **284:** 7017-7029.

Sundaresan, M., Yu, Z. X., Ferrans, V. J., Irani, K. and Finkel, T. (1995). Requirement for generation of H_2O_2 for platelet-derived growth factor signal transduction. *Science* **270:** 296-299.

Switala, J. and Loewen, P. C. (2002). Diversity of properties among catalases. *Arch. Biochem. Biophys.* **401:** 145-154.

Switala, J., O'Neil, J. O. and Loewen, P. C. (1999). Catalase HPII from *Escherichia coli* exhibit enhanced resistance to denaturation. *Biochemistry* **38:** 3895-3901.

Tenhaken, R., Levine, A., Brisson, L.F., Dixon, R.A. and Lamb, C. (1995). Function of the oxidative burst in hypersensitive disease resistance. *Proc. Natl. Acad. Sci. USA* **92:** 4158-4163.

Thomas, J.A., Morris, D.R. and Hager, L.P. (1970). Chloroperoxidase VII: classical peroxidatic, catalatic, and halogenating forms of the enzyme. *J. Biol. Chem.* **245:** 3129-3134.

Tkachenko, A., Nesterova, L. and Pshenichnov, M. (2001). The role of the natural polyamine putrescine in defence against oxidative stress in *Escherichia coli*. *Arch. Microbiol.* **176:** 155-157.

Toledano, M.B., Delaunay, A., Monceau, L. and Tacnet, F. (2004). Microbial H_2O_2 sensors are archetypical redox signalling modules. *Trends Biochem. Sci.* **29:** 351-357.

Touati, D. (2000). Iron and oxidative stress in bacteria. *Arch. Biochem. Biophys.* **373:** 1-6.

Touati, D., Jacques, M., Tardat, B., Bouchard, L. and Despied, L. (1995). Lethal oxidative damage and mutagenesis are generated by iron in delta fur mutants of *Escherichia coli*: protective role of superoxide dismutase. *J. Bacteriol.* **177:** 2305-2314.

Traber, M.G. and Atkinson, J. (2007). Vitamin E, antioxidant and nothing more. *Free Rad. Biol. Med.* **43:** 4–15.

Triggs-Raine, B.L., Doble, B.W., Mulvey, M.R., Sorby P.A. and Loewen, P.C. (1988). Nucleotide sequence of *katG*, encoding catalase HPI of *Escherichia coli*. *J. Bacteriol.* **170:** 4415-4419.

Vainshtein, B.K., Melik-Adamyan, W.R., Barynin, V.V., Vagin, A.A, Grebenko, A.I., Borisov, K.S., Fita, I. and Rossmann, M.G. (1986). Three-dimensional structure of catalase from *Penicillium vitale* at 2.0 Å resolution. *J. Mol. Biol.* **188:** 49-61.

Veal, E.A., Day, A.M. and Morgan, B.A. (2007). Hydrogen peroxide sensing and signalling. *Mol. Cell.* **26:** 1-14.

Vetrano, A.M., Heck, D.E., Mariano, T.M., Mishin, V., Laskin, D.L. and Laskin, J.D. (2005). Characterization of the oxidase activity in mammalian catalase. *J. Biol. Chem.* **280:** 35372-35381.

Vidossich, P., Alfonso-Prieto, M., Carpena, X., Fita, I., Loewen, P.C. and Rovira, C. (2010). The dynamic role of distal side residues in heme hydroperoxidase catalysis. Interplay between X-ray crystallography and *ab intio* MD simulations. *Arch. Biochem. Biophys.* **500:** 37-44.

Vidossich, P., Alfonso-Prieto, M., Carpena, X., Loewen, P.C., Fita, I. and Rovira, C. (2007). Versatility of the electronic structure of compound I in catalase-peroxidases. *J. Am. Chem. Soc.* **129:** 13436-13446.

Vieira, J. and Messing, J. (1987). Production of single-stranded plasmid DNA. *Methods Enzymol.* **153:** 3-11.

Visser, S.P. (2006). What external perturbations influence the electronic properties of catalase compound I? *Inorg. Chem.* **45:** 9551-9557.

von Ossowski, Hausner, G. and Loewen, P.C. (1993). Molecular evolutionary analysis based on the amino acid sequence of catalase. *J. Mol. Evol.* **37:** 71-76.

von Ossowski, I., Mulvey, M. R., Leco, P. A., Borys, A. and Loewen, P. C. (1991) Nucleotide sequence of *Eschericia coli katE*, which encodes catalase HPII. *J. Bacteriol.* 173, 514-520.

Wada, K., Tada, T., Nakamura, Y., Kinoshita, T., Tamoi, M., Shigeoka, S. and Nishimura, K. (2002). Crystallization and preliminary X-ray diffraction studies of catalase-peroxidase from *Synecococcus* PCC 7942. *Acta Crystallogr.* **D58:** 157-159.

Weber, H., Polen, T., Heuveling, J, Wendisch, V.F. and Hengge, R. (2005). Genome-wide analysis of the general stress response network in *Escherichia coli*: σ^S-dependent genes, promoters and sigma factor selectivity**.** *J. Bacteriol.* **187:** 1591-1603.

Weber, K., Pringle, J.R. and Osborn, M. (1972). Measurement of molecular weights by electrophoresis on SDS acrylamide gels. *Methods Enzymol.* **26:** 3-27.

Welinder, K.J. (1992). Superfamily of plant, fungal and bacterial peroxidases. *Curr. Opin. Struct. Biol.* **2:** 388-393.

Welinder, K.J. (1991). Bacterial catalase-peroxidases are gene duplicated members of the plant peroxidase superfamily. *Biochem. Biophys. Acta* **1080:** 215-220.

Whittaker, M.M., Barynin, V.V., Antonyuk, S.V. and Whittaker, J.W. (1999). The oxidized (3,3) state of manganese catalase: comparision of enzymes from *Thermus thermophilus* and *Lactobacillus plantarum*. *Biochemistry* **38:** 9126-9136.

Wu, F., Katsir, L.J., Seavy, M. and Gaffney, B.J. (2003). Role of radical formation at tyrosine 193 in the Allene Oxide Synthase domain of a Lipoxygenase-AOS fusion protein from Coral. *Biochemistry* **42:** 6871-6880.

Yamada, Y., Fujiwara, T., Sato, T., Igarashi, N. and Tanaka, N. (2002). The 2.0 Å crystal structure of catalase-peroxidase from *Haloarcula marismortui*. *Nat. Struct. Biol.* **9:** 691-695.

Yanisch-Perron, C., Vieira, J. and Messing, J. (1985). Improved M13 phage cloning vectors and host strains: nucleotide sequences of the M13mp18 and pUC19 vectors. *Gene* **33:** 103-119.

Zámocký, M., Furtmuller, P.G. and Obinger C. (2008). Evolution of catalases from bacteria to humans. *Antioxid. Redox Signal.* **10:** 1527-1547.

Zámocký, M., Jakopitsch, C., Vlasits, J. and Obinger C. (2007). Fungal catalase-peroxidases: a novel group of bifunctional oxidoreductases. *J. Biol. Inorg. Chem.* **12:** S97.

Zámocký, M. and Koller, F. (1999). Understanding the structure and function of catalases: clues from molecular evolution and in vitro mutagenesis. *Prog. Biophys. Mol. Biol.* **72:** 19-66.

Zhang, Y., Heym, B., Allen, B., Young, S. and Cole, S. (1992). The catalase-peroxidase gene and isoniazid resistance of *Mycobacterium tuberculosis*. *Nature* **358:** 591-593.

Zheng, M., Wang, X., Templeton, L.J., Smulski, D.R., LaRossa, R.A. and Storz, G. (2001). DNA microarray-mediated transcriptional profiling of the *Escherichia coli* response to hydrogen peroxide. *J. Bacteriol.* **183:** 4562-4570.

Zheng, M. and Storz, G. (2000). Redox sensing by prokaryotic transcription factors. *Biochem. Pharmacol.* **59:** 1-6.

Zheng, M., Aslund, F. and Storz, G. (1998). Activation of the OxyR transcription factor by reversible disulfide bond formation. *Science* **279:** 1718-1721.

Zhou, Y., Gottesman, S., Hoskins, J.R., Maurizi, M.R. and Wickner, S. (2001). The RssB response regulator directly targets σ^s for degradation by ClpXP. *Genes Dev.* **15:** 627-637.